CHARLES UNIVERSITY IN PRAGUE

FACULTY OF SCIENCE

Study program: Physical Chemistry

RNDr. Eliška Procházková

The Structure and Properties of Modified Nucleic Acid Components

Ph.D. Thesis

Supervisor: RNDr. Martin Dračínský, Ph.D.

Prague, 2015

Dedicated to

Doc. RNDr. Iva Zusková, CSc.

mentor, colleague and friend

DECLARATION

I declare that I wrote this thesis myself and that it represents the results of my own work under the supervision of RNDr. Martin Dračínský, Ph.D. All sources of literature have been properly cited in the Reference section. This work or its parts have not been previously used for obtaining any academic degree.

In Prague,…………………………

………………………………………

RNDr. Eliška Procházková

ACKNOWLEDGEMENTS

TABLE OF CONTENTS

LIST OF ABBREVIATIONS

1D	one-dimensional
2D	two-dimensional
ANPs	acyclic nucleoside phosphonates
APT	attached proton test
ATP	adenosine-5'-triphosphate
B3LYP	Becke's three-parameter hybrid functional with Lee-Yang-Parr correlation functional
COSY	correlation spectroscopy
CP-MAS	cross-polarization magic-angle spinning
DFT	density functional theory
DMSO	dimethyl sulfoxide
dNMR	dynamic nuclear magnetic resonance
DNA	deoxyribonucleic acid
FAD/FADH$_2$	flavin adenine dinucleotide
FDA	Food and Drug Administration
H-bonds	hydrogen bonds
HBV	hepatitis B virus
H/D exchange	hydrogen-to-deuterium exchange
HETCOR	heteronuclear correlation
HIV	human immunodeficiency virus
HMBC	heteronuclear multiple bond correlation
HPLC	high-performance liquid chromatography
HR-MS	mass spectrometry with high resolution
HSQC	heteronuclear single quantum correlation
IOCB AS CR	Institute of Organic Chemistry and Biochemistry, Academy of Sciences of the Czech Republic
NACs	nucleic acid components
NAD$^+$/NADH	nicotinamide adenine dinucleotide
NMR	nuclear magnetic resonance
NOE	nuclear Overhauser effect
PCM	polarizable continuum model
RAHB	resonance-assisted hydrogen bond
RNA	ribonucleic acid
ROESY	rotating frame nuclear Overhauser effect spectroscopy
SS-NMR	NMR spectroscopy in solid state
TMS	tetramethylsilane
UV/Vis spectrometry	spectrometry in ultraviolet and visible region

ABSTRACT

Modified nucleic acid components (nucleotides, nucleosides, nucleobases) display a wide range of biological activities such as antiviral, cytostatic, antimicrobial or antioxidative. Many of them are successfully used in clinical practice, for instance as anti-HIV drugs or in hepatitis B treatment. The first precondition for understanding biological effects is to evaluate the chemical structure as well as the conformation of the studied compounds correctly. For this purpose, solution-state nuclear magnetic resonance (NMR) spectroscopy in combination with mass spectrometry is the most frequently used method. Not only the structure, but also the physico-chemical properties can be investigated using NMR spectroscopy, for instance, conformational changes, tautomeric forms, protonation sites, acido-basic properties, non-covalent interactions, isotopic exchanges or interactions with biomolecules. Similarly to solutions, NMR spectroscopy can be employed in studies of nucleic acid components (NACs) in solid state. This technique found assertion after computational-chemistry methods development during the last decades. Different solid-state structures (polymorphic forms) or dynamics of these compounds can be established by solid-state NMR spectroscopy in combination with quantum-chemical calculations.

In this work, I dealt with the structure elucidation as well as the investigation of the physico-chemical properties of modified nucleotides, nucleosides and nucleobases using NMR spectroscopy both in solution state and solid state in combination with density functional theory (DFT) calculations of NMR parameters. For the structure determination, 1D in combination with 2D NMR experiments were employed; the configuration and conformation of the studied compounds were also investigated. During this analysis, we noticed a possibility of NMR signals misassignment in substituted purine derivatives, so we developed a new method for unambiguous NMR signal assignment in purines based on the measurement of heteronuclear coupling constants in combination with DFT calculations. The same approach including correlations between experimental and calculated data was applied for the development of a new method for the prediction of preferred tautomeric forms of purine derivatives in solution.

A non-covalent interaction essential for life is hydrogen bond (H-bond), which can be studied by NMR spectroscopy in detail. We studied nitrosopyrimidine derivatives with strong intramolecular H-bonds which stabilized two conformers, differing only in NO group orientation. We investigated the composition of the rotamers mixture in equilibrium depending on the pyrimidine substitution. From temperature-dependent ^{1}H NMR spectra, the rotational barriers of the nitroso group were estimated. In some cases, it was possible to separate both rotamers from each

other by column chromatography at room temperature and their purity was confirmed by SS-NMR spectra as well as by X-ray structure analysis. The kinetic data of the rotamer interconversion were measured to determine rotational barriers around C5-NO single bond. Experimental data were supported by DFT calculations.

Many biologically active compounds are unable to pass across the cell membrane, therefore, more lipophilic derivatives (prodrugs) are often prepared. They are designed with the aim of active compound release after a reaction with intracellular enzymes. For confirmation that newly prepared phosphoramidate derivatives could work as prodrugs and they are decomposed by carboxypeptidase in the supposed metabolic pathway, we studied their enzymatic decomposition using ^{31}P NMR spectroscopy. The monitoring of the reaction is based on the fact that the starting phosphoramidate has a chiral center at the phosphorus atom, so that it has two signals in proton decoupled ^{31}P NMR spectrum corresponding to two diastereoisomers. After several hours of the enzymatic reaction, a single ^{31}P signal is observed, which indicates that the final product does not contain a chiral center at the phosphorus atom. The same products were obtained after non-enzymatic hydrolysis with triethylamine and the suggested chemical structure was confirmed using ^{1}H, ^{13}C and 2D NMR experiments.

The solid-state structure of a given compound influences its biological effects and the information about their polymorphic structures is crucial for granting licenses obtained from regulatory authorities. For investigation of polymorphic crystals in this work, ^{13}C cross-polarization magic-angle spinning (CP-MAS) NMR spectroscopy was used. We prepared model polymorphic crystal forms of three pharmaceutically or industrially important compounds and characterized them using CP-MAS NMR spectroscopy as well as by Raman spectroscopy. The determined structures were confirmed by X-ray analysis. These data were supplemented by DFT calculations.

For biological properties investigation, the studied compounds are usually dissolved in DMSO, sometimes for a long time. We observed color changes of 5-aminopyrimidine derivatives dissolved in DMSO. We monitored these transformations by NMR and UV/Vis spectroscopy and we used series of chemical reactions to confirm the structure of the colorful products.

1 Introduction

1.1 Nucleic acid components (NACs)

1.1.1 Naturally occurring NACs

Naturally occurring NACs (namely nucleotides, nucleosides and nucleobases) play a key role as the building blocks of nucleic acids (DNA, RNA); they also interact with enzymes and other proteins as components of the cofactors and signal molecules, for instance, as second messengers.[1] Adenosine 5´-triphosphate (ATP) is well known as a macroergic molecule responsible for energy storage in cells (Fig. 1). NACs are also contained in the structure of cofactors essential for cellular metabolism such as nicotinamide adenine dinucleotide (NAD^+/NADH), flavin adenine dinucleotide (FAD, $FADH_2$), coenzyme A, S-methyladenosine *etc.*[2]
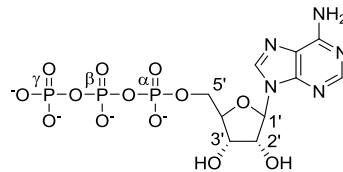
Figure 1. The structure of adenosine-5'-triphosphate (ATP).

Nucleotides consist of three parts: nitrogen-containing heterocycle (nucleobase), sugar part and phosphate. The structure of nucleobases is derived from purine and pyrimidine skeleton as shown in Fig. 2. These nucleobases have planar arrangement in space and they interact via π-π stacking as well as hydrogen bonds; one purine and one pyrimidine base are complementary to each other and they form a hydrogen-bonded base pair. This property is necessary condition for forming more complex structures such as DNA duplexes. The sugar part of the molecule is attached to the nucleobase (N^1 of pyrimidine or N^9 of purine) by N-glycosidic bond; β-D-ribose or 2'-deoxy-β-D-ribose form part of RNA or DNA, respectively. Phosphorylated nucleotides (triphosphates) serve as macroergic molecules and they play a key role in DNA synthesis. Nucleoside triphosphates are unstable and can be easily decomposed; inorganic phosphate is cleaved and the nucleoside diphosphate releases.
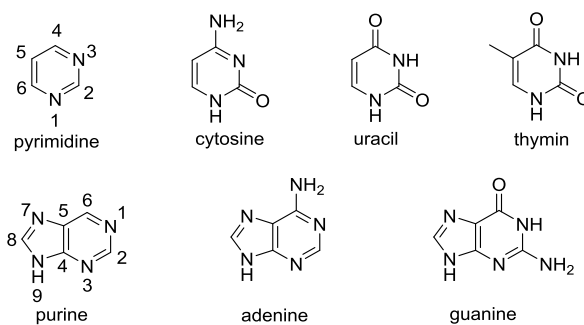
Figure 2. The structure of natural pyrimidine and purine nucleobases (N^1 and N^9 tautomers are shown) together with the structure and numbering of the parent heterocycles.

Another class of NACs important in biological systems are nucleosides; they are composed of a nucleobase and a sugar moiety. Their physico-chemical properties are significantly different from nucleotides mentioned above. They are not charged (the phosphate part is missing) and they are less soluble in water, leading to their better cell-membrane permeability.

1.1.2 Modified NACs

The aim of bioorganic and medicinal chemistry is to design and synthetize new biologically active compounds, which could be potentially used in chemotherapy. A very "popular" class of compounds are synthetically prepared analogs of metabolites - antimetabolites – their function as drug-like molecules is based on their structural similarity with naturally occurring substrates of the target enzymes. In the design of an antimetabolite, one has to take into account the differences in metabolic pathways of the host cell and the parasite (bacteria, virus, yeast, protozoa) or different metabolism of carcinoma cells with respect to healthy cells.

Many antimetabolites based on modified structures of NACs have important biological activity. For example, they can act as an interferon inducers used in therapy of chronic hepatitis C, as microtubule assembly inhibitors responsible for the cell cycle arrest at the G2/M transition or as inhibitors of pharmaceutically important enzymes such as HIV-reverse transcriptase, sulphotransferase, leukotriene A$_4$ hydrolase, phosphodiesterase or cyclin-dependent kinase.[3] Also their antioxidant activity has been found.[4] Nowadays, they are used as antiviral,[5,6] antitumor[7] and antimicrobial[8] agents.

1.1.2.1   Modifications of the nucleobase

The molecule of a nucleotide or nucleoside can be modified on the purine/pyrimidine skeleton as well as in the sugar part; nucleotides can be also modified in the phosphate chain. The heteroaromatic skeleton can be modified by heteroatoms (endocyclic substitution) or by a variety of substituents on the ring (exocyclic substitution). The most pharmaceutically important are aza/deaza-modified derivatives of purine as well as pyrimidine bases. As an example,

5-azacytidine (**1**) is a well-known cytostatics[9], 8-aza-7-deaza-hypoxanthine (**2**) called allopurinol is used against gout.[10] The analogs obtained after exocyclic substitution are, for instance, 5-fluorocytosine (**3**) exerting antifungal effects[11] or 6-mercaptopurine (**4**) used for antitumor treatment[12] (Fig. 3).
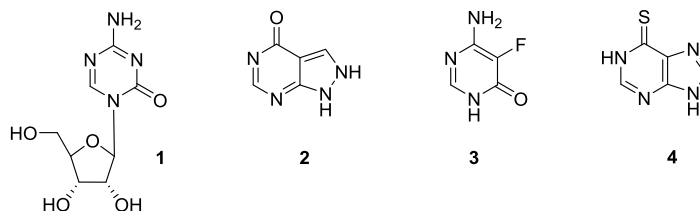
Figure 3. Examples of the structures of NACs modified on the nucleobase. 5-azacytidine **1** and allopurinol **2** are compounds with endocyclic modification of the base skeleton; 5-fluorocytosine **3** and 6-mercaptopurine **4** are substituted in position 5 and 6, respectively.

1.1.2.2   *Modification of the sugar part*

The second option for modification of nucleotides or nucleosides is the sugar part of the molecule, which can be modified in the same way as the nucleobase meaning the endocyclic or exocyclic substitution. These compounds exert a wide range of biological activities, for instance, lamivudine (**5**) with antiviral effects against hepatitis B virus (HBV)[13] as well as human immunodeficiency virus (HIV)[14] and gemcitabine (**6**) with antitumor activities[15] were described (Fig. 4).
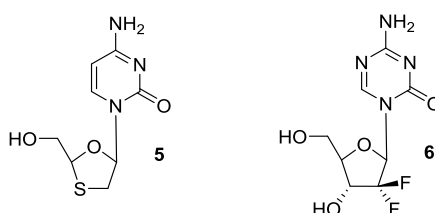
Figure 4. The structure of lamivudine with endocyclic substitution in the ribose ring (**5**) and gemcitabine (**6**) with exocyclic substitution on the ribose moiety.

Carbocyclic nucleosides

Nucleosides, where the ribose oxygen atom is replaced by a carbon atom, are called carbocyclic nucleoside derivatives and some of them exert antiviral and/or antibacterial activity. As an example, abacavir (**7**) displaying antiviral activity against HIV[16] is shown in Fig. 5.
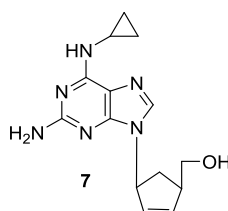
Figure 5. The structure of carbocyclic nucleoside abacavir (**7**).

Locked nucleosides

Nucleoside derivatives can be also bridged by short aliphatic chains leading to reduced flexibility of the ribose ring; these conformationally constrained compounds are called locked nucleosides and they are in the field of interest of medicinal chemists because of their antiviral activities.[17,18] It was discovered that the nucleosides locked in different conformations (described in 1.1.3.4) can interact with different enzymes.[19] As an example, carbocyclic locked nucleosides **8–11** designed as novel antivirotics from the group of Radim Nencka (IOCB AS CR) are introduced in Fig. 6.[18,20,21]
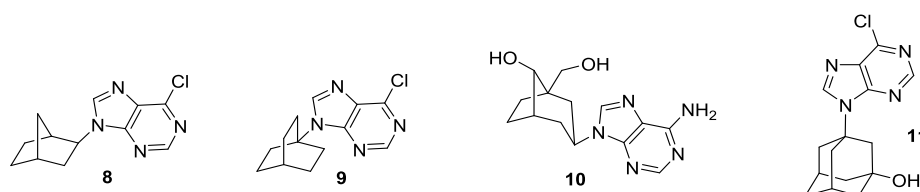
Figure 6. The structure of carbocyclic locked nucleosides **8–11** prepared as potential antivirotics.

The structure determination and conformational analysis of locked nucleoside derivatives studied by a combination of 1D and 2D NMR experiments will be discussed in detail in chapter 3.

Acyclic nucleosides

Another class of NACs modified in the sugar part are acyclic nucleoside derivatives, where the ribose ring is substituted by an acyclic chain with other places for possible modifications. Acyclic analogs are much more metabolically stable than the cyclic counterparts, because N-glycosidic bond between nucleobase and the sugar part is changed into N-alkyl bond. The most famous acyclic nucleoside is probably acyclovir **12** (Fig. 7), which is targeted against Herpes viruses.[22]
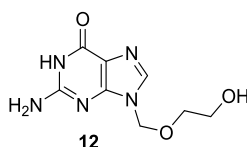
Figure 7. The structure of acyclovir (**12**), an acyclic nucleoside analog used in the treatment of Herpes *sp*.

Acyclic nucleoside phosphonates

Very important class of antiviral compounds – acyclic nucleoside phosphonates, (ANPs)[6] – was prepared and systematically studied by prof. Antonín Holý and his group (IOCB AS CR). In ANPs, the phosphate group is not attached through O-P bond, but through a methylene bridge $O\text{-}CH_2\text{-}P$, which provides them a higher metabolic stability. Nowadays, these compounds are considered as the most active against viruses and three of them (Fig. 8) are clinically used as antivirotics.

Adefovir (**13**) is active against retroviruses and DNA viruses,[23] its oral prodrug adefovir dipivoxil (commercialized under the trade name Hepsera™) works in the treatment of chronic HBV disease.[24] Another successfully used compound is tenofovir (**14**),[25] which exerts biological activity against retroviruses. It inhibits reverse transcriptase of HBV as well as HIV.[26] It is indicated for the treatment of long-lasting hepatitis B virus and it prevents cells from multiplying HIV in the body; more than 95 % of HIV-positive people in the world are treated with this drug. It is marketed as disoproxil fumarate prodrug called Viread™. The third clinically used compound of this class is cidofovir (**15**) with the brand name Vistide™. It is active mainly against DNA viruses. It has been approved by FDA in 1996 for treatment of cytomegalovirus retinitis[27] as well as against acyclovir-resistant Herpes *sp.* infections.[28]
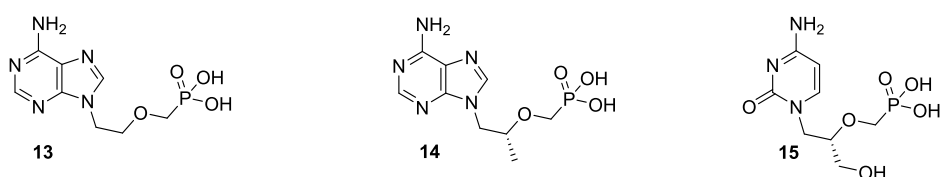
Figure 8. The structures of adefovir (**13**), tenofovir (**14**) and cidofovir (**15**), which are used in clinical practice.

1.1.3 Physico-chemical properties of NACs

Natural and modified nucleotides or nucleosides have very diverse structures leading to differences in a variety of their properties, such as different base-pairing, interactions with enzymes or metal ions and also tautomeric and conformational equilibria.

1.1.3.1 Tautomerism of nucleobases

Different tautomeric forms of a nucleobase can be found when a hydrogen atom changes its position in the heterocycle.[29] Different tautomers allow to form different hydrogen bonding arrangements and they impact various chemical processes, such as reactivity in alkylation or glycosidation reactions. The tautomeric form of the starting compound influences the regioselectivity of the reaction.[2] In a solution, there is usually an equilibrium mixture of several tautomers and the percentage of individual tautomers as well as exchange rates strongly depend on substituents, solvent and temperature.[30, 31] Because of the fast proton exchange in tautomers, only the time-averaged spectra are usually observable by nuclear magnetic resonance (NMR) spectroscopy at room temperature. The most suitable and commonly used tool for studying tautomeric equilibria is low-temperature NMR spectroscopy, where the motion of protons is slowed down and individual tautomers may be observed.[32] As an example, possible tautomeric forms of purine derivatives, hypoxanthine, is shown in Fig. 9. It was found that N^1,N^9 form is preferred in solution.[33,34]

N^1,N^9 tautomer N^1,N^7 tautomer N^3,N^9 tautomer N^3,N^7 tautomer O^6,N^9 tautomer
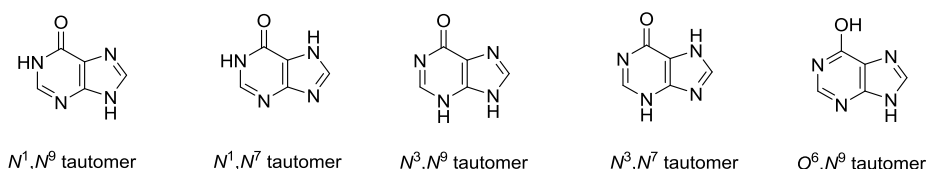
Figure 9. The selected tautomeric forms of hypoxanthine.

A new method for investigation of preferred tautomeric forms in purine derivatives based on a combination of experimental and calculated data will be discussed in chapter 4.

1.1.3.2 Protonation/Deprotonation

The nitrogen-containing heterocycle can offer places for protonation or deprotonation of nitrogen atoms allowing their participation in acid-base equilibria. Due to the fused imidazole ring, purine skeleton contains more protonation sites than pyrimidine ring. Protonation of a particular nitrogen atom leads to a dramatic change of its chemical shift and smaller chemical-shift changes of neighboring atoms. The most suitable tool for monitoring protonation or deprotonation is ^{15}N NMR spectroscopy, which clearly indicates the hydrogen atom bonding. Usually, the pH dependence of chemical shifts (NMR titration) is monitored to investigate acid-base properties of each site, such as acidic or basic dissociation constant K_A and K_B, respectively. As an example, protonated forms of hypoxanthine are shown in Fig. 10.

Neutral   Monocation   Dication
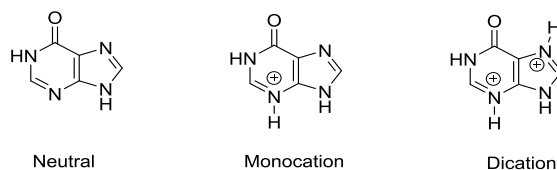
Figure 10. The structure of hypoxanthine monocation and dication studied by NMR spectroscopy.[35,36]

1.1.3.3 Base orientation

The orientation of a base with respect to a ribose ring is described by glycosidic torsion angle χ, which is defined for purine nucleosides as O4'-C1'-N9-C4 torsion angle (Fig. 11) and for pyrimidine derivatives as O4'-C1'-N1-C2 angle. If χ ranges between 90 and 270°, this conformation is called *anti*, on the other hand, when χ is between 0–90° or 270–360°, the conformation is termed *syn*. In naturally occurring nucleotides, nucleosides, *anti-* conformation is more frequent. The conformation of a nucleoside has a significant influence on interactions with other molecules in cell. *Anti-/syn-* conformation can be determined by heteronuclear (C-H) *J*-coupling analysis as well as by 2D ROESY experiment, which correlates close-in-space protons.
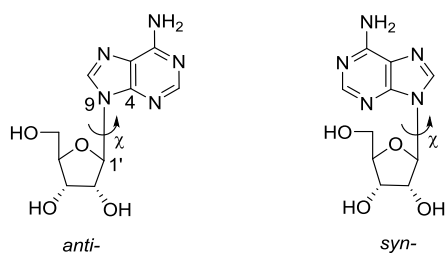
Figure 11. The two possible orientations of a nucleobase with respect to the ribose ring.

1.1.3.4   Conformation of the ribose ring

In general, it is well known that five-membered rings are flexible and can co-exist in several conformations in solution. The stereochemistry of the ribose ring is usually analyzed using the concept of pseudorotation, which was first introduced in cyclopentane by Kilpatrick *et al.*[37] Based on this work, Altona and Sundaralingam developed the method for a quantitative determination of five-membered ring conformation.[38] In the theory of pseudorotation, the conformation of the ribose ring is described by two parameters called phase angle P and maximum puckering amplitude $\varPhi_{MAX}$. For schematic representation of the furanose ring conformation based on the variation of P (0-360°), the pseudorotational cycle was defined (Fig. 12).[39] Each point on the circle represents a specific value of the phase angle of pseudorotation P; the cycle is divided into twenty increments (18° step) corresponding to twenty possible conformations of the furanose ring. The signs inside the ribose rings correspond to the signs of torsion angles $\varPhi_0$-$\varPhi_4$ described below. The capitals E or T meaning Envelope or Twist conformation, respectively, represent the shape of the furanose ring.
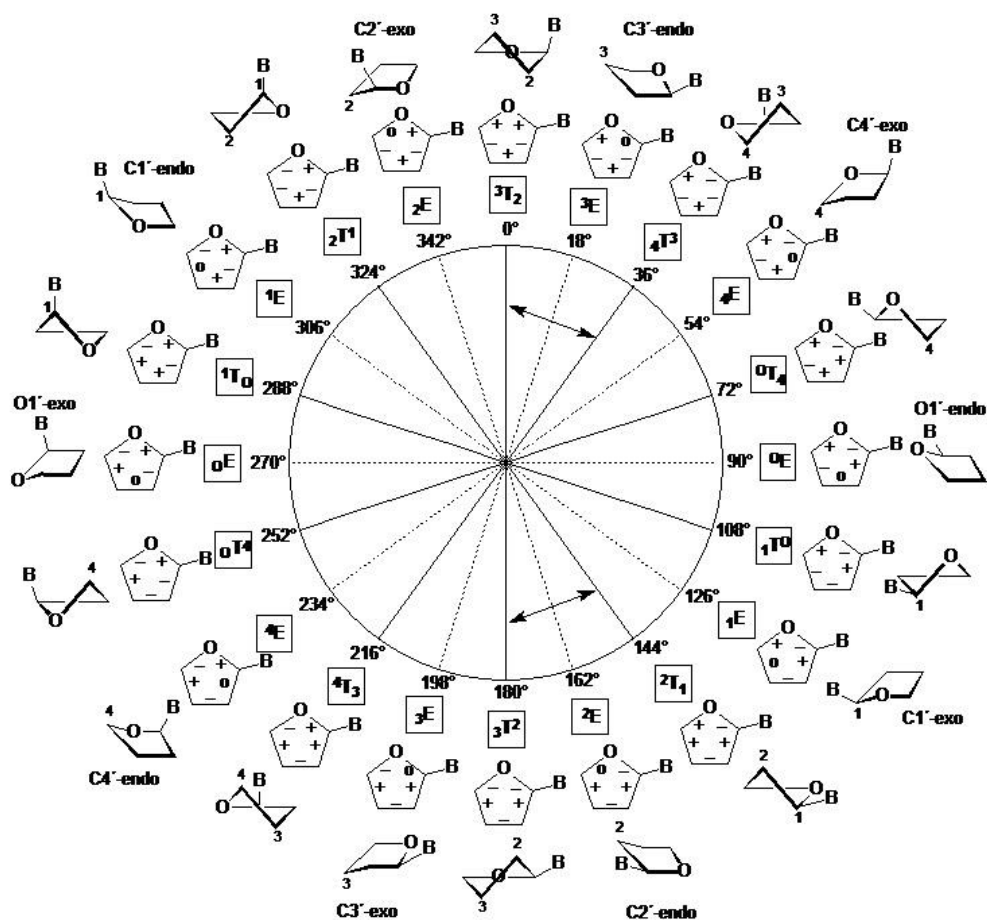
Figure 12. Pseudorotational cycle of the furanose ring. Each point on the circle represents a specific value of the phase angle of pseudorotation P (0–360°). The signs inside the ribose rings correspond to the signs of the torsion angles.

Phase angle is calculated from torsion (dihedral) angles Φ_0-Φ_4 (Fig. 13);[38] it tells us the information about the shape of the ribose ring; it indicates the atoms that are displaced from the plane formed by three (T conformation) or four (E conformation) ring atoms.

In naturally occurring nucleosides, phase angle P falls in the ranges 0-36° and 144–180°. Conformations with these phase angles are highlighted in Fig. 12 by arrows. The first one (0–36°) is denoted North (N-type) and the second one (144–180°) is called South (S-type).

Φ_0: C1-C2-C3-C4
Φ_1: C2-C3-C4-O
Φ_2: C3-C4-O-C1
Φ_3: C4-O-C1-C2
Φ_4: O-C1-C2-C3
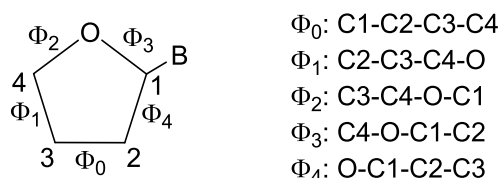
$$\tan P = \frac{(\Phi_2 + \Phi_4) - (\Phi_1 + \Phi_3)}{2\Phi_0(\sin 36 + \sin 72)}$$

Figure 13. Definition of the five endocyclic torsion angles Φ_0-Φ_4 in the ribose ring.

The second variable describing the ribose ring conformation is maximum puckering amplitude Φ_{MAX}, which characterizes maximal atom displacement and it can be calculated from the following equation.

$$\Phi_0 = \Phi_{MAX} \cos P$$

In naturally occurring nucleoside or nucleotide derivatives as well as in their modified counterparts, the values of Φ_{MAX} generally range approximately from 35 to 45°.[39] Therefore, Φ_{MAX} equal to 40° is often used as the input value for DFT calculations, which will be explained below (chapter 1.2.5).

The N-type conformation is also called C3'-endo (^{3}E) and the S-type is known as C2'-endo (^{2}E) (Fig. 14). Both conformations occur in nature and their relative concentration depend on the type of nucleic acid (A-DNA, B-DNA, RNA etc.), where the ribose ring is involved.
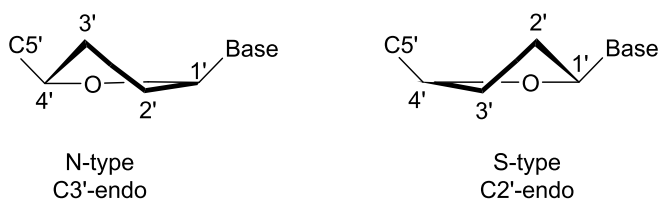
Figure 14. A schematic representation of the furanose conformations in nucleic acids.

The conformation of the ribose ring is crucial for the recognition by cellular enzymes.[40] For instance, it was found that North-type derivatives of a locked nucleoside are effectively bound by polymerases,[40] whereas the South counterparts are recognized by thymidine kinases.[19] From this reason, it is desired to study sugar conformation in newly prepared compounds.

In this work, the concept of pseudorotation was applied for investigation of the ribose ring conformation in locked nucleoside derivatives and it will be discussed in detail in chapter 3 in connection with the structure determination.

1.1.3.5   *Hydrogen bonds*

Very important non-covalent interaction in biological systems is hydrogen bond (H-bond). It is defined as a dipole-dipole attraction between an acidic hydrogen atom and highly electronegative atom such as nitrogen, oxygen *etc*. Intramolecular H-bonds decrease the molecular polarity, which leads to better membrane permeability.[41] The secondary structure of proteins is built by patterns of intramolecular H-bonds between the main-chain peptide groups. Furthermore, they play a key role in base-pairing in duplexes of nucleic acids.[42] If the duplex consists of higher number of C-G pairs containing three H-bonds, it is more stable than in the case of A-T pairs containing only two H-bonds. Sequence recognition *via* base-pairing is essential for DNA repair and gene regulation.[43]

The strength of intramolecular hydrogen bond is increased if a six-membered ring is formed and the linker atoms are sp^2-hybridized resulting in planar, conjugated systems. This phenomenon is called resonance-assisted hydrogen bonding (RAHB)

and it is mediated *via* enhanced π-delocalization.[44] It was published that six-membered hydrogen-bonded pseudorings can mimic aromatic rings.[45,46] For example, 5-nitrosopyrimidines with strong intramolecular H-bonds were proposed as purine mimics (Fig. 15).
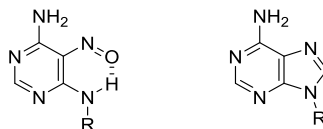
Figure 15. The structure of potential purine mimics; the shape of the heterocyclic base with intramolecular H-bond (left) is close to the purine skeleton structure (right).

A study of intramolecular H-bonds in 5-nitrosopyrimidine derivatives causing an interesting stereochemical behavior of these compounds will be discussed in detail in chapter 5.

1.2 NMR METHODS AND APPLICATIONS

The electronic distribution in molecules influences chemical properties and it is reflected in chemical shifts δ, spin-spin couplings J and other NMR parameters, which makes NMR spectroscopy an excellent tool for investigating structure, reactivity, molecular motions and intermolecular interactions of studied compounds especially small molecules such as NACs. [30,31,47]

Atomic nuclei with non-zero spin quantum number have nuclear magnetic momentum and that is why they are active in NMR spectroscopy. In homogenous magnetic field, spin states differ in energy and they are unequally populated. The energy-level transitions can be provoked by applying magnetic field with frequency ν resulting from the resonance condition:

$$\upsilon = \frac{\gamma B_0}{2\pi}$$

gyromagnetic ratio γ is a quantity characteristic for each nucleus and B_0 represents external magnetic field. In most cases, γ is positive, but sometimes (e.g. ^{15}N) it can be negative. The external magnetic field B_0 influences electron distribution and dynamics in the studied molecule, which leads to magnetic shielding of nuclei by electrons. Nuclei with different chemical environment are shielded differently and resonate at different frequencies. This fact makes NMR spectroscopy a perfect tool for chemists. The most suitable nuclei for NMR spectra measurements are those with spin one half such as ^{1}H, ^{13}C, ^{15}N, ^{19}F, or ^{31}P, commonly occurring in organic compounds. The natural abundance of magnetically active nuclides is, however, also very important parameter, which influences the overall sensitivity of a given nuclide. For example, the natural abundance of ^{1}H is 99.98 %, while that of ^{13}C is 1.11 %, only.

The chemical shift δ is defined as the difference between the resonance frequency ν of the observed nucleus and the standard reference frequency ν_{ref}

divided by v_{ref} and it is expressed in parts per million (ppm). The values of δ are typical for every type of functional groups, for instance, carbon nuclei of aromatic compounds resonate at lower field (higher δ) than aliphatic carbons. Every signal in a spectrum corresponds to a non-equivalent nucleus in the molecule.

$$\delta = \frac{v - v_{ref}}{v_{ref}} 10^6$$

The ^nJ-coupling (indirect spin-spin coupling) describes the interaction between nuclei via n chemical bonds. J-coupling between non-equivalent nuclei, meaning with different chemical environment, is visible in NMR spectrum as the distance between the lines in a multiplet (line-splitting). There is an approximate trend in the magnitudes of J-coupling showing that the more covalent bonds between the coupled nuclei are, the lower the J-coupling values are. The J-couplings can span a broad range of values, for instance between protons across 2–5 bonds can be approximately 0–20 Hz, whereas heteronuclear C-H coupling constants can be higher than 200 Hz (^1J (C-H)), depending significantly on carbon atom hybridization. J-coupling values also depend on the geometry of the molecule, which is described in detail in chapter 1.2.2.

The nuclear Overhauser effect (NOE) arises *via* through-space dipolar interactions of nuclear spins. It is based on a transfer of nuclear spin polarization from one nuclear spin population to another *via* cross-relaxation. This effect is crucial in many NMR techniques, not only to enhance otherwise insensitive NMR spectroscopic signals, but also to make unambiguous stereochemical assignment. As an example, ROESY experiment is based on NOE and it serves for the assignment of close-in-space nuclei (ca < 5 Å).[48]

1.2.1 NMR experiments

1.2.1.1   1D NMR experiments

^{1}H NMR experiment

The measurement of proton NMR spectra is probably the first instrumental analytical method of choice for structure determination in organic chemistry. With the use of external magnetic field B_0 equal to 11.74 T, the ^{1}H nuclide resonates at the frequency 500 MHz. ^{1}H NMR spectrum is approximately 10 ppm wide and it can be very roughly divided into three basic regions. The aliphatic proton signals are observable in the right-hand side of the spectrum, typically between 0 and approximately 3 ppm. For example, protons from CH_3 group in ethanol have the chemical shift around 1.0 ppm. The second region (ca. 3–6 ppm) contains protons in a heteroatom neighborhood (CH_2-OH). For example, CH_2 proton signal of ethanol is shifted to ca 3.4 ppm. The low-field region (6–10 ppm) contains signals coming from protons attached to sp^2-hybridized carbon atoms. For instance, electronic shielding caused by conjugated π-system in benzene shifts proton signals to values around 7.3

ppm. As a standard, tetramethylsilane (TMS) with the chemical shift equal to zero is used (δ_{TMS} = 0).

^{13}C NMR experiment

^{13}C NMR spectra provide another useful information about the structure of organic compounds. ^{13}C NMR spectrum range is approximately 200 ppm wide and it can be divided into three main regions similarly as in the case of ^{1}H NMR spectra described above. For instance, aliphatic carbon atom CH_3 in ethanol has chemical shift around 20 ppm, whereas the signal of the CH_2 group with neighboring oxygen atom (heteroatom) is shifted to ca 60 ppm. Aromatic and double bond region is between 120–170 ppm. For example, the chemical shift of carbon atoms in benzene is around 130 ppm. As a standard, tetramethylsilane (TMS) with the chemical shift equal to zero is used (δ_{TMS} = 0).

 It is more convenient to measure APT spectra (attached proton test) than common ^{13}C NMR spectra. It enables to distinguish carbon atom signals according to the number of attached protons. In APT spectra, signals of carbon atoms with odd number of protons (CH, CH$_3$) are turned down, while signals of carbon atoms with zero or two protons (C, CH$_2$) are oriented upwards. This significantly helps to assign ^{13}C NMR signals in more complicated structures.

Furthermore, in ^{13}C experiment without ^{1}H-decoupling, it is possible to see C-H spin-spin interactions as a splitting of carbon signals.

^{31}P NMR experiment

^{31}P NMR spectrum range is approximately 700 ppm wide and the chemical shifts are significantly influenced by the oxidation and coordination number of the phosphorus atom. As mentioned above, nucleoside triphosphates are very unstable; an inorganic phosphate is often cleaved spontaneously and the nucleoside diphosphate is released. This cleavage can be easily observed in ^{31}P NMR spectra. The ^{31}P nuclei of nucleoside triphosphates resonate approximately around -10 ppm (P$_\alpha$, P$_\gamma$) and -20 ppm (P$_\beta$). As an external standard, H_3PO_4 with chemical shift equal to zero is commonly used.

In this work, the measurement of ^{31}P NMR spectra allowed us to monitor the enzymatic decomposition of a phosphoramidate prodrug of a locked nucleoside derivative directly in the NMR tube. Furthermore, C-P spin-spin interactions visible in ^{13}C NMR spectra as a line-splitting were used for *in situ* structure determination of products of the decomposition. The results of this project will be introduced in chapter 6.

1.2.1.2   2D NMR experiments

The number of NMR signals, their position in 1D spectra (chemical shift δ) and their splitting (spin-spin interaction J) provide the first structural information about a compound. In simple structures, it is sufficient for structure determination; on the other hand, for the determination of more complicated structures, 2D NMR spectra

are measured. In this section, the most commonly used 2D NMR experiments in small-molecule NMR spectroscopy will be introduced. In 2D NMR experiments described below, both axes give chemical shifts and we call them 2D correlated NMR spectra. In all experiments except ROESY, a crosspeak found between two signals in 1D projections means that the corresponding nuclei have spin-spin interaction (J-coupling). On the other hand, in ROESY experiment, the crosspeaks correspond to through-space interactions. Homonuclear experiments correlate chemical shifts of the same nuclide, whereas heteronuclear experiments correlate chemical shifts of different nuclides. By combination of 1D (^{1}H, ^{13}C) and 2D (COSY, HSQC, HMBC, ROESY) NMR experiments, the structure of the studied molecule can be solved.

HSQC experiment

In heteronuclear single quantum correlation (HSQC), the crosspeaks correspond to heteronuclear spin-spin interaction of a proton with a heteroatom X (^{13}C, ^{15}N, ^{31}P) across one bond. ^{1}H,^{13}C-HSQC experiments are measured routinely and provide information which proton is directly attached (one-bond) to which carbon atom. HSQC experiment is more sensitive than previously used HETCOR because of polarization transfer from ^{1}H nuclei with high gyromagnetic ratio γ to low-γ heteronuclei and because of direct detection of ^{1}H signals and indirect detection of the heteronuclei. High sensitivity of this experiment is often exploited for indirect detection of insensitive nuclei such as ^{15}N with very low natural abundance (0.4 %) and low γ. ^{1}H,^{15}N-HSQC measurement provides an evidence of NH/NH$_2$ groups presence.

HMBC experiment

Heteronuclear multiple bond correlation (HMBC) correlates signals of protons and heteroatoms X (^{13}C, ^{15}N, *etc.*), which have J-coupling across two (^2J) and three (^3J) bonds. Sometimes, long-range couplings across four and five bonds (^4J and ^5J, respectively) can be also seen. ^{1}H,^{13}C-HMBC experiment is crucial mainly (but not only) for quaternary carbon atom signal assignment. ^{1}H,^{15}N–HMBC can help with the detection and assignment of ^{15}N signals of non-labeled compounds.

In this work, ^{1}H,^{13}C-HMBC experiment was employed to study long-range coupling constants in purine derivatives with the aim to improve NMR signal assignment. The results of this study are summarized in chapter 4.

COSY experiment

In homonuclear correlation spectroscopy experiment (COSY), crosspeaks provide information about J-couplings between the same nuclides. The most common experiment is ^{1}H,^{1}H-COSY. Crosspeaks from this spectrum correspond to J-couplings between protons on the same carbon atom (geminal coupling ^2J) or between protons in the neighboring positions (vicinal coupling ^3J), which is used for chain connectivity information. In some cases, long-range couplings (^4J, ^5J) are also observable.

Another important homonuclear 2D NMR spectrum is rotating frame nuclear Overhauser effect spectroscopy (ROESY), which is based on NOE described above. It correlates signals of protons occurring in space close to each other. The intensity of NOE signals decreases with a six-power distance between nuclei (the distance limit is ca. 5 Å). This measurement is useful for conformational analysis.

1.2.2 *J*-coupling analysis

As described above, indirect spin-spin interaction between neighboring nuclei is mostly mediated by bonding electrons. The values of coupling constants (*J*) are obtained from 1D NMR spectrum as the distance between lines in multiplets. From the values of *J*-coupling, it is possible to assess how many chemical bonds are between the coupled nuclei. Commonly observed interactions are across one bond ^1J (C-H) visible in ^{13}C spectra measured without broad-band decoupling; the couplings across two bonds ^2J and three bonds ^3J are called geminal and vicinal, respectively.

The ^3J-coupling value significantly depends on the torsion angle between the coupled nuclei. The relation $^3J \sim f (\Phi)$ is commonly used for investigation of conformation and configuration of studied compounds. The well-known curve describing the dependence of the torsion angle Φ on the vicinal coupling constant ^3J is Karplus equation: [49,50]

$$^3J(\Phi) = A \cos^2 \Phi + B \cos \Phi + C$$

where *A*, *B* and *C* are empirically obtained parameters suitable for selected class of compounds. Because of the cosine function, it is evident that for a torsion angle close to 90°, the coupling constant ^3J reaches the lowest value. On the other hand, when the torsion angle is close to 0° or 180°, the vicinal coupling constant tends to be the largest. The values of $^3J(H,H)$ depend also on other molecular parameters, such as electronegativity of the substituents, bond lengths and bond angles. Nowadays, many other empirical equations describing the dependence of ^3J on Φ are available, such as Altona, Diez-Donders[51] or Haasnoot-Altona[52] equation for various types of compounds.

In some cases, long-range couplings over more than three bonds are visible. If the bonds linking the coupled nuclei adopt planar W-like arrangement, long-range coupling constants are larger, see, for example, compounds **16**–**19** (Fig. 16).

Compound	^4J (Hz)
16	1-3
17	3-4
18	1-2
19	2-3
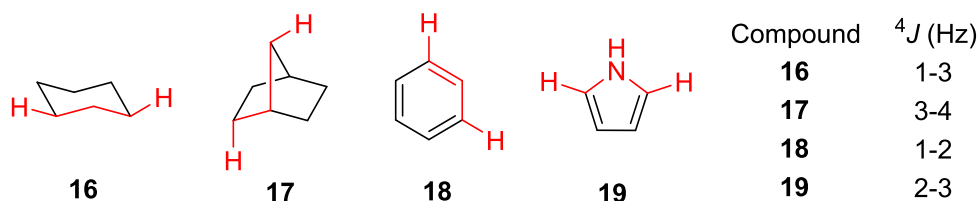
Figure 16. Examples of long-range coupling constants ^4J in compounds with W-like shaped pathway between the coupled nuclei (in red).

Multiple bonds in the pathway between the coupled nuclei also increase the value of long-range couplings. For instance, ^4J-couplings in alkene **20** or alkyne **21** derivatives are depicted in Fig. 17. Long-range couplings through five or more bonds can be observed rarely in NMR spectra, because their value is usually lower than the signal width. The preferences in pathway geometry between the coupled nuclei are the same as described in four-bond couplings; zig-zag pathway or multiple bonds increase the value of ^5J-coupling.

20 ^4J = 1-3 Hz   **21** ^4J = 2-3 Hz
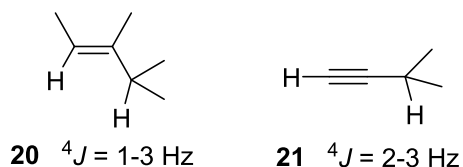
Figure 17. Long-range coupling constants in alkene (left) and alkyne (right) derivatives.

The most important coupling constants for conformational analysis are between protons J(H,H), but those between protons and carbons J(C,H) or between protons or carbons and other heteronuclei (^{19}F, ^{31}P) also provide useful information about the structure.

In this work, Karplus-like equations were used for conformational analysis of the ribose ring in locked nucleoside derivatives. It is based on the comparison between experimental and calculated J-couplings as described in detail in chapter 3.

1.2.3 Dynamic NMR spectroscopy

Dynamic processes such as conformational changes can be studied by dynamic NMR spectroscopy (dNMR). Atoms in different forms of a molecule (e.g. conformers) have different chemical shifts. Depending on the rate of interconversion between the individual forms, separated sets of signals for the individual forms or an averaged spectrum can be observed. Free energy barriers of the motional processes can be extracted from temperature-dependent NMR spectra. Using the dNMR method, the dynamic processes with the rate constant k between 10^{-1} and approximately 10^3 s^{-1} can be studied. As an example, dNMR method is frequently used to investigate tautomeric or conformational equilibria or to determine the barriers in compounds with sterically hindered rotation (e.g. atropisomers).

At lower temperature, the motional process is slowed down, which may lead in a two-state system, to observation of two sets of sharp signals corresponding to the two forms. When the temperature is increased, the exchange is faster and NMR signals are broader and closer to each other. At coalescence temperature T_c only one broad coalesced signal appears and further temperature increase leads to the single sharp signal in the spectrum.

The rate constant k_c at coalescence temperature T_c for two-site exchange can be estimated from equation:

$$k_c = \frac{\pi \Delta v}{\sqrt{2}} \approx 2.22 \Delta v$$

where $\Delta\nu$ is the difference of resonance frequency between the two signals in the absence of exchange. This value can be obtained from spectra recorded at temperatures, which are far below the coalescence temperature. This is a good approximation for estimating rate constant k_c, but it is valid only at single temperature (T_c) if the dynamic process follows the first-order kinetics, if the two singlets have equal intensities and if the studied nuclei are not coupled to each other.

For more complicated dynamic processes, a complete line-shape analysis must be done. After the measurement of ^{1}H NMR spectra at various temperatures, the shape of the signals is analyzed; simulated NMR spectra are calculated to fit the shape of experimental signals. From these simulations, the rate constant is extracted and used as an input for the Eyring equation.[53] The Eyring equation is an expression for the rate constant in the transition-state theory, from which we can calculate free energy barrier $\Delta G^{\ddagger}$ of the process.

$$k_{ex} = \frac{k_B T \kappa}{h} e^{-\frac{\Delta G^{\ddagger}}{RT}}$$

The transmission coefficient κ is set to unity, k_B is Boltzmann's constant, h is Planck's constant, R is universal gas constant and T is temperature.

The entropy of activation $\Delta S^{\ddagger}$ and enthalpy of activation $\Delta H^{\ddagger}$ can be obtained from Gibbs free energy of activation determined at various temperatures. To extract these thermodynamic quantities, the linear plot described by equation below is constructed. The enthalpy of activation $\Delta H^{\ddagger}$ is extracted from the slope of linear regression, whereas the entropy $\Delta S^{\ddagger}$ is obtained from the intercept.

$$ln\frac{k_{ex}}{T} = -\frac{\Delta H^{\ddagger}}{RT} + \frac{\Delta S^{\ddagger}}{R} + ln\frac{k_B}{h}$$

In this work, the experimental data obtained by the dNMR method were used for the determination of the rotational barriers in 5-nitrosopyrimidine derivatives, which were compared with the calculated values. These results are discussed in detail in chapter 5.

1.2.4 NMR spectroscopy in solid state

NMR spectroscopy in solid state (SS-NMR) is not as usually employed as the liquid-state technique, but it can provide useful information unavailable by NMR spectroscopy of solutions; for instance, describing polymorphic forms that is crucial in pharmaceutical industry. SS-NMR data are also very important in the crystal structure determination of compounds, for which single crystal for X-ray analysis was not obtained. The main difference between SS-NMR spectroscopy and NMR in liquid state is in the extensive averaging of various interactions in the liquid state caused by fast random motion of molecules; only the isotropic average of the interactions is observed in solution-state NMR spectra. In SS-NMR, these interactions are not averaged; for instance dipole-dipole, chemical shift anisotropy and quadrupolar

interactions can be observed in solid-state NMR spectra giving more information about the studied structure. NMR signals are, however, broadened by the anisotropic interactions, which complicates the interpretation of the spectra. It is possible to remove or at least suppress some of the mentioned interactions by MAS (see below) and high-power decoupling. The most suitable nuclei for NMR measurement in solids are those with one-half spin quantum number and with low natural abundance, where the homonuclear interactions are missing. Carbon nuclei ^{13}C perfectly fulfill these conditions and they are measured very often.

Nowadays, the most popular is cross-polarization magic-angle spinning (CP-MAS) NMR technique, where the cross-polarization from proton to carbon nuclei is used for sensitivity enhancement. Sample-spinning (rates 10–100 kHz) under the magic angle manages significant reducing of the line-broadening caused by anisotropic components of the NMR interactions. When the magic angle between rotation axis and external magnetic field B_0 is equal to 54.74°, the term $3cos^2\,\theta$ -1 occurring in equations describing the orientational dependence of NMR interactions is equal to zero. It leads to a suppression of the anisotropic interactions and the resulting NMR signals are significantly narrower.

With the development of DFT methods, which can complement the experimental data, SS-NMR spectroscopy opens new ways for studying various systems and gives rise to a novel method termed NMR crystallography, which has only recently come into common usage.

This method was performed in this thesis for the investigation of different polymorphic forms obtained by re-crystallization of the studied compounds from different solvents. These results are summarized in chapter 7.

1.2.5   NMR parameters calculations

In the last several decades, computational chemistry has become a very suitable tool to complement experimentally obtained NMR data or to predict reactivity or chemical properties of the studied compounds. The calculated NMR parameters and other physico-chemical quantities can effectively complement the data obtained from experimental NMR spectra.

In this work, I was using very common DFT (density functional theory) method for molecular modelling in almost all my projects. This method is based on the theorem that energy and properties of many-electron systems are uniquely determined by electron density $\rho(r)$; energy is a unique functional of electronic density. Becke's three-parameter hybrid functional (B3)[54] with the Lee-Yang-Parr (LYP)[55] correlation functional was used for all DFT calculations in this work.

First of all, the geometry of the studied molecule must be optimized; it means to find atom arrangement in space with the lowest energy (ground-state energy).[56] Usually, this procedure is done for a single molecule in vacuum; but in some cases, solvent influence must be taken into account. For this purpose, polarizable continuum model (PCM) of solvation is available for modelling solvent effects.

Calculations with PCM model usually simulates the structure and properties of the studied compound more realistically than vacuum calculations.

NMR parameters are frequently calculated using gauge-including-atomic-orbital (GIAO) method,[57] which provides chemical shielding constants of the studied nuclei. Indirect spin-spin interactions (*J*-couplings) are also routinely calculated by DFT methods.

Another important result in molecular modelling provides vibrational-frequency analysis. It can be used for confirmation that the optimized geometry is not a transition-state structure. Values of vibrational frequencies can be compared with the experimental infrared/Raman spectra. Furthermore, these data are also useful for calculations of thermodynamic parameters such as Gibbs energy, enthalpy or entropy.

Due to the geometry optimization and free electronic energy calculations, structures of conformers can be modelled and the energy differences can be used as input for the equilibrium constant calculation; the percentage of the individual conformers in solution can be predicted and it can be compared with the experimental data. Furthermore, geometry optimization of transition-state structures can provide free-energy barriers of chemical reactions or conformational changes. These predictions can support the kinetic data obtained from NMR measurements.

2 AIMS OF THE WORK

- ➲ The structure determination and conformational analysis of new potentially biologically active modified nucleic acid components.

- ➲ NMR methods development – a combination of experimental and theoretical approaches for a reliable signal assignment in purine derivatives and for the determination of the structure of preferred tautomeric forms in solution.

- ➲ The determination of intramolecular hydrogen-bond geometries and stabilities in 5-nitrosopyrimidine derivatives with two hydrogen-bond donors.

- ➲ The monitoring of the enzymatic decomposition of a prodrug of a biologically active locked carbocyclic nucleotide by ^{31}P NMR spectroscopy.

- ➲ The determination and characterization of polymorphic forms of model compounds (including modified nucleobase) by solid-state NMR spectroscopy.

- ➲ The structure determination of decomposition products of 5-aminopyrimidines stored in DMSO and the determination of the reaction mechanism.

3 STRUCTURE DETERMINATION – PAPERS I, II

The determination of the chemical structure during/after chemical synthesis is the first precondition for investigating biological and physico-chemical properties of newly prepared compounds. Nowadays, NMR spectroscopy is commonly used analytical method for the structure determination. The chemical structure of newly prepared compounds is often determined by a combination of 1D and 2D NMR experiments with mass spectrometry with high resolution (HR-MS). If necessary, the conformation of the studied compound may be also investigated by NMR spectroscopy. During my doctoral studies, I collaborated with synthetic chemists at the IOCB AS CR and determined or confirmed the structure of more than 700 compounds. In this chapter, as an example, NMR signal assignment and conformational analysis of conformationally constrained (locked) nucleosides with potential antivirotic activity will be described in detail.

3.1 NMR SIGNAL ASSIGNMENT

In this subsection, the NMR signal assignment of compound **22** (Fig. 18) will be discussed. This compound has been prepared by Michal Šála at the IOCB AS CR.
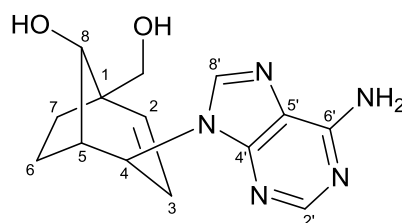
Figure 18. The chemical structure of compound **22** and the numbering.

^{1}H NMR spectrum of compound **22** with integrated signals is shown in Fig. 19. The integrals correspond to the number of protons in the molecule. The spectrum can be roughly divided into the aromatic region (around 8 ppm), double bond region (around 6 ppm) and aliphatic region (around 2 ppm). The signals of protons connected to a carbon neighboring with a heteroatom (CH_2OH) appear in the region between 3 and 5 ppm (heteroatomic region).
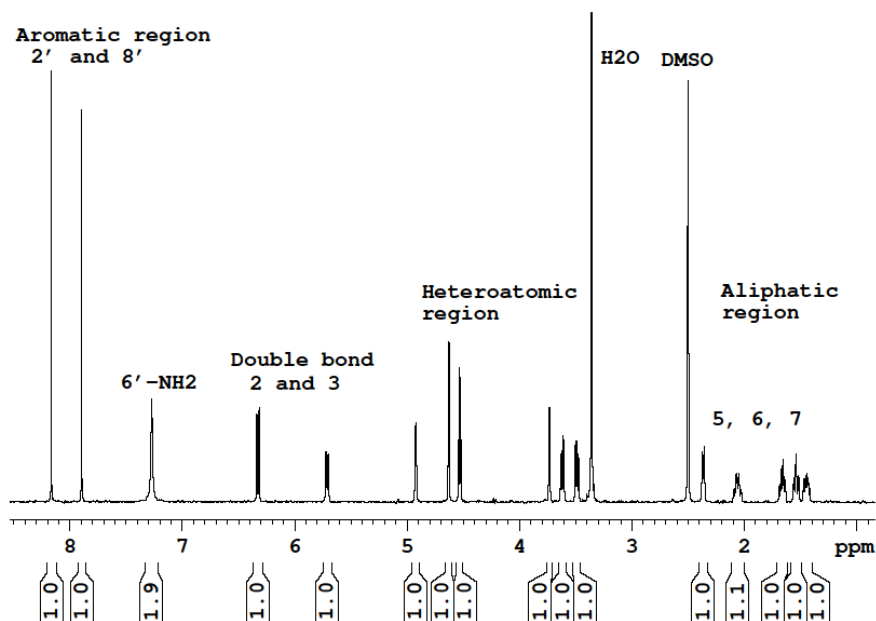
Figure 19. ^{1}H NMR spectrum of compound **22** measured in DMSO-d_6.

More information about the structure may be obtained from ^{13}C NMR spectra. As an example, ^{13}C APT spectrum of compound **22** is shown (Fig 20). In aromatic and double bond region (110–170 ppm), seven signals corresponding to five aromatic and two double-bond carbon atoms are present. Three upward oriented signals correspond to quaternary carbon atoms C4', C5'and C6' while four CH carbon signals come from C2', C8', C2 and C3. In the chemical-shift region of 40–80 ppm, there are signals corresponding to carbon atoms that are connected to a heteroatom (N, O) *via* one bond and bridgehead carbon atoms C1 and C5. The aliphatic region (20–40 ppm) contains signals of carbon atoms C6 and C7.
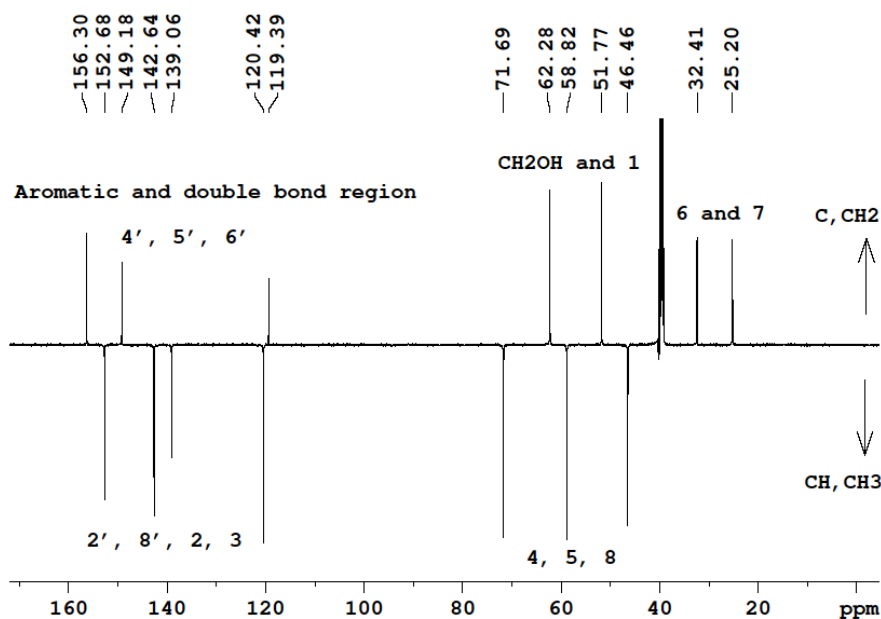
Figure 20. The ^{13}C APT spectrum of compound **22**. Carbon atom signals of CH_2 and quaternary carbons turn up, whereas CH and CH_3 signals turn down in this spectrum.

In ^{1}H,^{13}C-HMBC spectra, spin-spin interactions between protons and carbon atoms across two and three bonds are usually visible as crosspeaks. HMBC spectrum of compound **22** is depicted in Fig. 21 and four different parts (in color frames) of this spectrum are discussed below. For clarity, ^{1}H spectrum (x-axis) and ^{13}C APT spectrum (y-axis) were added.
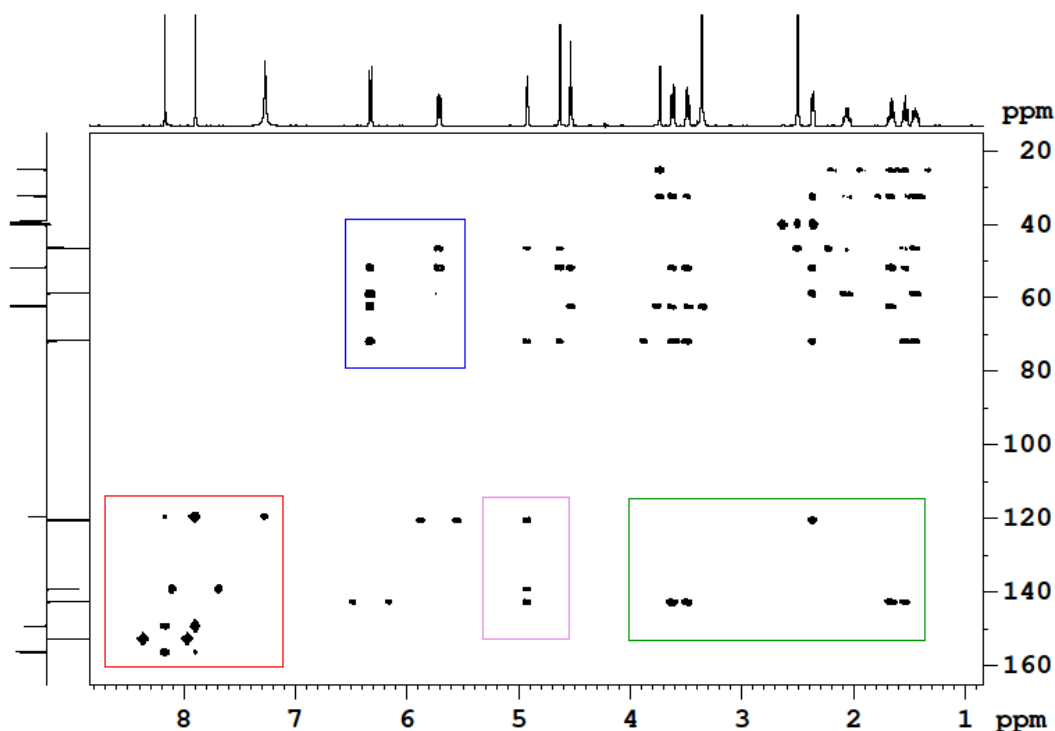
Figure 21. The ^{1}H,^{13}C-HMBC spectrum of compound **22** measured in DMSO-d_6.

The aromatic region of HMBC framed in red (expansion in Fig. 22) was used for NMR signal assignment of the purine skeleton of compound **22**. The 6'-NH$_2$ protons (7.27 ppm) have crosspeak (^3J-coupling) with C5' (119.4 ppm). It is known that ^3J(C,H) in aromatic systems are much larger than ^2J(C,H), therefore, ^2J(C6-NH$_2$) is not observed. Proton H2' has three-bond interactions with carbon atoms C4' and C6' and proton H8' has ^3J-coupling crosspeaks with carbon atoms C4' and C5'. By combination of this information, quaternary carbon atom signals were assigned as follows: C4' (149.2 ppm), C5' (119.4 ppm) and C6' (156.3 ppm).

In the same way, sp^2-hybridized carbon atoms of the double bond (C2 and C3) were assigned (green frame in HMBC in Fig. 21, expansion in Fig. 22). Carbon atom C2 (142.6 ppm) can have HMBC crosspeaks with protons around 1.5 ppm (H6 and H7 region) and CH$_2$OH protons (around 3.5 ppm), while carbon atom C3 (120.4 ppm) is too far away (more than three bonds) to have heteronuclear correlation with aliphatic protons H6 or H7.

The rest of the signals were assigned similarly, for instance, H4 proton correlations are shown in the pink expansion and double-bond proton correlations are shown in the blue expansion (Fig. 22).
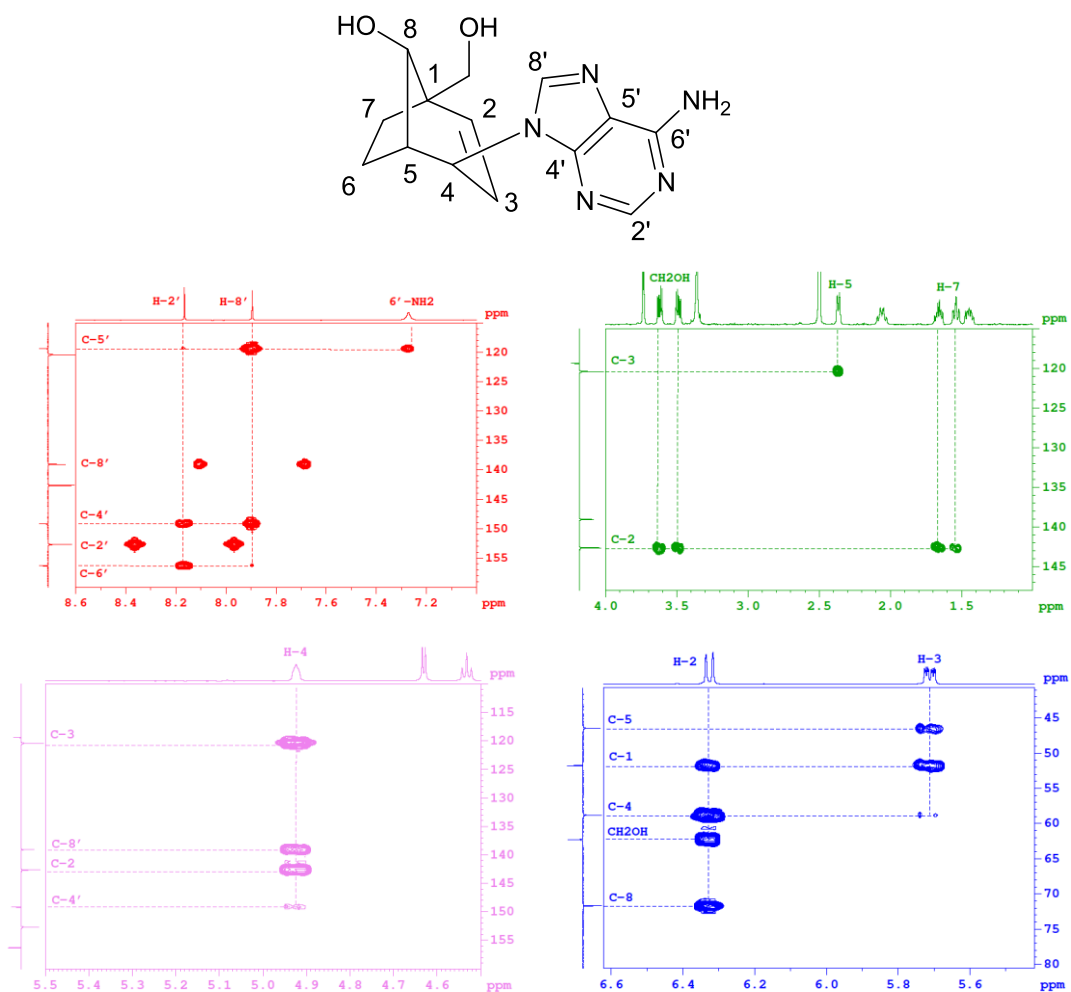
Figure 22. Parts of HMBC spectrum of compound **22**.

Most of the signals were assigned using ^{1}H,^{13}C-HMBC spectra as described above, but the rest of them (for instance H6, C6, C7 etc.) were assigned using ^{1}H,^{13}C-HSQC, where the crosspeaks correspond to one-bond proton-carbon interactions. The protons attached to a heteroatom (NH$_2$, OH) do not have crosspeaks in ^{1}H,^{13}C-HSQC as well as the quaternary carbon atoms (without any attached proton). From the aliphatic carbon atoms, only C1 (51.8 ppm) is quaternary, therefore, does not have a crosspeak in ^{1}H,^{13}C-HSQC (Fig. 23).
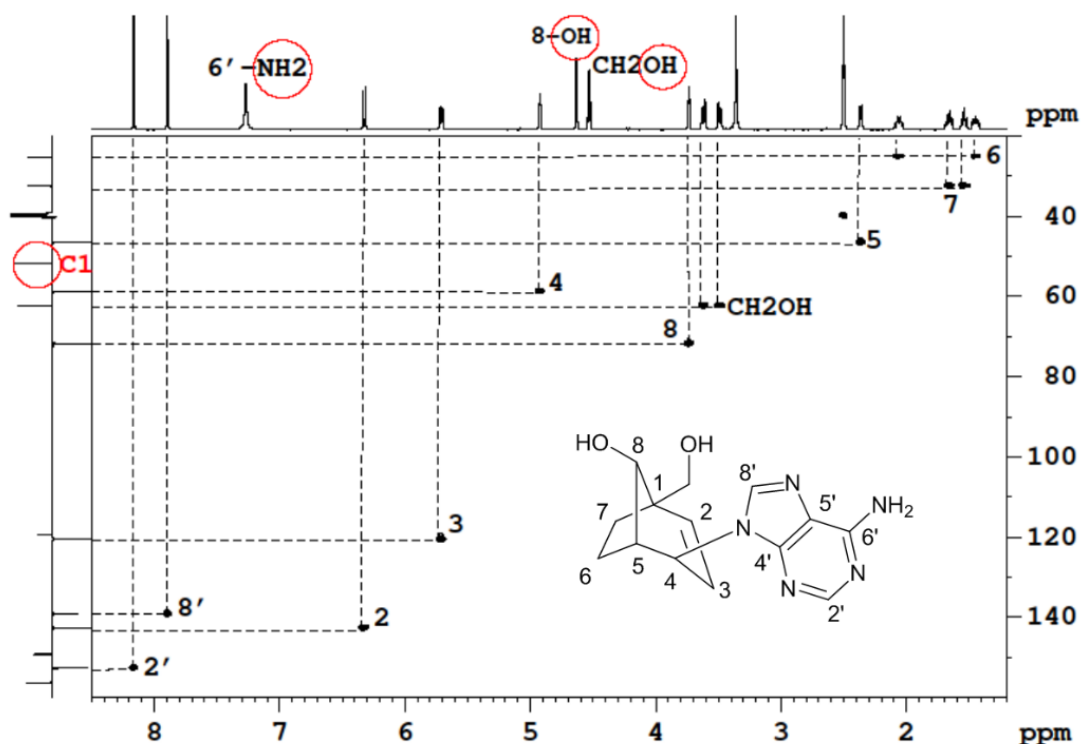
Figure 23. The ^{1}H,^{13}C-HSQC spectrum of compound **22**. The crosspeaks represent interaction between carbon atoms and the directly attached protons.

For determination of configuration at carbon atoms C4 and C8, two homonuclear 2D NMR spectra, COSY and ROESY, have been measured. As described previously, crosspeaks in ^{1}H,^{1}H-COSY spectra usually correspond to spin-spin interactions across two and three bonds. When the protons are in a W-like arrangement, it is possible to observe long-range couplings. Consequently, it was possible to confirm the stereochemistry at C8, because W-like long-range coupling between H8 and H7endo was found (Fig. 24 left). In the ROESY spectra, through-space interactions are observable. A ^{1}H,^{1}H-ROESY crosspeak corresponding to H8-H8' interaction (Fig. 24 right) confirmed the relative configuration at carbon atoms C8 and C4. Furthermore, crosspeaks corresponding to H4-H6endo and 8OH-H7exo were found in ^{1}H,^{1}H-ROESY, which further confirmed the stereochemical assignment at C4 and C8.
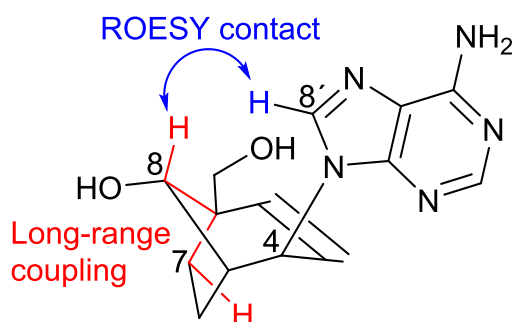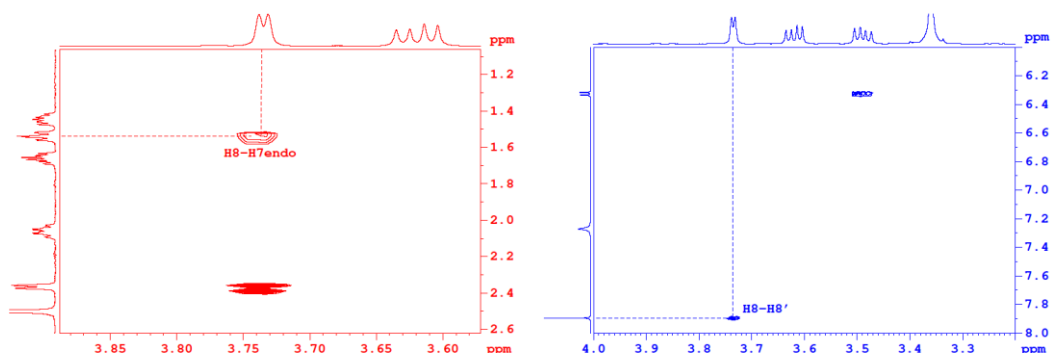
Figure 24. A part of the ^{1}H,^{1}H-COSY (in red) and ^{1}H,^{1}H-ROESY (in blue) spectra of compound **22**. The W-like shaped long-range interaction between H8 and H7-*endo* has clearly confirmed the configuration at carbon C8. The through-space interaction H8-H8' has confirmed the configuration at carbon atom C4.

Further confirmation of the stereochemical signal assignment of protons comes from analysis of *J*-couplings observable in ^{1}H NMR spectrum. The values of *J*-couplings significantly depend on the geometry of the molecule. From Karplus equation we can say that ca 90° torsion angle between two protons causes very low interaction between them and low (or zero) values of *J*-couplings are observed. For example, protons H5 and H8 have the torsion angle close to 90° and, therefore, no signal splitting due to the coupling between H5 and H8 was observed, see Table I for the most important vicinal proton-proton couplings in compound **22** and corresponding torsion angles $\varPhi$.
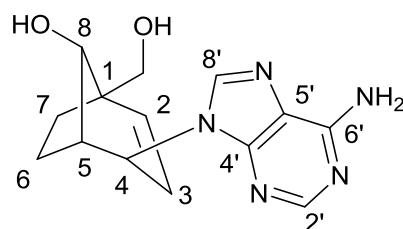
Table I. The experimental and calculated coupling constants (*J*-couplings) of compound **22** and corresponding calculated torsion angles $\varPhi$ (B3LYP/6-31+g(d,p)).

Interaction	$J_{\text{experiment}}$ (Hz)	$J_{\text{calculated}}$ (Hz)	$\varPhi_{\text{calculated}}$ (°)
H2-H3	9.5	9.3	0.2
H3-H4	3.9	4.1	-59.7
H4-H5	-	2.5	78.2
H5-H8	-	1.0	75.3
H5-H6ex	7.9	7.9	24.3
H5-H6en	-	0.7	-93.4
H6ex-H7en	2.4	2.3	-113.4
H6ex-H7ex	10.5	10.8	6.3
H6en-H7en	9.2	9.6	5.0
H6en-H7ex	6.2	4.8	124.6

The chemical structure and configuration of compound **22** determined by combination of 1D and 2D NMR spectra was complemented by DFT calculations. First, the geometry optimization was done to find the most stable conformer (Fig. 25). The interatomic distances were obtained to confirm that these interactions can be visible in the ROESY spectra. The H8-H8', H4-H6en and H7ex-8OH atom distances are around 2.5 Å and crosspeaks corresponding to the correlations between these atoms were successfully found in ROESY spectrum as described above. *J*-couplings calculated for the optimized structure are in very good agreement with measured values (Table I), which supported the results obtained from the NMR experiments.
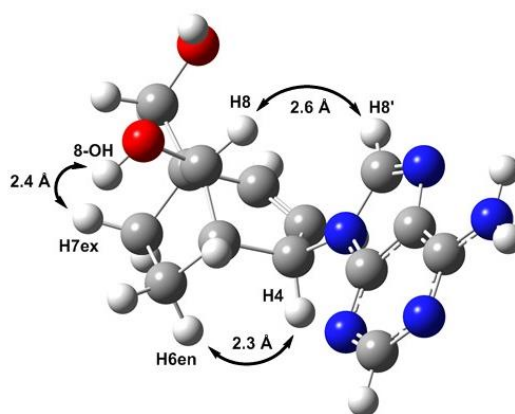
Figure 25. The optimized geometry of compound **22** obtained by DFT calculations (B3LYP/6-31+g(d,p)).

3.2 CONFORMATIONAL ANALYSIS

The ribose ring of naturally occurring nucleosides is flexible and may coexist in several conformations in solution. The conformation of these molecules can be studied by NMR spectroscopy. In some cases, a deeper insight into the conformation may be obtained by complementing experimental NMR data with DFT calculations. Covalent modifications of nucleosides may lead to locked nucleoside derivatives with reduced flexibility of the monosacharide ring. Conformationally restricted (locked) nucleosides have been synthetized as potential antivirotic agents. In this chapter, as an example, a conformational analysis of compound **23** (Fig. 26) will be discussed.
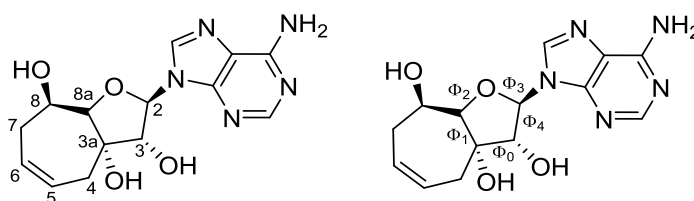
Figure 26. The chemical structure of compound **23** and the numbering of pseudosugar part of the molecule (left). Torsion (dihedral) angles Φ_0-Φ_4 (right).

Due to the presence of the seven-membered ring in compound **23** (prepared by Hubert Hřebabecký at the IOCB AS CR), the conformation of furanose ring is partially locked. Experimental *J*-coupling values obtained from ^{1}H NMR spectrum were compared with values calculated by two different approaches. First, the geometry of compound **23** was optimized at DFT level starting from four initial conformations with phase angles P = 0°, 90°, 180° and 270° and with maximum puckering amplitude Φ_{MAX} = 40°. After geometry optimization of all four initial geometries, only one conformer was found with torsion angles Φ_0-Φ_4: -30.8°, 20.5°, -0.8°, -19.5° and 31.5°, respectively. The obtained torsion angles were used as input for *J*-couplings calculated by empirical Haasnoot-Altona equation (J_{ALTONA} in Table II), which describes the dependence of the vicinal *J*-coupling values on the torsion angle between the coupled nuclei. *J*-couplings were also calculated by DFT method (J_{DFT} in Table II). Both theoretical approaches provided similar values, which fit well with the experimentally obtained *J*-couplings ($J_{EXPERIMENT}$ in Table II). From the obtained torsion angles, we can conclude that compound **23** is present in solution in South conformation (^{2}E) with phase angle P = 163° (Fig. 28).

Table II. Comparison of calculated coupling constants (*J*) of compound **23** by Haasnoot-Altona equation[52] and DFT method (B3LYP/6-31g (d)) with experimentally obtained values.

Interaction	J_{ALTONA} (Hz)	J_{DFT} (Hz)	$J_{EXPERIMENT}$ (Hz)
H2-H3	7.2	5.6	8.1
H8-H8a	1.3	1.0	1.6
H8-H7exo	2.0	2.0	1.7
H8-H7endo	5.0	4.9	4.3
H4exo-H5	-*	4.2	4.4

* Undefined for sp^2 hybridized carbon atoms (H5).
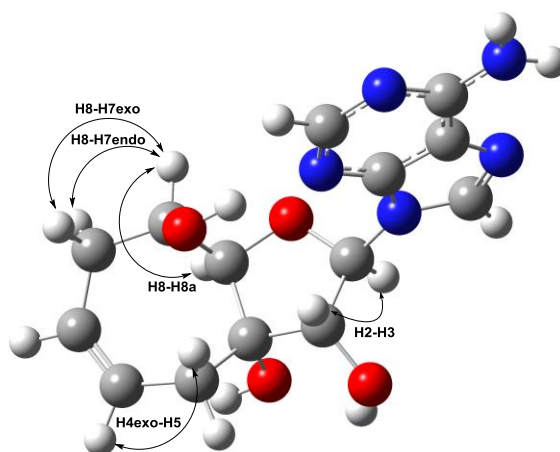
Figure 27. Optimized geometry of compound **23** (B3LYP/6-31+g(d,p)) and the spin-spin interactions described in the Table II.

The geometry optimization also showed that the adenine part of the molecule is oriented *syn* with respect to the ribose residue. The free-energy

difference between *syn-* and *anti-* conformation was calculated to be 5.4 kcal/mol. Only the *syn-* conformer was, therefore, used for *J*-coupling calculations.
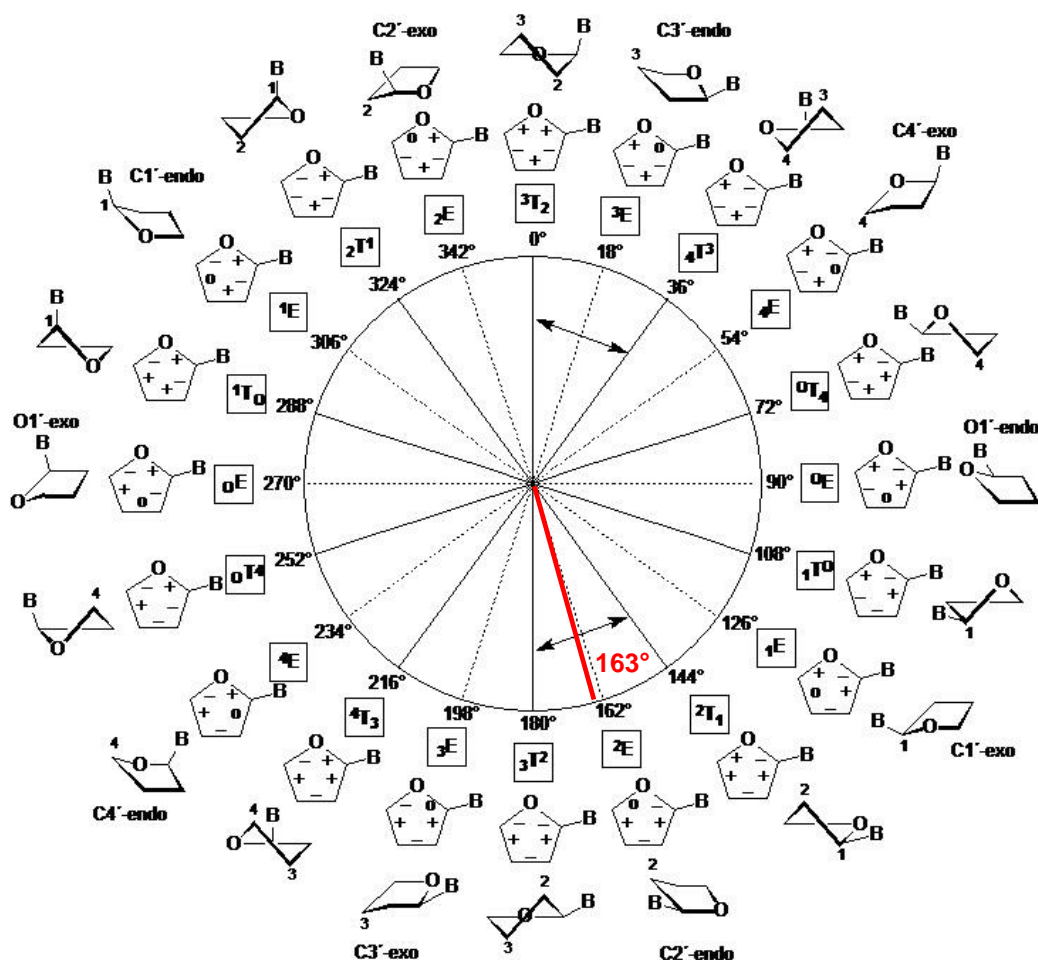
Figure 28. Pseudorotation cycle of a furanose ring. The determined South conformation of compound **23** with phase angle *P* = 163° (in red).

3.3 SUMMARY

In this chapter, the structure determination of compound **22** solved using a combination of 1D and 2D NMR spectra was shown. The configuration of compound **22** was investigated by a combination of experimentally obtained data (homonuclear 2D spectra COSY and ROESY) and DFT calculations of *J*-couplings. Both approaches provided the same geometry of compound **22**. The conformation of modified ribose ring in compound **23** was studied employing Altona-Sundaralingam formalism[39], which describes the ribose ring geometry by phase angle and maximum puckering amplitude. In compound **23**, the phase angle *P* = 163° and maximum puckering amplitude Φ_{MAX} = 32.9° were found. Compound **23** is present in solution in the South conformation ^{2}E.

4 NMR METHODS DEVELOPMENT – PAPERS III, IV

This chapter describes the results of two independent studies, which focused on the development of NMR methods for accurate signal assignment and the determination of the preferred tautomeric forms of purine derivatives in solution. At the beginning of every NMR study, all signals are assigned by commonly-used NMR techniques described in Chapter 3. For ^{13}C NMR signal assignment of purine derivatives, the three-bond heteronuclear couplings visible in ^{1}H,^{13}C-HMBC spectra as high-intensive crosspeaks are commonly used (Fig. 29 left). Simultaneously, there are sometimes two crosspeaks with lower intensity corresponding to the four- and five-bond coupling constants (long-range coupling constants) H8-C6 and H8-C2, respectively, (Fig. 29 right). From ^{1}H,^{13}C-HMBC spectrum, one can only qualitatively estimate J-couplings from crosspeak intensities, but it is generally expected that the four-bond H8-C6 crosspeak is always stronger than the five-bond one, meaning the four-bond coupling constant (^4J) is larger than the five-bond one (^5J). If the purine skeleton is substituted in both positions 2 and 6, C2 and C6 ^{13}C NMR signals are assigned using these heteronuclear long-range coupling constants ^4J and ^5J. We decided to investigate whether we can rely on the fact that ^5J is always lower than ^4J. The heteronuclear long-range coupling constants in a series of model compounds were estimated from the intensities of the corresponding HMBC crosspeaks or measured directly in proton-coupled ^{13}C NMR spectra. The obtained values were compared with DFT calculated data.
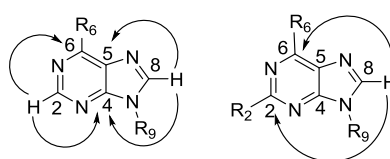
Figure 29. A schematic representation of heteronuclear H-C spin-spin interactions. Three-bond correlations (left) are commonly visible in HMBC, long-range couplings (right) are visible in HMBC as the crosspeaks with lower intensity.

^{13}C and ^{15}N NMR chemical shifts as well as ^{1}H-X coupling constants can be used not only to distinguish between different regioisomers, but also reflect equally well the positions of protons, which enables to study tautomeric equilibria. In the second study, experimental chemical shifts of a series of purine derivatives were complemented with DFT calculations. The comparison of the experimental and calculated data allowed to reveal the preferred tautomeric forms of the studied compounds.

4.1 STUDY OF HETERONUCLEAR LONG-RANGE COUPLING CONSTANTS

Heteronuclear (H,C) long-range coupling constants were studied on ten purine derivatives substituted with various substituents in positions 2 and 6. The studied compounds (Fig. 30.) have been prepared at the IOCB AS CR by Lucie Čechová and Petr Jansa. Measured coupling constants were compared to DFT calculated data (B3LYP/6-311++G(d,p)). For simplicity of the DFT calculations, the benzyl group was replaced by a methyl group and it was confirmed by a control calculation that this change caused only minor differences in the calculated coupling constants.

	R_2	R_6			R_2	R_6
24	NH_2	Cl		29	Cl	Cl
25	Cl	Cl		30	NH_2	Cl
26	H	Cl		31	OH	OH
27	NH_2	$NHCH_3$		32	Cl	OCH_3
28	NH_2	OH		33	Cl	NBu_2
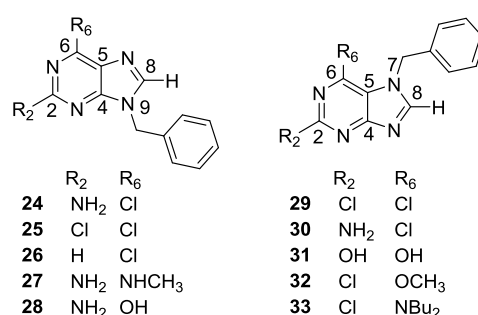
Figure 30. The chemical structure of studied compounds and their numbering. In compounds **28** and **31**, keto forms were used in DFT calculations.

The relative intensity of HMBC crosspeaks reflects, in general, the values of heteronuclear ([1]H-^{13}C) coupling constants. The observation of very small coupling constants J(C,H) depends on the match between the coupling constant and the experimental delay of the anti-phase evolution (1/2 J). For heteronuclear couplings lower than 1 Hz, the evolution delay should be larger than 500 ms, which leads, however, to a strong signal suppression by relaxation. After evolution delay optimization, the 50-ms delay was set for HMBC experiments in this study. Using this setup, the intensity of crosspeaks in HMBC spectra is mainly governed by the value of the J-coupling. The H8 regions of HMBC spectra of compounds **24–33** depicted in Fig. 30. show that the H8-C2 crosspeak can be more intensive than H8-C6 (compound **24**), equally intensive (compound **30**), less intensive (compound **27**) or it can be missing completely in the HMBC spectrum (compound **28**). It means that there are significant differences between long-range coupling constants in the differently substituted purines. To corroborate this finding, long-range coupling constants were calculated using DFT method. Calculated long-range coupling constants of compounds **24**, **27**, **28**, **30** (Table III) are in agreement with the findings obtained from HMBC spectra. For instance, in compound **24**, the calculated $^5J = 0.61$ Hz is higher than $^4J = 0.32$ Hz. It corresponds to the observation that the H8-C2 crosspeak in HMBC is stronger than the four-bond one (H8-C6). In the case of compound **30**, the calculated long-range coupling constants are close to each other

^5J = 0.75 Hz, ^4J = 0.79 Hz, corresponding to similar intensities of the crosspeaks in HMBC spectra.
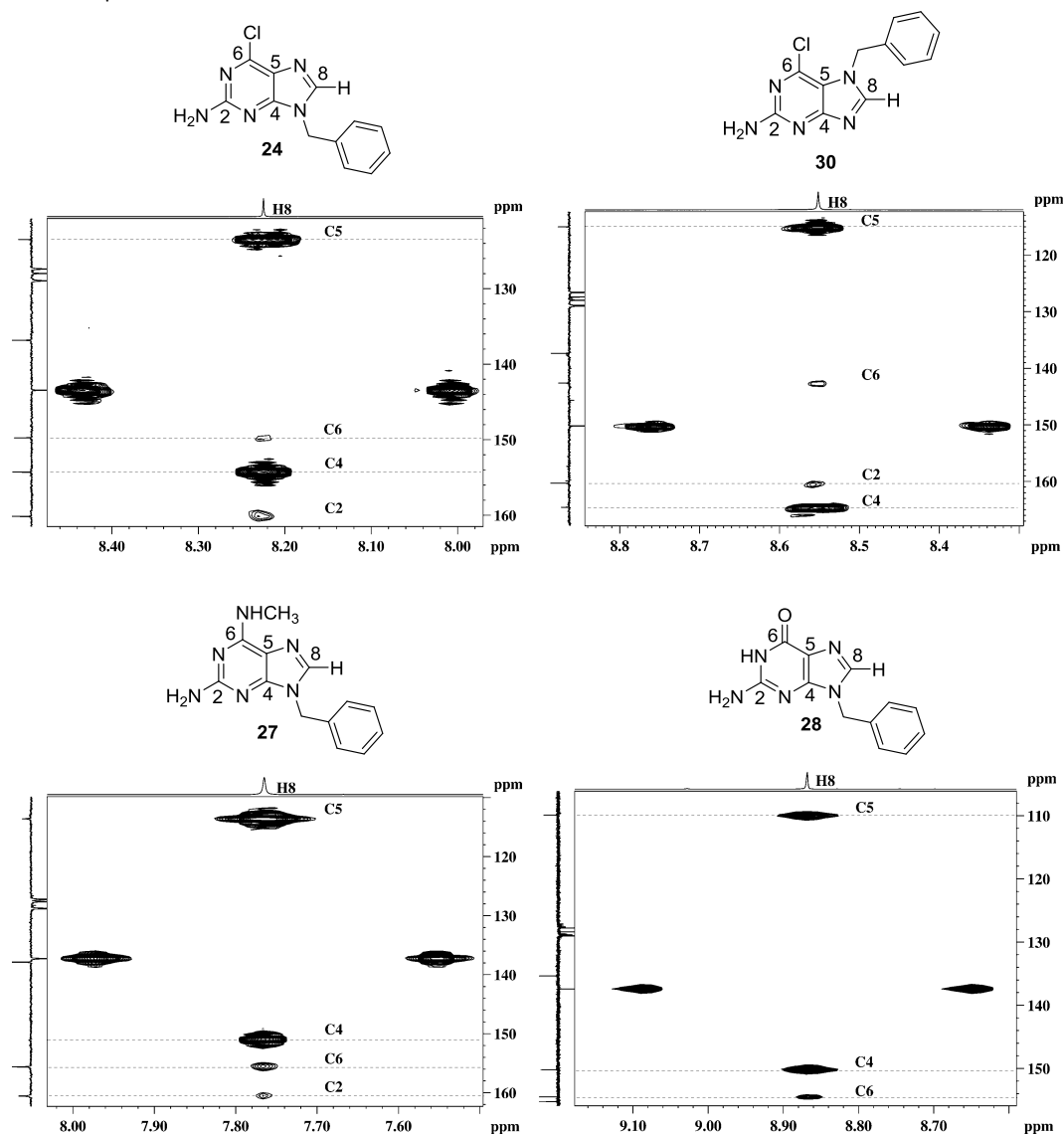
Figure 31. The H-8 region of the HMBC spectra of selected compounds. There are significant differences between the intensity of crosspeak H8-C2 and H8-C6. The H8-C6 crosspeak (^4J) is not always stronger than the H8-C2 (^5J).

Table III. The calculated five-bond ($^5J_{H8-C2}$) and four-bond ($^4J_{H8-C6}$) coupling constants of the selected compounds (B3LYP/6-311++g(d,p)).

Compound	$^5J_{H8-C2}$ (Hz)	$^4J_{H8-C6}$ (Hz)
24	0.61	0.32
30	0.75	0.79
27	0.56	0.66
28	0.34	0.92

The exact values of heteronuclear coupling constants can be obtained from the line splitting of proton-coupled ^{13}C NMR spectra. During this measurement, proton decoupling is on during relaxation delay to evolve NOE and switched of

during data acquisition. Split signals are less intensive than singlets obtained from ^{13}C NMR spectra acquired with proton decoupling. It leads to lower signal-to-noise ratio. Acquisition times must be longer as well as number of scans must be higher to obtain high-quality NMR spectrum. With respect to these facts, hydrogen-coupled ^{13}C NMR experiments are time-consuming and suitable only for high-concentrated samples or ^{13}C enriched compounds. As an example, a part of ^{13}C NMR spectra of compound **28** is shown in Fig. 32. The ^{13}C NMR spectrum with selective decoupling of H8 (Fig. 32) was measured to confirm that the line-splitting is really caused by the interaction of C2 and C6, respectively, with H8 atom.

The experimental values of heteronuclear *J*-couplings were compared with the calculated ones (Table IV) and they are in good agreement.
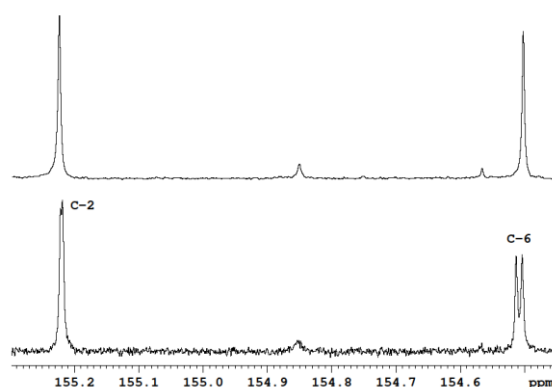
Table IV. Comparison of the experimental and calculated heteronuclear *J*-couplings.

Interaction	Experiment	Calculated
H8-C2	0.4	0.34
H8-C6	1.2	0.92

Figure 32. A part of hydrogen-coupled ^{13}C NMR spectrum (bottom) and ^{13}C NMR spectrum with selective H8 decoupling (top) of compound **28**.

The calculated values of H8-C2 (^5J) coupling constant depend significantly on the nature of the substituent in the position 2. The following order of the coupling values depending on the C2 substituent was observed: H < Cl < NH$_2$. Slightly different behavior was observed in guanine, hypoxanthine and xanthine (keto form in position C6), where very low H8-C2 coupling constants were found. Also the H8-C6 couplings (^4J) are primarily influenced by the nature of the C6 substituent. In keto forms of guanine, hypoxanthine and xanthine derivatives, the highest values of the coupling constants were found. Furthermore, in 7-methyl isomers, the long-range coupling constants, ^4J as well as ^5J, were higher than in the case of 9-methylisomers.

Based on these findings, it was shown that we cannot say that the four-bond coupling constant ^4J is always higher than the five-bond one (^5J). Depending on the substituents attached to the purine skeleton, the values of the coupling constants can change significantly. During the NMR signal assignment of purine derivatives one must keep in mind this fact, otherwise the signals could be incorrectly assigned.

4.2 METHOD FOR PREDICTION OF TAUTOMERIC FORMS

The tautomeric forms of purine derivatives were studied on a series of twenty four 6-substituted purines (Fig. 33) prepared by Michal Šála and Radim Nencka at the IOCB AS CR.
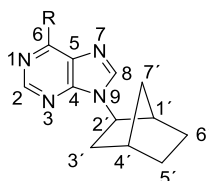
Figure 33. The general formula of the studied purine derivatives and the numbering. R = H, Cl, F, Br, CH_3, CF_3, OCH_3, SCH_3, CN, $COOCH_3$, $CONH_2$, OH, SH, NH_2, N_3, $N(CH_3)_2$, Ph, p-PhCl, p-PhF, p-PhtBu, p-PhPh, p-PhCN, p-PhOCH$_3$, p-PhNPh$_2$.

After NMR signal assignment, the shielding constants σ for every atom on the purine skeleton were calculated using a DFT method. For simplicity of the DFT calculations, the rigid bicycloheptane part of the molecule was replaced by a methyl group. The geometry optimizations and shielding constants calculations were performed in vacuum as well as with implicit solvent model (PCM) of DMSO solvation. For every atom in the purine skeleton of purine derivatives with one possible tautomeric form only, the correlation between experimentally obtained chemical shifts δ and calculated shielding constants σ was ploted. The correlations for carbon atoms as well as for nitrogen atoms (except carbon atom C6 and nitrogen atom N7 calculated in vacuum) fit well to a straight line ($R^2 > 0.96$); as an example, the correlation of the carbon atom C4 and the nitrogen atom N1 are shown in Fig. 34.
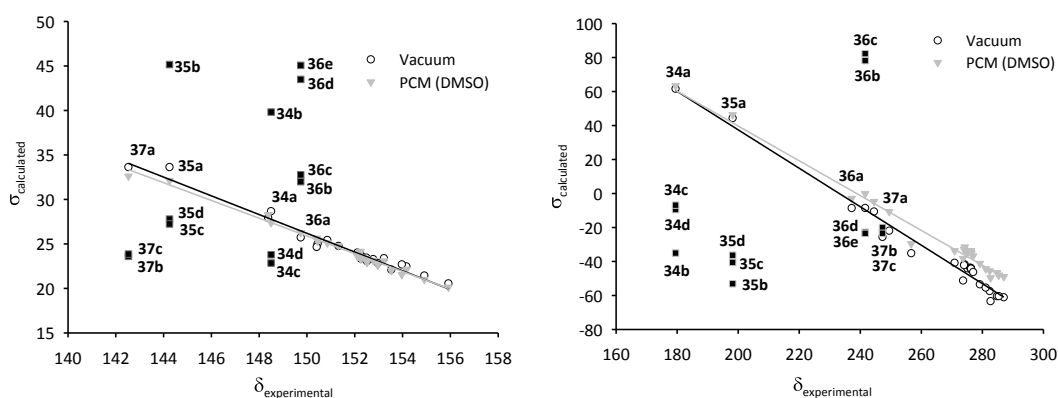
Figure 34. The correlation between the calculated shielding constants σ and the measured chemical shifts δ of the carbon atom C4 (left) and the nitrogen atom N1 (right). The black squares represent the tautomers/rotamers, which are not present in DMSO solution.

The poor correlation of nitrogen N7 shieldings ($R^2 = 0.37$) calculated in vacuum (Fig. 35) might be explained by stronger influence of solvation on the

electronic structure near the N7 atom and the vicinity of the substituents at C6. The largest deviations from the linear correlation for the carbon atom C6 were observed for substituents with heavy atoms (Cl, Br, S). It could be explained by relativistic effects contributing to the shielding of this carbon atom. The correlation for protons was rather modest (e.g. $R^2 = 0.35$ for H8 in vacuum) that could be caused by the inaccuracy of DFT calculations when neglecting vibrational averaging and interactions with explicit solvent molecules. Furthermore, in the small range of ^{1}H shifts, the same error causes larger relative error than in the case of carbon atoms or nitrogen atoms, respectively.
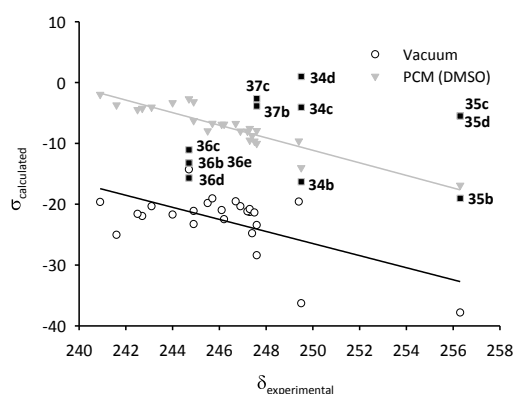
Figure 35. The correlation between the calculated shielding constants σ and the measured chemical shifts δ of the nitrogen atom N7. The black squares represent the tautomers/rotamers, which are not present in DMSO solution.

In compounds **34–36**, several tautomeric forms can exist in solution. Hypoxanthine derivative **34** and mercaptopurine derivative **35** can exist in four tautomer/rotamer forms (keto/enol tautomers) **34a–34d** and **35a–35d**, respectively (Fig. 36). The adenine derivative **36** can exist in five tautomer/rotamer forms **36a–36e** (Fig. 37). It has been determined previously that the keto form **34a**,[33,34] the thione form **35a**[58] and the amino form **36a**[59,60] are preferred in solution. These derivatives were used to validate the new method for prediction of the preferred tautomeric forms in purines. It is clear that only "**a**" forms fit well with the correlations (Fig. 34 and 35), meaning that these "**a**" forms are present in solution, whereas the other tautomer/rotamer forms **34b–34d**, **35b–35d** and **36b–36e** are far from the linear correlation, so these forms are not present or their relative concentration is low.
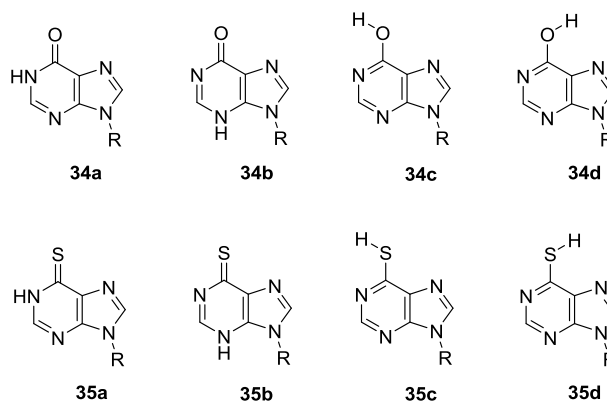
Figure 36. Possible tautomer/rotamer forms of compounds **34** and **35**.
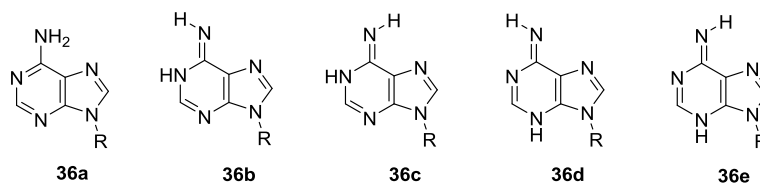
Figure 37. Possible tautomer/rotamer forms of compound **36**.

6-Azidopurine derivatives can exist in equilibrium between tetrazole **37a** and azido-azomethine forms **37b** and **37c** (Fig. 38) depending on external conditions like solvent or on different nature of the substituents.[61,62] It has been published that in polar solvents the equilibrium is shifted toward the tetrazole form.[63] According to the crystallographic data, 6-azidopurine exists in solid state as a pure tetrazole form.[64] The DFT calculations in vacuum show that the most stable form of compound **37** is azido-azomethine **37b**. In DMSO, the electronic energies of tetrazole form **37a** and azido-azomethine form **37b** are close to each other. From the shielding-shift correlations, it is evident that both azido-azomethine forms **37b** and **37c** are very far from the linear correlation (see e.g. carbon C4 in Fig. 34 left). It is clear that the tetrazole form **37a** is highly predominant in the DMSO solution.
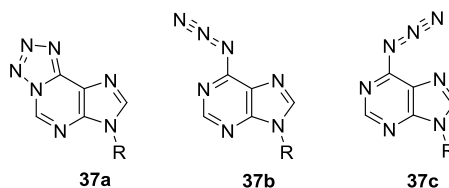
Figure 38. Possible forms of azidopurine **37**.

4.3 SUMMARY

In this work, two new NMR methods based on the combination of experimental and theoretical approaches relating to the purine derivatives were developed.

The first method employs heteronuclear long-range coupling constants across four and five bonds (^4J and ^5J, respectively) of the hydrogen atom H8 with carbon atoms C2 and C6 to assign the NMR signals correctly. Depending on the substituents attached to the purine skeleton, the values of the coupling constants can change significantly. We must take into account that five-bond coupling constant can be higher (and HMBC crosspeak more intensive) than the four-bond one ($^5J > ^4J$) and use the comparison of DFT-calculated and experimental ^4J and ^5J values for structural assignment of carbon atoms C2 and C6.

The second method is focused on the determination of preferred tautomeric forms in purine derivatives dissolved in DMSO using correlation between the experimental chemical shifts and the calculated shielding constants. The correlations constructed for every atom of purine skeleton were linear and the "**a**" forms of compounds **34–37** (Fig. 39) fit well with the correlation, whereas data for other tautomeric forms are far from the linear correlation.

34a   **35a**   **36a**   **37a**
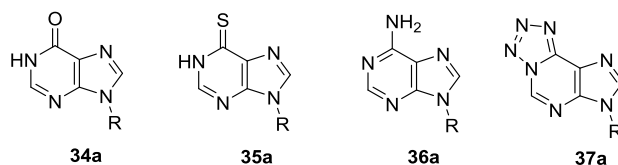
Figure 39. The preferred tautomeric forms determined by the correlation between experimental chemical shifts and the calculated shielding constants.

5 Hydrogen bonds in polysubstituted 5-nitroso-pyrimidines — papers V, VI

5-Nitrosopyrimidines are not naturally occurring but they display a wide range of biological effects such as cytostatic,[65,66] antifungal[67] or antimicrobial.[68] The nitroso group can form intramolecular hydrogen bonds (H-bonds) with suitable H-bond donors in the neighboring positions e.g. amino groups. In this arrangement, the shape of 5-nitrosopyrimidines is similar to purine derivatives and they might work as purine mimics. When two H-bond donors are attached to both carbon atoms in the neighboring positions, two H-bonds can be formed differing in the orientation of the nitroso group. Therefore, these molecules mimic two different purine derivatives and might be substrates for enzymes of two metabolic pathways.

We studied structure and physico-chemical properties of the rotamers of polysubstituted 5-nitrosopyrimidines with strong intramolecular H-bonds. The rotamers have different properties, for instance, we observed them as two sets of signals in NMR spectra (^{1}H, ^{13}C) in equilibrium mixture. We determined NMR parameters of both rotamers. Next, the substituent effects on the rotamer ratio in solution was studied as well as temperature dependence of ^{1}H NMR spectra that allowed us to determine the rotational barrier of the nitroso group. Electronic effects of substituents were also studied using UV/Vis spectrometry. In some cases, the rotamer separation was possible, so we determined the chemical structure of both rotamers in solid state using solid-state NMR spectroscopy and these data were confirmed by X-ray analysis. We also measured kinetics of rotamer interconversion using ^{1}H NMR spectroscopy and kinetic data are at disposal. The experimental data were supported by DFT calculations which fit well with our observations.

5.1 5-nitrosopyrimidines substituted with aromatic amines

For this work, a series of 5-nitrosopyrimidine derivatives with strong intramolecular H-bonds has been prepared (Fig. 40) by Lucie Čechová at the IOCB AS CR using a new microwave-assisted synthesis.[69] The first class of compounds with methoxy group in the position 4 and NH-aryl substituent in the position 6 on the pyrimidine skeleton (**38a**–**38i**) can form only one H-bond, whereas the second class of compounds with the amino substituents in both positions 4 and 6 could form two H-bonds. Due to the two possible H-bonds, the two conformers differing only in the

nitroso group orientation (rotamers) were observed in the NMR spectra as two sets of signals.
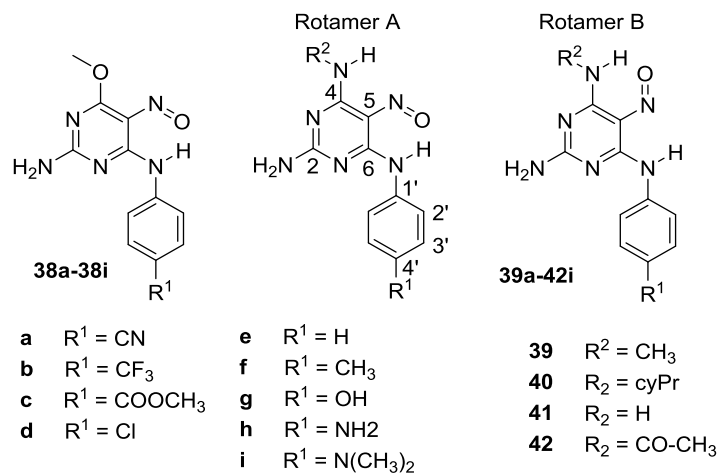
Figure 40. The structure of studied compounds.

5.1.1 NMR signal assignment

For the NMR signal assignment, ^{1}H, ^{13}C and 2D NMR spectra (HSQC, HMBC) were measured. Here, I would like to show the NMR signals assignment for compound **38e** as an example. Compound **38e** belongs to the first class of compounds, where only one H-bond can be formed, so only one conformer is stable and one set of signals was found in the spectra. From the chemical shifts, integration and multiplet analysis, the proton NMR signal assignment is clear (Fig. 41). The signal with the highest chemical shift above 13 ppm corresponds to the NH proton involved in the H-bond. The signals in the aromatic region (7–8 ppm) correspond to the phenyl residue. And the most shielded protons in methoxy group have NMR signal around 4 ppm.
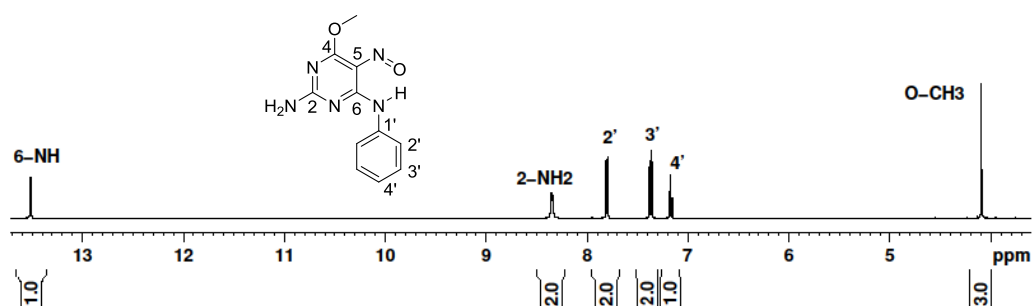
Figure 41. ^{1}H NMR spectrum of compound **38e** with signal assignment.

Next, the ^{13}C APT NMR spectrum was recorded. To assign all ^{13}C NMR signals, it was necessary to use 2D NMR spectra. One-bond C-H interactions are visible in HSQC spectrum as crosspeaks, see Fig. 42.
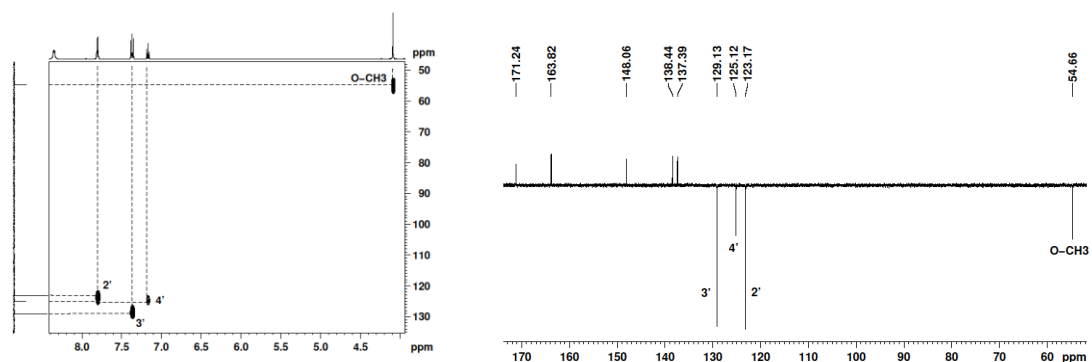
Figure 42. The ^{1}H,^{13}C-HSQC spectrum of compound **38e** (left) and assigned CH carbon atom signals in ^{13}C APT spectrum (right).

The last signals belonging to aromatic quaternary carbon atoms were assigned using ^{1}H,^{13}C-HMBC spectrum, where the crosspeaks correspond to the heteronuclear C-H multiple bond. In the HMBC spectrum of compound **38e**, strong H3'-C1', 6NH-C5 and CH$_3$-C4 crosspeaks were found and they determined chemical shifts of carbon atoms C1' (137.4 ppm), C4 (171.2 ppm) and C5 (138.4 ppm). In the case of W-like path between the nuclei, the four-bond (long-range) C-H interactions are usually visible as crosspeaks, but with weaker intensity. In this way, the carbon atom signals C2, C4 and C6 were assigned, see Fig. 43.
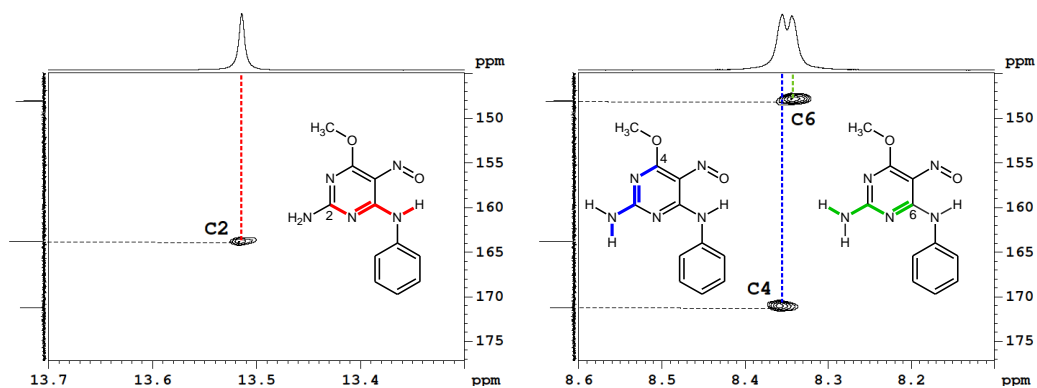
Figure 43. The ^{1}H,^{13}C-HMBC correlations of compound **38e** with the W-like arrangement between the aniline NH protons and C2 (left) and between the 2-amino protons and C4/C6 (right).

Using these 2D NMR spectra (HSQC and HMBC), it was possible to assign all NMR signals in ^{13}C NMR spectrum of compound **38e**, see Fig. 44. NMR signals of other studied compounds were assigned in the same way.
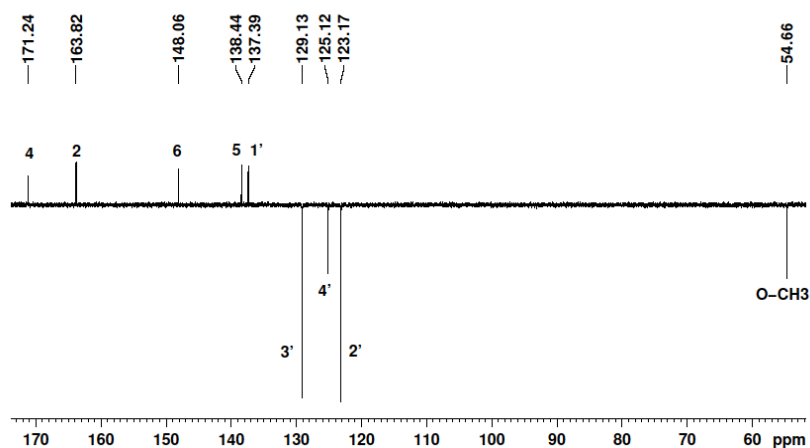
Figure 44. Complete ^{13}C NMR signal assignment of compound **38e**.

Usually, the stronger the hydrogen bond is, the higher chemical shift of proton involved in the H-bond is observed. Furthermore, electron-withdrawing substituents decrease the electron density in the studied molecule leading to smaller shieldings (higher chemical shifts). We observed an unexpected dependence of 6-NH chemical shifts on the *para*-substituents R^1. We found that in compounds with electron-donating substituents R^1 (with negative Hammett constants σ_P), the 6-NH chemical shift is slightly higher (Table V). As an explanation, in this type of molecules with a conjugated π-system, the electronic effects of the *para*-substituent R^1 are spread throughout the molecule. Electron-donating substituents increase the electron density also at the nitroso oxygen atom, which makes it a better H-bond acceptor.

Table V. The experimental chemical shifts of the 6-NH proton in compounds **38a–38i** in comparison to their electronic effects expressed by substituent Hammett constants σ_P.

Compound	*Para*-substituent R^1	Hammett constant σ_P [70]	Chemical shift δ_{NH} (ppm)
38a	CN	0.70	13.45
38b	CF$_3$	0.53	13.47
38c	COOCH$_3$	0.44	13.53
38d	Cl	0.24	13.46
38e	H	0	13.51
38f	CH$_3$	-0.14	13.52
38g	OH	-0.38	13.54
38h	NH$_2$	-0.57	13.65
38i	N(CH$_3$)$_2$	-0.63	13.67

5.1.2 Two rotamers = two sets of NMR signals

In the second class of compounds, methoxy group was replaced by NH-R[2] group, the second H-bond donor was thus inserted into the molecule and two rotamers were observable in ^{1}H and ^{13}C NMR spectra as two sets of signals. The rotamer ratio was determined from the ^{1}H NMR signals integration. For instance, in compound **42e**, 77 % of rotamer A was found (Fig. 45). In ^{13}C NMR spectrum of compound **42e**, the two sets of signals with intensities corresponding to the two rotamers concentration in equilibrium were also observed. The ^{1}H and ^{13}C NMR signals of both rotamers were assigned in the same way as described above.
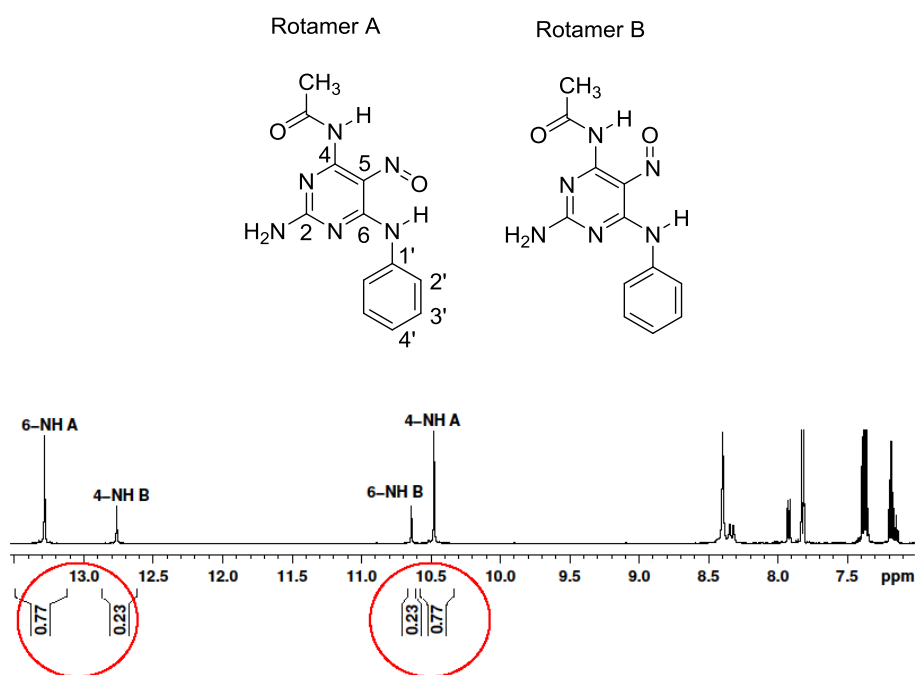
Figure 45. The low-field region of the ^{1}H NMR spectrum of compound **42e**. The rotamer ratio was determined by integration of the NH signals.
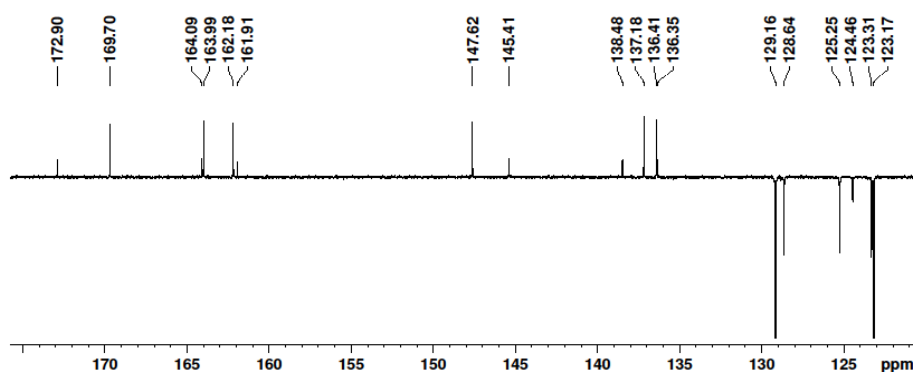
Figure 46. The low-field region of the APT ^{13}C spectrum of compound **42e**. Two sets of signals differing in the intensity correspond to two rotamers differing in their relative concentration in equilibrium. Rotamer A is the major one in this case.

5.1.3 The dependence of the rotamer ratio on substitution

The relative concentration of rotamer A ranged from 32 to 84 % in compounds **39a–42i** strongly depending on the *para* substituent R^1 of the phenylamino group at position 6, and the percentages correlated well with Hammett coefficients σ_P, see Fig. 47.
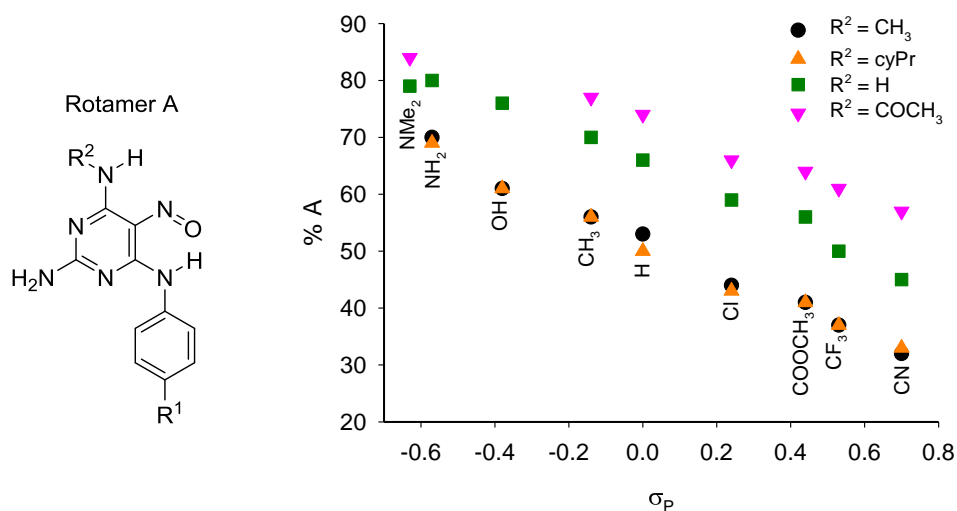
Figure 47. The dependence of the observed rotamer ratio of compounds **39–42** on the Hammett constant σ_P for the substituent in the *para* position of the phenylamino group (R^1).

In the series of compounds with R^2 = CH_3CO, the *para*-OH and *para*-NH_2 derivatives could not be prepared. Therefore, alternative derivatives with R^1 = NMe_2 were synthesized. Hammett coefficients σ_P of *para*-NH_2 and *para*-NMe_2 are very close (-0.57 and -0.63, respectively) as well as the resulting percentage of rotamer A in equilibrium (80 % and 79 %, respectively) in compounds **41h** and **41i**.

In general, it can be said that electron-withdrawing substituents R^1 decrease the concentration of rotamer A, whereas electron-donating substituents have the opposite effect. At the first sight, this behavior might be surprising; electron-donating groups increase the electron density in the aniline residue including the NH nitrogen, making the NH group less acidic and poorer H-bond donor. In our molecules, however, the conjugated π-electrons system enables the transfer of electronic substituent effects throughout the whole molecule. In this way, electron-donating substituents increase the electron density also at the nitroso oxygen atom, making it a better H-bond acceptor. The rotamer ratio can be predicted well using DFT calculations (data not shown).

5.1.4 Temperature dependence of ^{1}H NMR spectra

After the rotamer mixture heating, the nitroso group should rotate faster and only one set of signals should be observed in the NMR spectra. However, the intramolecular H-bonds stabilize the two rotamers and their interconversion is slow

even at elevated temperatures. For instance, temperature-dependent ^{1}H NMR spectra of compound **40e** are shown (Fig. 48) and it is seen that even at 140 °C no NH signals averaging was detected (Fig. 48 left). Only the two non-equivalent proton signals in the 2-amino group of both rotamers merged at 50 °C (Fig. 48 right). The temperature measurements above 140 °C were impossible because of the NMR probe temperature limitation.
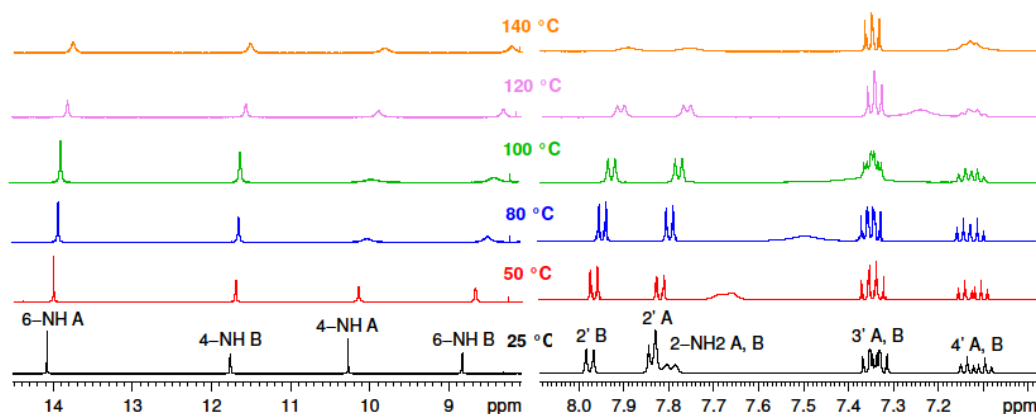
Figure 48. The NH-region (left) and the aromatic region (right) of the temperature-dependent ^{1}H NMR spectra of compound **40e**.

From these data it is clear that the rotational barrier is unusually high. From the NMR line-shape analysis of the NH protons, the rotational barrier higher than 20 kcal/mol has been determined. It led us to the idea that the individual rotamers might be separated. Unfortunately, for this class of compounds, it was not possible to separate them from each other even at low temperature.

5.1.5 UV/Vis spectrometry

Thanks to the nitroso group, the 5-nitrosopyrimidine derivatives are colorful compounds and their solutions have bright colors significantly dependent on the solvent. Furthermore, we found out that the color is strongly substituent-dependent and the Hammett-like correlation of the absorption spectra was observed. The UV/Vis spectra of these compounds in DMSO showed three transitions, one weak in the visible region (430–600 nm) and two strong transitions in the UV region (260–350 nm). For the interpretation of the UV/Vis spectra, the time-dependent density functional theory calculations (TD-DFT) have been used. The absorption in the visible region is caused by n $\rightarrow$ π* transitions, on the other hand, the UV bands are caused by π $\rightarrow$ π* transitions. The position of the absorption maximum in the visible region significantly depends on the *para* substituents (R^1), by contrast, the maxima in the UV region are only slightly substituent-dependent. Also the R^2-dependence was determined. The more electron-donating substituent R^2 is, the more hypsochromic shift was observed. For example, for the series with R^1 = H, the wavelength of the

absorption maxima in visible region decreases from 590 nm to 568, 564 and 562 nm for R^2 = CH_3CO, H, CH_3 and cyPr, respectively.

The UV/Vis absorption maxima of derivatives **39–42** are shifted by an almost constant shift with respect to the corresponding methoxy derivatives **38** indicating that the orientation of the nitroso group does not affect the electronic spectrum.

An interesting solvatochromic effect was observed. The UV/Vis spectra of compound **38e** dissolved in four different solvents were recorded and λ_{MAX} were found at 608, 594, 552 and 540 nm in acetone, DMSO, ethanol and methanol, respectively (Fig. 49).
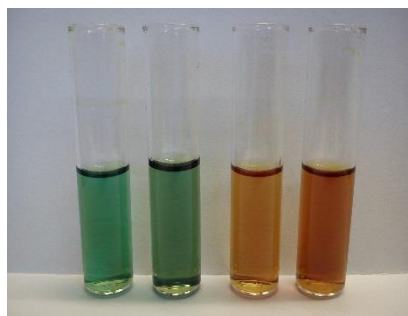
Figure 49. Compound **38e** dissolved in acetone, DMSO, ethanol and methanol (from left to right).

5.2 5-NITROSOPYRIMIDINES SUBSTITUTED WITH ALIPHATIC AMINES

Compounds **43–46** with aliphatic amine residues in positions 4 and 6 were prepared by Lucie Čechová and Zlatko Janeba at the IOCB AS CR. The physico-chemical properties of these compounds are really interesting; the rotational barrier was unusually high. We thus tried to separate the two rotamers from each other. Also here, there were two H-bond donors, two H-bonds were formed and the two stable rotamers were present in solution. The rotamer ratio was significantly substituent-dependent. To our surprise, it was possible to separate the two rotamers of compound **43** using column chromatography at room temperature. After the solvent evaporation from the chromatographic fractions, the two stable rotamers were obtained.
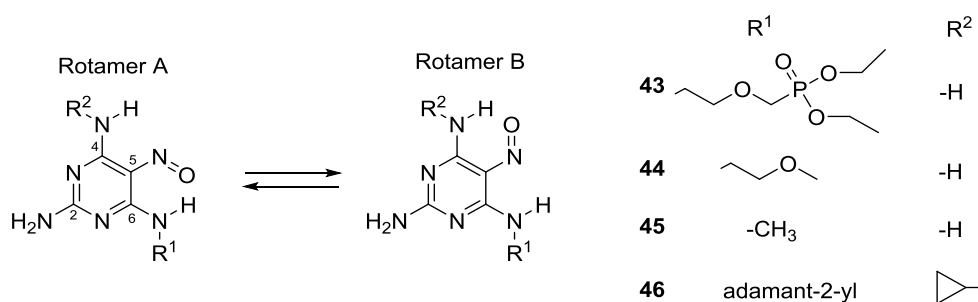
Figure 50. A new series of 5-nitrosopyrimidine derivatives substituted with aliphatic amines.

5.2.1 Influence of the NO group geometry on the chemical shifts

All NMR signals of both rotamers of the studied compounds were assigned using 1D and 2D NMR experiments described in 3.1. The orientation of the nitroso group has a significant influence on the chemical shift of the carbon atoms C4 and C6. For example, in aliphatic region of ^{1}H,^{13}C-HMBC spectrum of equilibrium mixture of compound **45** (Fig. 51), there are two crosspeaks between protons from methyl group and the carbon atom C6 for both rotamers – the major rotamer A (red) and the minor rotamer B (blue). It clearly shows the difference in chemical shifts of the carbon atom C6 between both rotamers. In rotamer A of compound **45**, where the nitroso oxygen atom is turned to the NH group at position 6, C6 carbon atom is more shielded (151.5 ppm) than in the case of rotamer B (163.8 ppm). These results were confirmed by DFT calculations. The experimental and calculated data for pyrimidine carbon atom chemical shifts are summarized in Table VI.
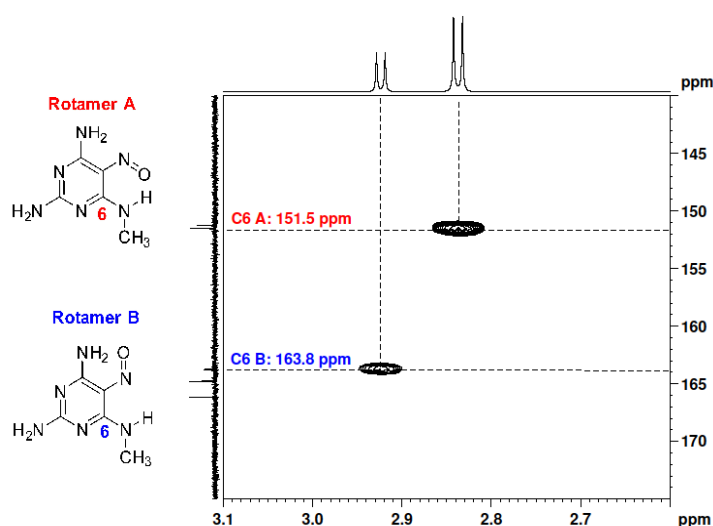
Figure 51. A part of the ^{1}H,^{13}C-HMBC spectrum of compound **45**. The crosspeaks correspond to the heteronuclear interactions between protons from the methyl group and the carbon atom C6.

Table VI. The experimental pyrimidine chemical shifts of rotamer A of compound **45** and the experimental and calculated (B3LYP/6-31+G(d,p)) chemical-shift differences between the two rotamers.

Atom	δ(A) exp. (ppm)	$\Delta\delta$ A-B exp.	$\Delta\delta$ A-B calc.
C-2	164.4	0	-0.3
C-4	166.2	14.9	17.0
C-5	136.9	-0.7	-0.7
C-6	151.5	-12.3	-13.5

The dependence of ^{15}N chemical shifts on the NO group orientation was also determined, the direct ^{15}N NMR spectrum could not be measured because of the low natural abundance of isotope ^{15}N. Instead, the indirect detection with 2D heteronuclear NMR experiments (^{1}H,^{15}N-HSQC, ^{1}H,^{15}N-HMBC) was used. The

nitrogen atoms with attached protons (NH, NH$_2$) are observable in ^{1}H,^{15}N-HSQC. The nitrogen atoms involved in the pyrimidine ring are observable in ^{1}H,^{15}N-HMBC (Fig. 52). There are significant differences between the chemical shifts of both rotamers. For instance, the nitrogen atom attached to the pyrimidine skeleton in the position 6 (6-**N**H) is less shielded in rotamer A (92.54 ppm) than in rotamer B (85.31 ppm). As a standard, nitromethane with the chemical shift at 381.7 ppm was used. These experiments have been confirmed by DFT calculations, see Table VII.
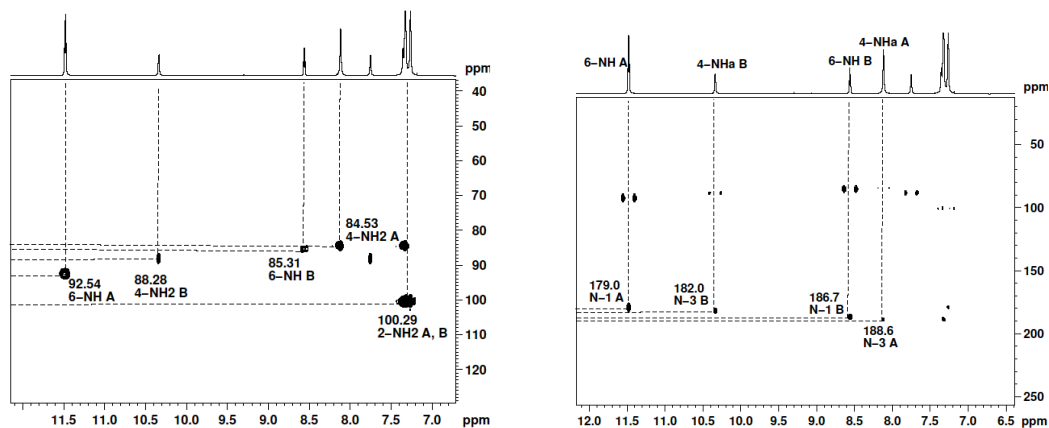
Figure 52. The NH region of ^{1}H,^{15}N-HSQC (left) and ^{1}H,^{15}N-HMBC (right) spectrum of equilibrium mixture of compound **43** in DMSO.

Table VII. The experimental nitrogen chemical shifts of rotamer A of compound **43** and the experimental and calculated (B3LYP/6-31+G(d,p)) chemical-shift differences between the two rotamers. To simplify the calculations, the phosphonate function was replaced by a methyl group.

Atom	δ(A) exp. (ppm)	$\Delta\delta$ A-B exp.	$\Delta\delta$ A-B calc.
N-1	179.0	-7.7	-4.2
N-3	188.6	6.6	3.8
4-NH$_2$	84.5	-3.8	-8.2
6-NH	92.5	7.2	7.4

5.2.2 Structure determination in solid state

After the gentle evaporation of solvents from chromatographically separated rotamers A and B of compound **43** (done by Lucie Čechová, IOCB AS CR), the solid-state ^{13}C NMR cross-polarization magic angle spinning (CP-MAS) spectra were measured. These data confirmed the rotamer purity (the minor rotamer NMR signal intensity was under the detection limit of solid-state NMR, ca. 5 %). The ^{13}C NMR signals of rotamer A were sharp indicating long-range order in the solid, whereas the signals of rotamer B were broader indicating amorphous structure. Interestingly, we

were able to observe slow re-crystallization of amorphous rotamer B into the stable crystalline rotamer A in solid-state ^{13}C NMR spectra within several months (Fig. 53).
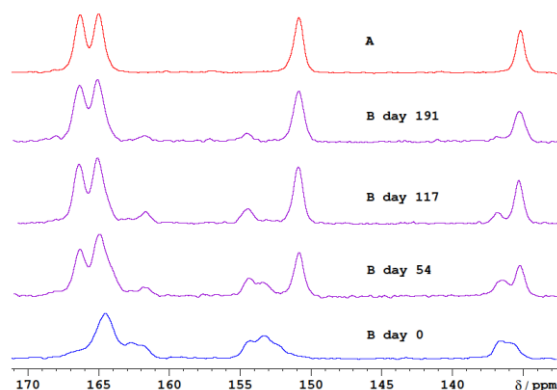
Figure 53. The aromatic region of the ^{13}C CP-MAS solid-state NMR spectra of planar rotamers **43A** and **43B**. Solid amorphous **43B** slowly transforms into the solid crystalline **43A**.

The geometry of the nitroso group was investigated using X-ray crystallography by Ivana Císařová (Faculty of Science, Charles University in Prague). Compound **43** was re-crystallized from dry acetone, only rotamer A was found in the X-ray structure (Fig. 54 left). After re-crystallization of compound **43** from acetone-water mixture, a disordered monohydrate with both nitroso group orientations was obtained (Fig. 54 right). Rotamer A was predominant (ca. 80 %).
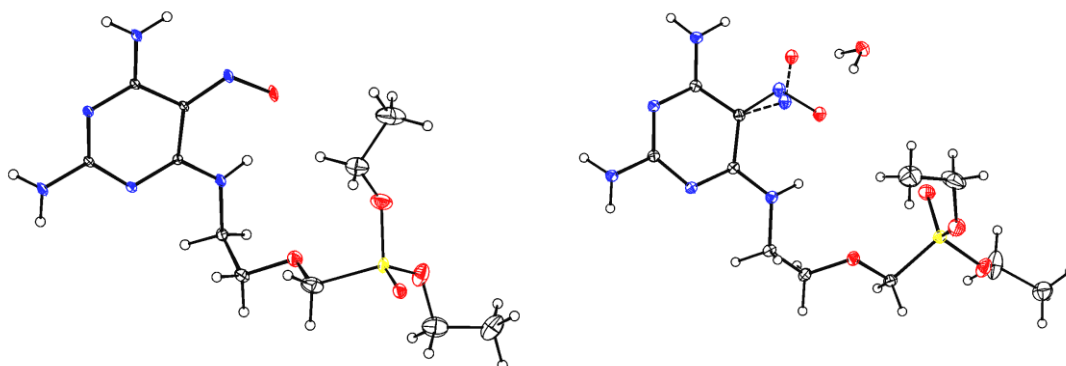
Figure 54. The X-ray structure of compound **43** re-crystallized from dry acetone (left) and from the acetone-water mixture (right). In the left structure, only rotamer A was found, whereas in the right structure, both rotamers appeared, rotamer A being predominant.

5.2.3 Kinetics of rotamer interconversion

Thanks to the chromatographic separation of the rotamers, the kinetics of their interconversion could be measured and for this purpose, solution-state ^{1}H NMR spectroscopy was used. The kinetic data of compound **43** are shown as an example. The NH proton NMR signals of the two rotamers are well separated and after their integration, the rotamer ratio in various times after dissolution (Fig. 55 left) was determined. From these data, kinetic curves (Fig. 55 right) were constructed and rate

constants k were determined. Gibbs free energy of activation $\Delta G^{\ddagger}$ (rotational barrier) was calculated from the Eyring equation.
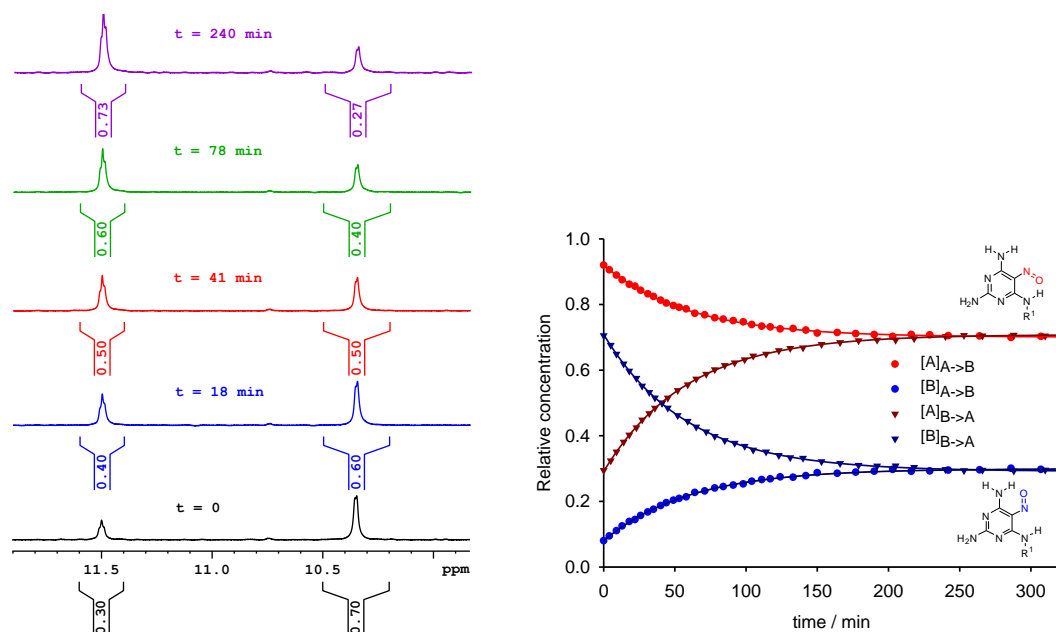
Figure 55. The kinetic measurement of rotamer interconversion in compound **43** in DMSO. Integrating ^{1}H NMR signals in various times after dissolution (left), the time dependence of relative concentrations was ploted (right).

As it can be seen in Fig. 55 right, we have measured kinetic data starting from almost pure rotamer A (90 % A) and from almost pure rotamer B (70 % B); the rotamer impurities were caused by the fast interconversion between them before the first NMR data could be acquired. After approximately four hours, the system was in equilibrium (73 % A + 27 % B), rate constant k = 1.21 x 10^{-4} s^{-1} was determined and Gibbs free energy of activation $\Delta G^{\ddagger}$ = 22.8 kcal/mol was calculated. The kinetic data for compounds **43–46** are summarized in Table VIII.

Table VIII. The kinetic data of compounds **43–46** and the relative concentration of rotamers in equilibrium.

Compound	Solvent	% A equilibrium	$k_{A \rightarrow B}$ /10^{-4} s^{-1}	$\Delta G^{\ddagger}$ /kcal . mol^{-1}
	DMSO	73	1.21	22.8
43	Methanol	67	1.07	22.9
	Acetone	71	1.64	22.6
44	DMSO	74	0.66	23.2
45	DMSO	64	0.92	23.0
46	DMSO	63	0.39	23.5
	Methanol	52	0.19	23.9

5.2.4 H/D isotopic exchange

The intramolecular hydrogen bonds reduce solvent accessibility to the hydrogen bond donor, which results in a slowing hydrogen-to-deuterium isotopic exchange. To confirm this fact, the isotopic exchange of proton 6-NH of compound **43** was investigated by ^{1}H NMR spectroscopy. This proton participates in the hydrogen bonding in rotamer A, in contrast to the rotamer B, where 6-NH is not involved in the hydrogen bonding. As expected, the H/D exchange is much slower in rotamer A (Fig. 56, red line) than in the case of rotamer B (Fig. 56, blue line).

As it is normal, the amino group protons in positon 2 were replaced by deuterium before the first spectrum could be acquired. Interestingly, both amino protons in position 4 were also exchanged despite the fact that the hydrogen bond in rotamer B is formed. It could be explained as follows: after the fast isotopic exchange of not H-bonded amino proton, the amino group rotates fast around the C4-NH$_2$ bond and the second hydrogen atom is exchanged to deuterium. This explanation was supported by DFT calculations of rotational barriers of the nitroso group around C5-NO bond and the amino group around C4-NH$_2$ bond. It was found out that the C4-NH$_2$ barrier is 5.6 kcal/mol lower than the C5-NO rotational barrier.
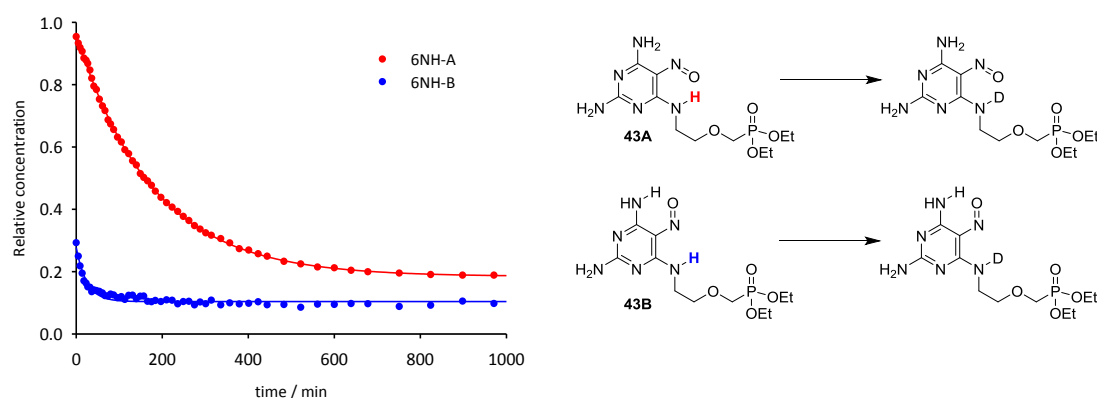
Figure 56. The progress of the H/D exchange of hydrogen atom 6-NH in equilibrium mixture of rotamers **43A** (in red) and **43B** (in blue) in DMSO-d_6-CD$_3$OD mixture (9:1).

5.3 SUMMARY

A new series of 5-nitrosopyrimidine derivatives with interesting physico-chemical properties was prepared. These compounds contain a system of strong intramolecular hydrogen bonds which allows the nitroso group to adopt two different orientations. It results in two stable conformers formation. The mixture composition in equilibrium is significantly substituent-dependent. From the temperature dependence we found out that the rotamer interconversion barrier is unusually high. The two rotamers of some derivatives could be chromatographically separated. Both chromatographic fractions were analyzed (after solvent

evaporation) using solid-state NMR and these data were confirmed by X-ray analysis. The rotamers were stable enough to measure kinetics of their interconversion in solution. The properties of these compounds are close to atropisomers, whose interconversion barrier is high enough to separate them. The main difference is that the atropisomers separation is allowed by sterically hindered rotation in contrast to our rotamers that are separable through strong intramolecular hydrogen bonding. This significant difference led us to make a distinction from relatively common atropisomers. We have suggested a term "planamerism", defining "planamers" (Fig. 57) as small aromatic molecule rotamers with a planar conjugated moiety that are isolable as chemical species.[71] It may be speculated that planamers might play an important role in disciplines involving the study of weak and reversible non-covalent interactions such as supramolecular assemblies or as potential biologically active compounds in the development of novel drug-like molecules.
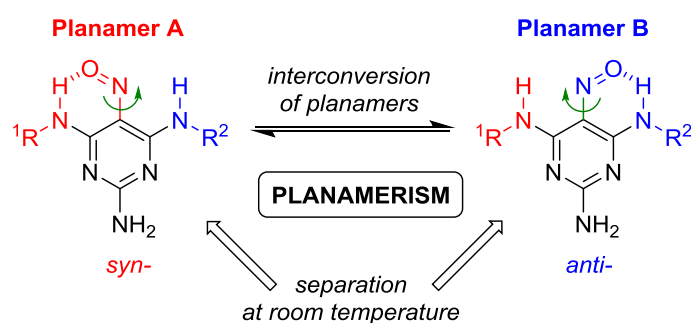
Figure 57. Planar rotamers have been separated by column chromatography at room temperature.

6 ENZYMATIC DECOMPOSITION MONITORED BY ^{31}P NMR SPECTROSCOPY – PAPER II

Many biologically active compounds are unable to pass across the cell membrane, therefore, more lipophilic derivatives (prodrugs) are often prepared. Frequently used prodrugs of modified nucleosides contain phosphoramidate moiety,[72] which can be easily cleaved by cellular enzymes and activated nucleoside (monophosphate) is released. The enzymatic cleavage can be monitored by ^{31}P NMR spectroscopy.[73]

This study deals with monitoring of the enzymatic decomposition of modified nucleosides with aryl phosphoramidate moiety (Fig. 58). Studied compounds have been prepared by Hubert Hřebabecký at the IOCB AS CR as potential antivirotics. It has been described for similar compounds that prodrug activation is initiated by the carboxyesterase-mediated hydrolysis of phosphoramidate derivative.[74] Enzymatic degradation was thus simulated using carboxypeptidase Y,[75] which possesses high structural homology to cathepsin A, an enzyme responsible for this conversion in humans. Chemical hydrolysis of the studied compounds in aqueous triethylamine solutions was also studied to confirm the chemical structure of intermediates and final products. It was found that the structural modification of the studied nucleoside derivatives is not significant enough to inhibit the enzyme and that the supposed metabolic reaction works well.
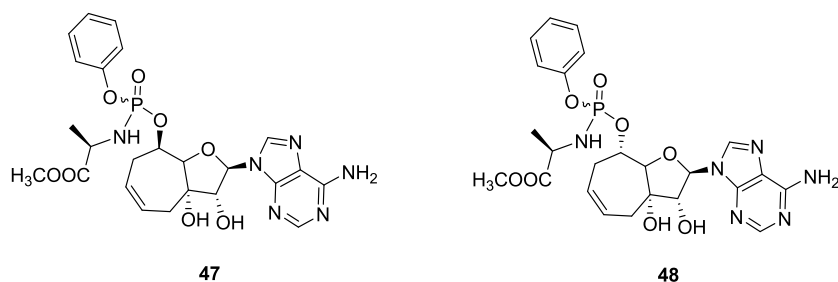
Figure 58. The chemical structure of the studied phosphoramidate derivatives.

The starting phosphoramidate derivative **47** has two signals in the proton decoupled ^{31}P NMR spectra corresponding to two diastereoisomers differing in the configuration of the chiral center at phosphorus atom. After the enzyme addition (Fig. 59 left), two new phosphorus signals of an intermediate **47a** appeared. It means that the intermediate still has the chiral center at phosphorus atom. After several hours, a single ^{31}P NMR signal was observed, which indicates that the final product **47b** does not contain a chiral centre at phosphorus atom. Similar progress of the reaction was observed after chemical hydrolysis of the starting phosphoramidate in

triethylamine solution (Fig. 59 right). The chemical-shift differences between enzymatic and chemical hydrolysis could be caused by the environment; the enzymatic hydrolysis was performed in Trizma buffer (pH 7.4), whereas the chemical hydrolysis was done in basic environment (pH 12.0).
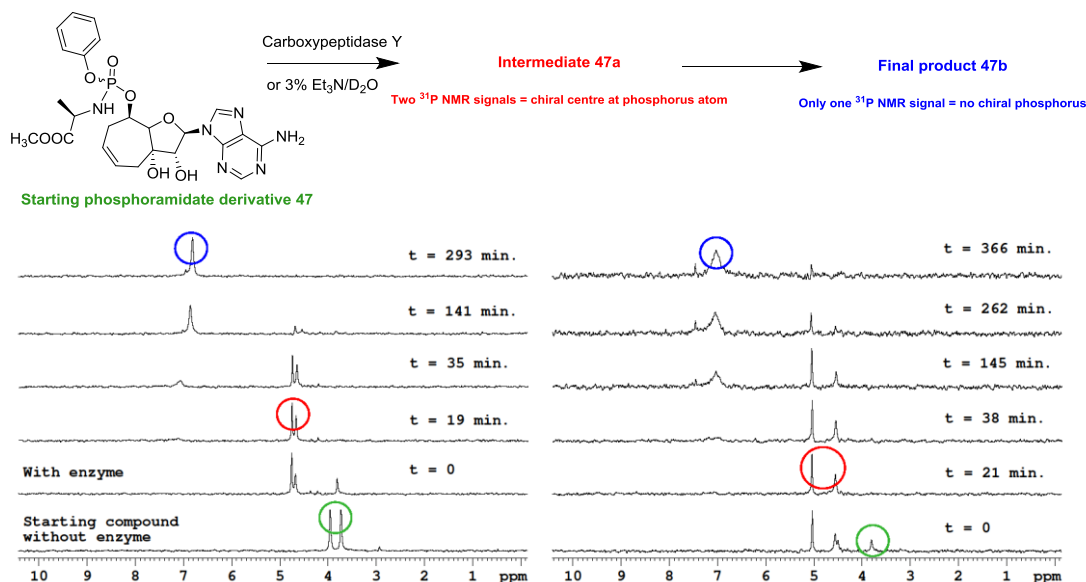
Figure 59. The enzymatic decomposition (left) and chemical hydrolysis (right) of the starting phosphoramidate derivative **47** monitored by ^{31}P NMR spectroscopy.

For compound **48**, similar progress of both enzymatic and chemical reactions was observed. The time dependence of relative concentration (Fig. 60 right) of the intermediate and the final product was obtained by integration of ^{31}P NMR spectra acquired at various times after the start of the chemical hydrolysis of compound **48** (Fig. 60 left).
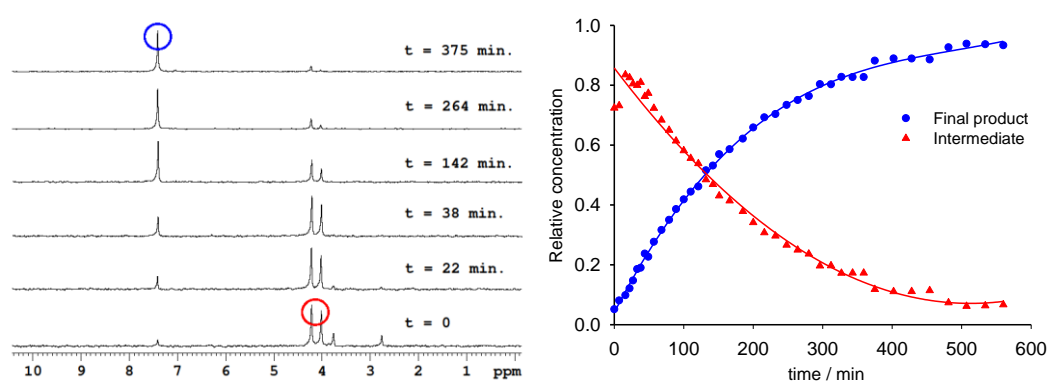
Figure 60. The progress of chemical hydrolysis of compound **48** monitored by ^{31}P NMR spectroscopy (left) and time dependence of relative concentrations obtained from integration of ^{31}P NMR spectra (right). Concentration of intermediate (red) decreased, whereas concentration of the final product (blue) increased.

6.1 *In situ* structure determination

In situ structure determination of intermediates **47a** and **48a**, respectively, was done during approximately the first two hours of the reaction, when the concentration of the intermediate was above 50 %. The structure determination is based on the analysis of C-P spin-spin interactions across 1–3 bonds visible in ^{13}C NMR spectra as a line splitting. It is clear that the methylester was hydrolyzed; the intensity of the signals corresponding to the methyl carbon atoms of methylester group (two signals around 52.55 ppm = two diastereoisomers) decreased whereas the intensity of methanol singlet signal (52.45 ppm) increased. The phenyl moiety is still attached to the molecule, signals corresponding to the carbon atoms in *ortho* position are still visible as two dublets (two, because of the two diastereoisomers and dublets because of the C-P interaction), Fig. 61.
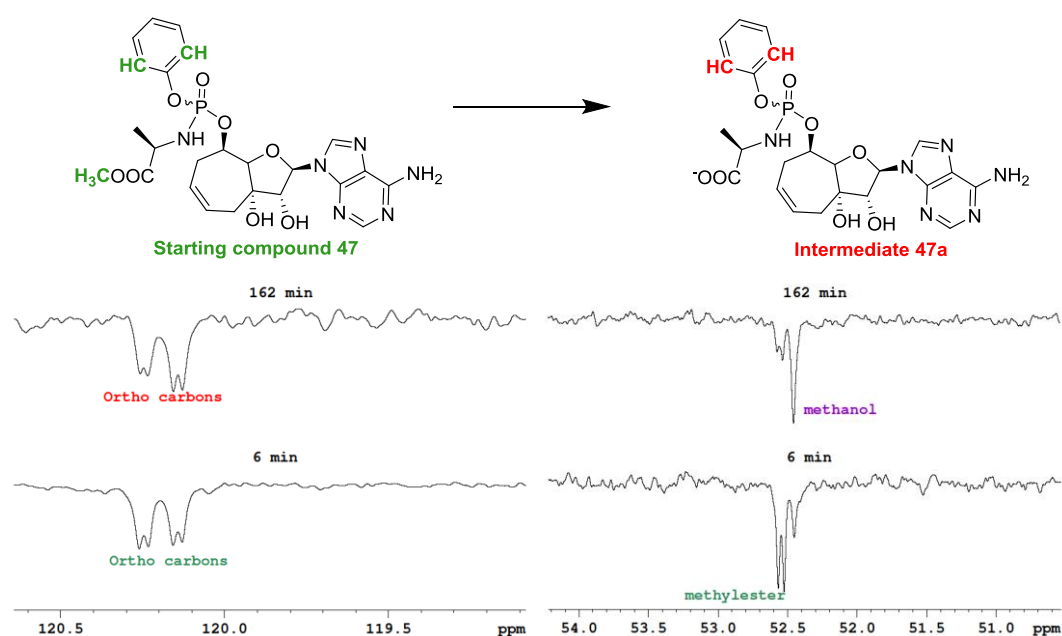
Figure 61. The ^{13}C NMR spectra of *ortho* carbons (left) and methoxy group (right) of compound **47**. The ^{13}C NMR spectra were accumulated at intervals 6–57 min (bottom) and 162–213 min (top) after the start of the chemical hydrolysis.

After several hours, the phenyl ring was cleaved and stable final product **47b** was obtained. The two dublets around 120.3 ppm corresponding to *ortho* carbons, disappeared and one singlet signal around 118.9 ppm corresponding to *ortho* carbon atoms of phenol appeared (Fig. 62). After the phenol release, there is no chiral center at the phosphorus atom, thus no two diastereoisomers exist.
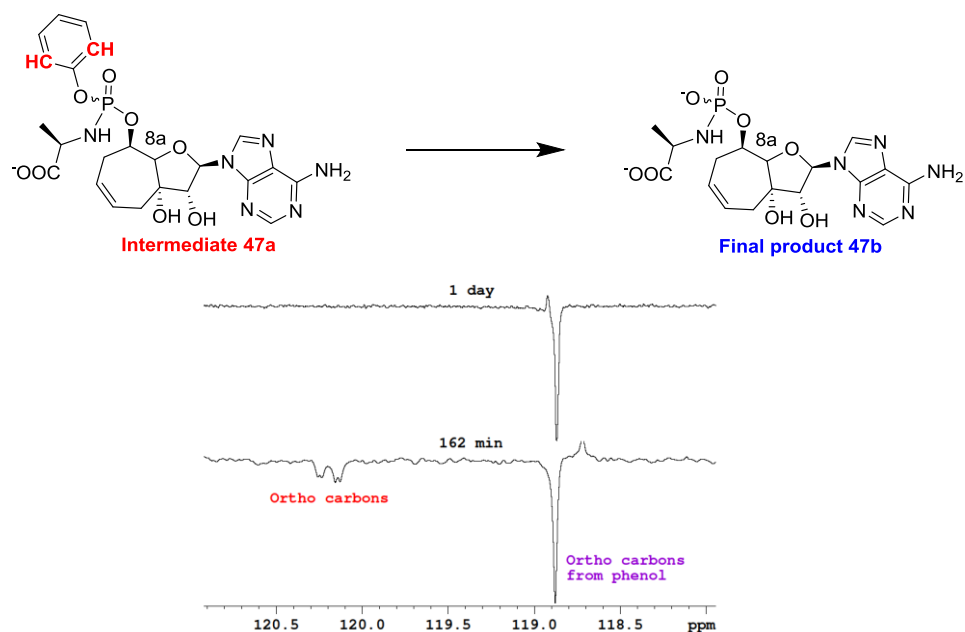
Figure 62. The ^{13}C APT spectra of *ortho* carbons.

The reaction mixture containing the final product was separated using HPLC; methanol and phenol were removed. It was confirmed by comparing of the ^{13}C NMR spectra of the reaction mixture before and after HPLC separation (Fig. 63). The ^{13}C NMR signals corresponding to phenol and methanol disappeared after HPLC separation.
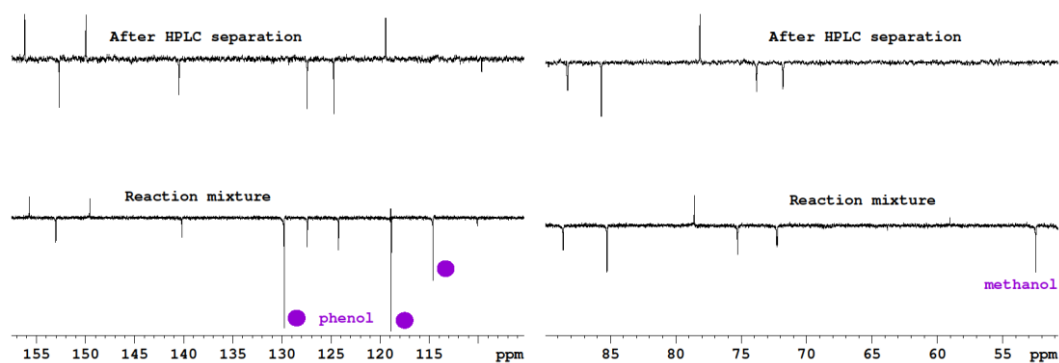
Figure 63. The aromatic region (left) and aliphatic region (right) of ^{13}C NMR spectra of the reaction mixture after chemical hydrolysis of compound **48** (bottom) and the reaction mixture after HPLC separation (top). NMR signals of phenol and methanol disappeared.

6.2 SUMMARY

The enzymatic cleavage of aryl phosphoramidate prodrug was successfully monitored by ^{31}P NMR spectroscopy. The decomposition was studied to confirm that the starting compound **47** can work as a prodrug and it is cleavable by intracellular enzymes. It was suggested previously that carboxypeptidases catalyze the first step

of the metabolic activation, which is the hydrolysis of the carboxylic ester function in the amino acid part of the molecule.[76] In this work, carboxypeptidase Y, an enzyme with high structural homology to human cathepsin A, was employed. It was found that the enzymatic cleavage of both compounds **47** and **48** consists of two steps. The intermediate **47a** (and **48a**, respectively) with chiral center at the phosphorus atom was obtained and the final product **47b** (and **48b**, respectively) does not contain the chiral center at the phosphorus atom, because phenolic substituent was removed by hydrolysis. The chemical structure of intermediate **47a** (and **48a**, respectively) and the final product **47b** (and **48b**, respectively) was determined by NMR spectroscopy (Fig. 64).
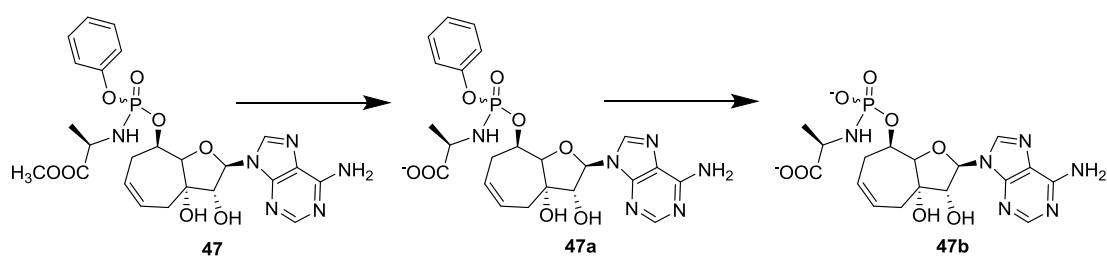
Figure 64. The proposed pathway of the enzymatic decomposition of the studied phosphoramidate prodrug.

7 Study of polymorphic forms by solid-state NMR spectroscopy – paper VII

Studies of polymorphic forms of pharmaceutically important compounds are in the field of interest of many research teams all over the world. The information about the polymorphic structure of these compounds is crucial for granting licenses obtained from regulatory authorities. The structure of polymorphs is usually studied by diffraction methods but solid-state NMR spectroscopy in combination with calculations can provide very useful information in the cases, where X-ray data are not available or where they are complicated by a disorder in the molecule. For this purpose, the ^{13}C cross-polarization magic-angle spinning (CP-MAS) NMR spectroscopy is often used. For example, to determine the number of non-equivalent molecules in asymmetric units in the crystal, it is sufficient simply to compare the number of the observed resonances with the number of non-equivalent carbon atoms of the studied molecule.

The aim of this work was to study polymorphic forms of three industrially important compounds, including methacrylamide (**49**), piracetam (**50**) and 2-thio-barbituric acid (**51**) (Fig. 65), by several spectroscopic methods, X-ray diffraction analysis and DFT calculations. The polymorphic structure differences visible in the NMR spectra of the studied compounds will be discussed in this chapter.

The desired polymorphic forms of studied compounds **49**–**51** were prepared by re-crystallization of commercially available samples from different solvents under described conditions.[77] The differences between their polymorphs range from a subtle change in the crystal packing (piracetam) over conformational (methacrylamide) and tautomeric (2-thiobarbituric acid) variations.

49a	**49b**	**50a, 50b**	**51a**	**51b**
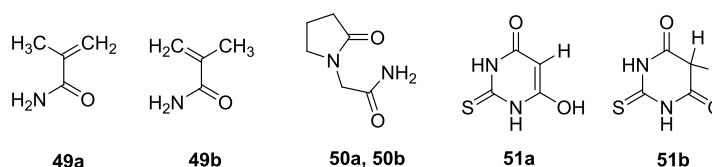
Figure 65. The chemical structure of model molecules: methacrylamide (**49**), piracetam (**50**) and 2-thiobarbituric acid (**51**).

7.1 Methacrylamide

Methacrylamide is widely industrially used as a key intermediate in acetone cyanohydrin process for the manufacture of methyl methacrylate and for a synthesis

of polymers. Two polymorphic forms of the compound are known.[78] The crystals of form I, prepared from hot $CHCl_3$ solution, are monoclinic, and contain *s-cis* conformer only (**49a**). Orthorhombic form II obtained from re-crystallization by slow cooling of warm aqueous solution of methacrylamide (**49b**) consists exclusively of *s-trans* conformer. It has not yet been possible to develop procedures for the isolation of the pure phases, only the enriched batches of either form I or II have been prepared.[78] We succeeded in the pure forms preparation, which was confirmed by X-ray analysis (done by Ivana Císařová at Faculty of Science, Charles University in Prague) and by the ^{13}C CP-MAS NMR spectra of both prepared pure forms. The chemical shifts of both polymorphic forms were only slightly different (Fig. 66).
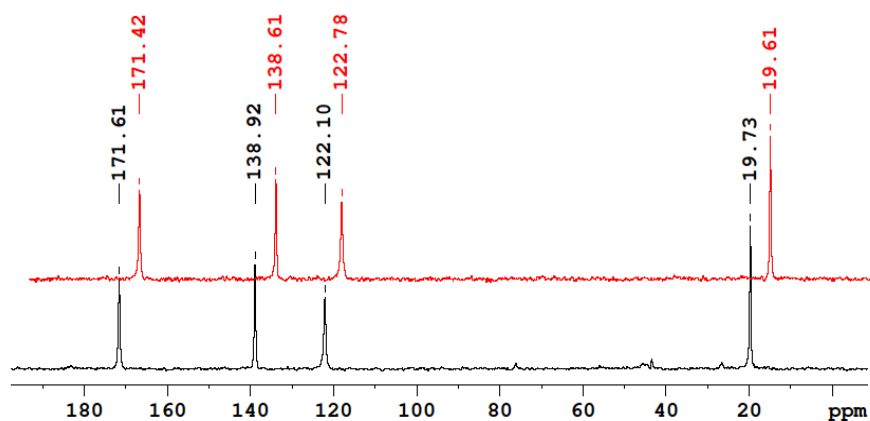
Figure 66. The solid-state ^{13}C NMR spectra of polymorphic crystals of methacrylamide re-crystallized from chloroform (red) as form **49a** and from water (black) as form **49b**. The red spectrum is offset by ~5 ppm for clarity. Crystalline glycine was used as a standard.

Furthermore, when sample **49b** was not completely dried before the NMR experiment, it was possible to observe the **49b** transformation into **49a** during several days. This process was monitored by a series of the ^{13}C CP-MAS NMR spectra (Fig. 67). The intensity of **49b** signals (in black) decreased whereas the intensity of new NMR signals corresponding to the form **49a** (in red) increased. The spectral changes are best observable in the region close to 122 ppm, where the left signal (122.78 ppm) corresponds to the form **49a** and the right signal (122.10 ppm) corresponds to form **49b**. This transformation may have been facilitated by the combined effect of residual solvent and higher pressure in the MAS rotor spinning at 12 kHz because it was not observed when the sample was dry or wet and stored without spinning.
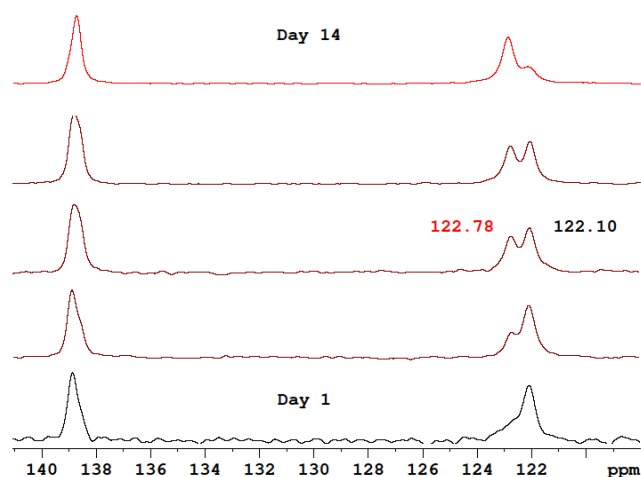
Figure 67. A part of the ^{13}C NMR spectra of methacrylamide polymorphic form **49b** at various times. After several days, the orthorhombic form **49b** (black) was transformed into the monoclinic form **49a** (red).

7.2 PIRACETAM

Piracetam (2-oxo-pyrrolidineacetamide) is pharmaceutically very important compound used to treat conditions of age-associated mental decline and disorders of the nervous system. The structures of five polymorphic forms have been described previously.[79,80] In our work, only triclinic form II (**50a**) and monoclinic form III (**50b**) have been studied. Form II has been prepared by re-crystallization from propan-2-ol, whereas form III has been prepared by re-crystallization from methanol. Although the molecular orientation of both forms **50a** and **50b** is almost identical, the different crystal packing induces specific shielding in the two crystal forms, which causes changes in the ^{13}C CP-MAS NMR chemical shifts (0.4–1.3 ppm) as shown in Fig. 68.
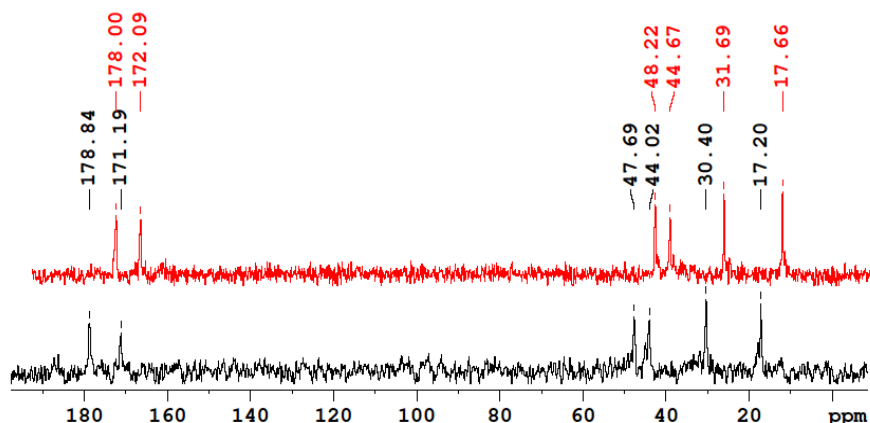
Figure 68. The solid-state ^{13}C NMR spectra of polymorphic crystals of piracetam re-crystallized from propan-2-ol (red) as form **50a** and from methanol (black) as form **50b**. The red spectrum is offset by ~5 ppm for clarity. Crystalline glycine was used as a standard.

7.3 2-Thiobarbituric acid

The third studied structure is 2-thiobarbituric acid that also belongs to a class of pharmaceutically important compounds. Six polymorphic forms and one hydrated form have been isolated and characterized.[81] For this study, two polymorphic forms II (**51a**) and III (**51b**) have been prepared by re-crystallization from absolute ethanol and dry acetonitrile, respectively. These two polymorphs contain two different tautomeric forms (**51a**-enol and **51b**-keto) and they are unambiguously distinguishable in ^{13}C CP-NMR spectra. The sp^2-hybridized carbon atom C5 in form **51a** is less shielded (82.75 ppm) than the sp^3-hybridized carbon C5 in form **51b** (40.93 ppm). Also other signals are significantly shifted (1.8–4.7 ppm). The measured spectra are depicted in Fig. 69.
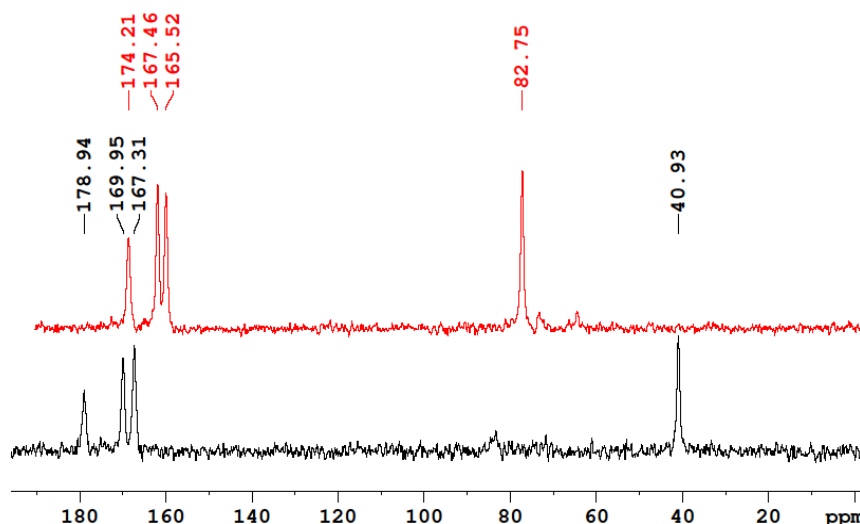
Figure 69. The solid-state ^{13}C NMR spectra of polymorphic crystals of thiobarbituric acid re-crystallized from ethanol (red) as form **51a** and from acetonitrile (black) as form **51b**. The red spectrum is offset by ~5 ppm for clarity. Crystalline glycine was used as a standard.

7.4 Summary

In this work, different polymorphic forms of three industrially important compounds have been prepared. The CP-MAS NMR data confirmed sample purity and good performance of the technique in polymorphic discrimination. We succeeded in preparing of the pure polymorphic crystals of methacrylamide which have not been published yet. The crystal structure of the desired orthorhombic form **49b** obtained after very slow re-crystallization from warm aqueous methacrylamide solution was confirmed by X-ray analysis. An interesting **49b**→**49a** transformation in solid state was detected using CP-MAS NMR spectra. The kinetic data of this process

were not obtained, because the rate of this transformation depended on the external conditions such as the sample spinning. The molecular geometry in both types of piracetam crystals (**50a** and **50b**) is the same, but the crystal packing is different, which induces different shielding as visible in CP-MAS NMR spectra. Two different tautomeric forms of 2-thiobarbituric acid were obtained in polymorphic forms **51a** and **51b**. Crystals **51a** consist of enol form of 2-thiobarbituric acid, whereas polymorphic form **51b** contained keto form of this compound, which was clearly determined by CP-MAS NMR spectroscopy.

^{13}C CP-MAS NMR spectroscopy is a suitable tool for polymorphic forms investigation, because even very small differences in the crystal structure lead to easily observable changes in the spectra. Solid-state NMR spectroscopy can thus be used as a fast and reliable technique for polymorphic purity determination.

8 STABILITY OF 5-AMINOPYRIMIDINES IN DMSO – PAPER VIII

For biological activity investigation, the studied compounds are usually dissolved in DMSO and these solutions are very often stored in a freezer for a long time. In our previous work,[4] when we studied antioxidative activities in a series of 5-aminopyrimidines (Fig. 70), color changes in DMSO solution were observed after several hours at room temperature (Fig. 71) as well as in a freezer.

This chapter will describe the chemical transformation of these compounds in DMSO studied by a consequences of chemical reactions with alloxan, by NMR and UV/Vis spectroscopy and proposed reaction mechanism. NMR spectroscopy was not suitable tool to determine the structures, because of very low solubility of the products, but it helped to elucidate the reaction mechanism as well as to monitor the progress of the transformations in DMSO.

	R^2	R^4	R^6
52	OH	OH	NH_2
53	NH_2	OH	NH_2
54	NH_2	NH_2	NH_2
55	OH	OH	OH
56	SH	OH	NH2
57	NH_2	OCH_3	OCH_3
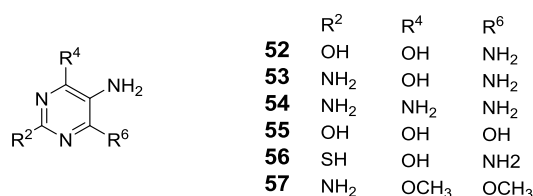
Figure 70. The general formula of the studied compounds.

Figure 71. The DMSO solutions of compounds **53**, **54**, **52**, **56** (from left to right) several hours after preparation. The solutions were colorless immediately after dissolution.

8.1   CHANGES OBSERVED BY NMR SPECTROSCOPY

Color changes were observable in DMSO as well as in DMSO-d_6 so they could be detected directly in an NMR tube. The kinetics of these transformations was monitored by ^{1}H NMR spectroscopy and by UV/Vis spectrometry. For illustration, the time-response changes in the ^{1}H NMR spectra of compound **53** are displayed in Fig. 72. The NMR signals of the starting compound (in red; 6.37 and 6.46 ppm) practically disappeared from the reaction mixture by day 7. The signals of the purple

intermediate product **53a** (in purple; 8.30; 8.60 and 10.95 ppm) appeared within only one day of incubation. On day 2, the signal of an ammonium cation was detected (in green; 7.09 ppm, J = 51 Hz). In several months, it was possible to observe the NMR signals of the final product of a successive reaction of **53**, the yellow **53b** (in yellow, 8.9 and 9.0 ppm). The low intensity of these signals was caused by the low solubility of **53b** in DMSO (it precipitated from the solution). The UV/Vis spectra confirmed the successive reactions (**53**→**53a**→**53b**), the isosbestic point at 365 nm was found.
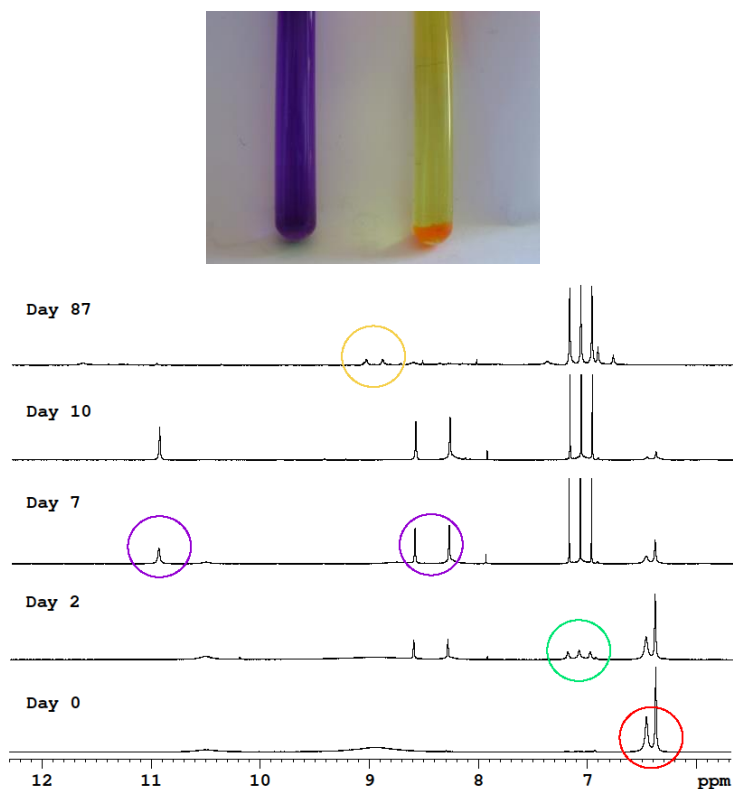
Figure 72. The time evolution of the ^{1}H NMR spectra of compound **53** in DMSO. The starting compound **53** (in red) reacted in DMSO to generate the intermediate product **53a** (in purple, the purple solution in the NMR tube). Simultaneously, the ammonium cation escaped (in green). Consequently, several months later, compound **53a** was converted into the final product **53b** (in yellow, the yellow solution in the NMR tube).

^{1}H NMR spectra have provided a clear evidence that an ammonium cation is present in the solution after the first reaction (**53**→**53a**) and the following mechanism has been proposed (Fig. 73). The starting compound **53** is oxidized by DMSO to pyrimidine-quinone-imine, while an ammonium cation is released. Subsequently, this unstable intermediate condenses with the 5-amino group of another molecule and purple intermediate **53a** arises. For comparison, 2,6-diamino-4-oxo-pyrimidine (compound **53** without the 5-amino group) was dissolved in DMSO and no changes were observed. Obviously, 5-amino group is crucial for the oxidation reactions. Several months later, the less soluble final product **53b** was obtained.
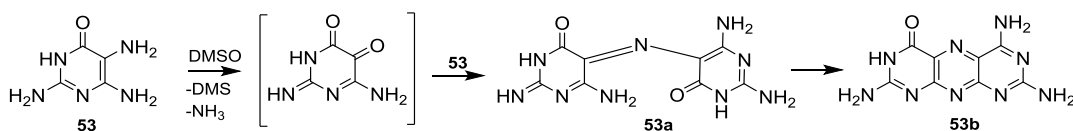
Figure 73. The proposed mechanism of the transformations of compound **53** in DMSO.

8.2 OXIDATION-CONDENSATION REACTIONS

Unfortunately, more information about the structure of the products were not obtained from the NMR spectra. The pyrimidopteridine products of the reactions were very poorly soluble and we were not able to acquire the ^{13}C NMR spectra or heteronuclear correlations of these products. Furthermore, in the ^{1}H NMR spectra of the starting compounds, the signals of the exchangeable protons (NH or OH) were very broad, probably because of a fast tautomer interconversion. For the structure determination, the chemical reactions with alloxan and hydrolysis by NaNO$_2$ in HCl were performed to compare UV/Vis spectra of our color products with previously described pyrimidopteridines. The observed oxidation-condensation reactions are depicted in Fig. 74.
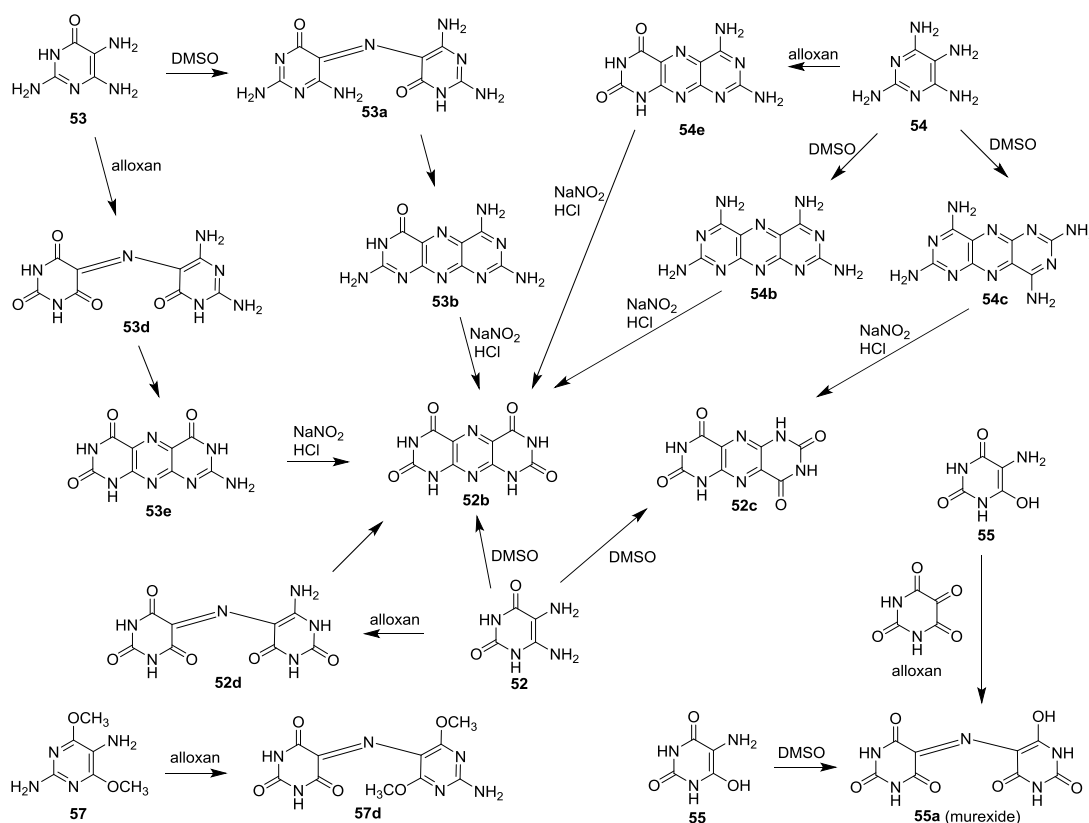
Figure 74. A series of the oxidation-condensation reactions of 5-aminopyrimidines with alloxan and with DMSO.

From the proposed mechanism introduced above, we can say that 5-amino group is transformed into oxo group which reacts with another pyrimidine molecule

quickly. To confirm the proposed mechanism, condensation reactions with alloxan (2,4,5,6-tetraoxo-pyrimidine) were performed. After the reaction of compound **52** with alloxan, obtained "open-form" **52d** spontaneously condensed, and the final product **52b** was obtained. Compound **53** reacted in the same way and products **53d** and **53e** were obtained. In the case of compound **54**, the "open-form" **54d** was not detected probably because of the fast intramolecular condensation into **54e**. After the condensation of 5-aminobarbituric acid **55** with alloxan, we ended up with the "open-form" **55a** and no subsequent intramolecular condensation was observed. It is not surprising, because in the molecule, no other amino group is present to condense into the "close-form". The ammonium salt of compound **55a** is called murexide and it is commercially available metalochromic indicator used in analytical chemistry for monitoring of calcium titrations. Therefore, we could compare not only UV/Vis spectra of our product **55a** (λ_{MAX} = 532 nm) with commercially available murexide, but also the ability of calcium chelation. In compound **56**, the changes in the UV/Vis spectra and the presence of ammonia cation suggest that similar oxidation and self-condensation reactions take place. Unfortunately, the isolation of the products failed, so reactions with this compound are not shown. Finally, the condensation of compound **57** with alloxan led to the stable "open-form" bipyrimidine derivative **57d**.

The "close-forms" **53e** and **54e** obtained from the reaction with alloxan and subsequent spontaneous intramolecular condensation were transformed into **52b** by the reaction with NaNO$_2$ in HCl. In the same way, the "close-forms" **53b** and **54b** obtained from DMSO oxidation and subsequent condensation were converted into **52b**. UV/Vis spectra of the final product **52b** obtained in different ways were in agreement with previously published data.[82]

8.3 Summary

We used consequence of chemical reactions and spectroscopic data to explain 5-aminopyrimidine transformations in DMSO and to determine the products of these transformations. HR-MS provided molecular formula of our products and UV/Vis spectra of the final products **52b** and **52c** were compared with literature.[82] Although it was impossible to use NMR spectra for structure determination, some relevant information were extracted and reaction mechanism of 5-aminopyrimidines transformations in DMSO was proposed.

9 SUMMARY

In this work, I focused on the structure determination of modified nucleic acid components, mainly (but not only) nucleoside derivatives, which have been prepared by synthetic chemists from the IOCB AS CR, namely the groups of Radim Nencka and Zlatko Janeba, with the aim to find novel potentially biologically active compounds. During my Ph.D. studies, I solved the chemical structure of more than 700 newly prepared compounds by NMR spectroscopy and, if necessary, complemented that with conformational analysis, because the correct structure assignment is a crucial step for biological activities screening and structure-activity relationship studies.

In this work, two new NMR methods have been developed to help with the structure determination of purine derivatives; quaternary carbon atom NMR signal assignment by heteronuclear (C-H) long-range coupling constants as well as preferred tautomeric forms have been studied in detail. These methods are based on the correlation between experimental and DFT-calculated NMR parameters.

Using NMR spectroscopy, physico-chemical properties such as the intramolecular interactions, stability or reactivity of modified nucleosides were studied. The most significant result published in this work is study of physico-chemical properties of 5-nitrosopyrimidine derivatives with strong intramolecular hydrogen bonds. In these compounds, interesting stereochemical behavior was observed. Due to unusually strong intramolecular H-bonds, two stable rotamers differing in nitroso group orientation were found and observed as two sets of NMR signals. The rotamer ratio in equilibrium strongly depends on the nature of substituents; the percentage of one rotamer can be tuned in a wide range of values (32–84 %). The influence of *p*-substituents on relative rotamer concentration correlates well with Hammett constants, where the substituents are aligned according to their electronic properties (donors, acceptors). Furthermore, in some cases, it was possible to separate the rotamers from each other and characterize them as individual chemical species. They exerted different retention factors in silica-gel chromatography and significantly different NMR spectra (^{1}H, ^{13}C, ^{15}N) in solution as well as in solid state. Because of their interesting stereochemical behavior, they were compared with well-known atropisomers, which are separable *via* sterically hindered rotation. In our rotamers, the mode of stabilization is strong intramolecular hydrogen bond. The rotational barriers were determined around 23 kcal/mol, which explains that pure rotamers could be isolated at room temperature.

References

(1)   Rosemeyer, H. *Chem. Biodivers.* **2004**, *1*, 361.

(2)   Bartl, T.; Zacharová, Z.; Sečkářová, P.; Kolehmainen, E.; Marek, R. *Eur. J. Org. Chem.* **2009**, *2009*, 1377.

(3)   Legraverend, M.; Grierson, D. S. *Bioorg. Med. Chem.* **2006**, *14*, 3987.

(4)   Procházková, E.; Jansa, P.; Dračínský, M.; Holý, A.; Mertlíková-Kaiserová, H. *Free Rad. Res.* **2012**, *46*, 61.

(5)   De Clercq, E.; Holý, A.; Rosenberg, I.; Sakuma, T.; Balzarini, J.; Maudgal, P. C. *Nature* **1986**, *323*, 464.

(6)   Holý, A. *Curr. Pharm. Des.* **2003**, *9*, 2567.

(7)   Kidwai, M.; Venkataramanan, R.; Mohan, R.; Sapra, P. *Curr. Med. Chem.* **2002**, *9*, 1209.

(8)   Kim, J. N.; Blount, K. F.; Puskarz, I.; Lim, J.; Link, K. H.; Breaker, R. R. *ACS Chem. Biol.* **2009**, *4*, 915.

(9)   Šorm, F.; Pískala, A.; Čihák, A.; Veselý, J. *Experientia* **1964**, *20*, 202.

(10)   Yue, T. F.; Gutman, A. B. *Am. J. Med.* **1964**, *37*, 885.

(11)   Chesney, P. J.; Teets, K. C.; Mulvihill, J. J.; Salit, I. E.; Marks, M. I. *J. Pediatr.* **1976**, *89*, 1017.

(12)   Skipper, H. E.; Thomson, J. R.; Elion, G. B.; Hitchings, G. H. *Cancer Res.* **1954**, *14*, 294.

(13)   Doong, S. L.; Tsai, C. H.; Schinazi, R. F.; Liotta, D. C.; Cheng, Y. C. *Proc. Natl. Acad. Sci. USA* **1991**, *88*, 8495.

(14)   Soudeyns, H.; Yao, X. I.; Gao, Q.; Belleau, B.; Kraus, J. L.; Nguyen-Ba, N.; Spira, B.; Wainberg, M. A. *Antimicrob. Agents Chemother.* **1991**, *35*, 1386.

(15)   Raguse, J. D.; Gath, H. J.; Bier, J.; Riess, H.; Oettle, H. *Clin. Oncol.* **2005**, *17*, 425.

(16)   Hughes, W.; McDowell, J. A.; Shenep, J.; Flynn, P.; Kline, M. W.; Yogev, R.; Symonds, W.; Lou, Y.; Hetherington, S. *Antimicrob. Agents Chemother.* **1999**, *43*, 609.

(17)   Dejmek, M.; Hřebabecký, H.; Šála, M.; Dračínský, M.; Procházková, E.; Leyssen, P.; Neyts, J.; Balzarini, J.; Nencka, R. *Bioorg. Med. Chem.* **2014**, *22*, 2974.

(18)   Dejmek, M.; Šála, M.; Plačková, P.; Hřebabecký, H.; Mascarell Borreda, L.; Neyts, J.; Dračínský, M.; Procházková, E.; Jansa, P.; Leyssen, P.; Mertliková-Kaiserová, H.; Nencka, R. *Arch. Pharm.* **2014**, *347*, 478.

(19)   Marquez, V. E.; Ben-Kasus, T.; Barchi, J. J., Jr.; Green, K. M.; Nicklaus, M. C.; Agbaria, R. *J. Am. Chem. Soc.* **2004**, *126*, 543.

(20)   Šála, M.; De Palma, A. M.; Hřebabecký, H.; Dejmek, M.; Dračínský, M.; Leyssen, P.; Neyts, J.; Mertlíková-Kaiserová, H.; Nencka, R. *Bioorg. Med. Chem. Lett.* **2011**, *21*, 4271.

(21)   Šála, M.; Dejmek, M.; Procházková, E.; Hřebabecký, H.; Rybáček, J.; Dračínský, M.; Novák, P.; Rosenbergová, Š.; Rosenberg, I.; Nencka, R. *Synthesis* **2015**.

(22)   Park, N. H.; Pavan-Langston, D.; McLean, S. L. *J. Infect. Dis.* **1979**, *140*, 802.

(23)   Pauwels, R.; Balzarini, J.; Schols, D.; Baba, M.; Desmyter, J.; Rosenberg, I.; Holý, A.; De Clercq, E. *Antimicrob. Agents Chemother.* **1988**, *32*, 1025.

(24)   De Clercq, E. *Int. J. Antimicrob. Agents* **1999**, *12*, 81.

(25) Holý, A.; Dvořáková, H.; Masojídková, M. *Collect. Czech. Chem. Commun.* **1995**, *60*, 1390.

(26) De Clercq, E. *Pharmacology* **2001**, *56*, 3.

(27) Snoeck, R.; Schols, D.; Andrei, G.; Neyts, J.; De Clercq, E. *Antiviral Res.* **1991**, *16*, 1.

(28) Chilukuri, S.; Rosen, T. *Dermatol. Clin.* **2003**, *21*, 311.

(29) Hanus, M.; Ryjáček, F.; Kabeláč, M.; Kubař, T.; Bogdan, T. V.; Trygubenko, S. A.; Hobza, P. *J. Am. Chem. Soc.* **2003**, *125*, 7678.

(30) Marek, R.; Sklenář, V. In *Annual Reports on NMR Spectroscopy*; Webb, A. G., Ed.; Elsevier Ltd: Oxford UK, 2005; Vol. 54, p 201.

(31) Dračínský, M.; Pohl, R. In *Annual Reports on NMR Spectroscopy*; Webb, A. G., Ed.; Elsevier Ltd: Oxford UK, 2014, p 59.

(32) Sečkářova, P.; Marek, R.; Maliňáková, K.; Kolehmainen, E.; Hocková, D.; Hocek, M.; Sklenář, V. *Tetrahedron Lett.* **2004**, *45*, 6259.

(33) Sheina, G. G.; Stepanian, S. G.; Radchenko, E. D.; Blagoi, Y. P. *J. Mol. Struct.* **1987**, *158*, 275.

(34) Ramaekers, R.; Maes, G.; Adamowicz, L.; Dkhissi, A. *J. Mol. Struct.* **2001**, *560*, 205.

(35) Benoit, R. L.; Frechette, M. *Can. J. Chem.* **1985**, *63*, 3053.

(36) Costas, M. E.; Acevedo-Chavez, R. *J. Solution Chem.* **2012**, *41*, 864.

(37) Kilpatrick, J. E.; Pitzer, K. S.; Spitzer, R. *J. Am. Chem. Soc.* **1947**, *69*, 2483.

(38) Altona, C.; Geise, H. J.; Romers, C. *Tetrahedron* **1968**, *24*, 13.

(39) Altona, C.; Sundaralingam, M. *J. Am. Chem. Soc.* **1972**, *94*, 8205.

(40) Marquez, V. E.; Siddiqui, M. A.; Ezzitouni, A.; Russ, P.; Wang, J.; Wagner, R. W.; Matteucci, M. D. *J. Med. Chem.* **1996**, *39*, 3739.

(41) Kuhn, B.; Mohr, P.; Stahl, M. *J. Med. Chem.* **2010**, *53*, 2601.

(42) Watson, J. D.; Crick, F. H. C. *Nature* **1953**, *171*, 737.

(43) Cisse, I. I.; Kim, H.; Ha, T. *Nat. Struct. Mol. Biol.* **2012**, *19*, 623.

(44) Gilli, G.; Bellucci, F.; Ferretti, V.; Bertolasi, V. *J. Am. Chem. Soc.* **1989**, *111*, 1023.

(45) Hodge, C. N.; Pierce, J. *Bioorg. Med. Chem. Lett.* **1993**, *3*, 1605.

(46) Menear, K. A.; Adcock, C.; Alonso, F. C.; Blackburn, K.; Copsey, L.; Drzewiecki, J.; Fundo, A.; Le Gall, A.; Gomez, S.; Javaid, H.; Lence, C. F.; Martin, N. M. B.; Mydlowski, C.; Smith, G. C. M. *Bioorg. Med. Chem. Lett.* **2008**, *18*, 3942.

(47) Standara, S.; Maliňáková, K.; Marek, R.; Marek, J.; Hocek, M.; Vaara, J.; Straka, M. *Phys. Chem. Chem. Phys.* **2010**, *12*, 5126.

(48) Simpson, J. H. *Organic structure determination using 2-D NMR spectroscopy, a problem-based approach*; 2nd ed.; Elsevier Inc., 2012.

(49) Gutowsky, H. S.; Karplus, M.; Grant, D. M. *J. Chem. Phys.* **1959**, *31*, 1278.

(50) Karplus, M. *J. Am. Chem. Soc.* **1963**, *85*, 2870.

(51) Diez, E.; San-Fabian, J.; Guilleme, J.; Altona, C.; Donders, L. A. *Mol. Phys.* **1989**, *68*, 49.

(52) Haasnoot, C. A. G.; de Leeuw, F. A. A. M.; Altona, C. *Tetrahedron* **1980**, *36*, 2783.

(53) Eyring, H. *J. Chem. Phys.* **1935**, *3*, 107.

(54) Becke, A. D. *J. Chem. Phys.* **1993**, *98*, 5648.

(55) Lee, C.; Yang, W.; Parr, R. G. *Phys. Rev. B* **1988**, *37*, 785.

(56) Leach, A. R. *Molecular Modelling: Principles and Applications*; Pearson Education Limited: Great Britain, 2001.

(57) Wolinski, K.; Hinton, J. F.; Pulay, P. *J. Am. Chem. Soc.* **1990**, *112*, 8251.

(58) Pazderski, L.; Lakomska, A.; Wojtczak, A.; Szlyk, E.; Sitkowski, J.; Kozerski, L.; Kamieński, B.; Kozmiński, B.; Toušek, J.; Marek, R. *J. Mol. Struct.* **2006**, *785*, 205.

(59) Chenon, M. T.; Pugmire, R. J.; Grant, D. M.; Panzica, R. P.; Townsend, L. B. *J. Am. Chem. Soc.* **1975**, *97*, 4636.

(60) Laxer, A.; Major, D. T.; Gottlieb, H. E.; Fischer, B. *J. Org. Chem.* **2001**, *66*, 5463.

(61) Temple, C. J.; Thorpe, M. C.; Coburn, W. C.; Montgomery, J. A. *J. Org. Chem.* **1966**, *31*, 935.

(62) Temple, C. J.; Kussner, C. L.; Montgomery, J. A. *J. Org. Chem.* **1966**, *31*, 2210.

(63) Sutherland, J. D.; Whitfield, J. N. *Tetrahedron* **1997**, *53*, 11595.

(64) Glusker, J. P.; Van der Helm, D.; Love, W. E.; Minkin, J. A.; Patterson, A. L. *Acta Cryst. B* **1968**, *24*, 359.

(65) O'Brien, D. E.; Baiocchi, F.; Robins, R. K.; Cheng, C. C. *J. Med. Chem.* **1963**, *6*, 467.

(66) Arris, C. E.; Boyle, F. T.; Calvert, A. H.; Curtin, N. J.; Endicott, J. A.; Garman, E. F.; Gibson, A. E.; Golding, B. T.; Grant, S.; Griffin, R. J.; Jewsbury, P.; Johnson, L. N.; Lawrie, A. M.; Newell, D. R.; Noble, M. E.; Sausville, E. A.; Schultz, R.; Yu, W. *J. Med. Chem.* **2000**, *43*, 2797.

(67) Olivella, M.; Marchal, A.; Nogueras, M.; Sanchez, A.; Melguizo, M.; Raimondi, M.; Zacchino, S.; Giannini, F.; Cobo, J.; Enriz, R. D. *Bioorg. Med. Chem.* **2012**, *20*, 6109.

(68) Olivella, M.; Marchal, A.; Nogueras, M.; Melguizo, M.; Lima, B.; Tapia, A.; Feresin, G. E.; Parravicini, O.; Giannini, F.; Andujar, S. A.; Cobo, J.; Enriz, R. D. *Arch. Pharm.* **2015**, *348*, 68.

(69) Procházková, E.; Čechová, L.; Janeba, Z.; Dračínský, M. *J. Org. Chem.* **2013**, *78*, 10121.

(70) Smith, M. B. M., J. *March's Advanced Organic Chemistry: Reactions, Mechanisms, and Structure*; 5th ed.; John Wiley & sons, 2001.

(71) Čechová, L.; Procházková, E.; Císařová, I.; Dračínský, M.; Janeba, Z. *Chem. Commun.* **2014**, *50*, 14892.

(72) McGuigan, C.; Sutton, P. W.; Cahard, D.; Turner, K.; O'Leary, G.; Wang, Y.; Gumbleton, M.; De Clercq, E.; Balzarini, J. *Antivir. Chem. Chemother.* **1998**, *9*, 473.

(73) Valette, G.; Pompon, A.; Girardet, J. L.; Cappellacci, L.; Franchetti, P.; Grifantini, M.; La Colla, P.; Loi, A. G.; Perigaud, C.; Gosselin, G.; Imbach, J. L. *J. Med. Chem.* **1996**, *39*, 1981.

(74) Winter, H.; Maeda, Y.; Mitsuya, H.; Žemlička, J. *J. Med. Chem.* **1996**, *39*, 3300.

(75) McGuigan, C.; Murziani, P.; Slusarczyk, M.; Gonczy, B.; Vande Voorde, J.; Liekens, S.; Balzarini, J. *J. Med. Chem.* **2011**, *54*, 7247.

(76) Saboulard, D.; Naesens, L.; Cahard, D.; Salgado, A.; Pathirana, R.; Velazquez, S.; McGuigan, C.; De Clercq, E.; Balzarini, J. *Mol. Pharmacol.* **1999**, *56*, 693.

(77) Dračínský, M.; Procházková, E.; Kessler, J.; Šebestík, J.; Matějka, P.; Bouř, P. *J. Phys. Chem. B* **2013**, *117*, 7297.

(78) Guo, C.; Hickey, M. B.; Guggenheim, E. R.; Enkelmann, V.; Foxman, B. M. *Chem. Commun.* **2005**, 2220.

(79) Fabbiani, F. P. A.; Allan, D. R.; David, W. I. F.; Davidson, A. J.; Lennie, A. R.; S., P.; Pulham, C. R.; E., W. J. *Cryst. Growth Des.* **2007**, *7*, 1115.

(80) Admiraal, G.; Eikelenboom, J. C.; Vos, A. *Acta Cryst. B* **1982**, *38*, 2600.

(81) Chierotti, M. R.; Ferrero, L.; Garino, N.; Gobetto, R.; Pellegrino, L.; Braga, D.; Grepioni, F.; Maini, L. *Chem. Eur. J.* **2010**, *16*, 4347.

(82) Taylor, E. C.; Loux, H. M.; Falco, E. A.; Hitchings, G. H. *J. Am. Chem. Soc.* **1955**, *77*, 2243.

Appendix

List of papers

1. Mertlíková-Kaiserová, H. – Rumlová, M. – Tloušťová, E. – **Procházková, E.** – Holý, A. – Votruba, I.: Point mutations in human guanylate kinase account for acquired resistence to anticancer nucleotide analogue PMEG. *Biochem. Pharmacol.* **2011**; 82, 131–138.

2. **Procházková, E.** – Jansa, P. – Dračínský, M. – Holý, A. - Mertlíková-Kaiserová, H.: Determination of the antioxidative activity of substituted 5-aminopyrimidines. *Free Rad. Res*. **2012**; 46, 61–67.

3. **Procházková, E.** – Čechová, L. – Jansa, P. – Dračínský, M.: Long-range heteronuclear coupling constants in 2,6-disubstituted purine derivatives. *Magn. Reson. Chem.* **2012**; 50, 295–298.

4. **Procházková, E.** – Šála, M. – Nencka, R. – Dračínský, M.: C^6-substituted purine derivatives: an experimental and theoretical ^{1}H, ^{13}C and ^{15}N NMR study. *Magn. Reson. Chem.* **2012**; 50, 181–186.

5. Jansa, P. – Baszczyňski, O. – **Procházková, E.** – Dračínský, M. – Janeba, Z.: Microwave-assisted hydrolysis of phosphonate diesters: an efficient protocol for the preparation of phosphonic acids. *Green Chem.* **2012**; 14, 2282–2288.

6. **Procházková, E.** – Jansa, P. – Březinová, A. – Čechová, L. - Mertlíková-Kaiserová, H. – Holý, A. – Dračínský, M.: Compound instability in dimethyl sulphoxide, case studies with 5-aminopyrimidines and the implications for compound storage and screening. *Bioorg. Med. Chem. Lett.* **2012**; 22, 6405–6409.

7. **Procházková, E.** – Čechová, L. – Janeba, Z. – Dračínský, M.: A switchable intramolecular hydrogen bond in polysubstituted 5-nitrosopyrimidines. *J. Org. Chem.* **2013**; 78, 10121–10133.

8. Dračínský, M. – **Procházková, E.** – Kessler, J. – Šebestík, J. – Matějka, J. – Bouř, P.: Resolution of organic polymorphic crystals by Raman spectroscopy. *J. Phys. Chem. B.* **2013**; 117, 7297–7307.

9. Čechová, L. – **Procházková, E.** – Císařová, I. – Dračínský, M. – Janeba, Z.: Separation of planar rotamers through intramolecular hydrogen bonding in polysubstituted 5-nitrosopyrimidines. *Chem. Commun.* **2014**; 50, 14892–14895.

10. Dejmek, M. – Šála, M. – Plačková, P. – Hřebabecký, H. – Borreda, L.M. – Neyts, J. – Dračínský, M. – **Procházková, E.** – Jansa, P. – Leyssen, P. – Mertlíková-Kaiserová, H. – Nencka, R.: Synthesis of Novel Purine-Based Coxsackievirus Inhibitors Bearing Polycylic Substituents at the N-9 Position. *Arch. Pharm. Chem. Life Sci.* **2014**; 347, 1–8.

11. Dejmek, M. – Hřebabecký, H. – Šála, M. – Dračínský, M. – **Procházková, E.** – Leyssen, P. – Neyts, J. – Balzarini, J. – Nencka, R.: From norbornane-based nucleotide analogs locked in South conformation to novel inhibitors of feline herpes virus. *Bioorg. Med. Chem.* **2014**; 22, 2974–2983.

12. Dejmek, M. – Šála, M. – Hřebabecký, H. – Dračínský, M. – **Procházková, E.** – Chalupská, D. – Klíma, M. – Plačková, P.; Hájek, M. – Andrei, G. – Naesens, L. – Leyssen, P. – Neyts, J. – Balzarini, J. – Bouřa, E. – Nencka, R.: Norbornane-based nucleoside and nucleotide analogues locked in North conformation. *Bioorg. Med. Chem.* **2015**; 23, 184–191.

13. Šála, M. – Dejmek, M. – **Procházková, E.** – Hřebabecký, H. – Rybáček, J. – Dračínský, M. – Novák, P. – Rosenbergová, Š. – Fukal, J. – Sychrovský, V. – Rosenberg, I. – Nencka, R.: Synthesis of locked cyclohexene and cyclohexane nucleic acids (LCeNA and LCNA) with modified adenosine units. *Org. Biomol. Chem.* **2015**; 13, 2703–2715.

14. Mejdrová, I. - Chalupská, D. - Kögler, M. - Šála, M. - Plačková, P. - Baumlová, A. - Hřebabecký, H. - **Procházková, E.** - Dejmek, M. - Guillon, R. - Strunin, D. - Weber, J. - Lee, G. - Birkus, G. - Mertlíková-Kaiserová, H. - Bouřa, E. – Nencka, R.: Highly selective PI4K IIIβ inhibitors and structural insight into their mode of action. *J. Med. Chem.* **2015**; 58, 3767–3793.

15. Šála, M. – Dejmek, M. – **Procházková, E.** – Hřebabecký, H. – Rybáček, J. – Dračínský, M. – Novák, P. – Rosenbergová, Š. – Rosenberg, I. – Nencka, R.: A new analogue of locked cyclohexane nucleic acids. *Synthesis* **2015**; DOI: 10.1055/s-0034-1380744.

16. Hřebabecký, H. – **Procházková, E**. – Šála, M. – Plačková, P. – Tloušťová, E. – Barauskas, O. – Lee, Y.J. – Tian, Y. – Mackman, R. – Nencka, R.: Synthesis of conformationally restricted 6- and 7- membered ring bicycloribonucleosides/tides and their recognition by kinases and polymerases. *Org. Biomol. Chem.* **2015**; under review.

LIST OF CONFERENCES

Lectures

1. *NMR studies of purine derivatives*
   Procházková E., Čechová L., Jansa P., Šála M., Nencka R, Dračínský M.
   XXVII. Central European NMR meeting 2012, Valtice, Czech Republic

2. *Strong intramolecular hydrogen bonds in 5-nitrosopyrimidines studied by NMR spectroscopy*
   Procházková E., Čechová L., Janeba Z., Dračínský M.
   XXVIII. Central European NMR meeting 2013, Valtice, Czech Republic

3. *Antioxidační účinky pyrimidinových derivátů a jejich stabilita v DMSO*
   Procházková E., Březinová A., Čechová L., Jansa P., Holý A., Mertlíková-Kaiserová H., Dračínský M.
   XIII. Mezioborové setkání mladých biologů, biochemiků a chemiků 2013, Žďár nad Sázavou, Czech Republic

4. *Conformational analysis and enzymatic decomposition of a locked nucleoside phosphoramidates using NMR spectroscopy*
   Procházková E., Hřebabecký H., Nencka R., Dračínský M.
   XXIX. Central European NMR meeting 2014, Valtice, Czech Republic

5. *Vliv substituentů na intramolekulární vodíkové vazby u polysubstituovaných 5-nitrosopyrimidinů*
   Procházková E., Čechová L., Janeba Z., Dračínský M.
   XIV. Mezioborové setkání mladých biologů, biochemiků a chemiků 2014, Milovy, Czech Republic

6. *"Planamerism": A novel stereochemical phenomenon?*
   Procházková E., Čechová L., Císařová I., Janeba Z., Dračínský M.
   XXX. Central European NMR meeting 2015, Valtice, Czech Republic

7. *Konformační analýza a enzymové štěpení fosforamidátového proléčiva konformačně uzamčeného nukleosidu*
   Procházková E., Hřebabecký H., Nencka R., Dračínský M.
   XV. Mezioborové setkání mladých biologů, biochemiků a chemiků 2015, Milovy, Czech Republic

Posters

1. *Antioxidative activity of substituted 5-aminopyrimidines and their oxidative self-condensation in dimethyl sulfoxide*
Procházková E., Březinová A., Jansa P., Holý A., Mertlíková-Kaiserová H., Dračínský M.
EuCheMS Chemistry congress 2012, Prague, Czech Republic

2. *Substituent effects on intramolecular hydrogen bonds in 5-nitrosopyrimidine derivatives*
Procházková E., Čechová L., Janeba Z., Dračínský M.
European Symposium on Organic Reactivity 2013, Prague, Czech Republic

3. *NMR investigation of strong intramolecular hydrogen bonds in 5-nitrosopyrimidines*
Procházková E., Čechová L., Janeba Z., Dračínský M.
A European Magnetic Resonance meeting 2013, Hersonissos, Crete, Greece

4. *NMR investigation of strong intramolecular hydrogen bonds in 5-nitrosopyrimidines*
Procházková E., Čechová L., Janeba Z., Dračínský M.
Small molecule NMR conference 2013, Santiago de Compostela, Spain

5. Enzymatic decomposition of a locked nucleoside phosphoramidate monitored by ^{31}P NMR spectroscopy
Procházková E., Hřebabecký H., Nencka R., Dračínský M.
Symposium on Chemistry of Nucleic Acid Components 2014, Český Krumlov, Czech Republic

6. *"Planamerism": A novel stereochemical phenomenon?*
Procházková E., Čechová L., Císařová I., Janeba Z., Dračínský M.
Small molecule NMR conference 2014, Atlanta, Georgia, USA

I.

Šála, M. – Dejmek, M. – **Procházková, E.** – Hřebabecký, H. – Rybáček, J. – Dračínský, M. – Novák, P. – Rosenbergová, Š. – Fukal, J. – Sychrovský, V. – Rosenberg, I. – Nencka, R.:

Synthesis of locked cyclohexene and cyclohexane nucleic acids (LCeNA and LCNA) with modified adenosine units.

Org. Biomol. Chem. **2015**; 13, 2703–2715.

Organic & Biomolecular Chemistry

PAPER

Synthesis of locked cyclohexene and cyclohexane nucleic acids (LCeNA and LCNA) with modified adenosine units†

Michal Šála,* Milan Dejmek, Eliška Procházková, Hubert Hřebabecký, Jiří Rybáček, Martin Dračínský, Pavel Novák, Šárka Rosenbergová, Jiří Fukal, Vladimír Sychrovský, Ivan Rosenberg and Radim Nencka*

We describe here the preparation of conformationally locked cyclohexane nucleic acids designed as hybrids between locked nucleic acids (LNAs) and cyclohexene nucleic acids (CeNAs), both of which excel in hybridization with complementary RNAs. We have accomplished the synthesis of these adenine derivatives starting from a simple ketoester and installed all four chiral centres by means of total synthesis. The acquired monomers were incorporated into nonamer oligonucleotides.

Introduction

Oligonucleotides with modified sugar moieties have found many applications in modern technologies such as antisense oligonucleotides, RNA interference (RNAi), ribozymes, DNAzymes and aptamers. The stabilization of the duplexes with complementary mRNA of interest is an essential concept for oligonucleotide-mediated regulation of the gene expression. Extensive hybridization with the target sequence and selectivity towards mRNA in comparison with affinity to complementary DNA are important features of the desired technologies.[1]

Although various sugar modifications have led to the enhancement of the hybridization properties of antisense oligonucleotides, probably the most famous modifications are based on monomers with a bridge between the 2′ and 4′ positions of the ribose ring. This results in the stabilization of the 3′-*endo* conformation and the formation of bridged nucleic acids (BNAs).[2] Imanishi's[3] and Wengel's[4] groups have independently synthesized monomers for 2′,4′-bridged nucleic acids/locked nucleic acids (LNA, **1**) and reported their hybridization properties after incorporation into oligonucleotides (Fig. 1). LNAs have also been successfully used for both RNAi[5] and selection of aptamers.[6] Since then, a number of compounds with alternative bridges (*e.g.* **2–4**) have been prepared, especially in order to increase the nuclease resistance of the resulting oligonucleosides.[7] Carba-LNAs (*e.g.* **2**)[8] have also

been prepared. They seem to possess a significantly increased nuclease resistance in comparison with traditional LNAs without a dramatic effect on the RNAse H mediated cleavage of the target RNA.[9] Recently LNAs modified on the nucleobase have been reported as well.[10]

In contrast to LNA-based oligonucleotides, which usually form stable duplexes with both RNA and DNA, cyclohexene nucleic acids (CeNA, **5**), developed by Herdewijn *et al.*, exert significant selectivity in hybridization with RNA over DNA.[11] The same research team has also suggested that the cyclohexene moiety can serve as an appropriate bioisostere of the
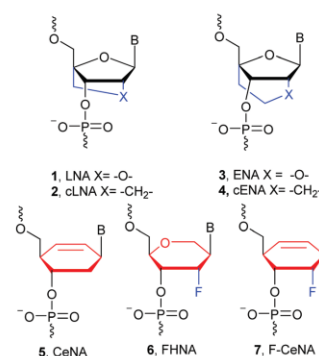
Fig. 1 The structures of selected nucleic acids with sugar modification including LNA analogues (1–4) and six-membered carbohydrate mimics (5–7).

Gilead Sciences & IOCB Research Centre, Institute of Organic Chemistry and Biochemistry, Academy of Sciences of the Czech Republic, v.v.i. Flemingovo n. 2, 16610 Prague, Czech Republic. E-mail: sala@uochb.cas.cz, nencka@uochb.cas.cz
†Electronic supplementary information (ESI) available. See DOI: 10.1039/c4ob02193b

This journal is © The Royal Society of Chemistry 2015

Org. Biomol. Chem., 2015, **13**, 2703–2715 | **2703**

natural furanose ring[11b] and proved that this pseudosugar exerts significant flexibility while being incorporated into the structure of oligonucleotides. The crystal structures of duplexes with complementary DNA and RNA oligomers have clearly demonstrated that the cyclohexene moiety can interconvert between two distinct conformations $^2H_3$ (similar to C2'-endo) and $^3H_2$ (similar to C3'-endo).[12,13]

Recently, Seth *et al.* have shown that 2'-fluoro hexitol nucleic acids (FHNA, **6**) exhibit higher duplex stability compared to 2'-fluoro CeNA (F-CeNA, **7**) due to higher rigidity and superior stabilization in C3'-endo-like conformation.[14,25]

The major objective of our presented study was the preparation of hybrid derivatives merging LNAs and CeNAs in order to stabilize the cyclohexene moiety in $^3H_2$ conformation resembling the C3'-endo, which is preferred by CeNA while forming a duplex with complementary RNA strands.[13] In addition, the synthesis of locked cyclohexene nucleic acid (LCeNA) monomers made it easy to obtain saturated monomers bearing a cyclohexane ring instead of the original cyclohexene one (LCNA).

Although the obvious way to reach these compounds in an asymmetric fashion led through extending the synthesis of CeNA by methods for the preparation of LNA from sugar precursors,[15] we decided to explore a synthetic approach, which would result in this type of compound starting from simple precursors avoiding the use of a chiral pool or enzymatic resolution of synthetically complicated nucleosides. In order to be able to determine the enantiomeric purity of our compounds, we initially performed racemic synthesis of the desired monomers (see the ESI†).

Results and discussion

The retrosynthetic analysis is outlined in Fig. 2. The crucial step of the synthesis is the construction of the first stereogenic centre by Michael conjugated addition of the acrolein to starting material **8** catalysed by the quinine based organocatalyst (Q-PHN-OH) immediately followed by cyclization to build a bicyclic ring system (bicyclo[3.2.1]octane). Further transform-
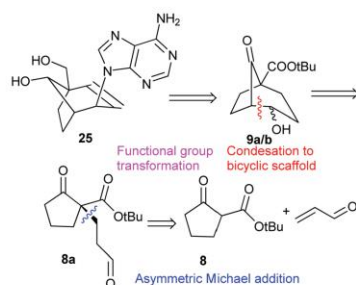
Fig. 2 Retrosynthetic analysis.

ations of the functional groups lead to the desired final nucleoside **25**.

The asymmetric synthesis of the desired monomers started from the ester **8**[16] (Scheme 1), which was treated with acrolein together with a quinine organocatalyst (Q-PHN-OH) by following the published synthetic protocol.[17] The crude aldehyde intermediate **8a** was cyclized with cesium carbonate[18] in toluene to afford a mixture of bicyclic compounds **9a** and **9b** (87% yield, 2 steps, ratio ~3 : 2, GC-MS analysis). Alcohols **9a** and **9b** were used as a mixture (Scheme 1), their keto group protected as a ketal and the ester group of **10** was reduced by lithium aluminum hydride to an inseparable diastereomeric mixture of alcohols **11**. The primary hydroxy group was protected by benzoylation at low temperature and the obtained mixture of the monobenzoylated compounds **13** (**13a**, **13b**, separable) and the dibenzoylated compound **12** (only the compound with an equatorial hydroxyl group was dibenzoylated) was separated. The benzoylation procedure employing BzCN was also attempted but without any improvement in the yields of the monobenzoylated products **13**. Compound **12** can be easily methanolyzed in high yield to the starting diol **11**,
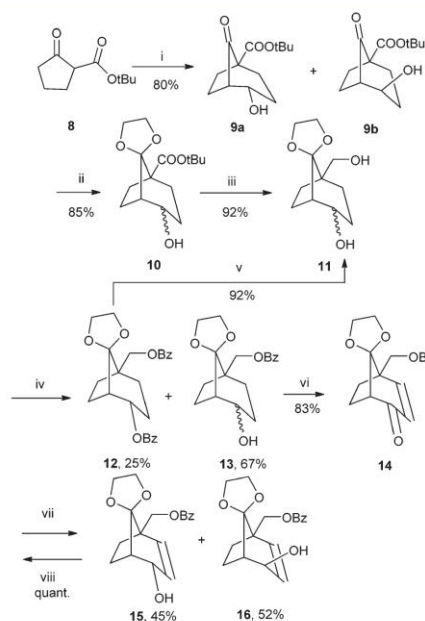
Scheme 1 Synthesis of compound **16**. Reagents and conditions: (i) (a) Q-PHN-OH,[17] acrolein, CH$_2$Cl$_2$, −25 °C; (b) Cs$_2$CO$_3$, toluene, r.t.. (ii) ethylene glycol, PPTS, benzene, 100 °C; (iii) LiAlH$_4$, Et$_2$O; (iv) BzCl, pyridine, CH$_2$Cl$_2$, −40 °C; (v) MeONa, MeOH; (vi) IBX, DMSO, TsOH, 90 °C; (vii), NaBH$_4$, CeCl$_3$, MeOH, 0 °C; (viii) MnO$_2$, CH$_2$Cl$_2$.

which can be re-used in the benzoylation reaction. In one step, the hydroxy group of **13** was oxidized to a keto group and a double bond was introduced to the scaffold by IBX oxidation according to the procedure described by Nicolaou.[19] This procedure progressed smoothly with an excellent yield (83%). Allylketone **14** was then subjected to the Luche reduction[20] and the obtained alcohols **15** and **16** were easily separated by column chromatography. The undesired alcohol **15** can be oxidized back to ketone **14** by manganese dioxide and thus recycled.

The ketone-protecting group of **16** was easily removed by the reaction with *p*-toluenesulfonic acid in a refluxing acetone–water mixture (Scheme 2). The keto group of the derivative **17** was then reduced to a hydroxy group by sodium triacetoxyborohydride. The hydroxy group in the position C-4 participates in this reaction and allows to prepare exclusively

the product with the desired orientation of the C-8 hydroxy group in diol **18**.[21] Although we tried numerous methodologies for the direct introduction of the purine nucleobase (including Tsuji–Trost reaction, Mitsunobu reaction and various direct alkylation methods) using diversely protected derivatives of compound **18** and its congeners with opposite configuration of the allylic hydroxyl, they all failed to give an appropriate product either due to low reactivity or undesired allylic rearrangements resulting in complex mixtures of products. Both the hydroxy groups were sequentially protected afterwards, the allylic hydroxyl was selectively protected by the TBDMS group and the C-8 hydroxyl by benzoylation. The TBDMS group was then cleaved by TBAF/acetic acid (the reaction mixture is less basic) at an elevated temperature (the reaction at r.t. is relatively slow) and the free allylic hydroxy group was converted to chloro derivative **21**, followed by the introduction of the azido group by NaN$_3$. At this stage, we were able to separate isomers **22** and **22a** (a product of the allylic rearrangement) and we also discovered that the undesired isomer **22a** can be easily converted to **22** by standing in acetonitrile solution or better by heating this solution overnight.[22] The allylic rearrangement of **22a** was monitored by ^{1}H NMR spectroscopy (see the ESI†).

The key amine **23** was prepared by the Staudinger reaction, followed by the removal of the benzoyl protecting groups under basic conditions (Scheme 2). A purine nucleobase was then introduced in moderate yield (42%) by a recently described MW-assisted build-up protocol.[23] Chloropurine derivative **24** was converted to adenine nucleoside **25** by ammonolysis with ethanolic ammonia under microwave conditions.[23,24] The enantiomeric purity of this LCeNA monomer **25** was determined by chiral HPLC, which assessed the enantiomeric purity above 98%. The saturated analogue **26** was obtained after hydrogenation in high yield (89%). Both nucleosides (**25** and **26**) were used as building blocks for the synthesis of monomeric phosphoramidite units, which were subsequently used for the solid-state oligonucleotide synthesis.

All the compounds were appropriately characterized by ^{1}H and ^{13}C NMR and also by 2D NMR techniques (COSY, HSQC, HMBC). The configuration of the chiral centres at C8 and C4 of compound **25** was confirmed by 2D NMR techniques (COSY, ROESY). In the COSY spectrum, 2- and 3-bond spin–spin interactions are visible as cross-peaks. When the hydrogen atoms are in a W-like arrangement, it is possible to see 4-bond long-range couplings. Due to this fact, it was possible to confirm stereochemistry at C-8, where we found W-like long-range couplings between H8 and H7 (Fig. 3 top). The configuration was also confirmed by the ROESY spectrum, where the cross-peaks correspond to the through-space interactions. The H8–H8′ cross-peak clearly determined not only the configuration at the C8 atom, but also the C4 atom; the nucleobase must be above the cycle. For nucleoside **25** we also calculated spin–spin coupling constants by the DFT method (B3LYP/6-31+G(d,p)), which were in agreement with the experimental data (see Table S3 in ESI†).

Scheme 2 Synthesis of nucleosides **25** and **26**. Reagents and conditions: (i) TsOH, acetone–H$_2$O, reflux; (ii) NaBH(OAc)$_3$, AcOH, CH$_3$CN, 0 °C to r.t.; (iii) (a) TBDMSCl, imidazole, CH$_2$Cl$_2$, 0 °C, (b) BzCl, pyridine, r.t.; (iv) TBAF, AcOH–THF, 60 °C; (v) NCS, PPh$_3$, CH$_2$Cl$_2$, 0 °C; (vi) NaN$_3$, DMF, 65 °C; (vii) CH$_3$CN, reflux; (ix) (a) PPh$_3$, THF, r.t., (b) H$_2$O, (c) KOH, EtOH–H$_2$O, reflux; (x) 4,6-dichloro-5-formamidopyrimidine, DIPEA, *n*-BuOH, MW, 160 °C; (xi) NH$_3$–EtOH, MW, 140 °C; (xii) H$_2$ (10 bar), Pd(OH)$_2$/C, MeOH, 50 °C.

This journal is © The Royal Society of Chemistry 2015

Org. Biomol. Chem., 2015, **13**, 2703–2715 | **2705**

Fig. 3 Region of COSY (in blue) and ROESY spectrum (in red) for compound **25**. W-like shaped long-range coupling constant between H8 and H7-*endo* clearly determined the configuration at carbon C-8. Through-space interaction H8–H8' confirmed the configuration at carbon C-4.

Synthesis of the phosphoramidites **29** and **31** which were used in the solid phase oligonucleotide synthesis is depicted in Scheme 3. We used a traditional approach and obtained the desired compounds in good yields. The obtained phosphoramidites **29** and **31** were then used in the classical trityl-off phosphoramidite method for solid-supported oligonucleotide synthesis.

The hybridization properties of the modified oligonucleotides with their natural DNA and RNA counterparts were evaluated by UV thermal denaturation experiments and the obtained T_m values were compared with those of the corresponding unmodified duplexes (Table 1).

To our surprise, a striking destabilization effect was observed for both LCeNA and LCNA. Although some destabili-
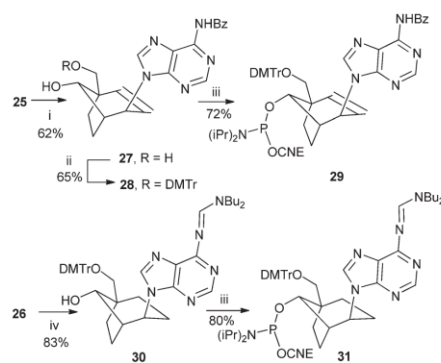
Scheme 3 Synthesis of phosphoramidites **29** and **31**. Reagents and conditions: (i) (a) TMSCl, pyridine, 0 °C, (b) BzCl, pyridine, r.t., (c) aq. NH₃, MeOH; (ii) DMTrCl, pyridine, r.t.; (iii) 2-cyanoethyl *N,N*-diisopropyl-chlorophosphoramidite, DIPEA, THF, r.t.; (iv) (a) dimethylacetal-*N,N*-dibutylformamide, MeOH, r.t., (b) DMTrCl, pyridine, r.t.; CNE = cyanoethyl.

Table 1 Thermal stability of modified oligonucleotide duplexes[a]

Oligonucleotide	ssRNA T_m $(\Delta T_m)^b$	ssDNA T_m $(\Delta T_m)^b$
5′-d(GCA²⁵TA²⁵TCA²⁵C)	22.0 (−4.3 °C)	No comp. form.
5′-r(GCA²⁵UA²⁵UCA²⁵C)	23.0 (−7.7 °C)	22.0 (-4.3 °C)
5′-d(GCA²⁶TA²⁶TCA²⁶C)	No comp. form.	No comp. form.
5′-r(GCA²⁶UA²⁶UCA²⁶C)	No comp. form.	No comp. form.

[a] 4 μM duplex in 50 mM NaH₂PO₄–Na₂HPO₄ pH 7.2 with 100 mM NaCl. [b] per modification.
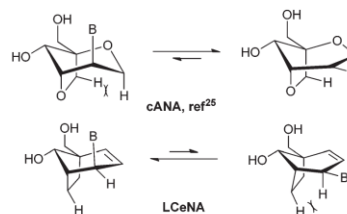
Fig. 4 In contrast to the preferred conformation of cANA, LCeNA should adopt a conformation that situates the nucleobase in an "axial-like" orientation due to the repulsion of the hydrogen atom of the −CH₂CH₂− bridge and the hydrogen atom vicinal to the nucleobase.

zation was observed by Migawa *et al.*[25] on structural related cANA derivatives, the drop in affinity is significantly larger in this case and cannot be clarified by the explanation suggested in their work, because the repulsion of the hydrogen in the bridge and the six-membered pseudosugar ring in cANA and LCeNA should lead to opposite effects (Fig. 4). Unfortunately,

2706 | *Org. Biomol. Chem.*, 2015, **13**, 2703–2715

This journal is © The Royal Society of Chemistry 2015

similar destabilization effects were observed also for homo-oligomers prepared from both LCeNA and LCNA subunits while hybridized with complementary oligothymidylates (see the ESI†).

To shed some light on the significant destabilization of the rLCeNA-RNA duplex, we performed the molecular dynamics simulations of RNA duplexes that included normal and locked units. (For a detailed analysis of the calculated results, structural models, and calculation method see ESI†). The values of backbone torsion angles α, γ, and δ calculated for the units of RNA oligonucleotides (Fig. S8–S13†) were analysed and statistical distributions of the torsion angles (Fig. S14†) were compared. The calculations unveiled a significant structural disorder of modified duplexes as compared to the A-RNA structure that was calculated for the duplex that included normal units. The deviations of modified oligonucleotides from canonical A-RNA occurred particularly owing to the irregular behaviour of the normal units neighbouring with modified units. The modified units were structurally more rigid though their behaviour was abnormal. In particular, the sugar of modified nucleosides was locked (δ torsion was *ca.* 60°) while the sugar of the normal units was flexible (δ torsion ranged from *ca.* 80° to *ca.* 160°). The overall values of α backbone torsions in the neighbourhood of modified residues were smaller by *ca.* 30° as compared to the typical value known for canonical A-RNA. The α-distribution calculated for locked units broadened, which indicated larger amplitudes of motion near phosphate. The α and γ torsions of phosphate groups bridging the locked unit with neighbouring normal units frequently flipped between the values characteristic to A-RNA, $\alpha/\gamma \approx 290°/70°$, and the values calculated owing to locked units, $\alpha/\gamma \approx 180°/180°$. The α-distributions of a normal A-RNA duplex were always single-modal and centered at 290° in contrast to bi- or even tri-modal α-distributions calculated in the neighbourhood of locked units (Fig. S14†). The calculations indicated instabilities and structural disorders of the normal residues in the neighbourhood of modified units. Moreover, the occurrence of α/γ flips depended on the positioning of phosphate groups with respect to 3′-end and 5′-end of locked units. The conformationally locked residues of RNA duplexes thus induced particularly irregular behaviour of backbone phosphates in the vicinity of the modified units.

Conclusions

In conclusion, we have prepared novel modified oligonucleotides containing monomers based on bicyclo[3.2.1]octene and octane skeletons as hybrids of CeNA/CNA and LNA. The appropriate monomers were synthesized from a simple achiral precursor – ketoester **8**. As far as we know, this is the first synthesis of the LNA analogues performed by a total synthetic approach. Our molecular dynamics calculations suggest that a surprisingly low affinity of the modified oligonucleotides towards the complementary DNA and RNA results from the irregular behaviour of the nucleotides neighbouring with the

locked units. The overall structure of the duplex containing locked units was significantly disordered and more conformationally labile in comparison with an A-RNA form of a normal duplex.

Experimental section

General

Melting points were determined on a Büchi B-540 apparatus. NMR spectra (δ, ppm; J, Hz) were measured on a Bruker Avance II-600 and/or Bruker Avance II-500 instruments (600.1 or 500.0 MHz for ^{1}H and 150.9 or 125.7 MHz for ^{13}C) in hexa-deuterated dimethyl sulfoxide and referenced to the solvent signal (δ 2.50 and 39.70, respectively). Mass spectra were measured on a LTQ Orbitrap XL (Thermo Fisher Scientific) by electrospray ionization (ESI). Column chromatography was performed on Silica gel 60 (Fluka) and thin-layer chromatography (TLC) on Silica gel 60 F254 foils (Merck). Solvents were evaporated at 2 kPa and bath temperature 30–60 °C; the compounds were dried at 13 Pa and 50 °C. The elemental analyses were obtained using a Perkin–Elmer CHN Analyzer 2400, Series II Sys (Perkin–Elmer). The elemental compositions for all compounds agreed to within ±0.4% of the calculated values. For all the tested compounds satisfactory elemental analysis was obtained supporting >95% purity. Optical rotation was measured on a polarimeter Autopol IV (Rudolph Research Analytical) at 589 nm wavelength in chloroform or methanol. Microwave syntheses were carried out using a CEM Discover instrument with a single-mode cavity and focused microwave heating (microwave power supply 0–300 W, 1 W increments, sealed vessel mode, pressure range 0–20 bar). GC-MS analyses were recorded by using a 5975B quadrupole mass spectrometer coupled to a 6890N gas chromatograph (Agilent, Santa Clara, CA, USA) equipped with a Phenomenex ZB-5 HT capillary column (30 m × 0.25 mm, film thickness 0.25 μm); temperature: 60 °C (2 min), then 10 °C min^{-1} to 320 °C (10 min).

Preparation of compounds 9a and 9b

To a mixture of starting material **8** (9.05 g, 49.1 mmol) and a catalyst Q-PHN-OH^{17} (2.40 g, 4.93 mmol, 0.1 eq.) in dry CH_2Cl_2 (100 mL) at −25 °C under an argon atmosphere, a solution of acrolein (8.23 mL, 123 mmol, 2.5 eq.) in CH_2Cl_2 (30 mL) was added dropwise. The reaction mixture was occasionally stirred (>95% of time without stirring) and kept at −25 °C for 24 h. Then the reaction mixture was poured into a silica gel column (200 g, Et_2O) and the crude product was eluted with Et_2O. Fractions containing the product were collected and evaporated to afford a crude intermediate (12.53 g) which was used immediately in the next step. The crude catalyst was then eluted from the column using methanol and recycled (chromatography on a silica gel column in CH_2Cl_2–ethanol 25 : 1). The crude intermediate was dissolved in toluene (350 mL), cesium carbonate (8.48 g, 26 mmol) was then added and the reaction mixture was stirred at r.t. overnight. Solids were removed by filtration through Celite and the filtrate was evaporated. The product

This journal is © The Royal Society of Chemistry 2015

Org. Biomol. Chem., 2015, **13**, 2703–2715 | **2707**

was purified on a silica gel column (250 g, toluene–ethyl acetate 3 : 1 → 2 : 1) to afford 9.416 g (80%) of the mixture **9a** and **9b** (GC chromatogram, Fig. S1†). Analytical samples of both isomers were obtained by column chromatography of the sample (300 mg of the mixture, 100 g of silica gel, toluene–ethyl acetate 3 : 1 → 2 : 1). For the determination of the optical purity of this step see the ESI.†

***tert*-Butyl (1*S*,4*S*,5*S*)-4-hydroxy-8-oxobicyclo[3.2.1]octane-1-carboxylate (9a).** Viscous oil. $[\alpha]_D^{20}$ = −22.8 (*c* 0.325, CHCl$_3$). Found: C, 65.26; H, 8.39. Calc. for C$_{13}$H$_{20}$O$_4$: C, 64.98; H, 8.39%. ^{1}H NMR (500 MHz, d6-DMSO): δ 1.39 (s, 9H, *t*Bu), 1.48–1.58 (m, 1H, H-3a), 1.67–1.87 (m, 5H, H-3b, H-7a, H-6ex, H-2), 1.90–1.97 (m, 1H, H-6en), 2.30–2.36 (m, 1H, H-7b), 2.38 (dd, J_{5-4} = 3.1, J_{5-6ex} = 6.7, 1H, H-5), 3.76–3.82 (m, 1H, H-4), 5.14 (d, J_{OH-4} = 4.5, 1H, OH). ^{13}C NMR (125.7 MHz, d6-DMSO): δ 16.02 (C-6), 26.52 and 26.63 (C-3 and C-7), 27.86 (C(CH$_3$)$_3$), 31.05 (C-2), 54.37 (C-5), 57.05 (C-1), 73.00 (C-4), 80.47 (C(CH$_3$)$_3$), 170.27 (COOtBu), 211.58 (C-8). ESI MS, *m/z* (rel%): 263 (100) [M + Na]. HRMS: calcd for [M + Na]: 263.12538, found: 263.12541.

***tert*-Butyl (1*S*,4*R*,5*S*)-4-hydroxy-8-oxobicyclo[3.2.1]octane-1-carboxylate (9b).** Viscous oil. $[\alpha]_D^{20}$ = −5.5 (*c* 0.381, CHCl$_3$). Found: C, 65.17; H, 8.56. Calc. for C$_{13}$H$_{20}$O$_4$: C, 64.98; H, 8.39%. ^{1}H NMR (500 MHz, d6-DMSO): δ 1.39 (s, 9H, *t*Bu), 1.49 (ddm, $J_{3ax-2ax}$ = 5.3, J_{gem} = 14.8, 1H, H-3ax), 1.57 (dddd, J_{6en-5} = 0.8, $J_{6en-7ex}$ = 4.4, $J_{6en-7en}$ = 10.8, J_{gem} = 13.3, 1H, H-6en), 1.77–1.85 (m, 2H, H-2eq, H-6ex), 1.87–1.95 (m, 2H, H-7en, H-3eq), 2.25–2.36 (m, 3H, H-5, H-2ax, H-7ex), 4.06–4.09 (m, 1H, H-4), 4.99 (dm,J_{OH-4} = 2.8, 1H, OH). ^{13}C NMR (125.7 MHz, d6-DMSO): δ 18.67 (C-6), 25.16 (C-7), 25.51(C-7), 27.94 (C(CH$_3$)$_3$), 33.35 (C-2), 51.96 (C-5), 57.28 (C-1), 76.38 (C-4), 80.34 (C(CH$_3$)$_3$), 170.42 (COOtBu), 211.44 (C-8). ESI MS, *m/z* (rel%): 263 (100) [M + Na]. HRMS: calcd for [M + Na]: 263.12538, found: 263.12541.

Preparation of compounds 10a and 10b

A mixture of alcohols **9a** and **9b** (9.1 g, 37.9 mmol) was dissolved in benzene (320 mL) and pyridinium *p*-toluenesulfonate (1.97 g, 7.8 mmol) and ethylene glycol (9.2 mL) were then added. The reaction mixture was heated to reflux with a Dean–Stark trap for 24 hours and then cooled to r.t., diluted with ethyl acetate (450 mL) and washed with water (300 mL) and saturated aq. sodium bicarbonate (2 × 300 mL). The organic phase was dried over sodium sulfate and evaporated. The residue was purified on a silica gel column (350 g, toluene–ethyl acetate 1 : 1) to obtain 9.15 g (85%) of the mixture of **10a** and **10b**. Analytical samples of both isomers were obtained after chromatography of the sample (300 mg of the mixture, toluene–ethyl acetate 3 : 1 → 2 : 1).

***tert*-Butyl (1*S*,4*S*,5*S*)-4-hydroxy-1*H*-spiro[bicyclo[3.2.1]octane-8,2′-[1,3]dioxolane]-1-carboxylate (10a).** Viscous oil. $[\alpha]_D^{20}$ = −22.4 (*c* 0.277, CHCl$_3$). Found: C, 63.24; H, 8.53. Calc. for C$_{15}$H$_{24}$O$_5$: C, 63.36; H, 8.51%. ^{1}H NMR (500 MHz, d6-DMSO): δ 1.14–1.22 (m, 1H, H-3eq), 1.32–1.49 (m, 12H, *t*Bu, H-2eq, H-6ex, H-7en), 1.54–1.60 (m, 1H, H-6en), 1.61–1.67 (m, 1H, H-3ax), 1.82 (dd, J_{5-4} = 3.1, J_{5-6ex} = 6.4, 1H, H-5), 1.95–2.02 (m,

1H, H-2ax), 2.17–2.24 (m, 1H, H-7ex), 3.76–3.91 (m, 5H, −OCH$_2$CH$_2$O−, H-4), 4.45 (d, J_{OH-4} = 4.6, 1H, OH). ^{13}C NMR (150.92 MHz, d6-DMSO): δ 17.70 (C-6), 26.37 (C-3), 27.80 (C(CH$_3$)$_3$), 28.10 (C-7), 29.85 (C-2), 49.23 (C-5), 52.38 (C-1), 63.93 and 65.42 (−OCH$_2$CH$_2$O−), 67.78 (C-4), 79.26 (C(CH$_3$)$_3$), 116.08 (C-8), 172.49 (COOtBu). ESI MS, *m/z* (rel%): 307 (100) [M + Na]. HRMS: calcd for [M + Na]: 307.15160, found: 307.15163.

***tert*-Butyl (1*S*,4*R*,5*S*)-4-hydroxy-1*H*-spiro[bicyclo[3.2.1]octane-8,2′-[1,3]dioxolane]-1-carboxylate (10b).** Viscous oil. $[\alpha]_D^{20}$ = −21.7 (*c* 0.373, CHCl$_3$). Found: C, 63.29; H, 8.69. Calc. for C$_{15}$H$_{24}$O$_5$: C, 63.36; H, 8.51%. ^{1}H NMR (500 MHz, d6-DMSO): δ 1.14 (ddd, $J_{6en-7ex}$ = 4.4, $J_{6en-7en}$ = 10.0, J_{gem} = 13.0, 1H, H-6en), 1.38 (s, 9H, *t*Bu), 1.39–1.46 (m, 2H, H-2eq, H-3eq), 1.56 (ddd, $J_{7en-6ex}$ = 4.7, $J_{7en-6en}$ = 10.8, J_{gem} = 13.3, 1H, H-7en), 1.64–1.73 (m, 2H, H-3ax, H-6ex), 1.91 (dd,J_{5-4} = 4.0, J_{5-6ex} = 7.2, 1H, H-5), 2.18 (dddm, $J_{7ex-6en}$ = 4.4, $J_{7ex-6ex}$ = 12.5, J_{gem} = 13.3, 1H, H-7ex), 2.32 (tdd, $J_{2ax-7ex}$ = 1.4, $J_{2ax-3ax}$ = 5.6, $J_{2ax-3eq}$ = J_{gem} = 13.7, 1H, H-2ax), 3.67–3.72 (m, 1H, H-4), 3.82–4.03 (m, 4H, −OCH$_2$CH$_2$O−), 4.14 (d, J_{OH-4} = 9.6, 1H, OH). ^{13}C NMR (125.7 MHz, d6-DMSO): δ 21.60 (C-6), 25.99 (C-3), 26.38 (C-7), 27.82 (C(CH$_3$)$_3$), 29.36 (C-2), 45.37 (C-5), 52.48 (C-1), 63.98 and 65.73 (−OCH$_2$CH$_2$O−), 72.65 (C-4), 79.48 (C(CH$_3$)$_3$), 116.32 (C-8), 172.00 (COOtBu). ESI MS, *m/z* (rel%): 307 (100) [M + Na]. HRMS: calcd for [M + Na]: 307.15160, found: 307.15165.

Preparation of compounds 13a and 13b

A mixture of alcohols **10a** and **10b** (9.79 g, 34.43 mmol) was dissolved in anhydrous ether (1000 mL) and cooled down with ice bath (argon atmosphere). A solution of LiAlH$_4$ in THF (60.5 mL, 1 M solution, 1.75 eq.) was added dropwise in 30 minutes. The reaction was allowed to slowly reach room temperature and was stirred overnight, then cooled again to 0 °C and quenched with ice. Solids were removed by filtration through a Celite pad and thoroughly washed with ethanol. The filtrate was concentrated and the residue was chromatographed on a silica gel column (300 g, ethyl acetate–ethanol 20 : 1) to afford an inseparable mixture of the diols (11, 6.86 g, 92%).

(1*S*,5*R*)-1-(Hydroxymethyl)spiro[bicyclo[3.2.1]octane-8,2′-[1,3]dioxolan-4-ol (11). Viscous oil. Found: C, 61.78; H, 8.43. Calc. for C$_{11}$H$_{18}$O$_4$: C, 61.66; H, 8.47%. CI MS, *m/z* (rel%): 214 (5) [M + H], 197 (100) [M − OH]. HRMS: calcd for [M + H]: 215.1283, found: 215.1286.

Benzoylation of the diol 11

Compound **11** (7.267 g, 33.9 mmol) was dissolved in CH$_2$Cl$_2$ (300 mL) and pyridine was added (5.5 mL, 68 mmol). The reaction mixture was cooled to −40 °C and a solution of benzoyl chloride (5.9 mL, 50.8 mmol) in CH$_2$Cl$_2$ (30 mL) was added dropwise for 1 h and the reaction mixture was stirred at −40 °C for 13 hours. The reaction was quenched with methanol and all volatiles were evaporated. The residue was dissolved in ethyl acetate (700 mL) and washed with water (300 mL) and satd sodium bicarbonate (300 mL), dried with sodium sulfate and evaporated. The residue was chromato-

2708 | *Org. Biomol. Chem.*, 2015, **13**, 2703–2715

This journal is © The Royal Society of Chemistry 2015

graphed on silica gel (400 g, toluene–ethyl acetate 4 : 1 → 1 : 1) to afford 3.580 g of **12** (25%) and 7.261 g of **13a** + **13b** (67%, mixture). The mixture of monobenzoylated compounds **13a** + **13b** was separated on a small scale by column chromatography (250 mg of the mixture, 100 g, toluene–ethyl acetate 2 : 1).

(1S,4S,5R)-1-((Benzoyloxy)methyl)spiro[bicyclo[3.2.1]octane-8,2′-[1,3]dioxolan]-4-yl benzoate (12). Light oil. $[\alpha]_D^{20}$ = +0 (c 0.312, CHCl₃), $[\alpha]_D^{20}$ = +4.0 (c 0.294, CH₃OH). Found: C, 71.35; H, 6.31. Calc. for C₂₅H₂₆O₆: C, 71.07; H, 6.20%. ¹H NMR (400 MHz, d6-DMSO): δ 1.60–1.76 (m, 5H, H-2a, H-2b, H-3ax, H-6b, H-7b), 1.78–1.92 (m, 2H, H-6a, H-7a), 1.95–2.02 (m, 1H, H-3eq), 2.27 (dd, J_{5-4} = 3.1, J_{5-6ex} = 6.0, 1H, H-5), 3.90–3.99 (m, 4H, –OCH₂CH₂O–), 4.22 and 4.29 (2 × d, 2H, J_{gem} = 10.9, BzOCH₂–), 5.25 (ddd, J_{4-5} = 3.1, J_{4-3eq} = 5.8, J_{4-3ax} = 10.6, H-4), 7.50–7.54 (m, 4H, Ph-m1, Ph-m2), 7.63–7.69 (m, 2H, Ph-p1, Ph-p2), 7.94–7.99 (m, 4H, Ph-o1, Ph-o2). ¹³C NMR (100.6 MHz, d6-DMSO): δ 19.28 (C-6), 23.29 (C-3), 28.32 (C-7), 28.94 (C-2), 44.98 (C-5), 45.00 (C-1), 64.20 and 65.31 (–OCH₂CH₂O–), 66.55 (BzOCH₂–), 73.07 (C-4), 115.45 (C-8), 128.92 and 129.00 (C-m1, C-m2), 129.28 (C-o2, C-o1), 129.98 and 130.17 (C-i1 and C-i2), 133.49 and 133.50 (C-p1, C-p2), 165.09 and 165.93 (2 × COO). CI MS, m/z (rel%): 423 (10) [M + H], 301 (100). HRMS: calcd for [M + H]: 423.1808, found: 423.1802.

((1R,2R,5S)-2-Hydroxyspiro[bicyclo[3.2.1]octane-8,2′-[1,3]-dioxolan]-5-yl)methyl benzoate (13a). Viscous oil. $[\alpha]_D^{20}$ = +6.3 (c 0.158, CHCl₃). Found: C, 68.19; H, 7.14. Calc. for C₁₈H₂₂O₅: C, 67.91; H, 6.97%. ¹H NMR (400 MHz, d6-DMSO): δ 1.24 (m, 1H, H-6b), 1.45–1.55 (m, 2H, H-2b, H-3b), 1.60–1.64 (m, 2H, H-7a, H-7b), 1.66–1.64 (m, 2H, H-3a, H-6a), 2.00 (dd, J_{5-4} = 4.2, J_{5-6ex} = 6.9, 1H, H-5), 2.06 (m, 1H, H-2a), 3.74 (m, 1H, H-4), 3.84–3.99 (m, 4H, –OCH₂CH₂O–), 4.11 (d, J_{OH-4} = 9.2, 1H, 4-OH), 4.18 and 4.24 (2 × d, 2H, J_{gem} = 10.8, BzOCH₂–), 7.54 (m, 2H, Ph-m), 7.66 (m, 1H, Ph-p), 7.96 (m, 2H, Ph-o). ¹³C NMR (100.6 MHz, d6-DMSO): δ 22.30 (C-6), 26.21 (C-3), 27.40 (C-7), 27.91 (C-2), 44.30 (C-5), 45.06 (C-1), 63.97 and 65.43 (–OCH₂CH₂O–), 66.88 (BzOCH₂–), 72.74 (C-4), 116.37 (C-8), 128.99 (C-m), 129.26 (C-o), 130.02 (C-i), 133.47 (C-p), 165.97 (COO). CI MS, m/z (rel%): 319 (25) [M + H], 301 (100). HRMS: calcd for [M + H]: 319.1545, found: 319.1546.

((1R,2S,5S)-2-Hydroxyspiro[bicyclo[3.2.1]octane-8,2′-[1,3]di-oxolan]-5-yl)methyl benzoate (13b). Viscous oil. $[\alpha]_D^{20}$ = +4.9 (c 0.284, CHCl₃). Found: C, 67.68; H, 7.21. Calc. for C₁₈H₂₂O₅: C, 67.91; H, 6.97%. ¹H NMR (400 MHz, d6-DMSO): δ 1.21–1.33 (m, 1H, H-3b), 1.42–1.54 (m, 3H, H-2b, H-6b, H-7b), 1.59–1.75 (m, 4H, H-2a, H-3a, H-6a, H-7a), 1.91 (dd, J_{5-4} = 3.0, J_{5-6ex} = 6.3, 1H, H-5), 3.83–3.89 (m, 5H, –OCH₂CH₂O–, H-4), 4.15 and 4.23 (2 × d, 2H, J_{gem} = 10.8, BzOCH₂–), 4.45 (d, J_{OH-4} = 4.7, 1H, 4-OH), 7.51–7.56 (m, 2H, Ph-m), 7.63–7.68 (m, 1H, Ph-p), 7.93–7.96 (m, 2H, Ph-o). ¹³C NMR (100.6 MHz, d6-DMSO): δ 18.46 (C-6), 26.87 (C-3), 28.56 (C-7), 29.12 (C-2), 44.88 (C-1), 48.01 (C-5), 63.94 and 65.15 (–OCH₂CH₂O–), 66.96 (BzOCH₂–), 68.00 (C-4), 115.89 (C-8), 128.98 (C-m), 129.25 (C-o), 130.04 (C-i), 133.46 (C-p), 165.96 (COO). CI MS, m/z (rel%): 319 (25) [M + H], 301 (100). HRMS: calcd for [M + H]: 319.1545, found: 319.1544.

Recyclation of diol 11 from 12

A freshly prepared sodium methoxide in methanol (prepared from 70 mg of sodium and 27 mL of absolute methanol) was added to a solution of the diol **12** (3.4 g, 8.1 mmol) in absolute methanol (55 mL). The reaction mixture was heated to 60 °C for 12 h and evaporated. The residue was chromatographed on a silica gel column (200 g, ethyl acetate) and 1.54 g (89%) of the recycled diol **11** was obtained. This diol was used again for the monobenzoylation reaction.

((1S,5R)-4-Oxospiro[bicyclo[3.2.1]oct[2]ene-8,2′-[1,3]dioxolan]-1-yl)methyl benzoate (14). A mixture of alcohols **13a** and **13b** (5.644 g, 17.73 mmol) was dissolved in DMSO (125 mL) and IBX (20.1 g, 71.8 mmol) and p-TsOH (1.013 g, 5.33 mmol) was then added. The reaction mixture was stirred at r.t. for 1 h and then heated to 90 °C for 16 h. A second portion of IBX (2 g) was added and heating was continued for another 3 h. After cooling, the reaction mixture was carefully poured into a satd solution of sodium bicarbonate (400 mL) and this mixture was extracted with ethyl acetate (3 × 500 mL). The combined organic phases were washed with a satd solution of sodium bicarbonate (2 × 600 mL), dried with sodium sulfate and evaporated. The product was purified on a silica gel column (250 g) with diethyl ether as a mobile phase to afford 4.618 g (83%) of the product **14**. An analytical sample was obtained by purification on a silica gel column (toluene–ethyl acetate 4 : 1). Viscous oil. $[\alpha]_D^{20}$ = +139.4 (c 0.307, CHCl₃). Found: C, 68.54; H, 5.87. Calc. for C₁₈H₁₈O₅: C, 68.78; H, 5.77%. ¹H NMR (500 MHz, d6-DMSO): δ 1.32–1.39 (m, 1H, H-6en), 1.68–1.74 (m, 1H, H-7en), 1.97–2.03 (m, H-7ex), 2.10–2.17 (m, 1H, H-6ex), 2.77 (ddm, 1H, J_{5-3} = 1.7, J_{5-6ex} = 7.7, 1H, H-5), 3.73–3.98 (m, 4H, –OCH₂CH₂O–), 4.44 and 4.51 (2 × d, 2H, J_{gem} = 11.1, BzOCH₂–), 6.09 (dd, J_{3-5} = 1.7, J_{3-2} = 9.9, 1H, H-3), 7.38 (d, J_{2-3} = 9.9, 1H, H-2), 7.53–7.56 (m, 2H, Ph-m), 7.65–7.69 (m, 1H, Ph-p), 7.96–7.98 (m, 2H, Ph-o). ¹³C NMR (125.7 MHz, d6-DMSO): δ 20.81 (C-6), 30.76 (C-7), 50.87 (C-1), 57.47 (C-5), 63.67 (BzOCH₂–), 65.15 and 65.40 (–OCH₂CH₂O–), 117.61 (C-8), 128.36 (C-3), 128.97 (C-m), 129.35 (C-o), 129.75 (C-i), 133.60 (C-p), 154.23 (C-2), 165.86 (COO), 200.87 (C-4). ESI MS, m/z (rel%): 337 (100) [M + Na]. HRMS: calcd for [M + Na]: 337.10464, found: 337.10469.

Preparation of compounds 15 and 16

To a solution of the starting material **14** (6.293 g, 20.02 mmol) in methanol (330 mL) at 0 °C, cerium(III) chloride heptahydrate (14.65 g, 35.3 mmol) was added and the reaction mixture was stirred at 0 °C for 1 h. Sodium borohydride (1.05 g, 27.8 mmol) was then added in three portions for 30 minutes, the reaction mixture was stirred at 0 °C for an additional hour, quenched with ice and evaporated. The residue was dissolved in ethyl acetate (600 mL) and washed with water (300 mL). The water phase was extracted with ethyl acetate (600 mL), the combined organic phases were dried with sodium sulfate and evaporated. The residue was chromatographed on silica gel (400 g, toluene–ethyl acetate 4 : 1 → 1 : 1) to afford 3.293 g of **16** (52%) and 2.827 g of **15** (45%) (both colourless oils).

This journal is © The Royal Society of Chemistry 2015

Org. Biomol. Chem., 2015, **13**, 2703–2715 | **2709**

((1S,4S,5R)-4-Hydroxyspiro[bicyclo[3.2.1]oct[2]ene-8,2′-[1,3]-dioxolan]-1-yl)methyl benzoate (15). $[\alpha]_D^{20}$ = +121.2 (c 0.307, CHCl$_3$). Found: C, 68.01; H, 6.57. Calc. for C$_{18}$H$_{20}$O$_5$: C, 68.34; H, 6.37%. ^{1}H NMR (500 MHz, d6-DMSO): δ 1.51–1.56 (m, 1H, H-6ex), 1.57–1.62 (m, 1H, H-7en), 1.74–1.79 (m, 1H, H-7ex), 1.92 (ddd, $J_{6en-7ex}$ = 6.6, $J_{6en-7en}$ = 9.8, J_{gem} = 13.3, 1H, H-6en), 2.09–2.12 (m, 1H, H-5), 3.80–3.93 (m, 4H, –OCH$_2$CH$_2$O–), 4.26 and 4.33 (2 × d, 2H, J_{gem} = 10.9, BzOCH$_2$–), 4.48 (bs, 1H, H-4), 4.80 (d, J_{OH-4} = 4.5, 1H, OH), 5.49 (dm, J_{3-2} = 9.7, 1H, H-3), 5.77 (dd, J_{2-4} = 1.7, J_{2-3} = 9.7, 1H, H-2), 7.53–7.55 (m, 2H, Ph-m), 7.64–7.67 (m, 1H, Ph-p), 7.94–7.96 (m, 2H, Ph-o). ^{13}C NMR (125.7 MHz, d6-DMSO): δ 18.09 (C-6), 33.29 (C-7), 46.62 (C-5), 47.28 (C-1), 64.24 and 65.33 (–OCH$_2$CH$_2$O–), 64.63 (BzOCH$_2$–), 71.01 (H-4), 116.59 (H-8), 128.95 (C-m), 129.29 (C-o), 129.86 (C-3), 129.97 (C-i), 131.21 (C-2), 133.48 (C-p), 165.86 (COO). ESI MS, m/z (rel%): 339 (100) [M + Na]. HRMS: calcd for [M + Na]: 339.12029, found: 339.12024.

((1S,4R,5R)-4-Hydroxyspiro[bicyclo[3.2.1]oct[2]ene-8,2′-[1,3]-dioxolan]-1-yl)methyl benzoate (16). $[\alpha]_D^{20}$ = +52.6 (c 0.312, CHCl$_3$). Found: C, 68.24; H, 6.40. Calc. for C$_{18}$H$_{20}$O$_5$: C, 68.34; H, 6.37%. ^{1}H NMR (500 MHz, d6-DMSO): δ 1.15 (dddd, J_{6en-5} = 1.1, $J_{6en-7ex}$ = 5.9, $J_{6en-7en}$ = 9.8, J_{gem} = 13.4, 1H, H-6en), 1.56–1.61 (m, 1H, H-7en), 1.70–1.76 (m, 1H, H-7ex), 1.83–1.91 (m, 1H, H-6ex), 2.10 (dm, J_{5-6ex} = 7.9, 1H, H-5), 3.80–3.98 (m, 6H, –OCH$_2$CH$_2$O–, H-4, 4-OH), 4.31 and 4.36 (2 × d, 2H, J_{gem} = 11.0, BzOCH$_2$–), 5.70 (ddd, J_{3-5} = 1.5, J_{3-4} = 3.4, J_{3-2} = 9.6, 1H, H-3), 5.92 (d, J_{2-3} = 9.6, 1H, H-2), 7.52–7.55 (m, 2H, Ph-m), 7.64–7.68 (m, 1H, Ph-p), 7.96–7.98 (m, 2H, Ph-o). ^{13}C NMR (125.7 MHz, d6-DMSO): δ 22.30 (C-6), 32.06 (C-7), 44.46 (C-5), 47.40 (C-1), 64.22 and 65.14 (–OCH$_2$CH$_2$O–), 64.77 (BzOCH$_2$–), 74.27 (C-4), 115.40 (C-8), 128.49 (C-3), 128.49 (C-m), 129.28 (C-o), 129.92 (C-i), 133.03 (C-p), 133.46 (C-2), 165.99 (COO). ESI MS, m/z (rel%): 339 (100) [M + Na]. HRMS: calcd for [M + Na]: 339.12029, found: 339.12026.

Recycling of alcohol 15 to ketone 14

To a solution of allyl alcohol **15** (2.088 g, 6.6 mmol) in CH$_2$Cl$_2$ (100 mL) manganese(IV) oxide (6.4 g, 10 eq., activated, ∼ 90%) was added in one portion and the reaction mixture was stirred overnight. Solids were removed by filtration on a Celite pad and thoroughly washed with ethyl acetate. The filtrate was evaporated and the crude **15** (quant. yield) was re-used in the Luche reduction. The analytical sample was obtained by silica gel chromatography (toluene–ethyl acetate 4 : 1). NMR spectra match those for **14**.

((1S,4R,5R)-4-Hydroxy-8-oxobicyclo[3.2.1]oct-2-en-1-yl)methyl benzoate (17). p-TsOH (2.38 g, 12.49 mmol) was added to a solution of allyl alcohol **16** (3.293 g, 10.41 mmol) in acetone (180 mL) and water (90 mL) and the reaction mixture was heated to reflux for 10 h and then to 50 °C for another 10 h. The reaction mixture was evaporated to half of the original volume and diluted with ethyl acetate (700 mL). The organic phase was washed with water (300 mL) and saturated aq. sodium bicarbonate (300 mL), dried over sodium sulfate and evaporated. The product was purified on a silica gel column (250 g, toluene–ethyl acetate 4 : 1 → 2 : 1) to afford 2.456 g

(87%) of **17** as viscous oil. $[\alpha]_D^{20}$ = +15.3 (c 0.326, CHCl$_3$). Found: C, 70.63; H, 6.27. Calc. for C$_{16}$H$_{16}$O$_4$: C, 70.57; H, 5.92%. ^{1}H NMR (500 MHz, d6-DMSO): δ 1.50–1.57 (m, 1H, H-6en), 1.86–1.95 (m, 2H, H-7en, H-7ex), 2.03–2.11 (m, 1H, H-6ex), 2.36 (dm, J_{5-6ex} = 8.4, 1H, H-5), 4.32 and 4.35 (2 × d, 2H, J_{gem} = 11.3, BzOCH$_2$–), 4.55 (bs, 1H, H-4), 5.39 (bs, 1H, 4-OH), 5.75 (ddd, J_{3-5} = 1.2, J_{3-4} = 3.8, J_{3-2} = 9.1, 1H, H-3), 5.96 (d, J_{2-3} = 9.1, 1H, H-2), 7.51–7.55 (m, 2H, Ph-m), 7.65–7.68 (m, 1H, Ph-p), 7.92–7.95 (m, 2H, Ph-o). ^{13}C NMR (125.7 MHz, d6-DMSO): δ 19.35 (C-6), 29.16 (C-7), 49.88 (C-1), 50.10 (C-5), 63.75 (BzOCH$_2$–), 79.92 (C-4), 129.01 (C-m), 129.39 (C-o), 129.56 (C-3), 129.74 (C-i), 133.55 and 133.66 (C-p and C-2), 165.86 (COO), 212.74 (C-8). ESI MS, m/z (rel%): 295 (100) [M + Na]. HRMS: calcd for [M + Na]: 295.09408, found: 295.09416.

((1S,4R,5R,8S)-4,8-Dihydroxybicyclo[3.2.1]oct-2-en-1-yl) methyl benzoate (18). To an ice-cooled solution of the keto derivative **17** (2.456 g, 9.02 mmol) in a mixture of acetonitrile (170 mL) and acetic acid (5.2 mL), sodium triacetoxyborohydride (2.87 g, 13.5 mmol) was added in four portions for 30 minutes. The reaction mixture was allowed to warm to r.t. and stirring was continued for 12 h. The reaction mixture was quenched with methanol and evaporated. The residue was dissolved in methanol and adsorbed on silica gel. Chromatography on a silica gel column (200 g) in ethyl acetate afforded 2.173 g (88%) of the product **18** as a white solid. M. p. 130–131 °C. $[\alpha]_D^{20}$ = −7.1 (c 0.320, CHCl$_3$). Found: C, 69.90; H, 6.60. Calc. for C$_{16}$H$_{18}$O$_4$: C, 70.06; H, 6.61%. ^{1}H NMR (500 MHz, d6-DMSO): δ 1.09–1.15 (m, 1H, H-6en), 1.43–1.48 (m, 1H, H-7en), 1.63–1.70 (m, 1H, H-7ex), 1.88–1.96 (m, 1H, H-6ex), 2.12 (dm, J_{5-6ex} = 8.0, 1H, H-5), 3.86–3.89 (m, 1H, H-4), 3.99 (d, J_{8-OH} = 4.0, 1H, H-8), 4.29 and 4.33 (2 × d, 2H, J_{gem} = 10.6, BzOCH$_2$–), 4.85 (d, J_{OH-8} = 4.0, 1H, 8-OH), 4.94 (d, J_{OH-4} = 5.2, 1H, 4-OH), 5.52 (ddd, J_{3-5} = 1.6, J_{3-4} = 3.9, J_{3-2} = 9.4, 1H, H-3), 5.85 (d, J_{2-3} = 9.4, 1H, H-2), 7.51–7.55 (m, 2H, Ph-m), 7.64–7.68 (m, 1H, Ph-p), 7.95–7.97 (m, 2H, Ph-o). ^{13}C NMR (125.7 MHz, d6-DMSO): δ 23.65 (C-6), 31.33 (C-7), 48.77 (C-5), 49.75 (C-1), 66.44 (BzOCH$_2$–), 72.08 (C-8), 73.25 (C-4), 128.12 (C-3), 128.93 (C-m), 129.35 (C-o), 130.21 (C-i), 133.46 (C-p), 135.73 (C-2), 166.07 (COO). ESI MS, m/z (rel%): 297 (100) [M + Na]. HRMS: calcd for [M + Na]: 297.10973, found: 297.10972.

((1S,4R,5S,8S)-8-(Benzoyloxy)-4-((tert-butyldimethylsilyl)oxy)-bicyclo[3.2.1]oct-2-en-1-yl)methyl benzoate (19). To an ice-cooled solution of diol **18** (2.419, 8.82 mmol) and imidazole (901 mg, 13.23 mmol) in CH$_2$Cl$_2$ (53 mL) was added TBDMSCl (total amount 1.6 g, 10.6 mmol) in two portions for 30 minutes and the reaction mixture was stirred at 0 °C for 16 h. Volatiles were evaporated, the residue was dissolved in ethyl acetate (700 mL) and the organic phase was washed with water (2 × 300 mL), dried with sodium sulfate, evaporated and co-evaporated with benzene (200 mL). The crude intermediate was dissolved in pyridine (50 mL) and then DMAP (catalytic amount) and benzoylchloride (2.05 mL 17.6 mmol) were added. The reaction mixture was left in the dark for 18 h. The reaction was then quenched with water and pyridine was evaporated. The residue was dissolved in ethyl acetate (700 mL) and washed with water (2 × 300 mL) and saturated aq. sodium

2710 | *Org. Biomol. Chem.*, 2015, **13**, 2703–2715

This journal is © The Royal Society of Chemistry 2015

bicarbonate (2 × 300 mL), dried with sodium sulfate and evaporated. The product was isolated by column chromatography on silica gel (250 g, hexanes–ethyl acetate 20 : 1) affording 3.691 g (85% over two steps) of **19** as an oil. $[\alpha]_D^{20}$ = +54.4 (*c* 0.375, CHCl₃). Found: C, 70.99; H, 7.36. Calc. for C₂₉H₃₆O₅Si: C, 70.70; H, 7.37%. ¹H NMR (500 MHz, d6-DMSO): δ 0.07 and 0.08 (2 × s, 2 × 3H, 2 × CH₃), 0.88 (s, 9H, *t*Bu), 1.33–1.39 (m, 1H, H-6en), 1.67–1.73 (m, 1H, H-7en), 1.95–2.01 (m, 1H, H-7ex), 2.04–2.12 (m, 1H, H-6ex), 2.38 (dm, J_{5-6ex} = 7.9, 1H, H-5), 4.17–4.19 (m, 1H, H-4), 4.34 and 4.41 (2 × d, 2H, J_{gem} = 11.1, BzOCH₂–), 5.46 (bs, 1H, H-8), 5.64 (ddd, J_{3-5} = 1.5, J_{3-4} = 4.1, J_{3-2} = 9.4, 1H, H-3), 5.96 (d, J_{2-3} = 9.4, 1H, H-2), 7.45–7.52 (m, 4H, Ph-*m*1, Ph-*m*2), 7.61–7.66 (m, 2H, Ph-*p*1, Ph-*p*2), 7.87–7.89 (m, 2H, Ph-*o*2), 7.95–7.97 (m, 2H, Ph-*o*1). ¹³C NMR (125.7 MHz, d6-DMSO): δ −4.30 and −4.55 (2 × CH₃), 17.99 (C (CH₃)₃), 22.92 (C-6), 25.91 (*t*Bu), 31.41 (C-7), 47.00 (C-5), 49.19 (C-1), 65.46 (BzOCH₂–), 73.87 (C-4), 77.11 (C-8), 127.98 (C-3), 128.87 and 128.96 (C-*m*1, C-*m*2), 129.27 (C-*o*2), 129.44 (C-*o*1), 129.81 and 130.02 (C-i1 and C-i2), 133.54 (C-*p*1, C-*p*2), 135.02 (C-2), 164.93 (COO-1), 165.70 (COO-2). ESI MS, *m/z* (rel%): 515 (100) [M + Na]. HRMS: calcd for [M + Na]: 515.22242, found: 515.22244.

((1S,4R,5R,8S)-8-(Benzoyloxy)-4-hydroxybicyclo[3.2.1]oct-2-en-1-yl)methyl benzoate (20). Silyl derivative **19** (2.910 g, 5.91 mmol) was dissolved in a mixture of THF (65 mL) and acetic acid (1.2 mL) under an argon atmosphere. The reaction mixture was treated with TBAF (8.9 mL, 1 M solution in THF) at r.t. After 30 minutes the reaction mixture was heated to 60 °C for 24 h and then evaporated. The residue was dissolved in ethyl acetate (700 mL) and washed with water (300 mL). The organic phase was dried with sodium sulfate and evaporated. Chromatography (silica gel 250 g, toluene–ethyl acetate 3 : 1) of the residue afforded 2.05 g (92%) of **20** as a viscous oil. $[\alpha]_D^{20}$ = +120.60 (*c* 0.329, CHCl₃). Found: C, 72.72; H, 6.10. Calc. for C₂₃H₂₂O₅: C, 73.00; H; 5.86%. ¹H NMR (500 MHz, d6-DMSO): δ 1.31–1.38 (m, 1H, H-6en), 1.69–1.74 (m, 1H, H-7en), 1.93–1.99 (m, 1H, H-7ex), 2.04–2.12 (m, 1H, H-6ex), 2.39 (d, J_{5-6ex} = 8.2, 1H, H-5), 4.00–4.03 (m, 1H, H-4), 4.32 and 4.38 (2 × d, 2H, J_{gem} = 11.1, BzOCH₂–), 5.24 (d, 1H, 4-OH), 5.48 (bs, 1H, H-8), 5.67 (ddd, J_{3-5} = 1.5, J_{3-4} = 3.9, J_{3-2} = 9.5, 1H, H-3), 5.96 (d, J_{2-3} = 9.5, 1H, H-2), 7.48–7.53 (m, 4H, Ph-*m*1, Ph-*m*2), 7.62–7.67 (m, 2H, Ph-*p*1, Ph-*p*2), 7.89–7.91 (m, 2H, Ph-*o*2), 7.95–7.97 (m, 2H, Ph-*o*1). ¹³C NMR (125.7 MHz, d6-DMSO): δ 23.46 (C-6), 31.79 (C-7), 46.88 (C-5), 49.18 (C-1), 65.51 (BzOCH₂–), 72.86 (C-4), 77.22 (C-8), 128.63 (C-3), 128.89 and 128.97 (C-*m*1, C-*m*2), 129.31 (C-*o*2), 129.38 (C-*o*1), 129.76 and 130.04 (C-i1 and C-i2), 133.52 (C-*p*1, C-*p*2), 134.67 (C-2), 165.05 (COO-1), 165.72 (COO-2). ESI MS, *m/z* (rel%): 401 (100) [M + Na]. HRMS: calcd for [M + Na]: 401.13594, found: 401.13608.

Preparation of compounds 22a and 22

A solution of PPh₃ (2.99 g, 11.4 mmol) and *N*-chlorosuccinimide (1.53 g, 11.45 mmol) in CH₂Cl₂ (32 mL) was stirred at 0 °C for 30 minutes. A solution of hydroxy derivative **20** (2.155 g, 5.65 mmol) in CH₂Cl₂ (32 mL + 5 mL for rinsing the flask) was then added dropwise for 30 minutes. The reaction

mixture was stirred at 0 °C for 2 h and then treated with methanol (5 mL) and evaporated. The residue was chromatographed on a silica gel column (250 g, hexanes–ethyl acetate 10 : 1) and the isolated intermediate was immediately used in the following step. Chloro derivative **21** was dissolved in DMF (44 mL) and treated with sodium azide (1.836 g, 28.3 mmol) at 65 °C for 12 h. Volatiles were evaporated, the residue was dissolved in ethyl acetate (350 mL) and washed with water (200 mL). The organic phase was dried with sodium sulfate, evaporated and the crude product was chromatographed on a silica gel column (250 g, hexanes–ethyl acetate 20 : 1 → 10 : 1) to afford **22a** (505 mg, 22% over 2 steps) and **22** (1.64 g, 72% over 2 steps, both were oils).

(1R,4S,5S,8S)-4-Azido-5-((benzoyloxy)methyl)bicyclo[3.2.1]-oct-2-en-8-yl benzoate (22a). ¹H NMR (500 MHz, d6-DMSO): δ 1.69–1.76 (m, 2H, H-7en, H-6ex), 2.11–2.19 (m, 2H, H-6en, H-7ex), 2.76–2.80 (m, 1H, H-1), 4.44 (d, 1H, J_{4-3} = 4.2, H-4), 4.47 and 4.52 (2 × d, 2H, J_{gem} = 11.0, BzOCH₂–), 5.19 (s, 1H, H-8), 5.77 (dd, J_{3-4} = 4.2, J_{3-2} = 9.3, 1H, H-3), 6.28 (dd, J_{2-1} = 6.9, J_{2-3} = 9.3, 1H, H-2), 7.49–7.54 (m, 4H, Ph-*m*1, Ph-*m*2), 7.64–7.69 (m, 2H, Ph-*p*1, Ph-*p*2), 7.97–8.00 (m, 4H, Ph-*o*2, Ph-*o*1). ¹³C NMR (125.7 MHz, d6-DMSO): δ 29.48 (C-6), 29.92 (C-7), 41.26 (C-1), 50.49 (C-5), 66.14 (C-4), 66.29 (BzOCH₂–), 77.69 (C-8), 122.20 (C-3), 128.85 and 128.94 (C-*m*1, C-*m*2), 129.34 and 129.42 (C-*o*1, C-*o*2), 129.48 and 129.57 (C-i1 and C-i2), 133.54 and 133.73 (C-*p*1, C-*p*2), 136.22 (C-2), 165.20 (8-COO), 165.63 (–CH₂OCOO). ESI MS, *m/z* (rel%): 426 (100) [M + Na]. HRMS: calcd for [M + Na]: 426.14243, found: 426.14233.

(1S,4R,5R,8S)-4-Azido-1-((benzoyloxy)methyl)bicyclo[3.2.1]-oct-2-en-8-yl benzoate (22). $[\alpha]_D^{20}$ = −10.2 (*c* 0.275, CHCl₃). Found: C, 68.45; H, 5.30; N, 10.11. Calc. for C₂₃H₂₁N₃O₄: C, 68.47; H, 5.25; N, 10.42%. ¹H NMR (500 MHz, d6-CDCl₃): δ 1.52 (ddd, $J_{6en-7ex}$ = 6.2, $J_{6en-7en}$ = 9.2, J_{gem} = 14.0, 1H, H-6en), 1.89–1.95 (m, 1H, H-7en), 2.04–2.11 (m, 1H, H-7ex), 2.21–2.29 (m, 1H, H-6en), 2.73 (dm, J_{5-6ex} = 8.1, 1H, H-5), 3.99 (t, J_{4-5} = 3.3, 1H, H-4), 4.39 and 4.56 (2 × d, 2H, J_{gem} = 11.2, BzOCH₂–), 5.49 (s, 1H, H-8), 5.73 (ddd, J_{3-5} = 1.6, J_{3-4} = 4.1, J_{3-2} = 9.5, 1H, H-3), 6.20 (d, 1H, J_{2-3} = 9.5, 1H, H-2), 7.39–7.45 (m, 4H, Ph-*m*1, Ph-*m*2), 7.52–7.58 (m, 2H, Ph-*p*1, Ph-*p*2), 7.99–8.02 (m, 4H, Ph-*o*2, Ph-*o*1). ¹³C NMR (125.7 MHz, CDCl₃): δ 24.96 (C-6), 32.73 (C-7), 44.74 (C-5), 49.15 (C-1), 64.81 (C-4), 65.17 (BzOCH₂), 76.76 (C-8), 122.80 (C-3), 128.39 and 128.44 (C-*m*1, C-*m*2), 129.56 and 129.64 (C-*o*1, C-*o*2), 129.75 and 129.99 (C-i1 and C-i2), 133.07 and 133.16 (C-*p*1, C-*p*2), 138.46 (C-2), 164.33 (COO-1), 165.40 (COO-2). ESI MS, *m/z* (rel%): 426 (100) [M + Na]. HRMS: calcd for [M + Na]: 426.14243, found: 426.14229.

Allylic rearrangement of 22a to 22

A solution of compound **22a** (505 mg, 1.25 mmol) in acetonitrile (35 mL) was heated to 95 °C for 24 h. The reaction mixture was evaporated and the residue was chromatographed (100 g, hexanes–ethyl acetate 10 : 1) to afford 241 mg (48%) of **22**.

(1S,4R,5R,8S)-4-Amino-1-(hydroxymethyl)bicyclo[3.2.1]oct-2-en-8-ol (23). Azido derivative **22** (1.64 g, 4.06 mmol) was dissolved in dry THF (20 mL, argon atmosphere) and then PPh₃

This journal is © The Royal Society of Chemistry 2015

Org. Biomol. Chem., 2015, **13**, 2703–2715 | 2711

(1.42 g, 5.41 mmol) was added. The reaction mixture was stirred for 20 h, then water (1.23 mL) was added and stirring was continued for another 20 h. The reaction mixture was evaporated and re-dissolved in EtOH–H_2O (18 mL, 1 : 1). Potassium hydroxide (1.2 g, 21.4 mmol) was added and the reaction mixture was heated to reflux for 5 h, neutralized with aq. HCl and purified on a DOWEX 50 (100 mL, H^+ cycle). The column was washed with water (400 mL), methanol (400 mL) and the product was then eluted with aq. NH_3–MeOH (1 : 4, v/v). Fractions containing the product were evaporated and the oily residue was converted to hydrochloride salt with hydrogen chloride in dioxane (2 M) (659 mg, 79%, slightly hygroscopic yellowish solid). $[\alpha]_D^{20} = -51.4$ (c 0.292, CH_3OH). Found: C, 51.21; H, 7.70; N, 6.23. Calc. for $C_9H_{16}ClNO_2 \cdot 1/3H_2O$: C, 51.06; H, 7.94; N, 6.62%. ^1H NMR (500 MHz, d6-DMSO): δ 1.26 (ddd, $J_{6en-7ex} = 5.9$, $J_{6en-7en} = 9.1$, $J_{gem} = 13.7$, 1H, H-6en), 1.37–1.43 (m, 1H, H-7en), 1.52–1.59 (m, 1H, H-7ex), 1.98–2.06 (m, 1H, H-6ex), 2.24 (d, $J_{5-6ex} = 8.0$, 1H, H-5), 3.41 (d, $J_{gem} = 10.7$, 1H, CHbOH), 3.52 (m, 2H, H-4, CHaOH), 4.00 (bs, 1H, H-8), 4.62 and 4.89 (2 × bs, 2H, 8-OH, CH_2OH), 5.48 (dd, $J_{3-5} = 1.7$, $J_{3-4} = 3.6$, $J_{3-2} = 9.5$, 1H, H-3), 6.13 (dd, $J_{2-4} = 0.8$, $J_{2-3} = 9.5$, 1H, H-2), 8.20 (bs, 3H, NH_3^+). ^{13}C NMR (125.7 MHz, d6-DMSO): δ 25.78 (C-6), 31.86 (C-7), 43.97 (C-5), 51.88 (C-4), 55.09 (C-4), 62.24 (CH_2OH), 71.21 (C-8), 120.68 (C-3), 142.49 (C-2). CI MS, m/z (rel %): 152 (100) [M + H-H_2O]. HRMS: calcd for [M + H]: 171.1181, found: 170.1176.

(1S,4R,5R,8S)-4-(6-Chloro-9H-purin-9-yl)-1-(hydroxymethyl)-bicyclo[3.2.1]oct-2-en-8-ol (24). A mixture of amine **23** (1 g, 4.9 mmol), 4,6-dichloro-5-formamido-pyrimidine (1.56 g, 7.35 mmol, prepared according to published procedure[26]) and DIPEA (2.9 mL, 14.7 mmol) in n-BuOH (25 mL) was heated in a sealed microwave reactor for 2 h at 140 °C. After evaporation the residue was chromatographed on a silica gel column (400 g) in ethyl acetate → ethyl acetate–toluene–acetone–ethanol (17 : 4 : 3 : 1) to afford **24** (631 mg, 42%). The analytical sample was crystalized from ethanol (white solid). M.p. 176.5–177 °C (decomposition, EtOH). $[\alpha]_D^{20} = -18.6$ (c 0.297, CH_3OH). Found: C, 54.50; H, 4.91; Cl, 11.30; N, 17.87. Calc. for $C_{14}H_{15}ClN_4O_2$: C, 54.82; H, 4.93; Cl, 11.56; N, 18.26%. ^1H NMR (500 MHz, d6-DMSO): δ 1.46–1.53 (m, 1H, H-6en), 1.54–1.60 (m, 1H, H-7en), 1.65–1.72 (m, 1H, H-7ex), 2.06–2.13 (m, 1H, H-6ex), 2.42 (dm, $J_{5-6ex} = 7.8$, 1H, H-5), 3.51 (dd, $J_{CH-OH} = 5.3$, $J_{gem} = 10.5$, 1H, CHbOH), 3.63 (dd, $J_{CH-OH} = 5.3$, $J_{gem} = 10.5$, 1H, CHaOH), 3.74 (d, $J_{8-OH} = 3.6$, 1H, H-8), 4.53 (t, $J_{OH-CH_2} = 5.3$, 1H, CH_2OH), 4.63 (d, $J_{OH-8} = 3.6$, 1H, 8-OH), 5.10–5.12 (m, 1H, H-4), 5.76 (ddd, $J_{3-5} = 1.7$, $J_{3-4} = 3.9$, $J_{3-2} = 9.4$, 1H, H-3), 6.40 (dd, $J_{2-4} = 1.2$, $J_{2-3} = 9.4$, 1H, H-2), 8.49 (s, 1H, H-8'), 8.83 (s, 1H, H-2'). ^{13}C NMR (125.7 MHz, d6-DMSO): δ 25.10 (C-6), 32.31 (C-7), 46.26 (C-5), 51.70 (C-1), 59.74 (C-4), 62.18 (CH_2OH), 71.81 (C-8), 119.57 (C-3), 131.47 (C-5'), 143.33 (C-2), 145.84 (C-8'), 149.32 (C-6'), 151.48 (C-4'), 151.67 (C-2'). ESI MS, m/z (rel%): 329/331 (100/33) [M + Na]. HRMS: calcd for [M + Na]: 329.07757, found: 329.07771.

(1S,4R,5R,8S)-4-(6-Amino-9H-purin-9-yl)-1-(hydroxymethyl)-bicyclo[3.2.1]oct-2-en-8-ol (25). A solution of chloropurine derivative **24** (540 mg, 1.76 mmol) was dissolved in ethanolic

ammonia (3.5 M, 6 mL) heated in a sealed microwave reactor at 140 °C for 1 h. The reaction mixture was evaporated and chromatographed on a silica gel column (200 g) in ethyl acetate → ethyl acetate–acetone–ethanol–H_2O (19 : 3 : 1.8 : 1.2) to afford 433 mg (86%) of the product **25**. The analytical sample was crystallized from ethanol (white solid).

Enantiomeric purity was determined by chiral HPLC on a Chirapak IA (Daicel) column with heptane–ethanol 2 : 1 + 0.1% Et_2NH as an eluent (Fig. S4 and S5†).

M.p. 158.5–159.5 °C (EtOH). $[\alpha]_D^{20} = -50.1$ (c 0.154, CH_3OH). Found: C, 53.48; H, 6.24; N, 22.14. Calc. for $C_{14}H_{17}N_5O_2 \cdot 1.5H_2O$: C, 53.49; H, 6.41; N, 22.28%. ^1H NMR (500 MHz, d6-DMSO): δ 1.41–1.48 (m, 1H, H-6en), 1.51–1.57 (m, 1H, H-7en), 1.63–1.70 (m, 1H, H-7ex), 2.02–2.10 (m, 1H, H-6ex), 2.37 (dm, $J_{5-6ex} = 7.9$, 1H, H-5), 3.49 (dd, $J_{CH-OH} = 5.5$, $J_{gem} = 10.5$, 1H, CHbOH), 3.62 (dd, $J_{CH-OH} = 5.5$, $J_{gem} = 10.5$, 1H, CHaOH), 3.73 (d, $J_{8-OH} = 3.5$, 1H, H-8), 4.53 (t, $J_{OH-CH_2} = 5.3$, 1H, CH_2OH), 4.63 (d, $J_{OH-8} = 3.5$, 1H, 8-OH), 4.91–4.93 (m, 1H, H-4), 5.71 (ddd, $J_{3-5} = 1.6$, $J_{3-4} = 3.9$, $J_{3-2} = 9.5$, 1H, H-3), 6.40 (dd, $J_{2-4} = 1.1$, $J_{2-3} = 9.5$, 1H, H-2), 7.27 (bs, 2H, NH_2), 7.90 (s, 1H, H-8'), 8.17 (s, 1H, H-2'). ^{13}C NMR (125.7 MHz, d6-DMSO): δ 25.20 (C-6), 32.41 (C-7), 46.46 (C-5), 51.77 (C-1), 58.82 (C-4), 62.28 (CH_2OH), 71.69 (C-8), 119.39 (C-5'), 120.42 (C-3), 139.06 (C-8'), 142.64 (C-2), 149.18 (C-4'), 151.68 (C-2'), 156.30 (C-6'). ESI MS, m/z (rel%): 310 (100) [M + Na]. HRMS: calcd for [M + H]: 288.14550, found: 288.14557; calcd for [M + Na]: 310.12745, found: 310.12747.

(1S,4R,5R,8S)-4-(6-Amino-9H-purin-9-yl)-1-(hydroxymethyl)-bicyclo[3.2.1]octan-8-ol (26). To a solution of nucleoside **25** (500 mg, 1.74 mmol) in methanol (50 mL) was added $Pd(OH)_2$/C (200 mg) and the reaction mixture was hydrogenated in a steel autoclave (10 bars of hydrogen) at 50 °C for 24 h. Solids were filtered off on a pad of Celite and the residue was chromatographed on a silica gel column (200 g, ethyl acetate → ethyl acetate–acetone–ethanol–H_2O (19 : 3 : 1.8 : 1.2)) to afford 450 mg (89%) of the product **26**. The analytical sample was crystalized from ethanol (white solid). M.p. 241.5–242.5 °C (EtOH). $[\alpha]_D^{20} = +54.5$ (c 0.301, CH_3OH). Found: C, 56.33; H, 6.46; N; 23.23. Calc. for $C_{14}H_{19}N_5O_2 \cdot 0.5H_2O$: C, 56.36; H, 6.76; N, 23.47%. ^1H NMR (600 MHz, d6-DMSO): δ 1.40–1.45 (m, 1H, H-7en), 1.52–1.58 (m, 3H, H-2eq, H-6en, H-7ex), 1.92–2.02 (m, 2H, H-2ax, H-6ex), 2.07–2.17 (m, 2H, H-3), 2.65 (dd, $J_{5-4} = 3.9$, $J_{5-6ex} = 7.0$, 1H, H-5), 3.32 (dd, $J_{CH-OH} = 5.0$, $J_{gem} = 10.5$, 1H, CHbOH), 3.38 (d, $J_{8-OH} = 3.5$, 1H, H-8), 3.53 (dd, $J_{CH-OH} = 5.0$, $J_{gem} = 10.5$, 1H, CHaOH), 4.32 (t, $J_{OH-CH_2} = 5.0$, 1H, CH_2OH), 4.42 (d, $J_{OH-8} = 3.5$, 1H, 8-OH), 4.52–4.54 (m, 1H, H-4), 7.21 (bs, 2H, NH_2), 8.14 (s, 1H, H-2'), 8.15 (s, 1H, H-8'). ^{13}C NMR (150.92 MHz, d6-DMSO): δ 21.51 (C-3), 25.63 (C-6), 28.26 (C-7), 31.75 (C-2), 47.10 (C-5), 49.54 (C-1), 56.99 (C-4), 64.92 (CH_2OH), 74.66 (C-8), 119.12 (C-5'), 138.98 (C-8'), 149.81 (C-4'), 152.44 (C-2'), 156.21 (C-6'). ESI MS, m/z (rel%): 312 (100) [M + Na]. HRMS: calcd for [M + H]: 290.16115, found: 290.16124; calcd for [M + Na]: 312.14310, found: 312.14315.

N-(9-((1R,2R,5S,8S)-8-Hydroxy-5-(hydroxymethyl)-bicyclo-[3.2.1]oct-3-en-2-yl)-9H-purin-6-yl)benzamide (27). Nucleoside **25** (550 mg, 1.91 mmol) was co-evaporated with pyridine (2 ×

2712 | Org. Biomol. Chem., 2015, **13**, 2703–2715

This journal is © The Royal Society of Chemistry 2015

15 mL), dissolved in pyridine (24 mL), cooled to 0 °C and then TMSCl (1.22 mL, 9.6 mmol) was added dropwise for 10 minutes. The reaction mixture was stirred at 0 °C for 1 h and then benzoyl chloride (1.11 mL, 9.6 mmol) was slowly added and the reaction mixture was left at 0 °C for 1 h and at r.t. for another 12 h. The mixture was cooled to 0 °C again, quenched with water (3.5 mL), and after 15 minutes aq. ammonia (6.4 mL, 25%) was added and after further 15 minutes the reaction mixture was evaporated. The residue was re-dissolved in methanol (17 mL) and aq. ammonia (12 mL, 25%) and after 1 h at r.t. evaporated. The residue was chromatographed on a silica gel column (100 g) in ethyl acetate → ethyl acetate–acetone–ethanol–H_2O (21 : 3 : 0.6 : 0.4) to afford 27 (464 mg, 62%) as a yellowish foam. $[\alpha]_D^{20}$ = −86.1 (c 0.296, CH_3OH). Found: C, 63.40; H, 5.46; N, 17.38. Calc. for $C_{21}H_{21}N_5O_3 \cdot 1/3H_2O$: C, 63.46; H, 5.50; N, 17.62%. ^1H NMR (600 MHz, d6-DMSO): δ 1.48–1.54 (m, 1H, H-6en), 1.55–1.60 (m, 1H, H-7en), 1.66–1.73 (m, 1H, H-7ex), 2.07–2.15 (m, 1H, H-6ex), 2.44 (dm, J_{5-6ex} = 8.0, 1H, H-5), 3.51 (dd, J_{CH-OH} = 5.1, J_{gem} = 10.5, 1H, CHbOH), 3.64 (dd, J_{CH-OH} = 5.1, J_{gem} = 10.5, 1H, CHaOH), 3.77 (d, J_{8-OH} = 3.5, 1H, H-8), 4.54 (t, J_{OH-CH_2} = 5.1, 1H, CH_2OH), 4.69 (d, J_{OH-8} = 3.5, 1H, 8-OH), 5.09–5.11 (m, 1H, H-4), 5.77 (ddd, J_{3-5} = 1.6, J_{3-4} = 3.9, J_{3-2} = 9.5, 1H, H-3), 6.39 (dd, J_{2-4} = 1.1, J_{2-3} = 9.5, 1H, H-2), 7.53–7.57 (m, 2H, Ph-m), 7.63–7.66 (m, 1H, Ph-p), 8.04–8.06 (m, 2H, Ph-o), 8.24 (s, 1H, H-8'), 8.77 (s, 1H, H-2'), 11.21 (bs, 1H, NH). ^{13}C NMR (150.92 MHz, d6-DMSO): δ 25.16 (C-6), 32.37 (C-7), 46.45 (C-5), 51.72 (C-1), 59.18 (C-4), 62.23 (CH$_2$OH), 71.82 (C-8), 119.96 (C-3), 126.09 (C-5'), 128.61 (C-m,o), 132.55 (C-p), 133.62 (C-i), 142.87 (C-8'), 143.04 (C-2), 150.48 (C-6'), 151.53 (C-2'), 151.98 (C-4'), 165.87 (COO). ESI MS, m/z (rel%): 414 (100) [M + Na]. HRMS: calcd for [M + Na]: 414.15366, found: 414.15359.

N-(9-((1R,2R,5S,8S)-5-(Bis(4-methoxyphenyl)-(phenyl)methoxy)-methyl-8-hydroxybicyclo[3.2.1]oct-3-en-2-yl)-9H-purin-6-yl)-benzamide (28).

Compound 27 (311 mg, 0.79 mmol) was co-evaporated with pyridine (2 × 7 mL) and then dissolved in pyridine (6 mL) and cooled to 0 °C. DMTrCl (404 mg, 1.19 mmol) was added in one portion and the reaction mixture was slowly warmed to r.t. and then stirred for 48 h. The reaction mixture was evaporated and the residue was dissolved in ethyl acetate (300 mL), washed with a satd solution of sodium bicarbonate (2 × 100 mL) and brine (100 mL), dried with sodium sulfate and evaporated. The residue was chromatographed on a silica gel column (150 g – deactivated with triethylamine, toluene–ethyl acetate 1 : 3) to afford 358 mg (65%) of the product 28 as a foam (contains some inseparable impurities according ^{13}C NMR, the compound was pure enough for the next step). $[\alpha]_D^{20}$ = −8.0 (c 0.313, CH_3OH). Found: C, 72.43; H, 5.83; N, 9.71. Calc. for $C_{42}H_{39}N_5O_5$: C, 72.71; H, 5.67; N, 10.09%. ^1H NMR (500 MHz, d6-DMSO): δ 1.50–1.56 (m, 1H, H-6en), 1.70 (m, 2H, H-7en, H-7ex), 2.08–2.15 (m, 1H, H-6ex), 2.48 (bs, 1H, H-5), 3.06 and 3.29 (2 × d, J_{gem} = 8.4, 2H, OCH$_2$), 3.74 (2 × s, 2 × 3H, 2 × OCH$_3$), 3.88 (bs, 1H, H-8), 4.76 (d, J_{8-OH} = 3.4, 1H, H-8), 5.13–5.15 (m, 1H, H-4), 5.82 (ddd, J_{3-5} = 1.6, J_{3-4} = 3.9, J_{3-2} = 9.4, 1H, H-3), 6.31 (dd, J_{2-4} = 1.1, J_{2-3} = 9.4, 1H, H-2), 6.89–6.92 (m, 4H, H-3″), 7.21–7.24 (m, 1H, 4‴), 7.28–7.30 (m,

4H, H-2″), 7.31–7.34 (m, 2H, H-3‴), 7.42–7.44 (m, 2H, H-2‴), 7.54–7.57 (m, 2H, Bz-m), 7.63–7.66 (m, 1H, Bz-p), 8.04–8.07 (m, 2H, Bz-o), 8.28 (s, 1H, H-8'), 8.79 (s, 1H, H-2'), 11.25 (bs, 1H, NH). ^{13}C NMR (125.7 MHz, d6-DMSO): δ 24.99 (C-6), 32.99 (C-7), 46.55 (C-5), 50.48 (C-1), 55.19 and 55.20 (2 × OCH$_3$), 59.20 (C-4), 64.87 (OCH$_2$), 72.14 (C-8), 85.10 (Ph$_3$CO–), 113.30 and 113.31 (2 × C-3″), 120.00 (C-3), 126.17 (C-5'), 126.75 (C-4‴), 127.92 and 127.96 (C-2″, C-3‴), 128.64 and 128.66 (Bz-o, Bz-m), 129.95 and 129.99 (2 × C-2″), 132.60 (Bz-p), 133.61 (Bz-i), 135.99 and 136.19 (2 × C-1″), 142.68 and 142.75 (C-2 and C-8'), 145.51 (C-1‴), 150.55 (C-6'), 151.61 (C-2'), 152.04 (C-4'), 158.16 and 158.17 (C-4″), 165.93 (COO). ESI MS, m/z (rel%): 716 (100) [M + Na]. HRMS: calcd for [M + Na]: 716.28434, found: 716.28429.

(1S,4R,5R,8S)-4-(6-Benzamido-9H-purin-9-yl)-1-((bis(4-methoxyphenyl)(phenyl)methoxy)methyl)bicyclo[3.2.1]oct-2-en-8-yl (2-cyanoethyl) diisopropylphosphoramidite (29).

Compound 28 (358 mg, 0.52 mmol) and DIPEA (0.353 mL, 2.05 mmol) were dissolved in dry THF (5 mL) and the flask was rinsed several times with argon. 2-Cyanoethyl N,N-diisopropyl-chloro-phosphoramidite (0.21 mL, 0.94 mmol) was added dropwise at r.t. for 15 minutes. The reaction mixture was stirred at r.t. for 3.5 h and then poured into the mixture of a satd solution of sodium bicarbonate with ice (100 mL). The water phase was extracted with ethyl acetate (2 × 200 mL) and the combined organic phases were dried with sodium sulfate and evaporated. The residue was co-evaporated with benzene (2 × 50 mL) and then chromatographed (100 g – deactivated with triethylamine, toluene–ethyl acetate 1 : 1 to afford 297 mg (72%) of the product 29 as a white foam. $^{31}P\{^1H\}$ NMR (202 MHz, d6-DMSO): 145.73, 145.21. ESI MS, m/z (rel%): 916 (100) [M + Na]. HRMS: calcd for [M + H]: 894.41025, found: 894.41126; calcd for [M + Na]: 916.39219, found: 916.39245.

N'-(9-((1R,2R,5S,8S)-5-((Bis(4-methoxyphenyl)-(phenyl)-methoxy)methyl)-8-hydroxybicyclo[3.2.1]octan-2-yl)-9H-purin-6-yl)-N,N-dibutylformimidamide (30).

Saturated nucleoside 26 (430 mg, 1.49 mmol) was suspended in methanol (10 mL), dimethylacetal-N,N-dibutylformamide (0.87 mL, 3.73 mmol) was then added in three portions and the reaction mixture was allowed to stir at r.t. for 11 h. A chromatography on a silica gel column (150 g, ethyl acetate → ethyl acetate–methanol 6 : 1) afforded a foam, which was directly used for the tritylation. The foam was co-evaporated with pyridine (2 × 10 mL), then dissolved in pyridine (10 mL) and cooled to 0 °C. DMTrCl (636 mg, 1.88 mmol) was added in one portion, the reaction mixture was slowly warmed to r.t. and then stirred for 48 h. Volatiles were evaporated and the residue was dissolved in ethyl acetate (300 mL), washed with a satd solution of sodium bicarbonate (2 × 150 mL) and brine (150 mL), dried with sodium sulfate, evaporated and chromatographed on a silica gel column (200 g – deactivated with triethylamine, ethyl acetate–acetone 10 : 1) to afford 727 mg (83%) of 30 as a white foam. $[\alpha]_D^{20}$ = −18.5 (c 0.313, CH_3OH). Found: C, 72.01; H, 7.40; N, 11.17. Calc. for $C_{44}H_{54}N_6O_4$: C, 72.30; H, 7.45; N, 11.50%. ^1H NMR (500 MHz, d6-DMSO): δ 0.93 (q, J_{4-3} = 7.5, 6H, 2 × CH$_3$), 1.28–1.37 (m, 4H, H-4), 1.46–1.51 (m, 1H, H-7″ex),

This journal is © The Royal Society of Chemistry 2015

Org. Biomol. Chem., 2015, 13, 2703–2715 | 2713

1.55–1.65 (m, 6H, H-2, H-6″en, H-7″en), 1.74–1.78 (m, 1H, H-2″ a), 1.94–2.00 (m, 1H, H-6″en), 2.04–2.11 (m, 1H, H-2″b), 2.15–2.20 (m, 2H, H-3″ax, H-3″eq), 2.71 (dd, $J_{5″-6″ex}$ = 7.3, $J_{5″-4″}$ = 3.8, H-5″), 2.90 and 3.40 (2 × d, J_{gem} = 8.4, 2H, OCH₂), 3.40 (d, $J_{8°OH}$ = 3.9, 1H, H-8″), 3.42–3.45 and 3.55–3.64 (2 × m, 2 × 2H, H-2), 3.73 (2 × s, 2 × 3H, 2 × OCH₃), 4.59–4.62 (m, 1H, H-4″), 6.86–6.89 (m, 4H, H-3‴), 7.19–7.22 (m, 1H, H-p), 7.24–7.27 (m, 4H, H-2‴), 7.28–7.31 (m, 2H, H-m), 7.39–7.41 (m, 2H, H-p), 8.33 (s, 1H, H-8′), 8.42 (s, 1H, H-2′), 8.96 (s, 1H, N═CH–NBu₂). ¹³C NMR (150.92 MHz, d6-DMSO): δ 13.77 and 13.95 (2 × CH₃), 19.34 and 19.83 (2 × C-3), 21.37 (C-3″), 25.45 (C-6″), 28.88 and 30.69 (2 × C-3), 29.22 (C-7″), 32.62 (C-2″), 44.55 and 51.07 (2 × C-1), 47.14 (C-5″), 48.68 (C-1″), 55.16 (2 × OCH₃), 57.12 (C-4″), 66.45 (OCH₂), 74.81 (C-8″), 84.91 (Ph₃CO–), 113.18 (C-3‴), 125.64 (C-5′), 126.61 and 127.85 and 127.97 (Ph-o, m, p), 129.96 and 129.98 (C-2‴), 136.19 and 136.38 (C-1″ ′), 140.98 (C-8′), 145.67 (Ph-i), 151.84 (C-2′), 151.88 (C-4′), 158.07 (C-4‴), 158.13 (N═CH–NBu₂), 159.52 (C-6′). ESI MS, m/z (rel %): 731 (100) [M + H]. HRMS: calcd for [M + H]: 731.42793, found: 731.42774.

(1S,4R,5R,8S)-1-((Bis(4-methoxyphenyl) (phenyl)methoxy)-methyl)-4-(6-(((dibutylamino) methylene)amino)-9H-purin-9-yl)-bicyclo[3.2.1]octan-8-yl (2-cyanoethyl) diisopropylphosphoramidite (31). Compound 30 (680 mg, 0.93 mmol) and DIPEA (0.71 mL, 4.08 mmol) were dissolved in dry THF (10 mL) and the flask was rinsed several times with argon. Then 2-cyanoethyl N,N-diisopropylchloro-phosphoramidite (0.42 mL, 1.88 mmol) was added dropwise at r.t. for 15 minutes. The reaction mixture was then stirred at r.t. for 3.5 h and then poured to the mixture of a satd solution of sodium bicarbonate with ice (150 mL). The water phase was extracted with ethyl acetate (2 × 250 mL) and the combined organic phases were dried with sodium sulfate and evaporated. The residue was co-evaporated with benzene (2 × 50 mL) and then chromato-graphed (100 g – deactivated with triethylamine, toluene–ethyl acetate 1 : 9) to afford 693 mg (80%) of the product 31 as a white foam. ³¹P{¹H} NMR (202 MHz, C₆D₆): 147.67, 146.63. ESI MS, m/z (rel%): 931 (100) [M + H]. HRMS: calcd for [M + H]: 931.53578, found: 931.53558; calcd for [M + Na]: 953.51772, found: 953.51730.

Synthesis of oligonucleotides

The oligonucleotides were synthesised from the appropriate monomers on a ~0.5 μmol scale by a standard trityl-off phos-phoramidite method using the LCAA CPG with attached 2′-deoxy-5′-O-dimethoxytritylcytidine-3′-O-hemisuccinate as the first nucleoside. Deprotection and release of oligonucleotides from CPG was achieved with gaseous ammonia (0.7 MPa) at r.t. for 12 h. Oligonucleotides were purified at 55 °C on DNAPac PA100 10 × 250 mm Nucleic Acid Column (Dionex) at a flow rate of 3 mL min⁻¹ using a linear gradient of sodium chloride (20 mM → 500 mM, 60 min) in 50 mM sodium acetate buffer pH 7.0 containing 20% (v) of acetonitrile. Desalting of pure oligonucleotides was performed on 10 μm Luna C18 (2) 10 × 100 mm column (Phenomenex) at a flow rate of 3 mL min⁻¹ using a gradient of acetonitrile (0 → 25%, 30 min) in 0.1 M

Table 2 Analytical data for oligonucleotides

Oligonucleotide	Calcd mass	Found mass
5′-d(GCA²⁵TA²⁵TCA²⁵C)	2790.82	2790.2
5′-r(GCA²⁵UA²⁵UCA²⁵C)	2858.76	2858.4
5′-d(GCA²⁶TA²⁶TCA²⁶C)	2796.82	2796.2
5′-r(GCA²⁶UA²⁶UCA²⁶C)	2864.76	2864.0

triethylammonium hydrogencarbonate. Desalted oligonucleo-tides were freeze-dried and characterized by MALDI TOF (Table 2).

Hybridization study

Thermal experiments with oligonucleotide complexes were performed at 260 nm using a CARY 100 Bio UV Spectrophoto-meter (Varian Inc.) equipped with a Peltier temperature con-troller and thermal analysis software. The aqueous solutions of modified and natural complementary strands (4 nmol of each) were mixed, freeze-dried and dissolved in 50 mM NaH₂PO₄ – Na₂HPO₄ pH 7.2 with 100 mM NaCl (1 mL) to give a 4 μM duplex solution. A heating–cooling cycle over a range of 15–60 °C with a gradient of 0.5 °C min⁻¹ was applied. The T_m value of each complex was determined from the first derivative plots (dA_{260}/dT versus temperature) as the temperature at a local maximum of dA_{260}/dT.

Acknowledgements

Notes and references

1 (a) C. J. Leumann, *Bioorg. Med. Chem.*, 2002, **10**, 841–854; (b) *Antisense Drug Technology: Principles, Strategies, and Applications*, ed. S. T. Crooke, CRC Press, Boca Raton, 2nd edn, 2007; (c) S. Kauppinen, B. Vester and J. Wengel, *Drug Discovery Today Technol.*, 2005, **2**, 287–290.

2 T. Imanishi and S. Obika, *Chem. Commun.*, 2002, 1653–1659.

3 S. Obika, D. Nanbu, Y. Hari, K. Morio, Y. In, T. Ishida and T. Imanishi, *Tetrahedron Lett.*, 1997, **38**, 8735–8738.

4 S. K. Singh, P. Nielsen, A. A. Koshkin and J. Wengel, *Chem. Commun.*, 1998, 455–456.

5 (a) R. N. Veedu and J. Wengel, *Chem. Biodiversity*, 2010, 7, 536–542; (b) T. P. Prakash, *Chem. Biodiversity*, 2011, **8**, 1616–1641.

6 (a) M. A. Campbell, B. Vester and J. Wengel, *Nucleic Acid Ther.*, 2011, **21**, A4; (b) K. K. Karlsen and J. Wengel, *Nucleic Acid Ther.*, 2012, **22**, 366–370; (c) A. S. Jorgensen, L. H. Hansen, B. Vester and J. Wengel, *Bioorg. Med. Chem.*

2714 | *Org. Biomol. Chem.*, 2015, **13**, 2703–2715

This journal is © The Royal Society of Chemistry 2015

Lett., 2014, **24**, 2273–2277; (*d*) M. Hollenstein, *Molecules*, 2012, **17**, 13569–13591.

7 H. Kaur, B. R. Babu and S. Maiti, *Chem. Rev.*, 2007, **107**, 4672–4697.

8 J. F. Xu, Y. Liu, C. Dupouy and J. Chattopadhyaya, *J. Org. Chem.*, 2009, **74**, 6534–6554.

9 (*a*) C. Zhou and J. Chattopadhyaya, *Chem. Rev.*, 2012, **112**, 3808–3832; (*b*) P. P. Seth, C. R. Allerson, A. Berdeja, A. Siwkowski, P. S. Pallan, H. Gaus, T. P. Prakash, A. T. Watt, M. Egli and E. E. Swayze, *J. Am. Chem. Soc.*, 2010, **132**, 14942–14950.

10 (*a*) M. Kaura, D. C. Guenther and P. J. Hrdlicka, *Org. Lett.*, 2014, **16**, 3311; (*b*) M. Kaura, P. Kumar and P. J. Hrdlicka, *J. Org. Chem.*, 2014, **79**, 6256–6268; (*c*) P. Kumar, M. E. Østergaard, B. Baral, B. A. Anderson, D. C. Guenther, M. Kaura, D. J. Raible, P. K. Sharma and P. J. Hrdlicka, *J. Org. Chem.*, 2014, **79**, 5047–5061.

11 (*a*) J. Wang, B. Verbeure, I. Luyten, E. Lescrinier, M. Froeyen, C. Hendrix, H. Rosemeyer, F. Seela, A. Van Aerschot and P. Herdewijn, *J. Am. Chem. Soc.*, 2000, **122**, 8595–8602; (*b*) P. Herdewijn and E. De Clercq, *Bioorg. Med. Chem. Lett.*, 2001, **11**, 1591–1597; (*c*) B. Verbeure, E. Lescrinier, J. Wang and P. Herdewijn, *Nucleic Acids Res.*, 2001, **29**, 4941–4947; (*d*) J. Wang, B. Verbeure, I. Luyten, M. Froeyen, C. Hendrix, H. Rosemeyer, F. Seela, A. Van Aerschot and P. Herdewijn, *Nucleosides, Nucleotides Nucleic Acids*, 2001, **20**, 785–788.

12 K. Robeyns, P. Herdewijn and L. Van Meervelt, *Artif. DNA: PNA & XNA*, 2010, **1**, 2–8.

13 M. Ovaere, P. Herdewijn and L. Van Meervelt, *Chem. – Eur. J.*, 2011, **17**, 7823–7830.

14 (*a*) M. Egli, P. S. Pallan, C. R. Allerson, T. P. Prakash, A. Berdeja, J. H. Yu, S. Lee, A. Watt, H. Gaus, B. Bhat, E. E. Swayze and P. P. Seth, *J. Am. Chem. Soc.*, 2011, **133**, 16642–16649; (*b*) P. P. Seth, J. H. Yu, A. Jazayeri,

P. S. Pallan, C. R. Allerson, M. E. Østergaard, F. W. Liu, P. Herdewijn, M. Egli and E. E. Swayze, *J. Org. Chem.*, 2012, **77**, 5074–5085; (*c*) M. E. Jung, T. A. Dwight, F. Vigant, M. E. Østergaard, E. E. Swayze and P. P. Seth, *Angew. Chem., Int. Ed.*, 2014, **37**, 9893–9897.

15 A. A. Koshkin, J. Fensholdt, H. M. Pfundheller and C. Lomholt, *J. Org. Chem.*, 2001, **66**, 8504–8512.

16 E. Abraham, C. W. Bailey, T. D. W. Claridge, S. G. Davies, K. B. Ling, B. Odell, T. L. Rees, P. M. Roberts, A. J. Russell, A. D. Smith, L. J. Smith, H. R. Storr, M. J. Sweet, A. L. Thompson, J. E. Thomson, G. E. Tranter and D. J. Watkin, *Tetrahedron: Asymmetry*, 2010, **21**, 1797–1815.

17 F. H. Wu, R. Hong, J. H. Khan, X. F. Liu and L. Deng, *Angew. Chem., Int. Ed.*, 2006, **45**, 4301–4305.

18 M.-H. Filippini, R. Faure and J. Rodriguez, *J. Org. Chem.*, 1995, **60**, 6872–6882.

19 K. C. Nicolau, Y.-L. Zhong and P. S. Baran, *J. Am. Chem. Soc.*, 2000, **122**, 7596–7597.

20 J. L. Luche, *J. Am. Chem. Soc.*, 1978, **100**, 2226–2227.

21 P. S. Jones, P. W. Smith, G. W. Hardy, P. D. Howes, R. J. Upton and R. C. Bethell, *Bioorg. Med. Chem. Lett.*, 1999, **9**, 605–610.

22 C. Ding, Y. Zhang, H. Chen, C. Wild, T. Wang, M. A. White, Q. Shen and J. Zhou, *Org. Lett.*, 2013, **15**, 3718–3721.

23 M. Dejmek, S. Kovačková, E. Zborníková, H. Hřebabecký, M. Šála, M. Dračínský and R. Nencka, *RSC Adv.*, 2012, **2**, 6970–6980.

24 M. Dejmek, M. Šála, P. Plačková, M. Hřebabecký, L. Mascarell Borredà, J. Neyts, M. Dračínský, E. Procházková, P. Jansa, P. Leyssen, H. Mertlíková-Kaiserová and R. Nencka, *Arch. Pharm.*, 2014, **347**, 478–485.

25 M. T. Migawa, T. P. Prakash, G. Vasquez, P. P. Seth and E. E. Swayze, *Org. Lett.*, 2013, **15**, 4316–4319.

26 M. R. Harnden, P. G. Wyatt, R. B. Boyd and D. Sutton, *J. Med. Chem.*, 1990, **33**, 187–196.

This journal is © The Royal Society of Chemistry 2015

Org. Biomol. Chem., 2015, **13**, 2703–2715 | **2715**

II.

Hřebabecký, H. – **Procházková, E**. – Šála, M. – Plačková, P. – Tloušťová, E. – Barauskas, O. – Lee, Y.J. – Tian, Y. – Mackman, R. – Nencka, R.:

Synthesis of conformationally restricted
6- and 7- membered ring bicycloribonucleosides/tides
and their recognition by kinases and polymerases.

Synthesis of conformationally restricted 6- and 7-membered ring bicycloribonucleosides/tides and their recognition by kinases and polymerases.

Hubert Hřebabecký,[a] Eliška Procházková,[a] Michal Šála,[a] Pavla Plačková,[a] Eva Tloušťová,[a] Ona Barauskas,[b] Yu-Jen Lee,[b] Yang Tian,[b] Richard Mackman[b] and Radim Nencka[a,*]

We prepared a novel series of conformationally restricted bicyclonucleosides and nucleotides. The synthetic approach employed a ring closing metathesis to provide access to both 6 and 7 membered saturated and unsaturated rings linking the 3' to 5' methylene groups of the sugar. The bicyclonucleoides were also transformed to the corresponding phosphoramidate prodrugs by an innovative one pot protocol of boronate ester protection, coupling of the phosphoryl chloridate and deprotection of the boronate. A similar strategy was also employed for the synthesis of the corresponding monophosphates as crucial intermediates for the synthesis of selected triphosphates. The biological properties of the nucleosides and monophosphate prodrugs were assessed for antiviral and cytostatic activities in cell based assays whilst the triphosphates were evaluated in enzymatic assays. The lack of significant effects suggests that the linkage of the 3' to 5' via a ring system and the subsequent conformational restriction of the ribose ring to the South conformation are incompatible with the kinases and polymerases that recognize nucleosides and their metabolites.

Introduction

Nucleosides and their phosphorylated metabolites (nucleotides) are vital components of living organisms. The recognition of nucleosides by proteins e.g. kinases involved in activation to the mono, di- and triphosphates, and the multiple roles of the triphosphate metabolites in providing energy for biological processes, and carrying genetic information, make understanding the protein-nucleoside/tide interactions valuable. One component of this interaction is the three dimensional conformation of the nucleoside/tide species in solution which has been well studied. The sugar ring of nucleosides/tides rapidly interconverts between the so called North (3'-endo) and South (2'-endo) conformations in solution (Figure 1). In addition to the sugar ring conformation, the orientation of 4'-5' bond (γ angle) and the orientation of the nucleobase are also essential features.[1, 2] Although a hydroxy group (or a phosphate group) at 5' position can rotate around the axis, the energetically preferred conformations are plus synclinal (+sc) and antiperiplanar (ap), which are equally populated in solutions of purine nucleosides, whereas +sc conformation is preferred in nucleotides.[1]

During interaction with their protein targets, nucleosides/tides presumably adopt the preferred binding conformation potentially with an entropic penalty. Given the flexibility of the sugar ring these interactions with proteins may favor one or more conformations. For example, Marquez and co-workers elegantly showed that deoxynucleosides/tides locked in South and North conformations can be efficiently recognized by different enzymes. Carbocyclic nucleoside derivatives N-MCT and S-MCT were designed to 'lock' the ring in the North and South conformation respectively. They discovered that the North conformation effectively binds to polymerases[3-5] whereas South is recognized by HSV-1 thymidine kinase.[6]

Recently, we have prepared a different pair of carbocyclic North/South adenosines[7,8] (as well as their analogues with other nucleobases), primarily inspired by LNA[9-11] monomers. The North derivatives were largely inactive against a panel of viruses (suggesting limited recognition by viral polymerases if one assumes the triphosphates were generated in the cells utilized), but phosphatidylinositol 4-kinase IIα bound the North-type adenosine derivative with affinity significantly exceeding that of adenosine.[7] Nucleoside triphosphate binding proteins are probably able to discriminate between nucleotides with different γ angles; however, there is no direct evidence of this to date. Taken together, our understanding of conformational preferences nucleosides/tides binding proteins is still rather limited yet fundamental to the design of selective therapeutics to address abnormalities in the pathways that lead to disease.
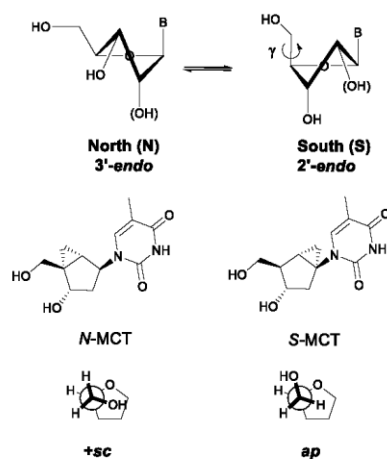
Figure 1. North and South conformation of natural nucleosides and examples of derivatives locked in these conformations.

In this study novel bicyclic adenosine nucleoside derivatives were designed that combine both the conformational restriction of the sugar moiety in the South orientation as well as provide for a defined γ angle (either +sc or ap). Furthermore, to interrogate whether the phosphorylated species can interact with proteins we have prepared monophosphate prodrugs in an attempt to deliver the monophosphate species into cells and potentially the triphosphate metabolite through activation by intracellular kinases. Finally, selected triphosphates were

prepared and evaluated for their recognition properties toward a variety of viral polymerases.

Results and discussion

Design and synthesis of a new series of bicyclic nucleoside and nucleotide derivatives

The design of the bicyclic adenosine derivatives was inspired by the work of Leumann et al., where bicyclic and tricyclic deoxynucleoside derivatives were utilized as monomers for oligonucleotide synthesis with duplex stabilizing properties.[12-15] In contrast to Leumann's work, we were primarily interested in the preparation of ribonuclosides/tides with six and seven membered, saturated and unsaturated, rings bridging between the 3' and 5' position of the ribo-sugar. To access these ring systems we envisaged utilizing a ring closing metathesis approach. Allose derivative 1[16] was selected as the starting material in the forward synthesis (Scheme 1). Deprotection and oxidative cleavage of the 5,6-diol was performed with periodic acid in ethyl acetate[17] to provide the 5-carboxaldehyde 2, which was then used directly in the next reaction with vinylmagnesium bromide or allylmagnesium bromide to provide dienes 3 and 6 respectively. The dienes 3 and 6 were then treated with 2nd generation Grubbs' catalyst in dichloromethane to generate the 6- and 7-membered ring intermediates as mixtures of diastereoisomers. The diastereoisomers were separated by chromatography on silica gel to yield compounds 4a (32%), 4b (18%), 7a (26%), and 7b (30%). The yields are calculated from starting allose derivative 1. Selective benzoylation of the compounds provided monobenzoates 5a (92 %), 5b (94%), 8a (89%), and 8b (74 %).
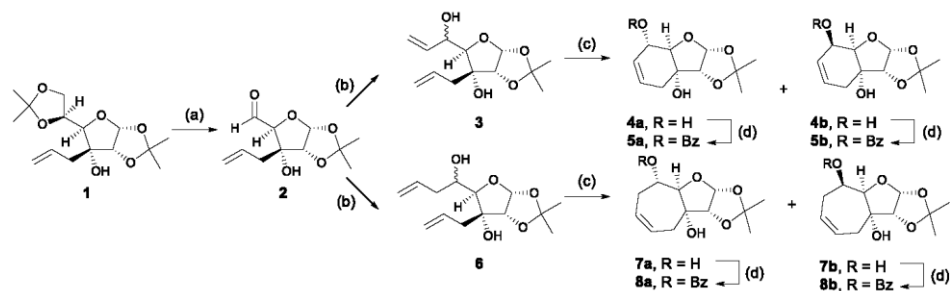
Scheme 1. Synthesis of sugar derivatives 5a, 5b and 7a, 7b. Reagents and conditions: (a) H₅IO₆, EtOAc, r.t., 5 h; (b) vinyl or allylmagnesium bromide, THF, 2 h at 0 °C and overnight at r.t.; (c) Grubbs' catalyst 2nd generation, DCM, 40 °C, 4 h, 32% of 4a, 18% of 4b, 26% of 7a and 30% of 7b from 1; (d) benzoyl chloride, pyridine, r.t., overnight, 92 % of 5a, 94% of 5b, 89% of 8a and 74 % of 8b.
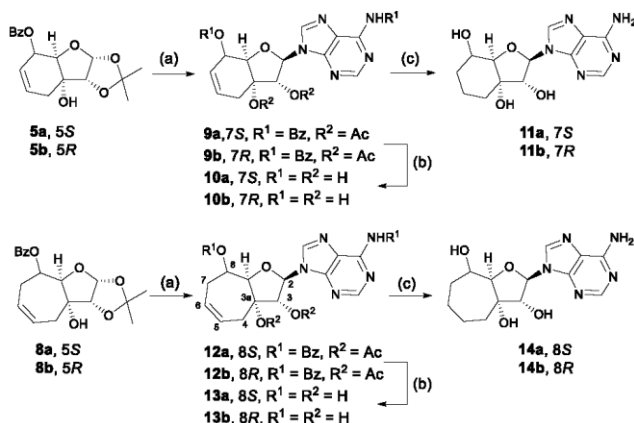
Scheme 2. Synthesis of free nucleoside analogues **10a**, **10b**, **11a**, **11b**, **13a**, **13b**, **14a**, **14b**. Reagents and conditions: (a) 1. 80% aq. TFA, r.t., 3 h; 2. Ac$_2$O, CH$_3$CN, DMAP, r.t., 16 h; 3. N^6-benzoyladenine, CH$_3$CN, SnCl$_4$, r.t., 3 h, 58% of **9a**, 55% of **9b**, 63% of **12a**, 76% of **12b**; (b) 0.1 M methanolic CH$_3$ONa, r.t., 16 h, 58% of **10a**, 92% of **10b**, 63% of **13a**, 66% of **13b**; (c) Pd(OH)$_2$/C, H$_2$, DMF, r.t., 16 h, 66% of **11a**, 70% of **11b**, 78% of **14a**, 75% of **14b**.
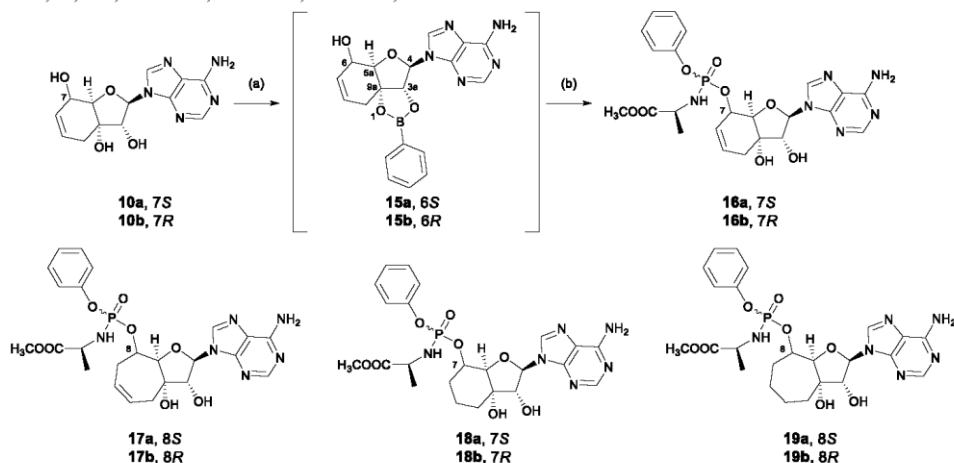
Scheme 3. Preparation of unprotected nucleotide analogue **16a** and **16b**. Reagents and conditions: (a) phenyl boronic acid, pyridine, heating; (b) N-[chloro(phenoxy)phosphoryl]-L-alaninate, 1-methylimidazole, THF, r.t., overnight, 54% of **16a**, 55% of **16b**. Structures of Pro-Tides **17a**, **17b**, **18a**, **18b**, **19a**, and **19b**.

Compounds **5a**, **5b**, **8a**, and **8b** were then converted to anomeric mixtures of acetates by treatment with aqueous trifluoroacetic acid followed by acetylation with acetic acid anhydride in acetonitrile, in the presence of 4-dimethylaminopyridine (Scheme 2). The sugar derivatives were then subjected to a Vorbrüggen reaction[18] with N^6-benzoyladenine in acetonitrile and Lewis acid catalyst, tin(IV) chloride, to afford the protected

nucleoside analogues, **9a** (58%), **9b** (55%), **12a** (63%), and **12b** (76%), respectively. Methanolysis with methanolic sodium methoxide yielded the free nucleosides **10a** (68%), **10b** (92%), **13a** (80%), and **13b** (66%). Hydrogenation of the unsaturated nucleosides on Pd(OH)$_2$/C in DMF led to saturated analogues **11a** (66%), **11b** (70%), **14a** (78%), and **14b** (75%), respectively.

The unambiguous transformation of the prepared nucleosides to monophosphate nucleotide prodrugs (Pro-Tides) required protection of the hydroxyl groups at positions 3 and 3a (Scheme 3). Typically an isopropylidine would suffice, but significant problems were encountered during acidic removal of the protecting group. A cyclic phenyl boronate was found to be the ideal protection. The unprotected nucleosides were treated with phenylboronic acid in boiling pyridine, which was slowly distilled off to azeotropically remove water. Subsequent reaction of the protected products with N-[chloro(phenoxy)phosphoryl]-L-alaninate in tetrahydrofuran in the presence of 1-methylimidazole[5] afforded the target Pro-Tides in 50 − 76% yields over two steps as 1:1 mixture of diastereomers (determined by NMR spectroscopy) due to the chiral phosphorus atom (Scheme 3).[19]
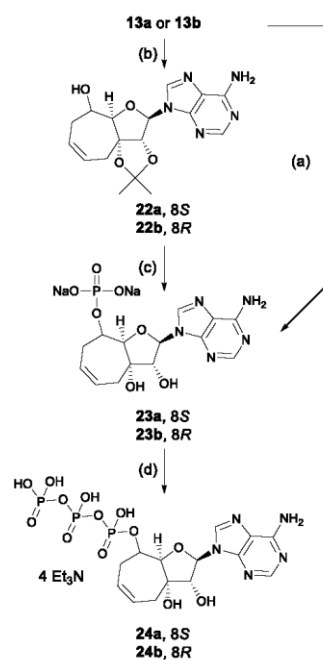
Scheme 4. Preparation of triphosphate anlogues **24a** and **24b**. Reagents and conditions: (a) 1. phenyl boronic acid, pyridine; 2. POCl$_3$, PO(OCH$_3$)$_3$, r.t., 4h; 3. H$_2$O, 0 °C, 26% of **23a**, 27% of **23b**; (b) 1. 2,2,-dimethoxypropane, DMF, H$_2$SO$_4$, 79% of **22a**, 69.5% of **22b**; (c) 1. POCl$_3$, PO(OCH$_3$)$_3$, r.t., 4h; 2. H$_2$O, 0 °C; 3. 50% aqueous TFA, r.t., 48 h, 38% of **23a**, 39% of **23b**; (d) 1. Dowex 50 (Et$_3$NH$^+$); 2. imidazole, PPh$_3$, Et$_3$N, 2,2′-dipyridyl disulfide, DMF-DMSO, r.t., overnight; 3. (nBu$_3$NH)$_2$P$_2$H$_2$O$_7$, DMSO, r.t., overnight.

In order to investigate the effect of the nucleosides **13a** and **13b** on the enzymatic level, we had to prepare the triphosphates that would mimic ATP in its South conformation. We achieved this goal by sequential synthesis of the monophosphates, followed by addition of pyrophosphate to generate of triphosphates. The yield of phosphates generated using a similar procedure to that described for the prodrugs via the cyclic boronate was generally very low (26% of **23a** and 27% of **23b**), therefore, we resorted back to the isopropylidene group. Isopropylidene derivatives **22a** and **22b** were prepared by a treatment of **13a** or **13b** with 2,2-dimethoxypropane in dimethylformamide in the presence of conc. H$_2$SO$_4$. Protected nucleosides **22a** and **22b** were converted to phosphate with POCl$_3$ in trimethyl phosphate and then deprotected with 50% aqueous trifluoroacetic acid. The crude product was purified and converted to the sodium salt providing nucleotide **23a** in 38% and **23b** in 39% yield respectively.

Triphosphates **24a** and **24b** were prepared from the triethylammonium salts, obtained by cation-exchange of the sodium salts **23a** and **23b** on Dowex 50 (Et$_3$NH$^+$). The triethylammonium salts were treated with imidazole, triphenylphosphine, triethylamine and 2,2′-dipyridyl disulfide in a mixture of DMSO and DMF at ambient temperature overnight. Reaction of the imidazolide intermediates that were generated with tributylammonium pyrophosphate led to the formartion of the crude triphosphates which were then purified by HPLC chromatography.

Conformational analysis of compound 13a

Due to the additional seven-membered ring in compound **13b**, the flexibility of the ribose ring is significantly reduced. Experimental J-coupling values obtained from ^{1}H NMR spectrum were compared with values calculated by two different approaches. First, the geometry of compound **13b** was optimized by DFT starting from four initial conformations. Torsion angles Φ_0 and Φ_3 with pucker amplitude Φ_{MAX} = 40° according to Altona-Sundaralingam[2] were set and four geometries with phase angles P = 0°, 90°, 180° and 270° were optimized. After geometry optimization of all four initial geometries, only one conformer was found with torsion angles Φ_0-Φ_4: -30.8°, 20.5°, -0.8°, -19.5° and 31.5°, respectively.

The obtained torsion angles were used as input for J-couplings calculated by empirical Haasnoot-Altona equation[20] (J_{ALTONA} in Table 1), which describes the dependence of vicinal J-coupling values on the torsion angle between the coupled nuclei. J-couplings were also calculated by DFT method (J_{DFT} in Table 1). Both theoretical approaches provided similar values, which fit well with the experimentally obtained J-couplings (J_{EXPER} in Table 1). From the obtained torsion angles, we can conclude that compound **13b** is present in a solution in South conformation (^{2}E) with phase angle P = 163°. The geometry optimization also indicated that the adenine nucleobase is oriented *syn* with respect to the ribose residue. The free energy difference between *syn-* and *anti-* conformation was calculated to be 5.4 kcal/mol. Only the *syn-* conformer was, therefore, used for J-coupling calculations.
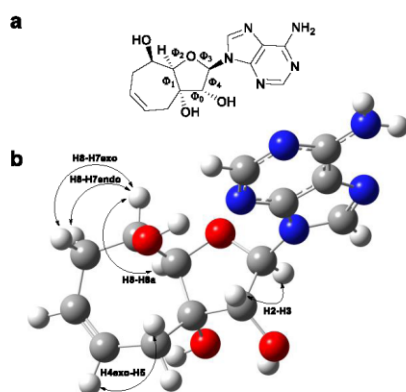
Figure 3. (a) The chemical structure of compound **13b** and the torsion angles Φ_0-Φ_4. (b) Optimized geometry of compound **13b** (B3LYP/6-31+g(d,p)) and the spin-spin interactions described in the Table 1.

Table 1. Comparison of calculated coupling constants (J) of compound **13b** by Haasnoot-Altona equation[20] and DFT method (B3LYP/6-31g (d)) with experimentally obtained values.

Interaction	J_{ALTONA} (Hz)	J_{DFT} (Hz)	J_{EXPER} (Hz)
H2-H3	7.2	5.6	8.1
H8-H8a	1.3	1.0	1.6
H8-H7exo	2.0	2.0	1.7
H8-H7endo	5.0	4.9	4.3
H4exo-H5	-[a]	4.2	4.4

[a] Undefined for sp^2 hybridized carbon atoms (H-5).

Biological evaluation of nucleoside derivatives and their monophosphate prodrugs in cell based assays

All the locked nucleoside derivatives (**10a**, **10b**, **11a**, **11b**, **13a**, **13b**, **14a**, and **14b**) were screened for cytostatic activity on several cell lines (HepG2, HL60, HeLa S3, CCRF-CEM) and all lacked cytostatic activity. These compounds were also screened for antiviral activity in a panel of viruses including HCV (1a, 1b, and 2a) (Huh-7 cells), HIV (MT4 cells), HRV (HeLa cells) and RSV (HEp-2 cells) and no activity was observed up to 50 uM of testing. Thus it was clear that no obvious protein recognition of the locked nucleosides was apparent from these initial experiments. Subsequently the phosphoramidate prodrugs were also evaluated in the same suite of assays and, in general, no activities up to assay limits were observed. The phospharamidate prodrug **17b** exerted modest antiviral activity against HCV 1a (EC$_{50}$ = 23 µM) that suggests this nucleoside monophosphate may have interactions with the enzymes responsible for activation to the triphosphate and subsequent inhibition of the viral polymerase, or alternatively targets other proteins that can impact the replication of HCV

Enzymatic decomposition of prodrugs 17a and 17b monitored by ^{31}P NMR spectroscopy

To further understand the lack of biological activity for the majority of the monophosphate prodrugs and confirm that the weakly active prodrug compound **17b** was being efficiently converted to the parent monophosphate inside the HCV replicon cells, we evaluated the prodrug breakdown process using carboxypeptidase Y. It is widely reported that the Pro-Tide prodrug breakdown is initiated by carboxypeptidases.[21] The starting phosphoramidate derivative **17b** has two signals in the proton decoupled ^{31}P NMR spectra corresponding to the two P diastereoisomers. After the enzyme addition (Figure 6b), two new phosphorus signals for intermediate **20b**[22] appeared which over several hours resolved to a single ^{31}P NMR signal for product **21b**. Similar progress of the reaction was observed after chemical hydrolysis of the starting phosphoramidate in triethylamine solution to yield the same final intermediate **21b**. For compound **17a**, similar progress of both enzymatic and chemical hydrolytic reaction was observed.

The final reaction mixture containing the product **21b**, methanol and phenol, was confirmed by comparing the ^{13}C NMR spectra of the reaction mixture before and after HPLC removal of MeOH and PhOH (Supporting information Figure S3.). The data with carboxypeptidase Y suggests that in the timescale of the cell based assays (3-5 days) the phosphoramidate prodrugs are being efficiently cleaved by esterases even though the position 8 (or 7 in the case of the 6 –membered ring) is sterically hindered. Whilst the data does not prove the intracellular formation of the monophosphate since further intracellular breakdown is necessary e.g. P-N bond cleavage by HINT enzymes to form the monophosphate, it does support that the breakdown process is not limited by the esterase cleavage and encouraged the preparation of the triphosphate species for evaluation.

Evaluation of triphosphates 24a and 24b in enzymatic assays

The triphosphate of nucleoside **17b**, i.e. **24b** was tested for inhibition of the HCV RNA-dependent RNA polymerase and found to be a weak inhibitor with IC$_{50}$ = 143 µM. Also, this triphosphate compound did not inhibit polymerase from influenza and human rhinovirus 16 (IC$_{50}$ were higher than 200 µM in both cases). Both triphosphate **24a** and **24b** were also evaluated in enzymatic assays of our current interest including phosphatidylinositol 4-kinases (PI4K IIIα, PI4K IIIβ, PI4K IIα) and adenylate cyclases from Bordetella pertussis and Antrax edema factor.

Starting phosphoramidate derivative 17a or 17b

Carboxypeptidase Y or 3% Et₃N/D₂O

Intermediate 20a or 20b
Two ³¹P NMR signals = chiral centre at phosphorus atom

Final product 21a or 21b
Only one ³¹P NMR signal = no chiral phosphorus
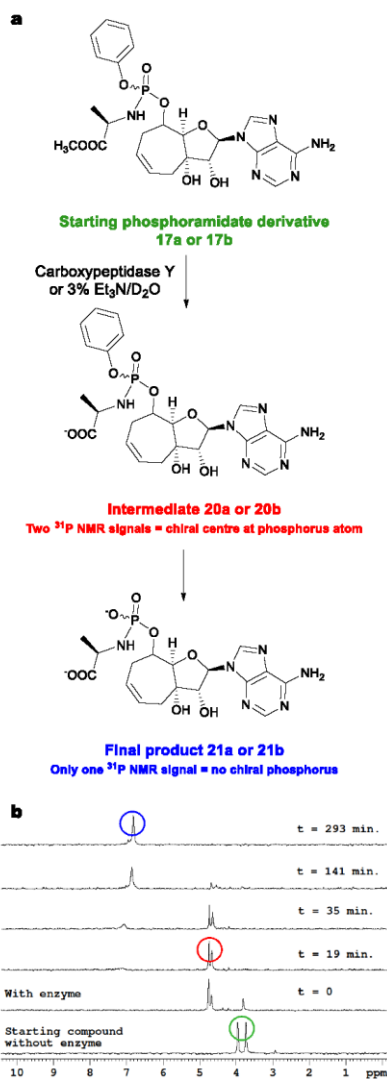
Figure 6. (a) Proposed breakdown pathway to phosphoramidate intermediate (b) Enzymatic decomposition of phosphoramidate derivative **17b** monitored by ³¹P NMR spectroscopy.

None of these enzymes were inhibited by these triphosphates. Altogether the data suggest that the triphosphates in the South conformation are not effective substrates for viral polymerases, consistent with the data of Marquez et al. on S-MCT analogs.

Conclusions

We report on a novel series of bicyclic ribonucleosides locked in South conformation through linking of the 3' and 5' methylene via ring closing metathesis methodologies. .

The efficient preparation of phosphoramidate prodrugs was achieved by employing a one-pot procedure involving a cyclic boronate protection of the cis-diol which can be easily removed after installation of the prodrug during work-up conditions.

All the bicyclic nucleoside derivatives and their prodrugs were screened in several cell-based assays in order to assess phenotypic engagement with cellular proteins. The lack of activity for the majority suggests the conformationally restricted sugars in the South orientation, and/or the additional atoms of the ring appended to the natural ribose sugar are not compatible with protein binding sites. In the one example, where modest activity was observed **17b**, evaluation of the triphosphate analog suggested the effect was likely non- specific. The results reported suggest that additional tools will be required to investigate the conformational aspects of sugars that favor nucleoside/tide interactions with proteins of interest.

Experimental

General

Melting points were determined on a Büchi B-540 apparatus. NMR spectra (δ, ppm; J, Hz) were measured on a Bruker Avance II-600 and/or Bruker Avance II-500 instruments (600.1 or 500.0 MHz for ¹H and 150.9 or 125.7 MHz for ¹³C) in hexadeuterated dimethyl sulfoxide and referenced to the solvent signal (δ 2.50 and 39.70 ppm, respectively). Mass spectra were measured on a LTQ Orbitrap XL (Thermo Fisher Scientific) using electrospray ionization (ESI). Column chromatography was performed on Silica gel 60 (Fluka) and thin-layer chromatography (TLC) on Silica gel 60 F254 foils (Merck). Solvents were evaporated at 2 kPa and bath temperature 30–60 °C; the compounds were dried at 13 Pa and 50 °C. The elemental analyses were obtained on a Perkin–Elmer CHN Analyzer 2400, Series II Sys (Perkin–Elmer). The elemental compositions for all compounds agreed to within ± 0.4% of the calculated values. For all the tested compounds satisfactory elemental analysis was obtained supporting > 95% purity. Optical rotation was measured on polarimeter Autopol IV (Rudolph Research Analytical) at 589 nm wavelength in chloroform or methanol.

Preparation of compounds 4a, 4b, 7a, and 7b

Periodic acid (7.07 g, 31.0 mmol) was added to a solution of 3-allyl-1,2:5,6-di-O-isopropylidene-α-D-allofuranose[2] (**1,** 8.41g, 28.0 mmol) in ethyl acetate (320 mL) and the mixture was stirred at room temperature under argon for 5 h, then filtered and evaporated. The residue was co-evaporated with toluene (2 x 100 mL) and dried under vacuum at 40 °C for 5 h. To a solution of thus obtained aldehyde in THF (200 mL) cooled to 0 °C was

added dropwise 1 M vinylmagnesium bromide solution in THF or 1 M allylmagnesium bromide solution in diethyl ether (80 mL), the mixture was stirred at 0 °C for 2 h and at room temperature overnight, cooled to 0 °C, treated with water (10 ml) and evaporated. The residue was triturated with ethyl acetate (200 ml), solids were filtered off and the solvent was removed in vacuo. The 2nd generation Grubbs catalyst (392 mg, 0.462 mmol) was added to a solution of the residue in dichloromethane and the solution was stirred at 40 °C under argon for 4 h, then at room temperature overnight and evaporated. Chromatography of the residue on silica gel (1 kg) in toluene – ethyl acetate (3:2) afforded compounds **4a** and **4b** or **7a** and **7b**.

(3a*R*,4a*R*,5*S*,8a*R*,8b*R*)-2,2-Dimethyl-3a,4a,5,8,8a,8b-hexahydro-[1,3]dioxolo[4,5-*b*]benzofuran-5,8a-diol (4a)

Yield 2.206 g (32% based on **1**) of a greyish solid foam. $[\alpha]_D^{20}$ +14.7 (c = 0.443, CHCl$_3$). Found: C, 57.86; H, 7.10. Calc. for C$_{11}$H$_{16}$O$_5$: C, 57.88; H, 7.07%. ^{1}H NMR (500 MHz, d6-DMSO): δ 1.26 (s, 3 H, CH$_3$exo), 1.47 (s, 3 H, CH$_3$endo), 1.84 (m, 1 H, H-8eq), 1.97 (m, 1 H, H-8ax), 3.96 (d, J_{4a-5} = 4.2, 1 H, H-4a), 4.14 (m, 1 H, H-5), 4.17 (d, J_{8b-3a} = 3.6, 1 H, H-8b), 4.79 (bs, 1 H, 5-OH), 5.04 (bs, 1 H, 8a-OH), 5.46–5.48 (m, 2 H, H-6, H-7), 5.68 (d, J_{3a-8b} = 3.6, 1 H, H-3a). ^{13}C NMR (125 MHz, d6-DMSO): δ 26.51 (CH$_3$exo), 26.55 (CH$_3$endo), 32.94 (C-8), 64.08 (C-5), 76.02 (C-4a), 76.09 (C-8a), 83.54 (C-8b), 103.56 (C-3a), 111.69 (C-2), 123.55 (C-7), 128.50 (C-6). HRMS (ESI): calcd. for C$_{11}$H$_{16}$O$_5$Na [M + Na] 251.08899; found: 251.08894.

(3a*R*,4a*R*,5*R*,8a*R*,8b*R*)-2,2-Dimethyl-3a,4a,5,8,8a,8b-hexahydro-[1,3]dioxolo[4,5-b]benzofuran-5,8a-diol (4b)

Yield 1.17 g (18% based on **1**) of a greyish crystals. M.p. 94-97 °C (diethyl ether). $[\alpha]_D^{20}$ +117 (c = 0.378, CHCl$_3$). Found: C, 57.86; H, 6.94. Calc. for C$_{11}$H$_{16}$O$_5$: C, 57.88; H, 7.07%. ^{1}H NMR (500 MHz, d6-DMSO): δ 1.26 (s, 3 H, CH$_3$exo), 1.47 (s, 3 H, CH$_3$endo), 1.76 (dm, J_{gem} = 18.0, 1 H, H-8eq), 2.04 (ddm, J_{gem} = 18.0, J_{8ax-7} = 5.7, 1 H, H-8ax), 3.81–3.91 (m, 2 H, H-4a, H-5), 4.11 (d, J_{8b-3a} = 3.8, 1 H, H-8b), 4.69 (s, 1 H, 8a-OH), 4.82 (d, J_{OH-5} = 5.9, 1 H, 5-OH), 5.62 (d, J_{3a-8b} = 3.8, 1 H, H-3a), 5.65 (m, 1 H, H-7), 5.69 (m, 1 H, H-6). ^{13}C NMR (125 MHz, d6-DMSO): δ 26.54 (CH$_3$exo), 26.68 (CH$_3$endo), 31.33 (C-8), 63.70 (C-5), 72.83 (C-8a), 80.34 (C-4a), 83.55 (C-8b), 103.11 (C-3a), 111.51 (C-2), 124.09 (C-7), 127.76 (C-6). ESI MS, *m/z* (%): 252.1 (15) [M + Na + H], 251.1 (100) [M + Na]. HRMS (ESI): calcd. for C$_{11}$H$_{16}$O$_5$Na [M + Na] 251.08899; found: 251.08895.

(3a*R*,4a*R*,5*S*,9a*R*,9b*R*)-2,2-Dimethyl-4a,5,6,9,9a,9b-hexahydro-3a*H*-cyclohepta[4,5]furo[2,3-d][1,3]dioxole-5,9a-diol (7a)

Yield 1.73 g (26% based on **1**) of a white crystals. M.p. 135.5-136.5 °C (diethyl ether). $[\alpha]_D^{20}$ +39.1 (c = 0.399, CHCl$_3$). Found: C, 59.47; H, 7.47. Calc. for C$_{25}$H$_{24}$O$_7$: C, 59.24; H, 7.49%. ^{1}H NMR (500 MHz, d6-DMSO): δ 1.26 (s, 3 H, CH$_3$ exo), 1.47 (s, 3 H, CH$_3$ endo), 1.91 (ddm, J_{gem} = 16.4, J_{6eq-7} = 8.2, J_{6eq-5} = 1.2, 1 H, H-6eq), 2.03 (ddm, J_{gem} = 17.4, J_{9ax-8} = 7.3, 1 H, H-9ax), 2.19 (dm, J_{gem} = 17.4, H-9eq), 2.45 (m, 1 H, H-6ax), 3.51 (m, 1 H, H-5), 3.68 (dd, J_{4a-5} = 7.1, J_{4a-9en} = 1.7, 1 H, H-4a), 3.98 (d,

J_{9b-3a} = 3.8, 1 H, H-9b), 4.64 (m, 1 H, 9a-OH), 4.95 (d, J_{OH-5} = 4.8, 1 H, 5-OH), 5.32 (m, 1H, H-8), 5.60 (m, 1 H, H-7), 5.70 (d, J_{3a-9b} = 3.8, 1 H, H-3a). ^{13}C NMR (125 MHz, d6-DMSO): δ 26.78 (CH$_3$ exo), 26.98 (CH$_3$ endo), 33.17 (C-6), 33.71 (C-9), 72.07 (C-5), 77.43 (C-9a), 85.58 (C-9b, 86.79 (C-4a), 102.92 (C-3a), 111.13 (C-2), 125.18 (C-8), 127.85 (C-7). HRMS (ESI): calcd. for C$_{12}$H$_{18}$O$_5$Na [M + Na] 265.10460; found: 265.10462.

(3a*R*,4a*R*,5*R*,9a*R*,9b*R*)-2,2-Dimethyl-4a,5,6,9,9a,9b-hexahydro-3a*H*-cyclohepta[4,5]furo[2,3-d][1,3]dioxole-5,9a-diol (7b)

Yield 2.06 g (30% based on **1**) of a white crystals. M.p. 79–80 °C (diethyl ether). $[\alpha]_D^{20}$ -5.1 (c = 0.454, CHCl$_3$). Found: C, 59.61; H, 7.57. Calc. for C$_{25}$H$_{24}$O$_7$: C, 59.24; H, 7.49%. ^{1}H NMR (500 MHz, d6-DMSO): δ 1.26 (s, 3 H, CH$_3$ exo), 1.46 (s, 3 H, CH$_3$ endo), 1.91 (ddm, J_{gem} = 14.4, J_{6eq-7} = 8.0, 1 H, H-6eq), 1.95 (ddd, J_{gem} = 14.4, J_{9ax-8} = 8.0, J_{9ax-4a} = 0.9, 1 H, H-9ax), 2.19 (dm, J_{gem} = 14.4, 1 H, H-9eq), 2.56 (m, 1 H, H-6ax), 3.57 (m, 1 H, H-5), 3.99 (d, J_{9b-3a} = 3.8, 1 H, H-9b), 4.00 (m, 1 H, H-4a), 4.71 (d, J_{OH-5} = 5.8, 1 H, 5-OH), 4.83 (t, J_{OH-9b} = J_{OH-9eq} = 0.7, 1 H, 9a-OH), 5.53 (m, 1 H, H-8), 5.71 (d, J_{3a-9b} = 3.8, 1 H, H-3a), 5.74 (m, 1 H, H-7). ^{13}C NMR (125 MHz, d6-DMSO): δ 26.66 and 26.73 (CH$_3$), 30.09 (C-6), 32.02 (C-9), 65.40 (C-5), 78.06 (C-9a), 83.20 (C-4a), 84.38 (C-9b), 102.95 (C-3a), 111.35 (C-2), 127.50 (C-8), 129.60 (C-7). ESI MS, *m/z* (%): 266.3 (14) [M + Na + H], 265.3 (100) [M + Na]. HRMS (ESI): calcd. for C$_{12}$H$_{18}$O$_5$Na [M + Na] 265.10464; found: 265.10461.

Selective benzoylation of 4a, 4b, 7a, and 7b

A solution of benzoyl chloride (0.67 mL, 5.77 mmol) in pyridine (9 ml) was added dropwise at room temperature within 20 min to a solution of dihydroxy derivative **4a**, **4b**, **7a**, and **7b** (5 mmol) in pyridine (20 mL) and the mixture was left overnight. Then water (2 mL) was added and, after 10 min, pyridine was evaporated. The residue was partitioned between ethyl acetate (50 mL) and water (20 mL). The organic phase was separated and washed with 5% hydrochloric acid (20 mL), water (20 mL), and 10% aqueous KHCO$_3$ (3 x 20 mL), dried over anhydrous Na$_2$SO$_4$ and evaporated. The residue was crystalized from cyclohexane.

(3a*R*,4a*R*,5*S*,8a*R*,8b*R*)-8a-Hydroxy-2,2-dimethyl-3a,4a,5,8,8a,8b-hexahydro-[1,3]dioxolo[4,5-b]benzofuran-5-yl benzoate (5a)

Yield 1.53 g (92%) of a white crystals. M.p. 104-106 °C. $[\alpha]_D^{20}$ +209.8 (c = 0.324, CHCl$_3$). Found: C, 65.16; H, 6.25. Calc. for C$_{18}$H$_{20}$O$_6$: C, 65.05; H, 6.07%. ^{1}H NMR (500 MHz, d6-DMSO): δ 1.28 (s, 3 H, CH$_3$exo), 1.46 (s, 3 H, H-CH$_3$endo), 1.93 (dm, J_{gem} = 18.6, 1 H, H-8eq), 2.21 (dd, J_{gem} = 18.6, J_{8ax-7} = 5.6, 1 H, H-8ax), 4.06 (m, 1 H, H-4a), 4.21 (d, J_{8b-3a} = 3.6, 1 H, H-8b), 5.15 (s, 1 H, 8a-OH), 5.32 (m, 1 H, H-5), 5.71 (d, J_{3a-8b} = 3.6, 1 H, H-3a), 5.79 (dm, J_{6-7} = 10.2, 1 H, H-6), 5.96 (m, 1 H, H-7), 7.52 (m, 2 H, H-3′, H-5′), 7.66 (tm, $J_{4'-3'}$ = $J_{4'-5'}$ = 7.4, 1 H, H-4′), 8.00 (m, 2 H, H-2′, H-6′). ^{13}C NMR (125 MHz, d6-DMSO): δ 26.41 (CH$_3$endo), 26.73 (CH$_3$exo), 31.41 (C-8), 66.11 (C-5), 72.57 (C-8a), 76.64 (C-4a), 85.53 (C-8b), 103.44 (C-3a), 111.93 (C-2), 121.75 (C-6), 128.80 (C-3′, C-5′), 128.97

(C-7), 129.73 (C-2′, C-6′), 129.92 (C-1′), 133.59 (C-4′), 165.26 (C=O). ESI MS, m/z (%): 356.1 (22) [M + Na + H], 355.1 (100) [M + Na]. HRMS (ESI): calcd. for $C_{18}H_{20}O_6Na$ [M + Na] 355.11521; found: 355.11516.

(3aR,4aR,5R,8aR,8bR)-8a-Hydroxy-2,2-dimethyl-3a,4a,5,8,8a,8b-hexahydro-[1,3]dioxolo[4,5-b]benzofuran-5-yl benzoate (5b)

Yield 1.56 g (94%) of a white crystals. M.p. 120.5–121.5 °C. $[\alpha]_D^{20}$ -50.9 (c = 0.456, CHCl₃). Found: C, 64.91; H, 5.90. Calc. for $C_{18}H_{20}O_6$: C, 65.05; H, 6.07%. ¹H NMR (500 MHz, d6-DMSO): δ 1.26 (s, 3 H, CH₃exo), 1.44 (s, 3 H, CH₃endo), 2.00 (m, 1 H, H-8eq), 2.13 (m, 1 H, H-8ax), 4.25 (d, J_{8b-3a} = 3.5, 1 H, H-8b), 4.28 (dd, J_{4a-5} = 4.5, J_{4a-8ax} = 1.7, 1 H, H-4a), 5.40 (s, 1 H, 8a-OH), 5.59–5.64 (m, 2 H, H-5, H-6), 5.76 (d, J_{3a-8b} = 3.5, 1 H, H-3a), 5.77 (m, 1 H, H-7), 7.55 (m, 2 H, H-3′, H-5′), 7.68 (m, 1 H, H-4′), 7.97 (m, 2 H, H-2′, H-6′). ¹³C NMR (125 MHz, d6-DMSO): δ 26.46 (CMe₂exo), 26.56 (CMe₂endo), 32.67 (C-8), 68.78 (C-5), 73.08 (C-4a), 76.42 (C-8a), 83.23 (C-8b), 103.87 (C-3a), 112.01 (C-2), 122.86 (C-6), 127.10 (C-7), 129.02 (C-3′, C-5′), 129.51 (C-2′, C-6′), 129.76 (C-1′), 133.74 (C-4′), 165.44 (C=O). ESI MS, m/z (%): 356.0 (20) [M + Na + H], 355.0 (100) [M + Na]. HRMS (ESI): calcd. for $C_{18}H_{20}O_6Na$ [M + Na] 355.11521; found: 355.11520.

(3aR,4aR,5S,9aR,9bR)-9a-Hydroxy-2,2-dimethyl-4a,5,6,9,9a,9b-hexahydro-3aH-cyclohepta[4,5]furo[2,3-d][1,3]dioxol-5-yl benzoate (8a)

Yield 1.54 g (89%) of a white crystals. M.p. 169-170 °C. $[\alpha]_D^{20}$ -7.3 (c = 0.259, CHCl₃). Found: C, 65.80; H, 6.50. Calc. for $C_{19}H_{22}O_6$: C, 65.88; H, 6.40%. ¹H NMR (500 MHz, d6-DMSO): δ 1.27 (s, 3 H, CH₃exo), 1.53 (s, 3 H, CH₃endo), 2.12 (ddd, J_{gem} = 16.0, J_{6eq-7} = 8.2, J_{6eq-5} = 1.5, 1 H, H-6eq), 2.18 (ddm, J_{gem} = 17.6, J_{9ax-8} = 7.4, 1 H, H-9ax), 2.35 (dm, J_{gem} = 17.6, 1 H, H-9eq), 2.66 (m, 1 H, H-6ax), 4.08 (d, J_{9b-3a} = 3.7, 1 H, H-9b), 4.15 (dd, J_{4a-5} = 7.6, J_{4a-9ax} = 1.4, 1 H, H-4a), 5.04 (s, 1 H, 9a-OH), 5.05 (ddd, J_{5-6ax} = 11.6, J_{5-6eq} = 1.5, J_{5-4a} = 7.6, 1 H, H-5), 5.49 (m, 1 H, H-8), 5.68 (m, 1 H, H-7), 5.74 (d, J_{3a-9b} = 3.7, 1 H, H-3a), 7.54 (m, 2 H, H-3′, H-5′), 7.67 (m, 1 H, H-4′), 7.95 (m, 2 H, H-2′, H-6′). ¹³C NMR (125 MHz, d6-DMSO): δ 26.71 (CH₃exo), 27.09 (CH₃endo), 29.34 (C-6), 33.45 (C-9), 75.63 (C-5), 77.69 (C-9a), 82.98 (C-4a), 85.43 (C-9b), 103.09 (C-3a), 111.56 (C-2), 126.22 (C-8), 126.31 (C-7), 129.01 (C-3′, C-5′), 129.36 (C-2′, C-6′), 129.94 (C-1′), 133.64 (C-4′), 165.05 (C=O). ESI MS, m/z (%): 370.1 (22) [M + Na + H], 369.1 (100) [M + Na]. HRMS (ESI): calcd. for $C_{19}H_{22}O_6Na$ [M + Na] 369.13086; found: 36913090.

(3aR,4aR,5R,9aR,9bR)-9a-Hydroxy-2,2-dimethyl-4a,5,6,9,9a,9b-hexahydro-3aH-cyclohepta[4,5]furo[2,3-d][1,3]dioxol-5-yl benzoate (8b)

Yield 1.28 g (74%) of a white crystals. M.p. 97.5-99.5 °C. $[\alpha]_D^{20}$ -17.6 (c = 0.33, CHCl₃). Found: C, 65.73; H, 6.36. Calc. for $C_{19}H_{22}O_6$: C, 65.88; H, 6.40%. ¹H NMR (500 MHz, d6-DMSO): δ 2.08-2.14 (m, 2 H, H-6B, H-10B), 2.33 (dm, J_{gem} = 1.0, 1 H, H-9A), 2.81 (m, 1 H, H-6A), 4.09 (d, J_{9b-3a} = 3.7, 1 H, H-9b),

4.17 (m, 1 H, 4a), 5.08 (dt, J_{5-6A} = 11.2, J_{5-6B} = J_{5-4a} = 2.4, 1 H, H-5), 5.15 (s, 1 H, 9a-OH), 5.69 (m, 1 H, H-8), 5.81 (d, J_{3a-9b} =3.7, 1 H, H-3a), 5.84 (m, 1 H, H-7), 7.54 (m, 2 H, H-3′, H-5′), 7.67 (m, 1 H, H-4′), 7.93 (m, 2 H, H-2′, H-6′). ¹³C NMR (125 MHz, d6-DMSO): δ 26.68 (C-6), 26.62 and 26.82 (2 × CH₃), 32.03 (C-9), 69.63 (C-5), 78.57 (C-9a), 80.59 (C-4a), 84.13 (C-9b), 103.25 (C-3a), 111.71 (C-2), 127.99 (C-7), 128.85 (C-8), 129.01 (C-3′, C-5′), 129.34 (C-2′, C-6′), 130.05 (C-1′), 133.63 (C-4′), 165.13 (COO). ESI MS, m/z (%): 370.1 (21) [M + Na + H], 369.1 (100) [M + Na]. HRMS (ESI): calcd. for $C_{19}H_{22}O_6Na$ [M + Na] 369.13086; found: 369.13078.

Synthesis of protected nucleosides 9a, 9b, 12a, and 12b

A solution of monobenzoate **5a**, **5b**, **8a** or **8b** (4 mmol) in 80% aqueous trifluoroacetic acid (12 mL) was left at room temperature for 3 h then evaporated and co-distilled with toluene (3 x 20 mL). Acetic anhydride (2.27 mL, 24.0 mmol) was added to a solution of the residue and dimethylaminopyridine (488 mg, 3.99 mmol) in acetonitrile (15 mL) and the mixture was left at room temperature overnight. Then methanol (~2 mL) was added and the solvents were evaporated. A solution of the residue in ethyl acetate (25 mL) was washed with water (20 mL) and 10% aqueous potassium hydrogen carbonate (2 x 20 mL), dried over anhydrous sodium sulfate and evaporated. To a stirred solution of the residue in acetonitrile (17 mL) was added benzoyladenine (1.05 g, 4.39 mmol) and then dropwise 1 M solution of tin(IV) chloride in dichloromethane (6 mL). The obtained solution was left at room temperature for 3 h and poured into a saturated aqueous solution of potassium hydrogen carbonate (70 mL). The mixture was extracted with ethyl acetate (2 x 100 mL) and the collected extracts were dried over sodium sulfate and evaporated. The residue was chromatographed on silica gel (200 g) in ethyl acetate – toluene (4 : 1).

(2R,3R,3aR,7S,7aR)-2-(6-Benzamido-9H-purin-9-yl)-7-(benzoyloxy)-2,3,3a,4,7,7a-hexahydrobenzofuran-3,3a-diyl diacetate (9a)

Yield 1.39 g (58%) of a white solid foam. $[\alpha]_D^{20}$ +87.0 (c = 0.300, CHCl₃). Found: C, 61.98; H, 4.60; N, 11.37. Calc. for $C_{31}H_{27}N_5O_8$: C, 62.31; H, 4.55; N, 11.72%. ¹H NMR (500 MHz, d6-DMSO): 2.18 (s, 3 H, 3a-OCOCH₃), 2.04 (s, 3 H, 3-OCOCH₃), δ 3.07 (m, 2 H, H-4), 4.75 (d, J_{7a-7} = 4.2, 1 H, H-7a), 5.93 (m, 1 H, H-6), 6.05 (m, 1 H, H-7), 6.06 (m, 1 H, H-5), 6.31 (d, J_{3-2} = 6.3, 1 H, H-3), 6.41 (d, J_{2-3} = 6.3, 1 H, H-2), 7.53 (m, 2 H, m-benzoyl), 7.55 (m, 2 H, m-benzoylamino), 7.65 (m, 1 H, p-benzoylamino), 7.67 (m, 1 H, p-benzoyl), 7.98 (m, 2 H, o-benzoyl), 8.05 (m, 2 H, o-benzoylamino), 8.76 (s, 1 H, H-8′), 8.80 (s, 1 H, H-2′), 11.28 (bs, 1 H, NH). ¹³C NMR (125 MHz, d6-DMSO): δ 20.55 (3-OCOCH₃), 21.67 (3a-OCOCH₃), 30.12 (C-4), 70.96 (C-7), 74.91 C-3), 80.83 (C-7a), 81.51 (C-3a), 86.09 (C-2), 124.23 (C-6), 126.18 (C-5′), 128.05 (C-5), 128.69, 128.72 (o-, m-benzoylamino), 129.02 (m-benzoyl), 129.46 (i-benzoyl), 129.53 (o-benzoyl), 132.73 (p-benzoylamino), 133.46 (i-benzoylamino), 133.85 (p-benzoyl), 144.35 (C-8′), 150.90 (C-6′), 151.98 (C-2′), 152.13 (C-4′), 165.18 (COO), 165.85 (CONH), 169.74 (3-OCOCH₃), 170.04 (3a-OCOCH₃). ESI MS,

m/z (%): 621.2 (36) [M + Na + H], 620.2 (100) [M + Na], 598.2 (24) [M + H]. HRMS (ESI): calcd. for $C_{31}H_{28}O_8N_5$ [M + H] 598.19324; found: 598.19326.

(2R,3R,3aR,7R, 7aR)-2-(6-Benzamido-9H-purin-9-yl)-7-(benzoyloxy)-2,3,3a,4,7,7a-hexahydrobenzofuran-3,3a-diyl diacetate (9b)

Yield 1.41 g (55%) of a white solid foam. $[\alpha]_D^{20}$ -23.2 (c = 0.263, CHCl$_3$). Found: C, 61.66; H, 4.70; N, 10.89. Calc. for $C_{31}H_{27}N_5O_8 \cdot 0.5\ CH_3COOC_2H_5$: C, 61.77; H, 4.87; N, 10.91%. ^{1}H NMR (500 MHz, d6-DMSO): δ 2.06 (s, 3 H, 3-OCOCH$_3$), 2.18 (s, 3 H, 3a-OCOCH$_3$), 2.78 (dm, J_{gem} = 18.0, 1 H, H-4B), 3.26 (ddm, J_{gem} = 18.0, J_{4A-5} = 4.7, 1 H, H-4A), 4.86 (dd, J_{7a-7} = 4.3, J_{7a-2} = 0.8, 1 H, H-7a), 5.83 (m, 1 H, H-7), 5.97 (m, 1 H, H-6), 5.99 (d, J_{3-2} = 5.7, 1 H, H-3), 6.03 (m, 1 H, H-5), 6.32 (d, J_{2-3} = 5.7, 1 H, H-2), 7.50 (m, 2 H, m-benzoyl), 7.55 (m, 2 H, m-benzoylamino), 7.63-7.67 (m, 2 H, p-benzoyl, p-benzoylamino), 7.94 (m, 2 H, o-benzoyl), 8.04 (m, 2 H, o-benzoylamino), 8.54 (s, 1 H, H-8′), 8.75 (s, 1 H, H-2′), 11.27 (bs, 1 H, NH). ^{13}C NMR (125 MHz, d6-DMSO): δ 20.54 (3-OCOCH$_3$), 21.45 (3a-OCOCH$_3$), 30.59 (C-4), 68.78 (C-7), 76.65 (C-3), 78.74 (C-7a), 80.61 (C-3a), 85.85 (C-2), 125.75 (C-5′), 126.00 (C-6), 126.61 (C-5), 128.69, 128.71 (o-, m-benzoylamino), 129.02 (m-benzoyl), 129.35 (i-benzoyl), 129.54 (o-benzoyl), 132.73 (p-benzoylamino), 133.41 (i-benzoylamino), 133.86 (p-benzoyl), 143.23 (C-8′), 150.89 (C-6′), 152.18 (C-2′), 152.23 (C-4′), 164.38 (COO), 165.82 (CONH), 169.69 (3-OCOCH$_3$), 169.88 (3a-OCOCH$_3$). ESI MS, m/z (%): 621.1 (34) [M + Na + H], 620.1 (100) [M + Na], 598.1 (30) [M + H]. HRMS (ESI): calcd. for $C_{31}H_{28}O_8N_5$ [M + H] 598.19324; found: 598.19337.

(2R,3R,3aR,8S,8aR)-2-(6-Benzamido-9H-purin-9-yl)-8-(benzoyloxy)-3,3a,4,7,8,8a-hexahydro-2H-cyclohepta[b]furan-3,3a-diyl diacetate (12a)

Yield 1.65 g (63%) of a white solid foam. $[\alpha]_D^{20}$ +41.8 (c = 0.385, CHCl$_3$). Found: C, 62.32; H, 5.00; N, 10.82. Calc. for $C_{32}H_{29}N_5O_8 \cdot 0.5\ CH_3COOC_2H_5$: C, 62.28; H, 5.07; N, 10.68%. ^{1}H NMR (500 MHz, d6-DMSO): δ 2.03 (s, 3 H, 3-OCOCH$_3$), 2.12 (s, 3 H, 3a-OCOCH$_3$), 2.54 (dm, J_{gem} = 16.4, 1 H, H-7B), 2.71 (m, 1 H, H-7A), 3.21 (dm, J_{gem} = 17.3, 1 H, H-4B), 3.36 (m, 1 H, H-4A), 4.62 (dd, J_{8a-2} = 1.3, J_{8a-8} = 7.9, 1 H, H-8a), 5.47 (ddd, J_{8-7A} = 11.0, J_{8-7B} = 2.4, J_{8a-8} = 7.9, 1 H, H-8), 5.58 (m, 1 H, H-5), 5.80 (m, 1 H, H-6), 6.02 (d, J_{3-2} = 5.1, 1 H, H-2), 6.26 (d, J_{2-3} = 5.1, 1 H, H-2), 7.52 (m, 2 H, m-benzoyl), 7.55 (m, 2 H, m-benzoylamino), 7.63-7.68 (m, 2 H, p-benzoylamino, p-benzoyl), 7.97 (m, 2 H, o-benzoyl), 8.04 (m, 2 H, o-benzoylamino), 8.68 (s, 1 H, H-8′), 8.79 (s, 1 H, H-2′), 11.28 (bs, 1 H, NH). ^{13}C NMR (125 MHz, d6-DMSO): δ 83.93 (C-8a), 20.51 (3-OCOCH$_3$), 21.15 (3a-OCOCH$_3$), 30.48 (C-7), 31.89 (C-4), 72.65 (C-8), 75.96 (C-3), 82.85 (C-3a), 87.17 (C-2), 124.37 (C-5), 125.93 (C-5′), 127.70 (C-6), 128.71, 128.61 (o-, m-benzoyl), 128.96 (m-benzoyl), 129.52 (o-benzoyl), 129.57 (i-benzoyl), 132.70 (p-benzoylamino), 133.48 (i-benzoylamino), 133.80 (p-benzoyl), 143.95 (C-8′), 150.91 (C-6′), 152.02 (C-4′),

152.11 (C-2′), 164.87 (COO), 165.83 (CONH), 169.20 (3-OCOCH$_3$), 169.34 (3a-OCOCH$_3$). ESI MS, m/z (%): 635.2 (37) [M + Na + H], 634.2 (100) [M + Na], 612.2 (31) [M + H]. HRMS (ESI): calcd. for $C_{32}H_{30}O_8N_5$ [M + H] 612.20889; found: 612.20911; calcd. for $C_{32}H_{29}O_8N_5Na$ [M + Na] 634.19083; found: 634.19089.

(2R,3R,3aR,8R,8aR)-2-(6-Benzamido-9H-purin-9-yl)-8-(benzoyloxy)-3,3a,4,7,8,8a-hexahydro-2H-cyclohepta[b]furan-3,3a-diyl diacetate (12b)

Yield 1.99 g (76%) of a white solid foam. $[\alpha]_D^{20}$ +25.0 (c = 0.428, CHCl$_3$). Found: C, 62.31; H, 4.90; N, 10.81. Calc. for $C_{32}H_{29}N_5O_8 \cdot 0.5\ CH_3COOC_2H_5$: C, 62.28; H, 5.07; N, 10.68%. ^{1}H NMR (500 MHz, d6-DMSO): δ 2.02 (s, 3 H, 3-OCOCH$_3$), 2.14 (s, 3 H, 3a-OCOCH$_3$), 2.54 (m, 1 H, H-7B), 2.89-3.02 (m, 2 H, H-4B, H-7A), 3.42 (dm, J_{gem} = 16.3, 1 H, H-4A), 4.87 (d, J_{8a-8} = 1.2, 1 H, H-8a), 5.63 (m, 1 H, H-5), 5.77-5.83 (m, 2 H, H-6, H-8), 6.29 (d, J_{3-2} = 7.2, 1 H, H-3), 6.37 (d, J_{2-3} = 7.2, 1 H, H-2), 7.51 (m, 2 H, m-benzoyl), 7.55 (m, 2 H, m-benzoylamino), 7.63-7.67 (m, 2 H, p-benzoylamino, p-benzoyl), 7.94 (m, 2 H, o-benzoyl), 8.04 (m, 2 H, o-benzoylamino), 8.61 (s, 1 H, H-2′), 8.64 (s, 1 H, H-8′), 11.27 (bs, 1 H, NH). ^{13}C NMR (125 MHz, d6-DMSO): δ 170.10 (3a-OCOCH$_3$), 169.59 (3a-OCOCH$_3$), 165.86 (CONH), 164.96 (COO), 152.34 (C-4′), 152.00 (C-2′), 150.88 (C-6′), 143.80 (C-8′), 133.72 (p-benzoyl), 133.44 (i-benzoylamino), 132.72 (p-benzoylamino), 129.61 (i-benzoyl), 129.50 (o-benzoyl), 128.97 (m-benzoyl), 128.69 (o-, m-benzoyl, C-6), 126.12 (C-5′), 123.20 (C-5), 84.71 (C-2), 84.70 (C-3a), 83.78 (C-8a), 73.83 (C-3), 70.34 (C-8), 31.19 (C-4), 29.94 (C-7), 21.71 (3a-OCOCH$_3$), 20.50 (3-OCOCH$_3$). HRMS (ESI): calcd. for $C_{32}H_{30}O_8N_5$ [M + H] 612.20889; found: 612.20890; calcd. for $C_{32}H_{29}O_8N_5Na$ [M + Na] 634.19083; found: 634.19062.

Deprotection of 9a, 9b, 12a, and 12b

A solution of the protected nucleoside 9a, 9b, 12a or 12b (2 mmol) in 0.1 M methanolic sodium methoxide (15 mL) was set at room temperature overnight. Water (0.5 mL) was then added and crystalline product was filtered off, washed with methanol and ether.

(2R,3R,3aS,7S,7aR)-2-(6-Amino-9H-purin-9-yl)-2,3,3a,4,7,7a-hexahydrobenzofuran-3,3a,7-triol (10a)

Yield 428 mg (68%) of a white crystals. M.p. 232-233.5 °C. $[\alpha]_D^{20}$ +30.4 (c = 0.289, DMF). Found: C, 49.78; H, 5.30; N, 22.28. Calc. for $C_{13}H_{15}N_5O_4 \cdot 0.5\ H_2O$: C, 49.68; H, 5.13; N, 22.15%. ^{1}H NMR (500 MHz, d6-DMSO): δ 0.52 (m, 1 H, H-4eq), 2.24 (dm, J_{gem} = 18.1, 1 H, H-4ax), 23.74 (d, J_{7a-7} = 6.2, 1 H, H-7a), 4.51 (m, 1 H, H-7), 4.82 (dd, J_{3-2} = 8.2, J_{3-OH} = 6.8, 1 H, H-3), 5.14 (d, J_{OH-7} = 5.9, 1 H, 7-OH), 5.16 (s, 1 H, 3a-OH), 5.51 (d, J_{OH-3} = 6.8, 1 H, 3-OH), 5.59 (dm, J_{6-5} = 10.0, 1 H, H-6), 5.66 (dm, J_{5-6} = 10.0, 1 H, H-5), 5.88 (d, J_{2-3} = 8.2, 1 H, H-2), 7.27 (d, 2 H, NH$_2$), 8.14 (s, 1 H, H-2′), 8.39 (s, 1 H, H-8′). ^{13}C NMR (125 MHz, d6-DMSO): δ 34.07 (C-4), 70.81 (C-7), 74.74 (C-3), 75.82 (C-3a), 86.18 (C-2), 88.99 (C-7a), 119.73 (C-5′), 124.53 (C-5), 130.40 (C-6), 141.14 (C-8′), 150.00 (C-4′),

152.73 (C-2′), 156.26 (C-6′). ESI MS, *m/z* (%): 329.2 (17) [M + Na + H], 328.2 (100) [M + Na], 306.2 (7) [M + H]. HRMS (ESI): calcd. for $C_{13}H_{15}O_4N_5Na$ [M + Na] 328.10163; found: 328.10159.

(2*R*,3*R*,3a*S*,7*R*,7a*R*)-2-(6-Amino-9*H*-purin-9-yl)-2,3,3a,4,7,7a-hexahydrobenzofuran-3,3a,7-triol (10b)

Yield 570 mg (92%) of a white crystals. M.p. 245.5-247 °C. $[\alpha]_D^{20}$ -60.8 (c = 0.311, DMF). Found: C, 50.60; H, 5.07; N, 22.57. Calc. for $C_{13}H_{15}N_5O_4 \cdot 0.25 \, H_2O$: C, 50.40; H, 5.04; N, 22.61%. ^{1}H NMR (500 MHz, d6-DMSO): δ 2.16 (dm, J_{gem} = 17.5, 1 H, H-4ax), 2.55 (dm, J_{gem} = 17.5, 1 H, H-4eq), 3.94 (d, J_{7a-7} = 4.5, 1 H, H-7a), 4.20 (q, J_{7-7a} = J_{7-OH} = 4.5, 1 H, H-7), 4.30 (t, J_{3-2} = J_{3-OH} = 7.3, 1 H, H-3), 5.11 (s,1 H, 3a-OH), 5.53 (d, J_{OH-3} = 6.7, 1 H, 3-OH), 5.60 (d, J_{OH-7} = 4.3, 1 H, 7-OH), 5.85 (d, J_{2-3} = 7.9, 1 H, H-2), 5.86 (m, 1 H, H-5), 5.90 (m, 1 H, H-6), 7.34 (d, 2 H, NH₂), 8.13 (s, 1 H, H-2′), 8.29 (s, 1 H, H-8′). ^{13}C NMR (125 MHz, d6-DMSO): δ 34.92 (C-4), 64.69 (C-7), 74.24 (C-3a), 78.15 (C-3), 85.79, 85.88 (C-2, C-7a), 119.30 (C-5′), 127.49 (C-5), 129.45 (C-6), 139.83 (C-8′), 149.73 (C-4′), 152.62 (C-2′), 156.32 (C-6′). ESI MS, *m/z* (%): 329.2 (16) [M + Na + H], 328.2 (100) [M + Na], 306.2 (8) [M + H]. HRMS (ESI): calcd. for $C_{13}H_{15}O_4N_5Na$ [M + Na] 328.10163; found: 328.10154.

(2*R*,3*R*,3a*S*,8*S*,8a*R*)-2-(6-Amino-9*H*-purin-9-yl)-3,3a,4,7,8,8a-hexahydro-2*H*-cyclohepta[b]furan-3,3a,8-triol (13a)

Yield 509 mg (80%) of a white crystals. M.p. 205.5-207 °C. $[\alpha]_D^{20}$ +0.5 (c = 0.389, DMF). Found: C, 52.48; H, 5.40; N, 21.65. Calc. for $C_{14}H_{17}N_5O_4$: C, 52.66; H, 5.37; N, 21.93%. HRMS (ESI): calcd. for $C_{14}H_{17}O_4N_5Na$ [M + Na] 342.11728; found: 342.11724. ^{1}H NMR (500 MHz, d6-DMSO): δ 2.22 (m, 1 H, H-7B), 2.40-2.49 (m, 3 H, 2 × H-4, H-7A), 3.72 (d, J_{8a-8} = 8.1, 1 H, H-8a), 3.92 (m, 1 H, H-8), 4.53 (m, 1 H, H-3), 4.84 (s, 1 H, 3a-OH), 4.89 (d, J_{OH-8} = 4.2, 1 H, 8-OH), 5.47-5.53 (m, 2 H, H-5, 3-OH), 5.60 (m, 1 H, H-6), 5.78 (d, J_{2-3} = 7.9, 1 H, H-2), 7.30 (brs, 2 H, NH₂), 8.14 (s, 1 H, H-2′), 8.35 (s, 1 H, H-8′). ^{13}C NMR (125 MHz, d6-DMSO): δ 33.60 (C-4), 34.42 (C-7), 68.57 (C-8), 70.86 (C-3a), 75.44 (C-3), 86.21 (C-2), 90.56 (C-8a), 119.54 (C-5′), 124.99 (C-5), 128.04 (C-6), 140.43 (C-8′), 149.93 (C-4′), 152.82 (C-2′), 156.29 (C-6′). ESI MS, *m/z* (%): 343.1 (18) [M + Na + H], 342.1 (100) [M + Na], 320.1 (10) [M + H].

(2*R*,3*R*,3a*S*,8*R*,8a*R*)-2-(6-Amino-9*H*-purin-9-yl)-3,3a,4,7,8,8a-hexahydro-2*H*-cyclohepta[b]furan-3,3a,8-triol (13b)

Yield 467 mg (66%) of a white crystals. M.p. 255-256 °C. $[\alpha]_D^{20}$ -25.5 (c = 0.364, DMF). Found: C, 52.30; H, 5.51; N, 21.61. Calc. for $C_{14}H_{17}N_5O_4$: C, 52.66; H, 5.37; N, 21.93%. ^{1}H NMR (500 MHz, d6-DMSO, 60 °C): δ 2.30-2.37 (m, 2H, H-4b, H-7b), 2.47 (m, 1 H, H-7a), 2.75 (dm, J_{gem} = 14.9, 1 H, H-4a), 4.05 (d, J_{8a-8} = 1.6, 1 H, H-8a), 4.08 (m, 1 H, H-8), 4.55 (bs, 1 H, 3a-OH), 4.60 (dd, J_{3-2} = 8.1, J_{3-OH} = 6.7, 1 H, H-3), 5.32 (d, J_{OH-3} = 6.7, 1 H, 3-OH), 5.53-5.62 (m, 2 H, H-5, H-6), 5.80 (d, J_{2-3} = 8.1, 1 H, H-2), 5.85 (bs, 1 H, 8-OH), 7.19 (s, 2 H, NH₂), 8.15 (s, 1 H, H-2′), 8.25 (s, 1H, H-8′). ^{13}C NMR (125 MHz, d6-DMSO): δ 33.20

(C-4), 33.73 (C-7), 68.26 (C-8), 75.78 (C-3), 79.58 (C-3a), 86.80 (C-2), 89.65 (C-8a), 119.74 (C-5′), 124.49 (C-5), 128.42 (C-6), 140.26 (C-8′), 149.14 (C-4′), 152.17 (C-2′), 156.28 (C-6′). ESI MS, *m/z* (%): 343.1 (15) [M + Na + H], 342.1 (100) [M + Na], 320.1 (36) [M + H]. HRMS (ESI): calcd. for $C_{14}H_{18}O_4N_5$ [M + H] 320.13533; found: 320.13536; calcd. for $C_{14}H_{17}O_4N_5Na$ [M + Na] 342.11728; found: 342.11727.

Preparation of saturated nucleosides 11a, 11b, 14a, and 14b

Palladium hydroxide on carbon (20 wt. %, 15 mg) was added to a solution of **10a**, **10b**, **13a** or **13b** (0.5 mmol) in dimethylformamide (2.5 ml) and the mixture was stirred under hydrogen at room temperature overnight. Catalyst was filtered off and the filtrate was evaporated. The solution of the residue in methanol (10 ml) was decolorized with charcoal and evaporated. The residue was crystalized from methanol.

(2*R*,3*R*,3a*S*,7*S*,7a*R*)-2-(6-Amino-9*H*-purin-9-yl)octahydrobenzofuran-3,3a,7-triol (11a)

Yield 102 mg (66%) of a white crystals. M.p. 234-236 °C. $[\alpha]_D^{20}$ -9.4 (c = 0.415, DMF). Found: C, 50.62; H, 5.63; N, 22.65. Calc. for $C_{13}H_{17}N_5O_4$: C, 50.81; H, 5.58; N, 22.79%. ^{1}H NMR (500 MHz, d6-DMSO): δ 1.13 (m, 1 H, H-6ax), 1.47-1.35 (m, 2 H, H-4ax, H-5ax), 1.56 (m, 1 H, H-5eq), 1.75 (m, 1 H, H-6eq), 1.99 (m, 1 H, H-4eq), 3.54 (d, J_{7a-7} = 8.1, 1 H, H-7a), 3.86 (m, 1 H, H-7), 4.82 (d, J_{OH-7} = 5.1, 1 H, 7-OH), 4.92 (dd, J_{3-2} = 8.1, J_{3-OH} = 5.7, 1 H, H-3), 5.01 (s, 1 H, 3a-OH), 5.36 (bd, J_{OH-3} = 5.7, 1 H, 3-OH), 5.98 (d, J_{2-3} = 8.1, 1 H, H-2), 7.26 (brs, 2H, NH₂), 8.16 (s, 1 H, H-2′), 8.46 (s, 1 H, H-8′). ^{13}C NMR (125 MHz, d6-DMSO): δ 19.24 (C-5), 32.26 (C-4), 32.74 (C-6), 72.29 and 72.32 (C-3, C-7), 77.59 (C-3a), 86.93 (C-2), 90.55 (C-7a), 119.61 (C-5′), 140.94 (C-8′), 150.23 (C-4′), 152.78 (C-2′), 156.25 (C-6′). HRMS (ESI): calcd. for $C_{13}H_{18}O_4N_5$ [M + H] 308.13533; found: 308.13522.

(2*R*,3*R*,3a*S*,7*R*,7a*R*)-2-(6-Amino-9*H*-purin-9-yl)octahydrobenzofuran-3,3a,7-triol (11b)

Yield 107 mg (70%) of a white crystals. M.p. 257-259 °C. $[\alpha]_D^{20}$ -43.5 (c = 0.352, methanol). Found: C, 50.78; H, 5.62; N, 22.53. Calc. for $C_{13}H_{17}N_5O_4$: C, 50.81; H, 5.58; N, 22.79%. ^{1}H NMR (600 MHz, d6-DMSO): δ 1.36-1.47 (m, 3 H, H-4ax, H-5b, H-6b), 1.61-1.69 (m, 2H, H-5a, H-5b), 1.95 (m, 1 H, H-4eq), 3.80 (d, J_{7a-7} = 4.3, 1 H, H-7a), 3.90 (m, 1 H, H-7), 4.45 (t, J_{OH-7} = J_{3-2} = 6.7, 1 H, H-3), 4.88 (s, 1 H, 3a-OH), 5.36 (d, J_{OH-3} = 6.5, 1 H, 3-OH), 5.57 (d, J_{OH-7} = 3.6, 1 H, 7-OH), 5.94 (d, J_{2-3} = 7.1, 1 H, H-2), 7.32 (brs, 2H, NH₂), 8.14 (s, 1 H, H-2′), 8.41 (s, 1 H, H-8′). ^{13}C NMR (151 MHz, d6-DMSO): δ 16.37 (C-5), 29.62 (C-6), 32.26 (C-4), 66.09 (C-7), 75.29 (C-3), 76.06 (C-3a), 84.79 (C-7a), 87.43 (C-2), 119.18 (C-5′), 140.03 (C-8′), 149.91 (C-4′), 152.62 (C-2′), 156.29 (C-6′). ESI MS, *m/z* (%): 331.1 (17) [M + Na + H], 330.1 (100) [M + Na], 308.1 (13) [M + H]. HRMS (ESI): calcd. for $C_{13}H_{18}O_4N_5$ [M + H] 308.13533; found: 308.13524; calcd. for $C_{13}H_{17}O_4N_5Na$ [M + Na] 330.11728; found: 330.11727.

(2R,3R,3aS,8S,8aR)-2-(6-Amino-9H-purin-9-yl)octahydro-2H-cyclohepta[b]furan-3,3a,8-triol (14a)

Yield 126 mg (78%) of a white crystals. M.p. 184-187 °C. [α]$_D^{20}$ -7.0 (c = 0.257, DMF). Found: C, 49.60; H, 6.05; N, 20.38. Calc. for C$_{13}$H$_{17}$N$_5$O$_4$H$_2$O: C, 49.55; H, 6.24; N, 20.64%. ESI MS, m/z (%): 345.3 (18) [M + Na + H], 344.3 (100) [M + Na]. ^{1}H NMR (500 MHz, d6-DMSO, 60 °C): δ 1.32 (m, 1 H, H-6b), 1.41-1.54 (m, 4 H, H-4b, H-5, H-7b), 1.71 (dm, J$_{gem}$ = 13.4, 1 H, H-6a), 1.81 (dm, J$_{gem}$ = 13.6, 1 H, H-7a), 1.92 (m, 1 H, H-4a), 3.63 (d, J$_{8a-8}$ = 9.4, 1 H, H-8a), 3.65 (dm, J$_{8-8a}$ = 9.4, 1 H, H-8), 4.36 (d, J$_{3-2}$ = 8.3, 1 H, H-3), 4.42, 4.61, 5.51 (3 x bs, 3 H, 3-OH, 3a-OH, 8-OH), 5.78 (d, J$_{2-3}$ = 8.3, 1 H, H-2), 7.28 (bs, 2 H, NH$_2$), 8.15 (s, 1 H, H-2′), 8.39 (s, 1 H, H-8′). ^{13}C NMR (125 MHz, d6-DMSO): δ 21.72 (C-5), 26.69 (C-6), 35.27 (C-7), 35.73 (C-4), 70.85 (C-8), 76.62 (C-3a), 77.61 (C-3), 85.16 (C-2), 92.31 (C-8a), 119.42 (C-5′), 140.20 (C-8′), 150.02 (C-4′), 152.81 (C-2′), 156.26 (C-6′). HRMS (ESI): calcd. for C$_{14}$H$_{19}$O$_4$N$_5$Na [M + Na] 344.13293; found: 344.13287.

(2R,3R,3aS,8R,8aR)-2-(6-Amino-9H-purin-9-yl)octahydro-2H-cyclohepta[b]furan-3,3a,8-triol (14b)

Yield 120 mg (75%) of a white crystals. M.p. 252.5-253.5 °C. [α]$_D^{20}$ -71.5 (c = 0.435, DMF). Found: C, 52.10; H, 5.85; N, 21.56. Calc. for C$_{14}$H$_{19}$N$_5$O$_4$: C, 52.33; H, 5.96; N, 21.79%. ^{1}H NMR (500 MHz, d6-DMSO): δ 1.40-1.48 (m, 2 H, H-5b, H-7b), 1.56-1.64 (m, 3 H, H-5a, H-6), 1.81-1.91 (m, 3 H, H-4, H-7a), 3.95-3.97 (m, 2 H, H-8, H-8a), 4.43 (dd, J$_{3-2}$ = 8.0, J$_{3-OH}$ = 6.0, 1 H, H-3), 4.45 (s, 1 H, 3a-OH), 5.45 (d, J$_{OH-3}$ = 6.0, 1 H, 3-OH), 5.75 (d, J$_{2-3}$ = 8.0, 1 H, H-2), 6.52 (bs, 1 H, 8-OH), 7.46 (bs, 2 H, NH$_2$), 8.13 (s, 1 H, H-2′), 8.30 (s, 1H, H-8′). ^{13}C NMR (125 MHz, d6-DMSO): δ 22.85 (C-5), 24.87 (C-6), 31.80 (C-7), 36.31 (C-4), 70.91 (C-8), 78.04 (C-3), 79.40 (C-3a), 88.56 (C-2), 92.48 (C-8a), 120.20 (C-5′), 141.17 (C-8′), 148.56 (C-4′), 152.16 (C-2′), 156.62 (C-6′). ESI MS, m/z (%): 345.2 (18) [M + Na + H], 344.2 (100) [M + Na], 322.3 (17) [M + H]. HRMS (ESI): calcd. for C$_{17}$H$_{22}$O$_4$N$_5$ [M + H] 344.13293; found: 344.13304.

Preparation of protected nucleotide analogues 16a, 16b, 17a, 17b, 18a, 18b, 19a, and 19b

Free nucleoside analogue 10a, 10b, 11a, 11b, 13a, 13b, 14a or 14b (0.5 mmol) was co-distiled with pyridine (3 x 5 mL) and the residue was dissolved in pyridine (8 mL). To the solution was added phenylboronic acid (65 mg, 0.533 mmol), pyridine (~6 mL) was distiled off at atmospheric pressure within 4 h and the remaining pyridine was evaporated under vacuum. A stirred solution of the residue in THF (2.5 mL) was treated under argon with a solution of N-[chloro(phenoxy)phosphoryl]-L-alaninate[6] (417 mg, 1.50 mmol) in THF (2.5 mL) and 1-methylimidazole (250 μL, 3.14 mmol). The mixture was stirred at room temperature overnight and then evaporated. A solution of the residue in chloroform (10mL) was washed with water (2 x 10 mL), dried over sodium sulfate and evaporated. Chromatography on silica gel in ethyl acetate – acetone – ethanol – water (100 : 15 : 6 : 4) and co-evaporation with methanol afforded the product as a solid foam.

(2S)-Methyl 2-[({[(2R,3R,3aS,7S,7aR)-2-(6-amino-9H-purin-9-yl)-3,3a-dihydroxy-2,3,3a,4,7,7a-hexahydrobenzofuran-7-yl]oxy} (phenoxy)phosphoryl)amino]propanoate (16a)

Yield 153 mg (54%) of a colourless solid foam. Found: C, 50.10; H, 5.17; N, 14.74; P, 5.50. Calc. for C$_{23}$H$_{27}$N$_6$O$_8$P·0.5CH$_3$OH: C, 50.18; H, 5.20; N, 14.49; P, 5.51%. ^{1}H NMR (500 MHz, d6-DMSO): δ 1.01 (d, J$_{CH3-CH}$ = 7.1, 1 H, CH$_3$-CH), 1.14 (d, J$_{CH3-CH}$ = 7.1, 3 H, CH$_3$-CH), 2.27 (m, 2 H, H-4eq), 2.60 (m, 2 H, H-4ax), 3.46 and 3.53 (2 x s, 6 H, OCH$_3$), 3.69 and 3.75 (2 x m, 2 H, Me-CH$_3$), 4.01 (d, J$_{7a-7}$ = 5.1, 1 H, H-7a), 4.03 (d, J$_{7a-7}$ = 5.2, 1 H, H-7a), 4.83 (d, J$_{3-2}$ = 8.1, 1 H, H-3), 4.89 (d, J$_{3-2}$ = 8.2, 1 H, H-3), 5.46 and 5.53 (2 x m, 2 H, H-7), 5.67 (dd, J$_{NH-CH}$ = 9.7, J$_{NH-P}$ = 12.4, 1 H, CH-NH), 5.73 (dm, J$_{6-5}$ = 10.2, 1 H, H-6), 5.83-5.88 (m, 4 H, CH-NH, H-5, H-6), 5.90 (d, J$_{2-3}$ = 8.1, 2 H, H-2), 6.92 (m, 2 H, o-phenyl), 7.04-7.19 (m, 6 H, m-phenyl, p-phenyl, o-phenyl), 7.27-7.33 (m, 6H, m-phenyl, NH$_2$), 8.08 and 8.10 (2 x s, 2 H, H-2′), 8.38 and 8.39 (2 x s, 2 H, H-8′). ^{13}C NMR (125 MHz, d6-DMSO): δ 19.58 (d, J$_{CH3-P}$ = 6.5, CH$_3$-CH), 19.74 (d, J$_{CH3-P}$ = 6.8, CH$_3$-CH), 33.17 and 33.29 (C-4), 49.86-49.89 (m, Me-CH), 51.85 and 51.95 (OCH$_3$), 74.02 and 74.04 (C-3), 75.90 (d, J$_{3a-P}$ = 0.8, C-3a), 75.93 (d, J$_{3a-P}$ = 0.9, C-3a), 77.45 (d, J$_{7-P}$ = 5.5, C-7), 77.62 (d, J$_{7-P}$ = 5.5, C-7), 86.11 and 86.16 (C-7a), 86.41and 86.55 (C-2), 119.83 and 119.85 (C-5′), 120.20 (d, J$_{o-P}$ = 4.7, o-phenyl), 120.34 (d, J$_{o-P}$ = 4.6, o-phenyl), 124.39 and 124.56 (p-phenyl), 125.59 (d, J$_{6-P}$ = 2.7, C-6), 125.67 (d, J$_{6-P}$ = 2.7, C-6), 127.94 and 127.98 (C-5), 129.45 and 129.67 (m-phenyl), 141.21 and 141.26 (C-8′), 149.78 and 149.81 (C-4′), 150.91(d, J$_{i-P}$ = 6.5, i-phenyl), 151.00 (d, J$_{i-P}$ = 6.6, i-phenyl), 152.67 and 152.69 (C-2′), 156.30 and 156.31 (C-6′), 173.65 (d, J$_{CO-P}$ = 5.5, C=O), 173.74 (d, J$_{CO-P}$ = 5.0, C=O). ESI MS, m/z (%): 570.4 (31) [M + Na + H], 569.4 (100) [M + Na], 547.4 (12) [M + H]. HRMS (ESI): calcd. for C$_{23}$H$_{28}$O$_8$N$_6$P [M + H] 547.17007; found: 547.17013.

(2S)-Methyl 2-[({[(2R,3R,3aS,7R,7aR)-2-(6-amino-9H-purin-9-yl)-3,3a-dihydroxy-2,3,3a,4,7,7a-hexahydrobenzofuran-7-yl]oxy}(phenoxy)phosphoryl)amino]propanoate (16b)

Yield 154 mg (55%) of a colourless solid foam. Found: C, 50.09; H, 5.25; N, 14.75; P, 5.33. Calc. for C$_{23}$H$_{27}$N$_6$O$_8$P·0.5CH$_3$OH: C, 50.18; H, 5.20; N, 14.49; P, 5.51%. ^{1}H NMR (500 MHz, d6-DMSO): δ 1.09 (d, J$_{CH3-CH}$ = 7.1, 3 H, CH$_3$-CH A), 1.15 (d, J$_{CH3-CH}$ = 7.2, 3 H, CH$_3$-CH B), 2.14-2.21m, 2 H, H-4b), 2.52-2.58 (m, 2 H, H-4a), 3.50 (s, 3 H, OCH$_3$ A), 3.52 (s, 3 H, OCH$_3$ B), 3.69 (m, 1 H, Me-CH A), 3.81 (m, 1 H, Me-CH B), 4.17-4.23 (m, 4 H, H-3, H-7), 4.95-5.01 (m, 2 H, H-7a), 5.38 (bs, 2 H, 3a-OH), 5.72 (bs, 2 H, 3-OH), 5.86 (d, J$_{2-3}$ = 7.7, 1 H, H-2 B), 5.88 (d, J$_{2-3}$ = 7.8, 1 H, H-2 A), 5.91-5.94 (m, 2 H, H-6), 5.96-6.08 (m, 4 H, CH-NH, H-5), 7.10-7.20 (m, 6 H, o-phenyl, p-phenyl), 7.27-7.37 (m, 8H, NH$_2$, m-phenyl), 8.16 (s, 1 H, H-2′ A), 8.17 (s, 1 H, H-2′ B), 8.20 (s, 1 H, H-8′ A), 8.26 (s, 1 H, H-8′ B). ^{13}C NMR (125 MHz, d6-DMSO): δ 19.74 (d, J$_{CH3-P}$ = 7.4, CH$_3$-CH A), 19.87 (d, J$_{CH3-P}$ = 6.6, CH$_3$-CH B), 34.48 (C-4 B), 34.53 (C-4 A), 49.73 (Me-CH A), 49.83 (Me-CH B), 51.97 (OCH$_3$ B), 51.98 (OCH$_3$ A), 70.61 (d, J$_{7-P}$ = 4.8, C-7 A), 71.11 (d, J$_{7-P}$ = 4.8, C-7 B), 73.98 (C-3a A), 74.06 (C-3a B), 77.76 (C-3 A), 78.05

(C-3 B), 83.36 (d, $J_{7a\text{-}P}$ = 6.2, C-7a A), 83.64 (d, $J_{7a\text{-}P}$ = 5.4, C-7a B), 84.60 (C-2 B), 84.68 (C-2 A), 118.93 (C-5′ B), 118.99 (C-5′ A), 120.24-120.32 (m, o-phenyl), 124.59 (p-phenyl B), 124.67 (p-phenyl A), 126.67 (d, $J_{o\text{-}P}$ = 2.8, o-phenyl A), 126.86 (d, $J_{o\text{-}P}$ = 3.1, o-phenyl B), 128.93 (C-5 B), 129.08 (C-5 A), 129.67 (m-phenyl B), 129.75 (m-phenyl A), 138.76 (C-8′ A), 138.76 (C-8′ B), 150.28 (C-4′ B), 150.31 (C-4′ A), 150.87 (d, $J_{i\text{-}P}$ = 6.1, i-phenyl B), 150.88 (d, $J_{i\text{-}P}$ = 6.0, i-phenyl A), 153.04 (C-2′ A), 153.05 (C-2′ B), 156.24 (C-6′ B), 156.26 (C-6′ A), 173.80 (d, $J_{CO\text{-}P}$ = 5.2, C=O B), 173.80 (d, $J_{CO\text{-}P}$ = 4.1, C=O A). ESI MS, m/z (%): 570.2 (30) [M + Na + H], 569.2 (100) [M + Na], 547.2 (41) [M + H]. HRMS (ESI): calcd. for $C_{23}H_{27}O_8N_6NaP$ [M + Na] 569.15202; found: 569.15175, calcd. for $C_{23}H_{28}O_8N_6P$ [M + H] 547.17007; found: 547.16996.

(2S)-Methyl 2-[({[(2R,3R,3aS,8S,8aR)-2-(6-amino-9H-purin-9-yl)-3,3a-dihydroxy-3,3a,4,7,8,8a-hexahydro-2H-cyclohepta[b]furan-8-yl]oxy}(phenoxy)phosphoryl)amino]propanoate (17a)

Yield 214 mg (76%) of a colourless solid foam. ESI MS, m/z (%): 584.2 (32) [M + Na + H], 583.2 (100) [M + Na], 561.2 (49) [M + H]. Found: C, 51.11; H, 5.20; N, 14.65; P, 5.32. Calc. for $C_{24}H_{29}N_6O_8P$: C, 51.43; H, 5.22; N, 14.99; P, 5.53%. ^{1}H NMR (600 MHz, d6-DMSO): δ 1.09 (d, $J_{CH3\text{-}CH}$ = 7.1, 3 H, CH₃-CH B), 1.16 (d, $J_{CH3\text{-}CH}$ = 7.1, 3 H, CH₃-CH A), 2.39-2.99 (m, 8 H, H-4, H-7), 2.99 (m, 2 H, H-4a), 3.55 (s, 3 H, OCH₃ A), 3.52 (s, 3 H, OCH₃ B), 3.77 (m, 2 H, Me-CH), 4.03 (d, $J_{8a\text{-}8}$ = 6.6, 1 H, H-8a B), 4.05 (d, $J_{8a\text{-}8}$ = 6.8, 1 H, H-8a A), 4.60 (m, 1 H, H-8 B), 4.69 (m, 1 H, H-8 A), 4.72 (d, $J_{3\text{-}2}$ = 8.0, 1 H, H-3 B), 4.75 (d, $J_{3\text{-}2}$ = 8.0, 1 H, H-3 A), 5.01 (bs, 1 H, 3a-OH B), 5.04 (bs, 1 H, 3a-OH A), 5.50-5.58 (m, 2 H, H-5), 5.60-5.64 (m, 4 H, H-6, 3-OH), 5.78 (m, 1 H, CH-NH B), 5.82 (d, $J_{2\text{-}3}$ = 8.0, 1 H, H-2 B), 5.83 (d, $J_{2\text{-}3}$ = 8.0, 1 H, H-2 A), 5.88 (m, 1 H, CH-NH A), 7.13-7.17 (m, 3 H, o-phenyl, p-phenyl B), 7.13-7.17 (m, 3 H, o-phenyl, p-phenyl A), 7.21 (m, 2 H, m-phenyl B), 7.29 (bs, 4 H, NH₂), 7.33 (m, 2 H, m-phenyl A), 8.37 (s, 1 H, H-8′ B), 8.39 (s, 1 H, H-8′ A). ^{13}C NMR (151 MHz, d6-DMSO): δ 124.46 (p-phenyl B), 120.40 (d, $J_{o\text{-}P}$ = 4.8, o-phenyl A), 120.30 (d, $J_{o\text{-}P}$ = 4.8, o-phenyl B), 119.61 (C-5′ A), 119.60 (C-5′ B), 87.85 (d, $J_{8a\text{-}P}$ = 6.0, C-8a A), 87.72 (d, $J_{8a\text{-}P}$ = 6.7, C-8a B), 86.09 (C-2 A), 86.08 (C-2 B), 78.12 (C-3a A), 77.93 (C-3a B), 75.29 − 75.18 (m, C-8), 73.64 (C-3 A), 73.56 (C-3 B), 52.01 (COOCH₃ A), 51.99 (OCH₃ B), 49.92 (Me-CH A), 49.68 (Me-CH B), 33.57 (C-7 A), 33.42 (C-7 B), 31.38 (C-4 A), 31.26 (C-4 B), 19.77 (d, $J_{CH3,P}$ = 6.1, CH₃-CH A), 19.71 (d, $J_{CH3,P}$ = 6.9, CH₃-CH B), 124.63 (p-phenyl A), 125.50 (C-5 B), 125.57 (C-5 A), 126.29 (C-6 B), 126.56 (C-6 A), 129.53 (m-phenyl B), 129.70 (m-phenyl A), 140.68 (C-8′ B), 140.70 (C-8′ A), 149.93 (C-4′ B), 149.94 (C-4′ A), 150.92 (d, $J_{i\text{-}P}$ = 6.6, i-phenyl B), 150.98 (d, $J_{i\text{-}P}$ = 6.6, i-phenyl A), 152.77 (C-2′ A), 156.30 (C-6′), 173.66 (d, $J_{CO\text{-}P}$ = 5.7, C=O B), 173.89 (d, $J_{CO\text{-}P}$ = 4.6, C=O A). HRMS (ESI): calcd. for $C_{24}H_{29}O_8N_6NaP$ [M + Na] 583.16767; found: 583.16760, calcd. for $C_{24}H_{30}O_8N_6P$ [M + H] 561.18572; found: 561.18578.

(2S)-Methyl 2-[({[(2R,3R,3aS,8R,8aR)-2-(6-amino-9H-purin-9-yl)-3,3a-dihydroxy-3,3a,4,7,8,8a-hexahydro-2H-cyclohepta[b]furan-8-yl]oxy}(phenoxy)phosphoryl)amino]propanoate (17b)

Yield 187 mg (66%) of a colourless solid foam. Found: C, 50.87; H, 5.30; N, 14.45; P, 5.32. Calc. for $C_{24}H_{29}N_6O_8P \cdot 0.5H_2O$: C, 50.62; H, 5.31; N, 14.76; P, 5.44%. ^{1}H NMR (500 MHz, d6-DMSO, 80 °C): δ 1.18 (d, $J_{CH3\text{-}CH}$ = 7.1, 3 H, CH₃-CH B), 1.22 (d, $J_{CH3\text{-}CH}$ = 7.1, 3 H, CH₃-CH A), 2.37-2.45 (m, 2 H, H-4b), 2.46-2.55 (m, 4 H, H-7), 2.97-3.03 (m, 2 H, H-4a), 3.55 (s, 3 H, OCH₃ B), 3.58 (s, 3 H, OCH₃ A), 3.81-3.88 (m, 2 H, Me-CH), 4.35 (m, 1 H, H-8a B), 4.38 (m, 1 H, H-8a A), 4.65-4.70 (m, 2 H, H-3), 4.77 (bs, 2 H, 3a-OH), 4.89 (m, 1 H, H-8 B), 4.93 (m, 1 H, H-8 A), 5.34 (bs, 2 H, 3-OH), 5.74-5.55 (m, 6 H, CH-NH, H-5, H-6), 5.87 (d, $J_{2\text{-}3}$ = 8.4, 1 H, H-2 B), 5.88 (d, $J_{2\text{-}3}$ = 8.5, 1 H, H-2 A), 6.98 (bs, 4 H, NH₂), 7.12-7.19 (m, 6 H, o-phenyl, p-phenyl), 7.30-7.34 (m, 4 H, m-phenyl), 8.16 (s, 1 H, H-2′B), 8.17 (s, 1 H, H-2′A), 8.28 (s, 1 H, H-8′B), 8.28 (s, 1 H, H-8′A). ^{13}C NMR (125 MHz, d6-DMSO): δ 19.26 (d, $J_{CH3\text{-}P}$ = 6.9, CH-CH₃ B), 19.50 (d, $J_{CH3\text{-}P}$ = 6.2, CH-CH₃ A), 31.59 (C-4), 33.65 and 33.67 (C-7), 49.69 and 49.77 (MeCH), 51.46 and 51.51 (OCH₃), 73.42 (C-3), 74.59 (d, $J_{8\text{-}P}$ = 5.8, C-8 B), 74.79 (d, $J_{8\text{-}P}$ = 6.1, C-8 A), 77.50-77.55 (m, C-3a), 84.51 and 84.61 (C-2), 87.24-87.34 (m, H-8a), 119.19 and 119.26 (C-5′), 119.93 (d, $J_{o\text{-}P}$ = 4.9, o-phenyl B), 119.96 (d, $J_{o\text{-}P}$ = 4.8, o-phenyl A), 124.13-124.21 (m, C-5, p-phenyl), 127.31 and 127.34 (C-6), 129.26 (m-phenyl), 139.50 and 139.65 (C-8′), 150.02 and 150.05 (C-4′), 150.70 (d, $J_{i\text{-}P}$ = 6.5, i-phenyl B), 150.73 (d, $J_{i\text{-}P}$ = 6.4, i-phenyl A), 152.48 (C-2′), 155.98 and 156.00 (C-6′), 173.19 (d, $J_{CO\text{-}P}$ = 5.3, C=O B), 173.33 (d, $J_{CO\text{-}P}$ = 4.7, C=O A). ESI MS, m/z (%): 584.3 (32) [M + Na + H], 583.3 (100) [M + Na], 561.3 (56) [M + H]. HRMS (ESI): calcd. for $C_{24}H_{30}O_8N_6NaP$ [M + Na] 561.18572; found: 561.18557.

(2S)-Methyl 2-[({[(2R,3R,3aS,7S,7aR)-2-(6-amino-9H-purin-9-yl)-3,3a-dihydroxyoctahydrobenzofuran-7-yl]oxy}(phenoxy)phosphoryl)amino]propanoate (18a)

Yield 147 mg (52%) of a colourless solid foam. Found: C, 50.20; H, 5.20; N, 14.61; P, 5.46. Calc. for $C_{23}H_{29}N_6O_8P \cdot 0.5$ CH₃OH: C, 50.00; H, 5.54; N, 14.89; P, 5.49%. ^{1}H NMR (500 MHz, d6-DMSO): δ 0.93 (d, $J_{CH3\text{-}CH}$ = 7.1, 3 H, CH₃-CH A), 1.10 (d, $J_{CH3\text{-}CH}$ = 7.1, 3 H, CH₃-CH B), 1.30 (m, 1 H, H-6b B), 1.38-1.54 (m, 5 H, H-4b, H-5b, H-6b A), 1.59 and 1.65 (2 x m, 2 H, H-5a), 1.98-2.05 (m, 3 H, H-4a, H-6a B), 2.17 (m, 1 H, H-6a A), 3.43 (s, 3 H, OCH₃ B), 3.52 (s, 3 H, OCH₃ A), 3.61 (m, 1 H, Me-CH B), 3.70 (m, 1 H, Me-CH A), 3.75 (d, $J_{7a\text{-}7}$ = 8.0, 1 H, H-7a B), 3.78 (d, $J_{7a\text{-}7}$ = 8.1, 1 H, H-7a A), 4.82-4.95 (m, 3 H, H-3 B, H-7), 4.98 (d, $J_{3\text{-}2}$ = 8.1, 1 H, H-3 A), 5.22 and 5.24 (2 x s, 2 H, 3a-OH), 5.36 (dd, $J_{NH\text{-}CH}$ = 9.5, $J_{NH\text{-}P}$ = 12.0, 1 H, CH-NH B), 5.47 (bs, 2 H, 3-OH), 5.70 (dd, $J_{NH\text{-}CH}$ = 10.0, $J_{NH\text{-}P}$ = 12.7, 1 H, CH-NH A), 6.01 (d, $J_{2\text{-}3}$ = 8.1, 1 H, H-2 B), 6.02 (d, $J_{2\text{-}3}$ = 8.1, 1 H, H-2 A), 6.88 (m, 2 H, o-phenyl A), 7.01 (m, 1 H, p-phenyl A), 7.07-7.15 (m, 5H, p-phenyl B, o-phenyl B, m-phenyl A), 7.23-7.25 (m, 4 H, NH₂), 7.31 (m, 2 H, m-phenyl B), 8.10 (s, 1 H, H-2′ A), 8.13 (s, 1 H, H-2′ B), 8.51 and 8.52 (2 x s, 2 H, H-8′). ^{13}C NMR (125 MHz, d6-DMSO): δ 19.50 (d, $J_{CH3\text{-}P}$ = 6.3, CH₃-CH), 19.70 (d, $J_{CH3\text{-}P}$ = 6.9, CH₃-CH), 30.59 and 30.62 (C-6), 31.70

and 31.74 (C-4), 49.69 and 49.77 (Me-CH), 51.81 and 51.93 (OCH$_3$), 72.20 and 72.35 (C-3), 77.82 (d, J_{3a-P} = 1.2, C-3a), 77.94 (d, J_{3a-P} = 1.4, C-3a), 79.41 (d, J_{7-P} = 5.9, C-7), 79.68 (d, J_{7-P} = 6.3, C-7), 87.48 and 87.54 (C-7a), 119.55 and 119.61 (C-5′), 120.10 (d, J_{o-P} = 5.0, o-phenyl), 120.43 (d, J_{o-P} = 4.8, o-phenyl), 124.15 and 124.49 (p-phenyl), 129.27 and 129.60 m-phenyl), 140.82 and 140.91 (C-8′), 150.06 and 150.10 (C-4′), 150.97 (d, J_{i-P} = 6.5, i-phenyl), 151.03 (d, J_{i-P} = 6.6, i-phenyl), 152.67 and 152.70 (C-2′), 156.23 and 156.25 (C-6′), 173.61 (d, J_{CO-P} = 6.3, C=O), 173.75 (d, J_{CO-P} = 5.2, C=O). ESI MS, m/z (%): 572.2 (30) [M + Na + H], 571.2 (100) [M + Na], 549.2 (29) [M + H]. HRMS (ESI): calcd. for C$_{23}$H$_{29}$O$_8$N$_6$NaP [M + Na] 571.16767; found: 569.16739, calcd. for C$_{23}$H$_{30}$O$_8$N$_6$P [M + H] 549.18572; found: 549.18571.

(2S)-Methyl 2-[({[(2R,3R,3aS,7R,7aR)-2-(6-amino-9H-purin-9-yl)-3,3a-dihydroxyoctahydrobenzofuran-7-yl]oxy}(phenoxy)phosphoryl)amino]propanoate (18b)

Yield 165 mg (60%) of a colourless solid foam. Found: C, 50.02; H, 5.38; N, 14.98; P, 5.50. Calc. for C$_{23}$H$_{29}$N$_6$O$_8$P: C, 50.37; H, 5.33; N, 15.32; P, 5.65%. ^{1}H NMR (500 MHz, d6-DMSO): δ 1.09 (d, J_{CH3-CH} = 7.1, 3 H, CH$_3$-CH A), 1.15 (d, J_{CH3-CH} = 7.0, 3 H, CH$_3$-CH B), 1.51-1.71 (m, 8 H, H-4b, H-5, H-6b), 1.79-1.98 (m, 4 H, H-4a, H-6a), 3.49 (s, 3 H, OCH$_3$ A), 3.53 (s, 3 H, OCH$_3$ B), 3.63 (m, 1 H, Me-CH A), 3.79 (m, 1 H, Me-CH B), 4.00 (d, J_{7a-7} = 3.9, 1 H, H-7a B), 4.02 (d, J_{7a-7} = 4.3, 1 H, H-7a A), 4.25 (d, J_{3-2} = 5.0, 1 H, H-3 B), 4.29 (d, J_{3-2} = 5.8, 1 H, H-3 A), 4.57-4.66 (m, 2 H, H-7), 5.13 (bs, 2 H, 3a-OH), 5.68 (bs, 2 H, 3-OH), 5.85 (d, J_{2-3} = 5.0, 1 H, H-2 B), 5.92 (d, J_{2-3} = 5.8, 1 H, H-2 A), 5.92 (dd, J_{NH-CH} = 10.2, J_{NH-P} = 13.4, 1 H, CH-NH A), 6.01 (dd, J_{NH-CH} = 10.1, J_{NH-P} = 12.8, 1 H, CH-NH B), 7.13-7.24 (m, 6 H, o-phenyl, p-phenyl), 7.32-7.38 (m, 8H, NH$_2$, m-phenyl), 8.17 (s, 1 H, H-2′ A), 8.18 (s, 1 H, H-2′ B), 8.34 (s, 1 H, H-8′ A), 8.40 (s, 1 H, H-8′ B). ^{13}C NMR (125 MHz, d6-DMSO): δ 17.65 (C-5 A), 18.33 (C-5 B), 19.78 (d, J_{CH3-P} = 7.5, CH$_3$-CH A), 19.88 (d, J_{CH3-P} = 6.5, CH$_3$-CH B), 27.09 (C-6 B), 27.36 (C-6 A), 31.78 (C-4), 49.61 (Me-CH A), 49.84 (Me-CH B), 51.95 (OCH$_3$ A), 51.98 (OCH$_3$ B), 73.58 (d, J_{7-P} = 3.7, C-7 A), 74.08 (d, J_{7-P} = 5.2, C-7 B), 75.44 (C-3 A), 76.16 (C-3a A), 76.23 (C-3 B), 76.33 (C-3a B), 80.36 (C-7a B), 80.89 (C-7a A), 87.62 (C-2 A), 88.66 (C-2 B), 119.04 (C-5′ B), 119.08 (C-5′ A), 120.27 and 120.31 (o-phenyl), 124.56 (p-phenyl B), 124.64 (p-phenyl A), 129.71 (m-phenyl B), 129.77 (m-phenyl A), 138.93 (C-8′ A), 139.31 (C-8′ B), 150.00 (C-4′ B), 150.20 (C-4′ A), 150.93 (d, J_{i-P} = 5.9, i-phenyl A), 150.97 (d, J_{i-P} = 6.3, i-phenyl B), 153.03 (C-2′), 156.29 (C-6′ B), 156.30 (C-6′ A), 173.75-173.81 (m, C=O). ESI MS, m/z (%): 572.4 (28) [M + Na + H], 571.4 (100) [M + Na], 549.3 (12) [M + H]. HRMS (ESI): calcd. for C$_{23}$H$_{29}$O$_8$N$_6$NaP [M + Na] 571.16767; found: 571.16749.

(2S)-Methyl 2-[({[(2R,3R,3aS,8S,8aR)-2-(6-amino-9H-purin-9-yl)-3,3a-dihydroxyoctahydro-2H-cyclohepta[b]furan-8-yl]oxy}(phenoxy)phosphoryl)amino]propanoate (19a)

Yield 142 mg (50%) of a colourless solid foam. Found: C, 51.21; H, 5.58; N, 14.63; P, 5.32. Calc. for C$_{24}$H$_{31}$N$_6$O$_8$P: C, 51.24; H, 5.55; N, 14.94; P, 5.51%. ^{1}H NMR (500 MHz, d6-DMSO): δ

0.94 (d, J_{CH3-CH} = 7.1, 3 H, CH$_3$-CH B), 1.09 (d, J_{CH3-CH} = 7.1, 3 H, CH$_3$-CH B), 1.31-1.43 (m, 2 H, H-6b), 1.50-1.58 (m, 6 H, H-4b, H-5), 1.60-1.79 (m, 4 H, H-7b, H-6a), 1.93-2.00 (m, 3 H, H-7a B, 4a), 2.26 (m, 1 H, H-7a A), 3.46 and 3.51 (2 x s, 6 H, OCH$_3$), 3.65-3.73 (2 x m, 2 H, Me-CH), 3.87 (d, J_{8a-8} = 9.0, 1 H, H-8a B), 3.90 (d, J_{8a-8} = 9.2, 1 H, H-8a A), 4.39 (d, J_{3-2} = 8.4, 1 H, H-3 B), 4.42 (d, J_{3-2} = 8.4, 1 H, H-3 A), 4.49 and 4.54 (2 x m, 2 H, H-8), 4.82 (bs, 2 H, 3a-OH), 5.44 (dd, J_{NH-CH} = 10.1, J_{NH-P} = 11.6, 1 H, CH-NH A), 5.63 (bs, 2 H, 3-OH), 5.75 (dd, J_{NH-CH} = 10.1, J_{NH-P} = 12.7, 1 H, CH-NH B), 5.83 (d, J_{2-3} = 8.4, 1 H, H-2 B), 5.84 (d, J_{2-3} = 8.4, 1 H, H-2 A), 6.97-7.03 (m, 3 H, o-phenyl B, p-phenyl B), 7.05-7.15 (m, 5 H, o-phenyl A, p-phenyl A, m-phenyl B), 7.28 (bs, 4 H, NH$_2$), 7.30 (m, 2 H, m-phenyl A), 8.14 (2 x s, 2 H, H-2′), 8.46 and 8.46 (2 x s, 2 H, H-8′). ^{13}C NMR (125 MHz, d6-DMSO): δ 19.64 (d, J_{CH3-P} = 5.2, CH$_3$-CH), 19.72 (d, J_{CH3-P} = 6.8, CH$_3$-CH), 21.57 (C-5), 25.70 and 25.89 (C-6), 33.01 and 33.16 (C-7), 35.43 and 35.49 (C-4), 49.48 and 49.77 (Me-CH), 51.92 (OCH$_3$), 76.32 and 76.52 (C-3a), 77.21 and 77.42 (C-3), 78.24 (d, J_{8-P} = 6.3, C-8), 78.33 (d, J_{8-P} = 5.6, C-8), 84.34 and 84.36 (C-2), 89.76 (d, J_{8a-P} = 5.8, C-8a), 89.82 (d, J_{8a-P} = 6.4, C-8a), 119.15 and 119.21 (C-5′), 120.31 (d, J_{o-P} = 4.6, o-phenyl), 120.47 (d, J_{o-P} = 4.5, o-phenyl), 124.19 and 124.55 (p-phenyl), 129.28 and 129. 64 (m-phenyl), 139.84 and 139.88 (C-8′), 150.20 and 150.23 (C-4′), 151.03 (d, J_{i-P} = 6.6, i-phenyl), 151.06 (d, J_{i-P} = 6.7, i-phenyl), 152.86 C-2′), 156.24 (C-6′), 173.61 (d, J_{CO-P} = 6.8, C=O), 173.85 (d, J_{CO-P} = 5.3, C=O). HRMS (ESI): calcd. for C$_{24}$H$_{31}$O$_8$N$_6$NaP [M + Na] 585.18332; found: 585.18308, calcd. for C$_{24}$H$_{32}$O$_8$N$_6$P [M + H] 563.20137; found: 563.20133.

(2S)-Methyl 2-[({[(2R,3R,3aS,8R,8aR)-2-(6-amino-9H-purin-9-yl)-3,3a-dihydroxyoctahydro-2H-cyclohepta[b]furan-8-yl]oxy}(phenoxy)phosphoryl)amino]propanoate (19b)

Yield 144 mg (51%) of a colourless solid foam. Found: C, 50.98; H, 5.74; N, 14.58; P, 5.34. Calc. for C$_{24}$H$_{31}$N$_6$O$_8$P: C, 51.24; H, 5.55; N, 14.94; P, 5.51%. ^{1}H NMR (500 MHz, d6-DMSO): δ 1.04 (d, $J_{CH3- CH}$ = 7.1, 3 H, CH$_3$-CH), 1.13 (d, $J_{CH3- CH}$ = 7.1, 3 H, CH$_3$-CH), 1.53-1.73 (m, 12 H, H-4b, H-7b, H-5, H-6), 1.85-1.94 (m, 2 H, H-4a), 2.21 (m, 2 H, H-7a), 3.50 and 3.55 (2 x s, 6 H, OCH$_3$), 3.79 and 3.88 (2 x m, Me-CH), 4.05-4.06 (m, 2 H, H-8a), 4.15 and 4.27 (2 x m, 2 H, H-3), 4.61-4.68 (m, 2 H, H-8), 4.73 (bs, 2 H, 3a-OH), 5.57 (bs, 2 H, 3-OH), 5.87 (d, J_{2-3} = 8.5, 1 H, H-2), 5.92 (d, J_{2-3} = 8.5, 1 H, H-2), 5.95 (dd, J_{NH-CH} = 10.1, J_{NH-P} = 13.1, 1 H, CH-NH), 6.13 (dd, J_{NH-CH} = 10.4, J_{NH-P} = 12.3, 1 H, CH-NH), 7.14-7.20 (m, 4H, o-phenyl, p-phenyl), 7.23 (m, 2 H, o-phenyl), 7.29 (bs, 2 H, NH$_2$), 7.32-7.40 (m, 4 H, m-phenyl), 8.14 and 8.15 (2 x s, 2 H, H-2′), 8.38 and 8.45 (2 x s, 2 H, H-8′). ^{13}C NMR (125 MHz, d6-DMSO): δ 19.72 (d, J_{CH3-P} = 7.2, CH$_3$-CH), 20.11 (d, J_{CH3-P} = 5.6, CH$_3$-CH), 22.38 (C-5), 24.7 (C-6), 30.15 and 30.27 (C-7), 35.72 (C-4), 49.89 and 50.01 (Me-CH), 52.02 and 52.07 (O-CH$_3$), 77.32 (d, J_{8-P} = 6.0, C-8), 77.90 (d, J_{8-P} = 6.3, C-8), 77.90 and 78.40 (C-3), 78.47 and 78.71 (C-3a), 84.03 and 84.47 (C-2), 89.38 and 89. 43 (C-8a), 118.81 and 119.05 (C-5′), 120.40 (d, J_{o-P} = 4.6, o-phenyl), 120.52 (d, J_{o-P} = 4.3, o-phenyl), 124.68 and 124.76 (p-phenyl), 129.74 and 129.79 (m-phenyl), 138.87 and 139.45 (C-8′), 150.33 and 150.45

(C-4′), 150.97 (d, $J_{i\text{-}P}$ = 6.2, *i*-phenyl), 151.00 (d, $J_{i\text{-}P}$ = 6.5, *i*-phenyl), 152.91 and 152.96 (C-2′), 156.21 and 156.25 (C-6′), 173.75-173.82 (m, C=O). ESI MS, *m/z* (%): 586.2 (33) [M + Na + H], 585.2 (100) [M + Na], 563.2 (18) [M + H]. HRMS (ESI): calcd. for $C_{24}H_{32}O_8N_6P$ [M + H] 563.20137; found: 563.20136.

Preparation of isopropylidene derivatives 22a and 22b

2,2-Dimethoxypropane (5 mL) and conc. H_2SO_4 (120 μL) were added to a solution of **13a** or **13b** (319 mg, 1.0 mmol) in dimethyl formamide (6 mL) and the mixture was stirred at ambient temperature for 24 h. Then was neutralized with pulverized $KHCO_3$ and evaporated. The residue was triturated with water, solid was filtred off, washed with water, dried and chromatographed on silica gel (40 g) in ethyl acetate – acetone–ethanol – water (400 : 30 : 12 : 8).

(3a*R*,4*R*,5a*R*,6*S*,10a*R*)-4-(6-Amino-9*H*-purin-9-yl)-2,2-dimethyl-3a,4,5a,6,7,10-hexahydrocyclohepta[2,3]furo[3,4-d][1,3]dioxol-6-ol (22a)

Yield 285 mg (79%) of **22a** as white crystals. M.p. 179-180 °C. $[\alpha]_D^{20}$ -48.7 (c = 0.406, MeOH). Found: C, 56.46; H, 6.03; N, 19.18. Calc. for $C_{17}H_{21}N_5O_4$: C, 56.82; H, 5.89; N, 19.49%. ^{1}H NMR (500 MHz, d6-DMSO): δ 1.32 (s, 3 H, 2-CH₃), 1.55 (s, 3 H, 2-CH₃), 2.16 (dd, J_{gem} = 17.2, $J_{7b\text{-}8}$ = 7.3, 1 H, H-7b), 2.32 (bm, 1 H, H-7a), 2.43 (ddm, J_{gem} = 17.3, $J_{10b\text{-}9}$ = 7.8, 1 H, H-10b), 3.13 (dm, J_{gem} = 17.3, 1 H, H-10a), 3.82-3.85 (m, 2 H, H-5a, H-6a), 4.93 (d, $J_{3a\text{-}4}$ = 2.8, 1 H, H-3a), 5.13 (d, $J_{OH\text{-}6}$ = 4.2, 1 H, OH), 5.50 (m, 1 H, H-9), 5.60 (m, 1 H, H-8), 6.08 (d, $J_{4\text{-}3a}$ = 2.8, 1 H, H-4), 7.35 (bs, 2 H, 6′-NH₂), 8.17 (s, 1 H, H-2′), 8.37 (s, 1 H, H-8′). ^{13}C NMR (125 MHz, d6-DMSO): δ 27.40 (2-CH₃), 28.40 (2-CH₃), 34.14 (C-10), 34.48 (C-7), 69.34 (C-6), 87.40 (C-4), 89.25 (C-10a), 89.30 (C-3a), 91.77 (C-5a), 114.90 (C-2), 119.30 (C-5′), 125.24 (C-9), 127.27 (C-8), 139.77 (C-8′), 149.22 (C-4′), 153.09 (C-2′), 156.33 (C-6′). ESI MS, *m/z* (%): 383.2 (21) [M + Na + H], 382.2 (100) [M + Na], 360.2 (9) [M + H]. HRMS (ESI): calcd. for $C_{17}H_{22}O_4N_5$ [M + H] 360.16663; found: 360.16664; calcd. for $C_{17}H_{21}O_4N_5Na$ [M + Na] 382.14858; found: 382.14857.

(3a*R*,4*R*,5a*R*,6*R*,10a*R*)-4-(6-Amino-9*H*-purin-9-yl)-2,2-dimethyl-3a,4,5a,6,7,10-hexahydrocyclohepta[2,3]furo[3,4-d][1,3]dioxol-6-ol (22b)

Yield 250 mg (69.5%) of **22b** as white crystals. M.p. 264-266 °C. $[\alpha]_D^{20}$ -19.7 (c = 0.299, DMF). Found: C, 56.52; H, 5.92; N, 19.19. Calc. for $C_{17}H_{21}N_5O_4$: C, 56.82; H, 5.89; N, 19.49%. ^{1}H NMR (500 MHz, d6-DMSO): δ 1.38 (s, 3 H, 2-CH₃), 1.55 (s, 3 H, 2-CH₃), 2.35-2.39 (m, 2 H, H-7a, H-7b), 2.59 (dm, J_{gem} = 13.6, 1 H, H-10b), 2.91 (m, 1 H, H-10a), 4.23 (m, 1 H, H-6), 4.27 (m, 1 H, H-5a), 4.98 (d, $J_{3a\text{-}4}$ = 3.7, 1 H, H-3a), 5.33 (bs, 1 H, OH), 5.54-5.56 (m, 2 H, H-8, H-9), 6.12 (d, $J_{4\text{-}3a}$ = 3.7, 1 H, H-4), 7.35 (bs, 2 H, 6′-NH₂), 8.16 (s, 1 H, H-2′), 8.32 (s, 1 H, H-8′). ^{13}C NMR (125.8 MHz, d6-DMSO): δ 28.41 (2-CH₃), 28.83 (2-CH₃), 33.62 (C-10), 33.99 (C-7), 66.94 (C-6), 87.72 (C-4), 89.03 (C-3a), 91.02 (C-5a), 91.99 (C-10a), 114.31 (C-2), 118.96 (C-5′), 123.36 and 129.05 (C-8, C-9), 138.90 (C-8′), 149.28 (C-4′), 153.05 (C-2′), 156.31 (C-6′). ESI MS, *m/z* (%): 383.1 (22)

[M + Na + H], 382.1 (100) [M + Na], 360.1 (10) [M + H]. HRMS (ESI): calcd. for $C_{17}H_{22}O_4N_5$ [M + H] 360.16663; found: 360.16660.

Preparation of phosphates 23a and 23b

Method A: To a stirred solution of **22a** or **22b** (179 mg, 0.5 mmol) in trimethyl phosphate (1.2 mL) cooled to 0°C was dropwise added POCl₃ (213 μL, 2.25 mmol). The mixture was stirred at ambient temperature for 4 h and then cooled to 0°C. Water was added (0.8 mL) and the mixture was neutralized with aqueous ammonia and applied onto Dowex 50 (H⁺) column (30 mL). Column was eluted with water (200 mL) and then with 2.5 % aqueous ammonia. UV absorbing fractions were collected and evaporated. A solution of the residue in 50% aqueous trifluoroacetic acid (2 mL) was kept at room temperature for 48 h, then evaporated and twice co-evaporated with water. A solution of the residue in water was neutralized with aqueous ammonia and adsorbed on silica gel, which was placed on a top of silica gel column (40 mL). Elution with 2-propanol – water – conc. aqueous ammonia (15 : 4 : 2) afforded crude **23a** or **23b**, which were re-purified on Dowex 50 (H⁺) column (15 mL) by elution with water (100 mL) and 2.5 % aqueous ammonia. UV absorbing fraction were collected, concentrated and converted to sodium salt using Dowex 50 (Na⁺) column (30 mL) by elution of the column with water and subsequent evaporation of UV absorbing fractions.

(2*R*,3*R*,3a*S*,8*S*,8a*R*)-2-(6-Amino-9*H*-purin-9-yl)-3,3a-dihydroxy-3,3a,4,7,8,8a-hexahydro-2*H*-cyclohepta[b]furan-8-yl dihydrogen phosphate, disodium salt (23a)

Yield 89 mg (38%) of phosphate **23a**, as a yellowish amorphous solid. $[\alpha]_D^{20}$ 21.4 (c = 0.392, H₂O). Found: C, 36.71; H, 4.21; N, 14.98; P, 6.45. Calc. for $C_{14}H_{18}N_5Na_2O_7P \cdot H_2O$: C, 36.45; H, 3.93; N, 15.18; P, 6.71%. ^{1}H NMR (500 MHz, D₂O): δ 2.51-2.58 (m, 2 H, H-4b, H-7b), 2.71-2.79 (m, 2 H, H-4a, H-7a), 4.26 (d, $J_{8a\text{-}8}$ = 7.4, 1 H, H-8a), 4.51 (m, 1 H, H-8), 4.59 (d, $J_{3\text{-}2}$ = 7.9, 1 H, H-3), 5.63 (dm, $J_{5\text{-}6}$ = 11.5, 1 H, H-5), 5.73 (dm, $J_{6\text{-}5}$ = 11.5, 1 H, H-6), 5.98 (d, $J_{2\text{-}3}$ = 7.9, 1 H, H-2), 8.16 (s, 1 H, H-2′), 8.41 (s, 1 H, H-8′). ^{13}C NMR (125 MHz, D₂O): δ 35.01 (C-7), 35.54 (C-4), 75.26 (d, $J_{8\text{-}P}$ = 5.2, C-8), 78.41 (C-3), 81.27 (C-3a), 87.82 (C-2), 91.42 (d, $J_{8a\text{-}P}$ = 6.1, C-8a), 121.33 (C-5′), 126.72 (C-5), 130.61 (C-6), 142.84 (C-8′), 151.87 (C-4′), 155.48 (C-2′), 158.09 (C-6′). negESI MS, *m/z* (%): 399.0 (15) [M], 398.0 (100) [M - H]. HRMS (negESI): calcd. for $C_{14}H_{17}O_7N_5P$ [M - H] 398.08711; found: 398.08702.

(2*R*,3*R*,3a*S*,8*R*,8a*R*)-2-(6-Amino-9*H*-purin-9-yl)-3,3a-dihydroxy-3,3a,4,7,8,8a-hexahydro-2*H*-cyclohepta[b]furan-8-yl phosphate disodium salt (23b).

Yield 91 mg (39%) of phosphate **23b**, as a yellowish amorfous solid. $[\alpha]_D^{20}$ 26.0 (c = 0.308, H₂O). Found: C, 36.33; H, 4.14; N, 14.86; P, 6.40. Calc. for $C_{14}H_{18}N_5Na_2O_7P \cdot H_2O$: C, 36.45; H, 3.93; N, 15.18; P, 6.71%. ^{1}H NMR (500 MHz, D₂O): δ 8.49 (bs, 1 H, H-8′), 8.20 (s, 1 H, H-2′), 6.04 (d, $J_{2\text{-}3}$ = 8.5, 1 H, H-2), 5.74 (m, 1 H, H-6), 5.67 (m, 1 H, H-5), 4.73 – 4.68 (m, 2 H, H-3, H-8), 4.50 (bs, 1 H, H-8a), 2.82 – 2.48 (m, 4 H, H-4, H-7). ^{13}C NMR

(125MHz, D$_2$O): δ 158.24 (C-6′), 155.62 (C-2′), 152.20 (C-4′), 142.76 (C-8′), 131.69 (C-6), 126.13 (C-5), 121.27 (C-5′), 91.91 (d, $J_{8a,P}$ = 4.7, C-8a), 86.79 (C-2), 81.28 (C-3a), 78.31 (C-3), 74.66 (C-8), 35.53 (C-4), 34.99 (C-7). ESI MS, m/z (%): 400.2 (51) [M + Na], 342.2 (41), 320.2 (100). negESI MS, m/z (%): 399.1 (20) [M], 398.1 (100) [M - 1]. HRMS (ESI): calcd. for C$_{14}$H$_{19}$O$_7$N$_5$P [M + H] 400.10166; found: 400.1078. HRMS (negESI): calcd. for C$_{14}$H$_{17}$O$_7$N$_5$P [M - H] 398.08711; found: 400.08716.

Method B: Nucleoside analogue **13a** or **13b** (160 mg, 0.5 mmol) was co-distilled with pyridine (3 x 5 mL) and dissolved in pyridine (8 mL). To the solution was added phenylboronic acid (65 mg, 0.53 mmol), pyridine (~6 mL) was distilled off at atmospheric pressure within 4 h and the remaining pyridine was evaporated under vacuum. To a stirred solution of the residue in trimethyl phosphate (1.2 mL) cooled to 0°C was dropwise added POCl$_3$ (213 µL, 2.25 mmol). The mixture was stirred at ambient temperature for 4 h. The reaction mixture was worked up as in Method A. It was obtained 60 mg (26%) of **23a** and 62 mg (27%) of nucleotide analogue **23b**.

Preparation of triphosphates 24a and 24b

A solution of phosphate **23a** or **23b** in water (0.2 mL) was placed on a top of Dowex 50 (Et$_3$NH$^+$) column (10 mL) and the column was eluted with water. UV absorbing fractions were collected and evaporated. A mixture of the residue, imidazole (51 mg, 0.75 mmol) and triphenylphosphine (131 mg, 0.5 mmol) was co-distilled with DMF (3 x 3 mL). To a solution of the residue in DMSO (0.25 mL) and DMF (0.5 mL) were added triethylamine (24.5 µL, 0.175 mmol) and 2,2′dipyridyl disulfide (110 mg, 0.5 mmol) and the mixture was stirred at room temperature under argon atmosphere overnight. The mixture was then added dropwise at 0 °C to a mixture of acetone (15 mL), diethylether (15 mL) and saturated solution of NaClO$_4$·H$_2$O in acetone (0.15 mL). The precipitate was centrifuged at 0 °C and washed with a mixture of diethylether- acetone (1:1, 2 x 20 mL) and ether (2 x 20 mL), both at 0 °C. The residue was dried over P$_2$O$_5$ in vacuum overnight. Dry imidazolide was disolved in 0.5 M solution of (nBu$_3$NH)$_2$P$_2$H$_2$O$_7$ in DMSO (0.3 mL) and the solution was left at room temperature overnight. Crude triphosphate was purified by reverse phase HPLC.

(2R,3R,3aS,8R,8aR)-2-(6-Amino-9H-purin-9-yl)-3,3a-dihydroxy-3,3a,4,7,8,8a-hexahydro-2H-cyclohepta[b]furan-8-yl triphosphate, tetra(triethylammonium) salt (24a)

A white amorfous solid. ^{1}H NMR (500 MHz, MeOD): δ 1.21 (t, $J_{CH3,CH2}$ = 7.3, 36 H, NCH$_2$CH$_3$), 2.39-2.92 (m, 4 H, H-4, H-7), 3.01 (q, $J_{CH2-CH3}$ = 7.3, 24 H, NCH$_2$CH$_3$), 4.55-4.88 (m, 3 H, H-3, H-8, H-8a), 5.59 (m, 1 H, H-5), 5.69 (m, 1 H, H-6), 6.01 (d, J_{2-3} = 8.3, 1 H, H-2), 8.19 (s, 1 H, H-2′), 8.43 (bs, 1 H, H-8′). ^{13}C NMR (125 MHz, MeOD): δ 9.66 (NCH$_2$CH$_3$), 33.72 (C-7), 35.10 (C-4), 47.23 (NCH$_2$CH$_3$), 75.03 (d, J_{8-P} = 5.0, C-8), 79.79 (C-3a), 86.68 (C-2), 90.50 (C-8a), 120.47 (C-5′), 125.09 (C-5), 130.04 (C-6), 141.69 (C-8′), 151.66 (C-4′), 154.07 (C-2′), 157.45 (C-6′). C-3 was not detected. ^{31}P NMR (202 MHz,

MeOD): δ 10.36 (d, $J_{\gamma-\beta}$ = 20.9, γ-P), 11.81 (d, $J_{\alpha-\beta}$ = 19.7, α-P), 23.70 (dd, $J_{\beta-\alpha}$ = 19.7, $J_{\beta-\gamma}$ = 20.9, β-P). negESI MS, m/z (%): 559.0 (25) [M], 558.0 (84) [M - H], 479.0 (33) [M - HPO$_3$], 478.0 (100) [M – H$_2$PO$_3$]. HRMS (negESI): calcd. for C$_{14}$H$_{19}$O$_{13}$N$_5$P$_3$ [M - H] 558.01977; found: 558.01932.

(2R,3R,3aS,8S,8aR)-2-(6-Amino-9H-purin-9-yl)-3,3a-dihydroxy-3,3a,4,7,8,8a-hexahydro-2H-cyclohepta[b]furan-8-yl triphosphate, tetra(triethylammonium) salt (24b)

A white amorfous solid. ^{1}H NMR (500 MHz, MeOD): δ 1.21 (t, $J_{CH3-CH2}$ = 7.3, 36 H, NCH$_2$CH$_3$), 2.44 (dd, J_{gem} = 16.5, J_{4B-5} = 6.8, 1 H, H-4B), 2.63 (dm, J_{gem} = 18.1, 1H, H-7B), 2.93-3.07 (m, 26 H, H-4A, H-7A, NCH$_2$CH$_3$), 4.45 (d, J_{8a-8} = 6.0, 1 H, H-8a), 4.71 (m, 1 H, H-8), 4.78 (d, J_{3-2} = 8.2, 1 H, H-3), 5.55-5.64 (m, 2 H, H-5, H-6), 5.97 (d, J_{2-3} = 8.2, 1 H, H-2), 8.19 (s, 1 H, H-2′), 8.42 (s, 1 H, H-8′). ^{13}C NMR (125 MHz, MeOD): δ 9.69 (NCH$_2$CH$_3$), 32.97 (d, J_{7-P} = 2.9, C-7), 34.85 (C-4), 47.21 (NCH$_2$CH$_3$), 74.96 (d, J_{8-P} = 6.0, C-8), 75.87 (C-3), 79.80 (C-3a), 87.58 (C-2), 89.75 (d, J_{8a-P} = 5.6, C-8a), 120.65 (C-5′), 125.55 (C-5), 128.58 (C-6), 142.01 (C-8′), 151.46 (C-4′), 154.00 (C-2′), 157.44 (C-6′). ^{31}P NMR (202 MHz, MeOD): δ 10.28 (d, $J_{\square-\square}$ = 21.1, γ-P), 11.73 (d, $J_{\square-\square}$ = 19.8, α-P), 23.79 (dd, $J_{\square-\square}$ = 19.8, $J_{\square-\square}$ = 21.1, β-P). negESI MS, m/z (%): 559.0 (12) [M], 558.0 (71) [M - H], 479.0 (20) [M - HPO$_3$], 478.0 (100) [M – H$_2$PO$_3$]. HRMS (negESI): calcd. for C$_{14}$H$_{19}$O$_{13}$N$_5$P$_3$ [M - H] 558.01977; found: 558.01935.

Carboxypeptidase Y Assay.

The phosphoramidate derivative **17a** or **17b** (5.0 mg) was dissolved in acetone-d_δ (200 µL) and then 400 µL of Trizma (tris(hydroxymethyl)aminomethane) buffer (pH 7.4) was added at room temperature (25°C). ^{31}P NMR spectrum (202 MHz with H$_3$PO$_4$ as external standard) of this sample was measured to obtain ^{31}P chemical shifts of the starting phosphoramidate. Next, carboxypeptidase Y (0.3 mg dissolved in 200 µL of Trizma buffer) was added and ^{31}P NMR spectra were recorded in various times after the addition (25°C).

Chemical hydrolysis.

The studied compound **17a** or **17b** (5.4 mg) was dissolved in 500 µL of triethylamine aqueous solution (3 % Et$_3$N in D$_2$O) and ^{31}P NMR spectra (202 MHz with H$_3$PO$_4$ as external standard) were recorded forthwith at room temperature (25°C) and then at various times after the sample preparation.

Screening of antiviral activity

The anti-rhinovirus activity of test compounds was measured in H1-HeLa cells. Compounds were prepared in replicate 3-fold serial dilutions in DMSO (384-well format), and 0.1 µL of these dilutions were transferred acoustically to assay plates with an Echo instrument. H1-HeLa cells in RPMI medium supplemented with 10 % heat inactivated FBS and antibiotics were premixed in batch with mixture of HRV1A, HRV14, and HRV16 at a TCID$_{90}$ of 4X for each strain. After three day incubation at 33°C, virus-induced cytopathic effects were determined by a Cell-titer Glo viability assay (Promega, Madison, WI).
Anti HCV activity of compounds was determined in multiplex assay using HUH 7-lunet stably replicating I389luc-ubi-neo/NS3-3′/ET genotype 1b replicon and 2aLucNeo-25 cell line

encoding a genotype 2a JFH-1 replicon. Cells were maintained in Dulbecco DMEM medium supplemented with GlutaMAX (Invitrogen), 10% FBS (not heat-inactivated), 1mg/mL G-418, Pen-Strep, and non-essential amino acids. Cells were plated into 384-well assay plates with 1600 cells per well and treated with serial dilutions of compounds. Following three day incubation, the activity of Renilla luciferase was quantified using the Dual-Glo luciferase assay system from Promega (Promega, Madison, WI).

Inhibition of the activity of PI4Ks

The lipid kinase activity was determined by ADP-Glo Kinase Assay (Promega) measuring the amount of ADP produced during the kinase reaction. Reactions were carried out in a total volume of 5 µl and contained PI4K enzyme (final concentrations for PI4K IIIβ was 4ng/µL, for PI4K IIIα was 2ng/µL, and for PI4K IIα was 2ng/µL) in kinase buffer (20mM TRIS pH 7.5; 5 mM MgCl$_2$; 0.2% Triton-X; 0.1 mg/mLBSA; 2mM DTT), PI/PS (lipid kinase substrate) in kinase buffer (final concentration = 50 µM), inhibitors (10 mM stock solutions in DMSO were diluted with kinase buffer to final concentration dependent on inhibitor's activity, e.g. 400-0,01; 300-0,0001; 150-0,00001 µM for PI4K IIIβ), and the reaction was started by adding ATP in kinase buffer (final concentration 100 µM). This reaction was carried out for 60 min/25°C and the amount of hydrolyzed ATP was measured according to the manufacturer's protocol (add ADP/Glo Reagent to terminate the kinase reaction and deplete the remaining ATP, then add Kinase Detection Reagent to simultaneously convert ADP to ATP and allow the newly synthesized ATP to be measured using a luciferase/luciferin reaction). Luminescence was measured using spectrophotometer TECAN infinite M 1000.

Acknowledgements

Notes and references

^{a} Institute of Organic Chemistry and Biochemistry, Academy of Sciences of the Czech Republic, v.v.i., Gilead Sciences & IOCB Research Centre, 166 10 Prague 6, Czech Republic.

^{b} Gilead Sciences, Inc., 333 Lakeside Drive, Foster City, CA 94404, United States.

Electronic Supplementary Information (ESI) available: details of chemical hydrolysis monitored by NMR spetroscopy. See DOI: 10.1039/b000000x/

1. G. M. Blackburn, M. J. Gait, D. Loakes and D. M. Williams, *Nucleic Acids in Chemistry and Biology, Third Edition*, 2006, 13-75.

2. C. Altona and M. Sundaralingam, *J. Am. Chem. Soc.*, 1972, **94**, 8205-8212.

3. V. E. Marquez, A. Ezzitouni, P. Russ, M. A. Siddiqui, H. Ford, R. J. Feldman, H. Mitsuya, C. George and J. J. Barchi, *J. Am. Chem. Soc.*, 1998, **120**, 2780-2789.

4. V. E. Marquez, M. A. Siddiqui, A. Ezzitouni, P. Russ, J. Y. Wang, R. W. Wagner and M. D. Matteucci, *J. Med. Chem.*, 1996, **39**, 3739-3747.

5. V. E. Marquez, S. H. Hughes, S. Sei and R. Agbaria, *Antiviral Res.*, 2006, **71**, 268-275.

6. V. E. Marquez, T. Ben-Kasus, J. J. Barchi, K. M. Green, M. C. Nicklaus and R. Agbaria, *J. Am. Chem. Soc.*, 2004, **126**, 543-549.

7. M. Dejmek, M. Šála, H. Hřebabecký, M. Dračínský, E. Procházková, D. Chalupska, M. Klíma, P. Plačková, M. Hájek, G. Andrei, L. Naesens, P. Leyssen, J. Neyts, J. Balzarini, E. Boura and R. Nencka, *Bioorg. Med. Chem.*, 2015, **23**, 184-191.

8. M. Dejmek, H. Hřebabecký, M. Šála, M. Dračínský, E. Procházková, P. Leyssen, J. Neyts, J. Balzarini and R. Nencka, *Bioorg. Med. Chem.*, 2014, **22**, 2974-2983.

9. S. Kauppinen, B. Vester and J. Wengel, *Drug Discov. Today Technol.*, 2005, **2**, 287-290.

10. R. N. Veedu and J. Wengel, *Chem. Biodivers.*, 2010, **7**, 536-542.

11. M. Šála, M. Dejmek, E. Procházková, H. Hřebabecký, J. Rybáček, M. Dračínský, P. Novák, S. Rosenbergová, J. Fukal, V. Sychrovský, I. Rosenberg and R. Nencka, *Org. Biomol.Chem.*, 2015, **13**, 2703-2715.

12. C. J. Leumann, *Bioorg. Med. Chem.*, 2002, **10**, 841-854.

13. A. Stauffiger and C. J. Leumann, *Eur. J. Org. Chem.*, 2009, 1153-1162.

14. P. Silhar and C. J. Leumann, *Bioorg. Med. Chem.*, 2010, **18**, 7786-7793.

15. M. Hollenstein and C. J. Leumann, *ChemBioChem*, 2014, **15**, 1901-1904.

16. S. Hanessian and D. J. Ritson, *J. Org. Chem.*, 2006, **71**, 9807-9817.

17. M. J. Robins, S. F. Wnuk, X. D. Yang, C. S. Yuan, R. T. Borchardt, J. Balzarini and E. De Clercq, *J. Med. Chem.*, 1998, **41**, 3857-3864.

18. U. Niedballa and H. Vorbrüggen, *J. Org. Chem.*, 1974, **39**, 3654-3660.

19. During the preparation of this manuscript, Mayes et al. also reported utilization of similar technique for installation of different type of phosphoramidate prodrugs and according to our experience this procedure can be applied to a variety of other nucleoside substrates with results significantly exceeding the traditional approaches.
B. A. Mayes, J. Arumugasamy, E. Baloglu, D. Bauer, A. Becker, N. Chaudhuri, G. M. Latham, J. Li, S. Mathieu, F. P. McGarry, E. Rosinovsky, A. Stewart, C. Trochet, J. Wang and A. Moussa, *Org. Process Res. Dev.*, 2014, **18**, 717-724.

20. C. A. G. Haasnoot, F. A. A. M. de Leeuw and C. Altona, *Tetrahedron*, 1980, **36**, 2783-2792.

21. C. McGuigan, P. Murziani, M. Slusarczyk, B. Gonczy, J. Vande Voorde, S. Liekens and J. Balzarini, *J. Med. Chem.*, 2011, **54**, 7247-7258.

22. *In situ* structure determination of intermediate **20b** was performed during approximately the first two hours of the reaction, when the concentration of the intermediate was above 50 %. The structure determination is based on the *in situ* analysis of C-P spin-spin interactions across 1-3 bonds visible in ^{13}C NMR spectra as a line splitting. It is clear that the methylester was hydrolyzed; the intensity of the signals corresponding to the methyl of methylester group (two signals = two diastereoisomers around 52.55 ppm) decreased whereas the intensity of methanol single signal (52.45 ppm) increased. Phenyl moiety is still attached to the molecule, signals corresponding to the carbon atoms in *ortho* position are still two dublets (two, because of the two diastereoisomers and dublets because of the C-P interaction). After several hours, the phenyl ring was cleaved and the stable final product was

obtained. The two dublets around 120.3 ppm, corresponding to *ortho* carbons, disappeared and one singlet signal around 118.9 ppm corresponding to *ortho* carbons of phenol appeared (Supporting information Figure S1). After the phenol release, there is no chiral center at the phosphorus atom, thus no two diastereoisomers exist. It is visible, for instance, in ^{13}C NMR spectra of carbon atom 8a, where the two dublets (87.8 ppm) corresponding to the two diastereoisomers of the intermediate disappeared and one dublet (88.6 ppm) coming from carbon atom 8a of the final product appeared (Supporting information S2).

III.

Procházková, E. – Čechová, L. – Jansa, P. – Dračínský, M.:

Long-range heteronuclear coupling constants in
2,6-disubstituted purine derivatives.

Magn. Reson. Chem. **2012**; 50, 295–298.

Research Article

Long-range heteronuclear coupling constants in 2,6-disubstituted purine derivatives

Eliška Procházková,[a] Lucie Čechová,[a] Petr Jansa[a] and Martin Dračínský[a]*

Four- and five-bond heteronuclear *J*-couplings between the hydrogen H-8 and carbons C-6 and C-2 in a series of 7- and 9-benzyl substituted purine derivaties with various substituents in positions 2 and 6 were studied by coupled ^{13}C NMR and H,C-HMBC experiments and by DFT calculations. We have found that for some of the derivatives, the five-bond coupling H8-C2 is higher than the four-bond H8-C6 coupling, which is also evidenced by a stronger crosspeak in the HMBC. This finding contradicts the generally accepted opinion that only strong three-bond crosspeaks and one weak four-bond H8-C6 crosspeak can be observed in the HMBC spectra of purine derivatives. The misinterpretation of HMBC spectra may lead to an incorrect determination of the purine derivatives' structure. Copyright © 2012 John Wiley & Sons, Ltd.

Supporting information may be found in the online version of this article.

Introduction

Naturally occurring purines are the basic constituents of nucleic acids; they also interact with enzymes and other proteins as components of the cofactors and signal molecules.[1] Adenosine 5′-triphosphate (ATP) controls the energy metabolism of cells, and nicotinamide adenine dinucleotide (NAD+, NADH) and flavin adenine dinucleotide (FAD, FADH$_2$) are the key cofactors not only of the cellular citric acid cycle, which is involved in the cellular oxidation/reduction processes.[2] Another molecule of biological relevance is acetyl-coenzyme A, which is of central importance for metabolism.

Purine derivatives bearing diverse types of substituents display a broad spectrum of biological activities,[3] including an interferon-inducing effect or more often an inhibitory effect against leukotriene A$_4$ hydrolase, sulfotransferase, phosphodiesterase, kinase, and other enzymes.[4] Modified nucleosides and nucleotides are very important classes of compounds used in the therapy of a wide variety of diseases, since they can act as antiviral,[5–8] antitumor[9,10] or antimicrobial[11] agents.

The distribution of electrons around the purine skeleton affects not only its chemical properties and reactivity but also the NMR parameters. The nature of the substituent is reflected in the NMR chemical shifts and nuclear spin–spin coupling constants, which makes NMR spectroscopy an excellent tool for investigating and interpreting the structure, reactivity and intermolecular interactions in terms of the electron distribution.[12] The ^{13}C and ^{15}N NMR chemical shifts as well as ^{1}H–X coupling constants can be used not only to distinguish between different regioisomers,[13] but also to reflect equally well the positions of protons, which enables the study of the tautomeric equilibria.[2,14–20]

The assignment of the carbon signals is usually done using three-bond H-C heteronuclear *J*-coupling.[21] A schematic graphical representation of the 'building blocks' for the assignment of purine derivatives signals with C-6 substituents is given in Fig. 1. It is generally believed that, for derivatives substituted at both positions 2 and 6, small four-bond interactions H8-C6 can be

used for the assignment of the carbon signals. The H8-C6 coupling can be identified in the HMBC spectra as a crosspeak with lower intensity.[22]

In this paper, we present a combined experimental and computational study of the four- and five-bond heteronuclear couplings H8-C6 and H8-C2. The experimentally studied compounds are depicted in Fig. 2. We demonstrate that the five-bond coupling is of a comparable magnitude with the four-bond coupling and a structure determination based on the HMBC patterns can lead to incorrect structures and/or the incorrect assignment of signals.

Experiment

The syntheses of compounds **1–4** and **6–7** have been described previously.[23–25] For the selective preparation of 7-substituted purines, an alternative synthetic approach could be used.[26] The preparation of compounds **5**, **9** and **10** will be described in a separate paper with the description of their biological activities. Briefly, compound **5** was obtained after hydrolysis of compound **1**; compound **9** was prepared by methanolysis of compound **6**, and compounds **8** and **10** were prepared by microwave-assisted reactions of compound **6** with 1 M hydrochloric acid (compound **8**) or with dibutylamine (compound **10**).

The NMR spectra were measured on a Bruker Avance 600 (with ^{1}H at 600.13 MHz and ^{13}C at a frequency of 150.92 MHz) and/or Bruker Avance 500 (with ^{1}H at 499.95 MHz and ^{13}C at 125.71 MHz) using a 5 mm TXI cryoprobe and about 5–10 mg of sample in 0.6 ml of CDCl$_3$ or DMSO-d_6. The chemical shifts are given in δ-scale (with the ^{1}H and ^{13}C referenced to TMS or to

---

* *Correspondence to: Martin Dračínský, Institute of Organic Chemistry and Biochemistry, Academy of Sciences, Flemingovo náměstí 2, 166 10 Prague, Czech Republic. E-mail: dracinsky@uochb.cas.cz*

a *Institute of Organic Chemistry and Biochemistry, Academy of Sciences, Flemingovo náměstí 2, 166 10 Prague, Czech Republic*
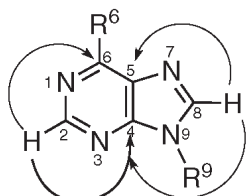
Figure 1. Schematic representation of the 'HMBC building blocks' (three-bond coupling pathways) for the assignment of purine derivatives signals with C-6 substituents.
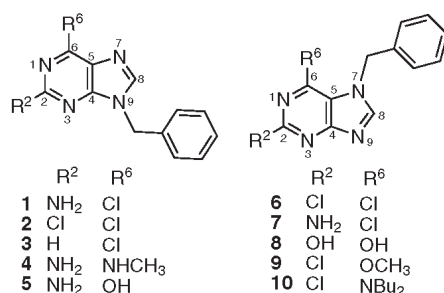

	R^2	R^6		R^2	R^6
1	NH$_2$	Cl	**6**	Cl	Cl
2	Cl	Cl	**7**	NH$_2$	Cl
3	H	Cl	**8**	OH	OH
4	NH$_2$	NHCH$_3$	**9**	Cl	OCH$_3$
5	NH$_2$	OH	**10**	Cl	NBu$_2$

Figure 2. The studied compounds and their numbering.

DMSO using δ(DMSO) 2.50 and 39.7 ppm, respectively). The typical experimental conditions for the ^{1}H NMR spectra were 32 scans, a spectral width of 6 kHz, and an acquisition time of 5 s, yielding 60 K data points. The FIDs were zero-filled to 128 K data points. The coupled ^{13}C NMR spectra were acquired using a gated decoupling pulse sequence (decoupling during d1). The ^{13}C spectra were also acquired with selective decoupling of H-8. The coupled ^{13}C and selectively decoupled ^{13}C experiments (30 mg of a sample dissolved in 0.6 ml of a solvent) were acquired with a spectral width of 70 ppm, offset of 135 ppm, d1 = 3 s, acquisition time of 3.7 s yielding 64 K data points, which were zero-filled to 128 K data points. The 2D-homonuclear (H,H-COSY) and 2D-heteronuclear (H,C-HSQC and H,C-HMBC) experiments were performed for the structural assignments of the ^{1}H and ^{13}C signals (using standard 2D-NMR pulse sequences of Bruker software).

The geometry optimizations and NMR parameters calculations were conducted using the Gaussian 09 software package.[27] All of the structures were optimized at the DFT level of theory using the B3LYP functional.[28,29] For geometry optimization, the standard 6-31 + G(d,p) basis set was used, and for the shielding and coupling constants, a slightly larger 6-311++G(d,p) basis set was utilized. The vibrational frequencies and free energies were calculated for all of the optimized structures, and the stationary-point character (a minimum) was thus confirmed. The optimizations and shielding- and coupling-constant calculations were done in vacuum. We have previously explored various approaches for modeling the solvent effects on the calculation of NMR parameters. We have shown that a large number of molecular dynamics snapshot geometries have to be averaged to model the solvent

effects reasonably and that implicit solvent models (e.g. PCM) fail in the calculation of the solvent effects on NMR parameters.[30,31] Further discrepancy between the calculated and experimental data can be caused by the inaccuracy of the DFT calculations and neglecting vibrational averaging.[32]

The NMR spectra signal assignment (C-1' - C-4' correspond to C-*ipso*, C-*ortho*, C-*meta* and C-*para* of the benzyl substituent) is given as follows:

9-Benzyl-6-chloro-9*H*-purin-2-amine (**1**): ^{13}C NMR (150.9 MHz, DMSO): δ = 46.3 (CH$_2$); 123.5 (C-5); 127.4 (C-2'), 128.0 (C-4'), 129.0 (C-3'); 136.8 (C-1'); 143.5 (C-8); 149.7 (C-6); 154.3 (C-4); 160.1 (C-2) ppm. ^{1}H NMR (600.1 MHz, DMSO): δ = 5.29 (s, 2H, CH$_2$); 6.92 (bs, 2H, NH$_2$); 7.26 – 7.38 (m, 5H, H-2', H-3', H-4'), 8.22 (s, H-8) ppm.

9-Benzyl-2,6-dichloro-9*H*-purine (**2**): ^{13}C NMR (125.7 MHz, CDCl$_3$): δ = 48.0 (CH$_2$); 128.0 (C-2'), 129.0 (C-4'), 129.3 (C-3'); 130.6 (C-5); 133.9 (C-1'); 145.5 (C-8); 151.8 (C-6); 153.1 (C-4 and C-2) ppm. ^{1}H NMR (499.9 MHz, CDCl$_3$): δ = 5.42 (s, 2H, CH$_2$); 7.32 (m, 2H, H-2'); 7.36 – 7.41 (m, 3H, H-3', H-4'), 8.07 (s, H-8) ppm.

9-Benzyl-6-chloro-9*H*-purine (**3**) ^{13}C NMR (125.7 MHz, DMSO): δ = 47.3 (CH$_2$); 127.9 (C-2'), 128.3 (C-4'), 129.0 (C-3'); 131.0 (C-5); 136.2 (C-1'); 147.7 (C-8); 149.4 (C-6); 151.9 (C-2); 152.0 (C-4) ppm. ^{1}H NMR (499.9 MHz, DMSO): δ = 5.42 (s, 2H, CH$_2$); 7.32 (m, 2H, H-2'); 7.36 – 7.41 (m, 3H, H-3', H-4'), 8.07 (s, H-8) ppm.

9-Benzyl-*N*^{6}-methyl-9*H*-purin-2,6-diamine (**4**): ^{13}C NMR (125.7 MHz, DMSO): δ = 27.2 (CH$_3$); 45.6 (CH$_2$); 113.6 (C-5); 127.2 (C-2'), 127.6 (C-4'), 128.8 (C-3'); 137.3 (C-8); 137.9 (C-1'); 151.0 (C-4); 155.6 (C-6); 160.6 (C-2) ppm. ^{1}H NMR (499.9 MHz, DMSO): δ = 5.42 (s, 2H, CH$_2$); 7.32 (m, 2H, H-2'); 7.36 – 7.41 (m, 3H, H-3', H-4'), 8.07 (s, H-8) ppm.

9-Benzylguanine (**5**): ^{13}C NMR (150.9 MHz, DMSO): δ = 47.8 (CH$_2$); 110.4 (C-5); 128.2 (C-2'), 128.8 (C-4'), 129.5 (C-3'); 135.8 (C-1'); 137.9 (C-8); 150.7 (C-4); 155.0 (C-6); 155.7 (C-2) ppm. ^{1}H NMR (600.1 MHz, DMSO): δ = 5.30 (s, 2H, CH$_2$); 7.05 (bs, 2H, NH$_2$); 7.28 – 7.40 (m, 5H, H-2', H-3', H-4'), 8.87 (s, H-8) ppm.

7-Benzyl-2,6-dichloro-7*H*-purine (**6**): ^{13}C NMR (125.7 MHz, CDCl$_3$): δ = 50.9 (CH$_2$); 121.7 (C-5); 127.0 (C-2'), 129.0 (C-4'), 129.4 (C-3'); 134.1 (C-1'); 143.9 (C-6); 150.4 (C-8); 153.2 (C-2); 163.5 (C-4) ppm. ^{1}H NMR (499.9 MHz, CDCl$_3$): δ = 5.69 (s, 2H, CH$_2$); 7.18 (m, 2H, H-2'); 7.36 – 7.42 (m, 3H, H-3', H-4'), 8.27 (s, H-8) ppm.

7-Benzyl-6-chloro-7*H*-purin-2-amine (**7**): ^{13}C NMR (125.7 MHz, DMSO): δ = 49.4 (CH$_2$); 115.0 (C-5); 126.6 (C-2'), 128.0 (C-4'), 129.0 (C-3'); 137.4 (C-1'); 142.6 (C-6); 150.2 (C-8); 160.3 (C-2); 164.6 (C-4) ppm. ^{1}H NMR (499.9 MHz, DMSO): δ = 5.56 (s, 2H, CH$_2$); 6.64 (bs, 2H, NH$_2$); 7.13 (m, 2H, H-2'); 7.27 -7.36 (m, 3H, H-3', H-4'), 8.55 (s, H-8) ppm.

7-Benzylxanthine (**8**): ^{13}C NMR (125.7 MHz, DMSO): δ = 49.0 (CH$_2$); 106.2 (C-5); 127.7 (C-2'), 128.1 (C-4'), 128.8 (C-3'); 137.3 (C-1'); 142.8 (C-8); 149.7 (C-4'); 151.4 (C-2); 155.7 (C-6) ppm. ^{1}H NMR (499.9 MHz, DMSO): δ = 5.41 (s, 2H, CH$_2$); 7.27 – 7.36 (m, 5H, H-2', H-3', H-4'), 8.13 (s, H-8); 10.87 (bs, 1H) and 11.58 (bs, 1H, H-1 and H-3) ppm.

7-Benzyl-2-chloro-6-methoxy-7*H*-purin (**9**): ^{13}C NMR (125.7 MHz, DMSO): δ = 50.2 (CH$_2$); 55.1 (CH$_3$); 111.8 (C-5); 127.5 (C-2'), 128.2 (C-4'), 128.9 (C-3'); 136.8 (C-1'); 148.5 (C-8); 151.3 (C-2); 157.5 (C-6); 162.8 (C-4) ppm. ^{1}H NMR (499.9 MHz, DMSO): δ = 4.05 (s, 3H, CH$_3$); 5.54 (s, 2H, CH$_2$); 7.27 – 7.31 (m, 5H, H-2', H-4'), 7.35 (m, 2H, H-3'); 8.73 (s, H-8) ppm.

7-Benzyl-*N*,*N*-dibutyl-2-chloro-7*H*-purin-6-amine (**10**): ^{13}C NMR (125.7 MHz, DMSO): δ = 13.8 (C-4''); 19.5 (C-3''); 29.1 (C-2''); 49.5 (C-1''); 50.9 (CH$_2$); 113.8 (C-5); 126.3 (C-2'), 128.0 (C-4'), 128.9 (C-3'); 137.0 (C-1'); 149.9 (C-8); 151.9 (C-2); 155.6 (C-6); 163.6 (C-4) ppm.

^{1}H NMR (499.9 MHz, DMSO): δ = 0.75 (t, 6H, $J_{4'',3''}$ = 7.3, H-4''); 1.01 (m, 4H, H-3''); 1.35 (m, 4H, H-2''); 3.39 (m, 4H, H-1''); 5.56 (s, 2H, CH_2); 6.97 (m, 2H, H-2'); 7.24 – 7.32 (m, 3H, H-3', H-4'), 8.62 (s, H-8) ppm.

Results and Discussion

In a typical HMBC spectrum of 2,6-disubstituted purine derivatives (refer to Fig. 3), we can observe strong three-bond cross-peaks between the hydrogen H-8 and carbons C-4 and C-5. The strong crosspeaks are accompanied by one or two weak cross-peaks corresponding to H8-C6 and/or H8-C2. The stronger crosspeak from these two low-intensity crosspeaks is believed to be the H8-C6 correlation.[22] However, we have observed that for many purine derivatives, the long-range crosspeaks are of a comparable magnitude, and in some cases, the magnitude of the H8-C2 crosspeak is larger than that of the H8-C6 crosspeak. The intensity of a HMBC crosspeak is dependent on the match between heteronuclear coupling constant and the experimental delay of the anti-phase evolution (1/2 J). For heteronuclear couplings lower than 1 Hz, the evolution delay should be larger than 500 ms, which leads to a strong signal suppression by relaxation. We performed optimization of the evolution delay and we have observed that for longer delays, the gain of intensity of the weak crosspeaks was overridden by the relaxation losses. Therefore, all the HMBC spectra reported in this paper were measured with evolution delay of 50 ms. Using this setup, the intensity of the long-range HMBC crosspeaks is mainly governed by the value of the J-coupling. The HMBC spectra of all of the studied compounds are shown in Supporting information.

The long-range heteronuclear coupling can be observed in hydrogen-coupled ^{13}C spectra. Because of the small values of the four- and five-bond coupling constants, line narrowing and longer acquisition times are necessary, which makes this technique possible only for concentrated samples or ^{13}C labeled compounds. We measured the coupled ^{13}C spectra of compounds 2, 5 and 6. A part of the coupled spectrum of compound 5 depicting the signals of C-2 and C-6 is shown in Figure S11 in the SI. For comparison, the spectrum obtained with a selective decoupling of H-8 is also shown in the figure. The experimental values of the long-range coupling constants obtained from the coupled ^{13}C spectra are discussed below. Given the experimental difficulties in obtaining the coupled spectra, we estimated qualitatively the couplings and their relative intensities from the HMBC spectra.
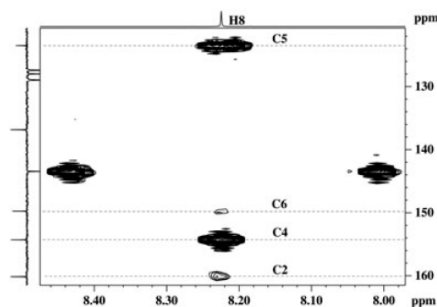

Figure 3. The H-8 region of the HMBC spectrum of compound 1.

The uncertainty in the signal assignment based on the HMBC patterns may lead to incorrect structure determination. For some 7-substituted purine derivatives, the spatial proximity obtained from the NOE experiments can be used to determine the structure unequivocally. This approach is demonstrated on compound 10. In the ROESY spectrum of compound 10, we observed crosspeaks between the benzyl part of the molecule and the dibutylamino part, which is possible only for the 7-benzyl-6-dibutylamino derivative. In some cases, the assignment of the carbon signal could be obtained from the HMBC spectra observing the crosspeaks of the NH_2, $HNCH_3$ or OCH_3 groups. For some derivatives, the spectral assignment could be done only with the help of calculated chemical shifts.

We performed geometry optimization and shielding- and coupling-constant calculations for a series of purine derivatives with various substituents in positions 2 and 6 and a methyl substituent in position 7 or 9. We believe that the change of the benzyl substituent to a methyl group can cause only minor differences in the calculated coupling constants, while the calculations are much less demanding. We confirmed this for compound 6. The differences in the calculated H8-C2 and H8-C6 coupling constants between compound 6 (7-benzylderivative) and 2,6-dichloro-7-methyl-7H-purine were lower than 0.01 Hz.

Both the calculated J(H8-C2) and J(H8-C6) were always positive. Interestingly, the calculated values of J(H2-C8) were always negative, and the absolute values were close to 0.2 Hz, which is in agreement with the lack of crosspeaks between H-2 and C-8 in the HMBC spectra of the purine derivatives. For all derivatives with the same substituents in both positions 2 and 6 except for the dihydroxyderivatives, the calculated chemical shift of C-6 was lower than that of C-2 by 1–6 ppm for 9-methyl- and by 11–19 ppm for the 7-methylderivatives.

In the HMBC spectrum of compound 1 (Fig. 3), we observed weak crosspeaks to both C-2 and C-6 with the C-2 crosspeak being slightly more intensive. This observation is in agreement with the calculated coupling constants (Table 1, Entry 8), where the H8-C2 coupling was 0.61 Hz compared to 0.32 Hz of the H8-C6 coupling. The signals of the carbon atoms C2 and C4 are unfortunately overlapped in the spectrum of compound 2, and therefore, the H8-C2 crosspeak (if present) is overlapped by the strong H8-C4 crosspeak in the HMBC spectrum. We measured the coupled ^{13}C NMR spectrum and ascertained that the experimental long-range couplings 0.4 and 0.3 Hz were very close to the calculated values (0.52 and 0.19 Hz, Table 1, Entry 4). In agreement with the small value of the H8-C6 coupling constant, no H8-C6 crosspeak was observed in the HMBC spectrum. Similarly, in the HMBC spectrum of compound 3, we did not observe any H8-C6 crosspeak, and the H8-C2 crosspeak (if present) was overlapped by the strong H8-C4 signal. This finding is consistent with the rather small calculated couplings (Table 1, Entry 3). In the HMBC spectra of compound 4, the H8-C2 crosspeak was weaker than the H8-C6 crosspeak, which is again in agreement with the calculated coupling constants. We measured the coupled ^{13}C NMR spectrum of compound 5, and the experimental coupling constants (1.2 Hz for the H8-C6 and 0.4 for the H8-C2 coupling) were in excellent agreement with the calculated values 0.92 and 0.34 Hz, respectively (Table 1, Entry 10). In addition, the H8-C2 crosspeak was missing in the HMBC spectrum.

We obtained the experimental H8-C2 and H8-C6 coupling constants of compound 6 from the coupled ^{13}C spectrum, and again, the calculated values (0.86 and 0.73 Hz, Table 1, Entry 4) agreed

Table 1. The calculated heteronuclear coupling constants J(H8-C2) and J(H8-C6) in substituted 9- and 7-methylpurines

Entry	R^2	R^6	9-isomer		7-isomer	
			J(H8-C2)	J(H8-C6)	J(H8-C2)	J(H8-C6)
1	H	H	0.32	0.36	0.61	0.93
2	Cl	H	0.48	0.34	0.79	0.89
3	H	Cl	0.35	0.21	0.65	0.89
4	Cl	Cl	0.52	0.19	0.86	0.73
5	H	NH₂	0.35	0.55	0.60	0.81
6	NH₂	H	0.57	0.46	0.68	0.96
7	NH₂	NH₂	0.57	0.62	0.68	0.84
8	NH₂	Cl	0.61	0.32	0.75	0.79
9	Cl	NH-CH₃	0.49	0.58	0.76	0.80
10	NH₂	OH[a]	0.34	0.92	0.41	1.2
11	OH[a]	OH[a]	0.36	0.75	0.27	1.1
12	H	OH[a]	0.16	0.85	0.36	1.1
13	Cl	OCH₃	0.49	0.44	0.80	0.73
14	Cl	N(CH₃)₂	0.54	0.64	0.79	0.74
15	NH₂	NH-CH₃	0.56	0.66	0.67	0.86

[a]Keto forms of the guanine, hypoxanthine and xanthine bases were used in the calculations.

excellently with the experimental ones (0.8 and 0.7 Hz). Crosspeaks of equal intensity were observed in the HMBC spectrum of this compound. Similarly, in the HMBC spectra of compounds **7**, **9** and **10**, both crosspeaks H8-C2 and H8-C6 were observed, and their intensities were almost identical, which is in line with the calculated coupling constant values 0.7–0.8 Hz for all the couplings. In contrast to that the calculated value of the H8-C2 coupling constant (0.27 Hz) in compound **8** is much smaller than the H8-C6 coupling constant (1.1 Hz), which is, indeed, manifested in the HMBC spectrum by a missing H8-C2 crosspeak.

Based on a careful analysis of the calculated long-range coupling constants, we can conclude that the value of H8-C2 coupling depends primarily on the nature of the substituent in the position 2. The following order of the coupling values depending on the C-2 substituent was observed: H < Cl < NH₂. Exceptions from this rule are the keto forms of guanine, hypoxanthine and xanthine, which have always very low H8-C2 coupling. Similarly, the H8-C6 coupling value is dominated by the nature of the C-6 substituent, with the keto forms of guanine, hypoxanthine and xanthine having the highest values of the coupling. 7-methylisomers always have both H8-C2 and H8-C6 coupling constants values higher than the 9-methylisomers.

Conclusions

We have demonstrated both experimentally and by DFT calculations that the four- and five-bond heteronuclear *J*-couplings of the hydrogen H-8 with carbon atoms C-6 and C-2 may be of a comparable size. Depending on the substituents attached to the purine skeleton, the values of the coupling constants can change significantly. For proper structure determination and signal assignment, care must be taken with this issue and one cannot rely on small crosspeaks in the HMBC spectra, which can be caused by both H8-C2 and H8-C6 interactions. The DFT calculated coupling constants were shown to agree very well with the experimental data. An alternative for the structure determination

and signal assignment could be also the comparison of calculated and experimental chemical shifts.[20]

References

[1] H. Rosemeyer. *Chem. Biodivers.* **2004**, *1*, 361–401.
[2] T. Bartl, Z. Zacharová, P. Sečkářová, E. Kolehmainen, R. Marek. *Eur. J. Org. Chem.* **2009**, 1377–1383.
[3] I. Collins, J. J. Caldwell, 10.11 - Bicyclic 5–6 Systems: Purines, in *Comprehensive Heterocyclic Chemistry III*, vol. 10 (Eds: A. R. Katritzky, C. A. Ramsden, E. F. V. Scriven, J. K. Taylor), Elsevier, Oxford, **2008** pp. 525–597.
[4] M. Legraverend, D. S. Grierson. *Bioorg. Med. Chem.* **2006**, *14*, 3987–4006.
[5] E. De Clercq, A. Holý, I. Rosenberg, T. Sakuma, J. Balzarini, P. C. Maudgal. *Nature* **1986**, *323*, 464–467.
[6] A. Holý. *Curr. Pharm. Des.* **2003**, *9*, 2567–2592.
[7] E. De Clercq, A. Holý. *Nat. Rev. Drug Discovery* **2005**, *4*, 928–940.
[8] C. Simons, Q. P. Wu, T. T. Htar. *Curr. Top. Med. Chem.* **2005**, *5*, 1191–1203.
[9] M. Kidwai, R. Venkataramanan, R. Mohan, P. Sapra. *Curr. Med. Chem.* **2002**, *9*, 1209–1228.
[10] N. R. Kode, S. Phadtare. *Molecules* **2011**, *16*, 5840–5860.
[11] J. N. Kim, K. F. Blount, I. Puskarz, J. Lim, K. H. Link, R. R. Breaker. *ACS Chem. Biol.* **2009**, *4*, 915–927.
[12] S. Standara, K. Maliňáková, R. Marek, J. Marek, M. Hocek, J. Vaara, M. Straka. *Phys. Chem. Chem. Phys.* **2010**, *12*, 5126–5139.
[13] R. Marek, J. Brus, J. Toušek, L. Kovacs, D. Hocková. *Magn. Res. Chem.* **2002**, *40*, 353–360.
[14] O. Tsikouris, T. Bartl, J. Tousek, N. Lougiakis, T. Tite, P. Marakos, N. Pouli, E. Mikros, R. Marek. *Magn. Reson. Chem.* **2008**, *46*, 643–649.
[15] M. T. Chenon, R. J. Pugmire, D. M. Grant, R. P. Panzica, L. B. Townsend. *J. Am. Chem. Soc.* **1975**, *97*, 4627–4636.
[16] J. Kongsted, K. Aidas, K. V. Mikkelsen. *Phys. Chem. Chem. Phys.* **2010**, *12*, 761–768.
[17] N. C. Gonnella, H. Nakanishi, J. B. Holtwick, D. S. Horowitz, K. Kanamori, N. J. Leonard, J. D. Roberts. *J. Am. Chem. Soc.* **1983**, *105*, 2050–2055.
[18] M. Dračínský, P. Jansa, J. Chocholoušová, J. Vacek, S. Kovačková, A. Holý. *Eur. J. Org. Chem.* **2010**.
[19] M. Dračínský, P. Jansa, K. Ahonen, M. Buděšínský. *Eur. J. Org. Chem.* **2011**, 1544–1551.
[20] E. Procházková, M. Šála, R. Nencka, M. Dračínský. *Magn. Res. Chem.* **2012** in press. DOI: 10.1002/mrc.2864.
[21] T. Dieckmann, J. Feigon. *Curr. Opin. Struc. Biol.* **1994**, *4*, 745–749.
[22] R. Marek, V. Sklenář. *Annu. Rep. NMR Spectrosc.* **2004**, *54*, 201–242.
[23] A. Holý, J. Günter, H. Dvořáková, M. Masojídková, G. Andrei, R. Snoeck, J. Balzarini, E. De Clercq. *J. Med. Chem.* **1999**, *42*, 2064–2086.
[24] C. Dalby, C. Bleasdale, W. Clegg, M. R. J. Elsegood, B. T. Golding, R. J. Griffin. *Angew. Chem. Int. Ed.* **1993**, *32*, 1696–1697.
[25] L. Čechová, P. Jansa, M. Šála, M. Dračínský, A. Holý, Z. Janeba. *Tetrahedron* **2011**, *67*, 866–871.
[26] V. Kotek, N. Chudikova, T. Tobrman, D. Dvorak. *Org. Lett.* **2010**, *12*, 5724–5727.
[27] M. J. Frisch, G. W. Trucks, H. B. Schlegel, G. E. Scuseria, M. A. Robb, J. R. Cheeseman, G. Scalmani, V. Barone, B. Mennucci, G. A. Petersson, H. Nakatsuji, X. Caricato, X. Li, H. P. Hratchian, A. F. Izmaylov, J. Bloino, G. Zheng, J. L. Sonnenberg, M. Hada, M. Ehara, K. Toyota, R. Fukuda, J. Hasegawa, M. Ishida, T. Nakajima, Y. Honda, O. Kitao, H. Nakai, T. Vreven, J. J. A. Montgomery, J. E. Peralta, F. Ogliaro, M. Bearpark, J. J. Heyd, E. Brothers, K. N. Kudin, V. N. Staroverov, R. Kobayashi, J. Normand, K. Raghavachari, A. Rendell, J. C. Burant, S. S. Iyengar, J. Tomasi, M. Cossi, N. Rega, J. M. Millam, M. Klene, J. E. Knox, J. B. Cross, V. Bakken, C. Adamo, J. Jaramillo, R. Gomperts, R. E. Stratmann, O. Yazyev, A. J. Austin, R. Cammi, C. Pomelli, J. W. Ochterski, R. L. Martin, K. Morokuma, V. G. Zakrzewski, G. A. Voth, P. Salvador, J. J. Dannenberg, S. Dapprich, A. D. Daniels, O. Farkas, J. B. Foresman, J. V. Ortiz, J. Cioslowski, D. J. Fox, *Gaussian 09, Revision A.02*, Gaussian, Inc., Wallingford CT, **2009**.
[28] A. D. Becke. *J. Chem. Phys.* **1993**, *98*, 5648–5652.
[29] C. T. Lee, W. T. Yang, R. G. Parr. *Phys. Rev. B* **1988**, *37*, 785–789.
[30] M. Dračínský, P. Bouř. *J. Chem. Theory Comput.* **2010**, *6*, 288–299.
[31] M. Dračínský, J. Kaminský, P. Bouř. *J. Phys. Chem. B* **2009**, *113*, 14698–14707.
[32] M. Dračínský, J. Kaminský, P. Bouř. *J. Chem. Phys.* **2009**, *130*, 094106.

IV.

Procházková, E. – Šála, M. – Nencka, R. – Dračínský, M.:

C^6-substituted purine derivatives: an experimental and theoretical ^{1}H, ^{13}C and ^{15}N NMR study.

Research Article

C⁶-substituted purine derivatives: an experimental and theoretical ¹H, ¹³C and ¹⁵N NMR study

Eliška Procházková, Michal Šála, Radim Nencka and Martin Dračínský*

We measured the ¹H, ¹³C and ¹⁵N chemical shifts for a series of purine derivatives bearing a norbornane substituent in position 9 and various substituents in position 6. The experimental data were complemented with density functional theory (DFT) calculations. The comparison of the calculated and experimental chemical shifts provided us with information about the tautomer and conformational equilibria of the studied compounds. Copyright © 2012 John Wiley & Sons, Ltd.

Supporting information may be found in the online version of this article.

Introduction

The characterization of purine bases and the emphasis on the significant role they play in living systems have attracted the attention of many scientific teams and been an important stimulus for intensive investigations in this field. Not only are purines the basic constituents of nucleic acids, but they also interact with enzymes and other proteins as components of cofactors and signal molecules. Adenosine 5'-triphosphate controls the energy metabolism of every cell, and nicotinamide adenine dinucleotide (NAD+, NADH) and flavin adenine dinucleotide (FAD, FADH₂) are key coenzymes of the cellular citric acid cycle that is involved in the cellular oxidation/reduction processes. Another molecule of biological relevance is acetyl-coenzyme A, which is of central importance for the metabolism. Naturally occurring purines have been excellently reviewed recently.[1] Purine derivatives bearing diverse types of substituents display a broad spectrum of biological activities, including an interferon-inducing effect or, more often, an inhibitory effect against leukotriene A₄ hydrolase, sulfotransferase, phosphodiesterase, kinase and other enzymes.[2]

Modified nucleosides and nucleotides are very important classes of compounds used in the therapy of a wide variety of diseases because they can act as antiviral, antitumor or antimicrobial agents. Nucleosides in which the furanose-ring oxygen is replaced with a methylene, ethylene or vinylene group are called carbocyclic nucleosides, and these compounds typically excel in enzymatic as well as chemical stability, which makes them an attractive research target.[3–8]

Because the carbocycle conformation might prove vital for the nucleoside's biological activity,[9,10] we have decided to focus on conformationally restricted carbocyclic nucleosides with variously substituted norbornane as a pseudosugar part and substituted purine as a nucleobase.[11,12] The substitutions on both these structural parts were examined extensively – first, a number of compounds with a modified bicycle skeleton was prepared, and then, because 9-norbornyl-6-chloropurine was identified as one of the most active compounds against Coxsackie virus B3 (EC₅₀

0.81 μM),[11] diverse modifications in position 6 of the purine nucleobase were performed to determine the structure–activity relations.[12]

The nature of the substituent is reflected in the NMR chemical shifts and nuclear spin–spin coupling constants, which makes NMR spectroscopy an excellent tool for investigating and interpreting the reactivity and intermolecular interactions in terms of the electron distribution.[13] The ¹³C and ¹⁵N NMR chemical shifts as well as ¹H–X coupling constants can be used not only to distinguish between different regioisomers,[14] but they reflect equally well the positions of protons, which enables the study of tautomeric equilibria.[15–21] ¹⁵N NMR spectroscopy has proven to be particularly useful in investigating protonation equilibria, probing hydrogen bonding and describing purine complexes with metal ions, because nitrogen atoms are directly involved in these processes.[22,23]

In this paper, we present the experimental ¹H, ¹³C and ¹⁵N data of a series of 24 purine derivatives with a bicyclo[2.2.1] hept-2-yl substituent in position 9 and various substituents in position 6. The general formula of the studied compounds is depicted in Fig. 1. The experimental data were complemented with DFT calculations of the chemical shifts. The comparison of the experimental and calculated data made it possible to reveal the preferred tautomeric and conformational forms of the compounds.

Experimental

Compounds **1–15** were synthesized according to ref.[12] The synthesis of compounds **16–24** will be described elsewhere.

* Correspondence to: Martin Dračínský, Institute of Organic Chemistry and Biochemistry, Academy of Sciences, Flemingovo náměstí 2, 166 10 Prague, Czech Republic. E-mail: dracinsky@uochb.cas.cz

Institute of Organic Chemistry and Biochemistry, Academy of Sciences, Prague, Czech Republic
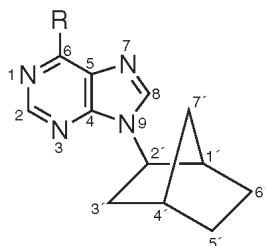
Figure 1. The general formula of the studied purine derivatives.

The NMR spectra were measured on a Bruker Avance 600 (with ^{1}H at 600.13 MHz, ^{13}C at 150.92 MHz and ^{15}N at 60.82 frequency) and/or Bruker Avance 500 (with ^{1}H at 499.95 MHz and ^{13}C at 125.71 MHz) using a 5 mm TXI cryo-probe and about 5–10 mg of sample in 0.6 ml of dimethyl sulfoxide (DMSO)-d_6. The chemical shifts are given in δ-scale (with the ^{1}H and ^{13}C referenced to DMSO using δ (DMSO) 2.50 and 39.7 ppm, respectively). The ^{15}N chemical shifts were determined and assigned using gradient-enhanced ^{1}H-^{15}N multiple-bond correlation experiments (gHMBC[24,25]). Nitromethane was used as external standard (δ 381.7) for the ^{15}N chemical shifts. The typical experimental conditions for the ^{1}H NMR spectra were 32 scans, a spectral width of 6 kHz and an acquisition time of 5 s, yielding 60 K data points. The FIDs were zero filled to 128 K data points. The 2D-homonuclear (H,H-COSY) and 2D-heteronuclear (H,C-HSQC and H,C-HMBC) experiments were performed for the structural assignments of ^{1}H and ^{13}C signals (with standard 2D-NMR pulse sequences of Bruker software being used). The chemical shifts of the bicycloheptane part of compound **1**: ^{13}C NMR (150.92 MHz, DMSO): δ = 27.01 (C-6´), 27.96 (C-5´), 35.85 (C-7´), 35.91 (C-4´), 37.76 (C-3´), 42.24 (C-1´), 57.57 (C-2´) ppm. ^{1}H NMR (600.13 MHz, DMSO): δ = 1.27 (m, 2H, H-5´*endo* and H-7´a); 1.41 (dddd, 1H, J_{gem} = 12.1, $J_{6´en,5´en}$ = 9.0, $J_{6´en,5´ex}$ = 4.0, $J_{6´en,7´b}$ = 2.3, H-6´*endo*); 1.54 (m, 1H, H-5´*exo*); 1.62 (tt, 1H, J_{gem} = $J_{6´ex,5´ex}$ = 12.2, $J_{6´ex,5´en}$ = $J_{6´ex,1´}$ = 4.5, H-6´*exo*); 1.73 (dm, 1H, J_{gem} = 10.3, H-7´b); 2.00 (ddd, 1H, J_{gem} = 13.3, $J_{3´en,2´}$ = 8.5, $J_{3´en,7´a}$ = 2.4, H-3´*endo*); 2.07 (m, 1H, H-3´*exo*); 2.43 (bt, 1H, $J_{4´,3´ex}$ = $J_{4´,5´ex}$ = 4.3, H-4´); 2.52 (bd, 1H, $J_{1´,6´ex}$ = 4.6, H-1´); 4.57 (ddd, 1H, $J_{2´,3´en}$ = 8.5, $J_{2´,3´ex}$ = 4.5, $J_{2´,7´a}$ = 1.4, H-2´) ppm.

The geometry optimizations and chemical-shift calculations were conducted using the Gaussian 09 software package.[26] All of the structures were optimized at the DFT level of theory using the B3LYP functional.[27,28] The vibrational frequencies and free energies were calculated for all of the optimized structures, and the stationary point character (a minimum) was thus confirmed. In some calculations, the solvent effects were treated implicitly by the polarizable continuum model (PCM) method[29,30] with a DMSO solvent. Two different combinations of geometry optimization and chemical-shift calculations were used for all of the compounds (B3LYP/6-311++G**// B3LYP/6-31+G** and B3LYP/6-311++G**/PCM//B3LYP/6-311++G**/PCM).

Results and Discussion

The ^{1}H, ^{13}C and ^{15}N NMR chemical shifts of compounds **1–24** in DMSO-d_6 solutions were determined and assigned as described

in the experimental section. The chemical shifts of the purine parts of the molecules are reported in Tables 1 and 2. There were only very small differences between the ^{1}H and ^{13}C chemical shifts of the bicycloheptane part of compounds **1–24** (typically below 0.1 ppm); in the experimental part, only the data for compound **1** are listed.

Calculations

We performed geometry optimization and shielding constant calculations for all the studied compounds. The bicycloheptane part of the molecules was replaced with a methyl group. The reason for the replacement was twofold: (i) the experimental chemical shifts of the bicycloheptane part of the molecules were almost identical, which indicated that the conformation (rotation around the N9-C2´ bond) was conserved in the whole series; and (ii) the calculations were less computationally demanding, whereas all the chemical shift tendencies of the purine part of the molecules remained in the methyl derivatives. We used two different approaches for the calculations. The optimizations and shielding constant calculations were performed in vacuum and with the PCM of DMSO solvation. We have previously explored different approaches for modeling solvent effects on the calculation of NMR parameters. We have shown that implicit solvent models (e.g. PCM) fail in the calculation of solvent effects on NMR parameters.[31,32] However, the implicit solvent model also can influence the calculated shielding constants indirectly by providing a better molecular structure in the solution.

As discussed below, for some derivatives in the series, more tautomers/rotamers were taken into account in the calculations. The correlations between the experimental chemical shifts and

Table 1. The experimental ^{1}H and ^{15}N chemical shifts of purine parts of compounds **1–24**

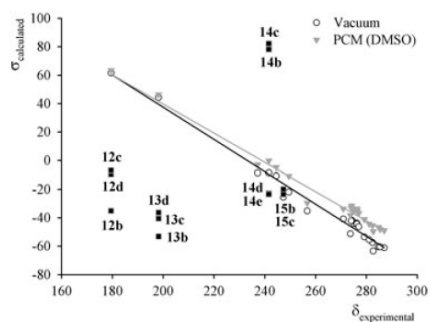| Compound	R	N-1	N-3	N-7	N-9	H-2	H-8
1	H	284.8	258.6	246.2	180.5	8.93	8.77
2	Cl	279.2	257.8	244.9	184.4	8.77	8.85
3	F	249.5	259.8	240.9	184.5	8.67	8.83
4	Br	287.0	256.8	247.4	184.3	8.71	8.86
5	CH$_3$	285.4	253.8	246.1	180.7	8.74	8.64
6	CF$_3$	273.7	268.0	242.7	183.2	9.12	9.02
7	OCH$_3$	244.5	246.9	244.0	182.5	8.51	8.52
8	SCH$_3$	270.9	245.8	243.1	182.2	8.72	8.60
9	CN	282.7	268.1	242.5	183.7	9.11	9.10
10	COOCH$_3$	282.4	267.1	247.6	182.7	9.03	8.90
11	CONH$_2$	281.1	265.3	244.9	182.4	9.01	8.90
12	OH	179.5	222.2	249.5	187.0	8.03	8.22
13	SH	198.2	230.6	256.3	185.7	8.19	8.44
14	NH$_2$	241.6	232.2	244.7	181.1	8.12	8.26
15	N$_3$	247.3	257.6	247.6	188.6	10.08	8.80
16	N(CH$_3$)$_2$	237.2	230.7	249.4	181.7	8.20	8.27
17	Ph	276.4	256.6	246.9	181.7	9.03	8.24
18	*p*-PhCl	275.1	257.0	245.5	181.0	8.98	8.84
19	*p*-PhF	276.0	257.0	246.7	181.9	9.00	8.23
20	*p*-PhtBu	276.3	256.0	247.3	181.6	9.01	8.21
21	*p*-PhPh	276.3	257.1	247.2	181.7	9.04	8.25
22	*p*-PhCN	277.0	259.7	245.7	182.2	9.06	8.96
23	*p*-PhOCH$_3$	274.2	254.4	247.3	181.5	8.96	8.20
24	*p*-PhNPh$_2$	274.0	255.2	247.5	181.2	8.95	8.18

Table 2. The experimental ^{13}C chemical shifts of purine parts of compounds 1–24

Compound	R	C-2	C-4	C-5	C-6	C-8
1	H	152.0	151.3	134.3	148.0	145.0
2	Cl	151.5	152.1	131.4	149.1	145.6
3	F	151.2	155.9	119.8	158.9	145.4
4	Br	151.5	150.9	134.0	141.8	145.4
5	CH$_3$	151.5	150.5	133.0	158.0	143.4
6	CF$_3$	151.4	154.2	130.2	142.7	148.0
7	OCH$_3$	151.4	152.2	121.2	160.4	141.8
8	SCH$_3$	151.4	148.4	131.3	159.9	142.6
9	CN	152.1	153.2	135.5	128.8	148.9
10	COOCH$_3$	151.4	154.0	132.1	144.8	147.1
11	CONH$_2$	151.4	153.5	131.5	147.6	146.2
12	OH	145.4	148.5	124.5	157.0	138.1
13	SH	144.8	144.3	135.5	176.0	141.0
14	NH$_2$	152.4	149.7	119.3	156.2	138.8
15	N$_3$	135.6	142.5	120.3	145.7	142.3
16	N(CH$_3$)$_2$	151.6	150.4	119.8	154.3	137.5
17	Ph	152.1	152.5	131.4	154.7	141.8
18	p-PhCl	151.8	152.8	130.9	151.3	144.8
19	p-PhF	152.1	152.5	131.1	153.5	141.8
20	p-PhtBu	152.1	152.4	131.3	154.9	141.6
21	p-PhPh	152.1	152.5	131.4	154.3	141.8
22	p-PhCN	152.1	153.0	131.8	152.0	142.6
23	p-PhOCH$_3$	152.1	152.3	130.8	154.3	141.3
24	p-PhNPh$_2$	152.1	152.2	130.9	154.4	141.2

calculated shieldings were generally very good for all nitrogen atoms (Figs 2 and 3 and Figures S1 and S2 in Supporting Information) and all carbon atoms (Figs 4 and 5 and Figures S3–S5 in the SI) except for nitrogen N-7 calculated in vacuum and carbon C-6. The poor correlation of the nitrogen N-7 shieldings calculated in vacuum might be explained by stronger influence of solvation on the electronic structure near the N-7 atom and the vicinity of the substituents at C-6. The largest deviations from the linear correlation for carbon C-6 were observed for substituents with heavy atoms (Cl, Br, S), suggesting that the relativistic corrections of the calculated shielding constants should be considered for

Figure 3. The correlation of the calculated shielding constants of nitrogen atom N-7 with the experimental chemical shifts. The black squares represent the tautomers/rotamers, which were not involved in the correlation.
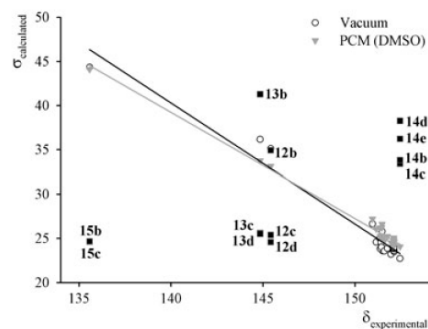
Figure 4. The correlation of the calculated shielding constants of carbon atom C-2 with the experimental chemical shifts. The black squares represent the tautomers/rotamers, which were not involved in the correlation.

Figure 2. The correlation of the calculated shielding constants of nitrogen atom N-1 with the experimental chemical shifts. The black squares represent the tautomers/rotamers, which were not involved in the correlation.
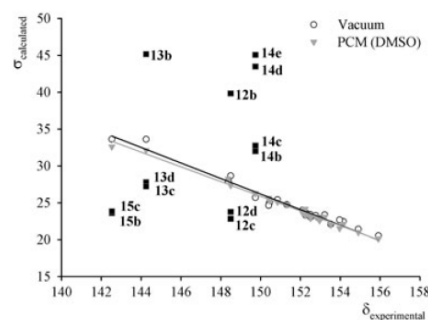
Figure 5. The correlation of the calculated shielding constants of carbon atom C-4 with the experimental chemical shifts. The black squares represent the tautomers/rotamers, which were not involved in the correlation.

precise calculations. The correlation for hydrogen atoms was rather modest (Figures S6 and S7 in SI). The possible sources of errors are the inaccuracy of DFT calculations and neglecting vibrational averaging.[33] The calculated shieldings for H-8 also

Table 3. The calculated relative electronic energies and molar ratios of two conformations of compounds **7**, **8**, **10** and **11**. All of the energies are in kcal/mol

		$E_{vac}{}^a$	x_{vac}	$E_{DMSO}{}^b$	x_{DMSO}
7	N1-C6-X-C ~ 0°	0.00	0.995	0.00	0.994
	N1-C6-X-C ~ 180°	3.09	0.005	2.99	0.006
8	N1-C6-X-C ~ 0°	0.00	0.973	0.00	0.978
	N1-C6-X-C ~ 180°	2.13	0.027	2.24	0.022
10	N1-C6-C = O ~ 0°	0.00	0.519	0.00	0.533
	N1-C6-C = O ~ 180°	0.04	0.481	0.08	0.467
11	N1-C6-C = O ~ 0°	0.00	0.511	0.00	0.727
	N1-C6-C = O ~ 180°	0.03	0.489	0.58	0.273

^{a}B3LYP/6-31 + G**
^{b}B3LYP/611++G**/PCM

Figure 6. Possible tautomer/rotamer forms of compounds **12** and **13**.

might be affected by the replacement of the bicycloheptane ring by a methyl group. The parameters of the linear regression are given in Table S1.

Two rotamers around the C6-X bond (X = C, O, S) were examined for compounds **7**, **8**, **10** and **11**. In the case of **7** and **8**, the conformation with the N1-C6-X-C torsion angle close to 180° was 2–3 kcal/mol less stable than the conformation with the N1-C6-X-C torsion angle close to 0° (Table 3), and only the low-energy conformer was considered in the correlations. For compounds **10** and **11**, a ratio close to 1 : 1 of two conformers was found, and a weighted average of the shielding constants was considered in the correlations. The shieldings of nitrogen N-1 calculated for the two conformations were found to be more distant from the linear fit than the weighted average.

The hypoxanthine derivative **12** and mercaptopurine derivative **13** can exist in four tautomer/rotamer forms **12a–12 d** and **13a–13 d** as depicted in Fig. 6. The adenine derivative **14** can exist in five tautomer/rotamer forms (Fig. 7). It follows from the comparison of the electronic energies of the optimized structures (Table 4) that only the keto form **12a**, the thione form **13a** and the amino form **14a** are probably populated in solution. This also was confirmed by the calculated and experimental NMR data, where only the calculated data for **12a** and **13a** correlate well with the experimental chemical shifts (Figs 2–5 and Figures S1–S7). The calculated shieldings for the higher energy forms are far from the linear correlation. The same tautomer preferences for adenine,[34–36] hypoxanthine[37,38] and mercaptopurine[34,39–41] were found previously.

Azidopurine nucleotides easily and efficiently yield photocross-linking products and were long ago proposed[42] as photoaffinity labels for studies of protein-DNA/RNA and RNA/RNA interactions. Apart from its photochemical and biological activity, the 6-azidopurine (as well as 2-azidopurine) system shows an interesting feature of the existence in an equilibrium of two possible tautomeric forms[43,44] of fused tetrazole **15a** and azido-azomethine **15b** or **15c** structures (Fig. 8). Extensive studies[43–45] on this phenomenon have been performed, leading to the conclusion that, in polar solvents, the equilibrium is shifted toward the tetrazole form.[46,47] The crystallographic data indicate

Figure 7. Possible tautomer/rotamer forms of compound **14**.

Table 4. The calculated relative electronic energies of the tautomers/rotamers of compounds **12–15**. All of the energies are in kcal/mol

	$E_{vac}{}^a$	$E_{DMSO}{}^b$		$E_{vac}{}^a$	$E_{DMSO}{}^b$		$E_{vac}{}^a$	$E_{DMSO}{}^b$		$E_{vac}{}^a$	$E_{DMSO}{}^b$
12a	0.0	0.0	**13a**	0.0	0.0	**14a**	0.0	0.0	**15a**	1.66	0.02
12b	20.5	10.8	**13b**	21.90	11.45	**14b**	19.28	12.04	**15b**	0.00	0.00
12c	3.23	8.58	**13c**	3.13	9.41	**14c**	12.33	9.72	**15c**	2.37	2.18
12 d	4.50	9.60	**13 d**	2.49	8.93	**14 d**	32.08	20.01			
						14e	32.21	20.12			

^{a}B3LYP/6-31 + G**
^{b}B3LYP/611++G**/PCM

Figure 8. Possible forms of azidopurine **15**.
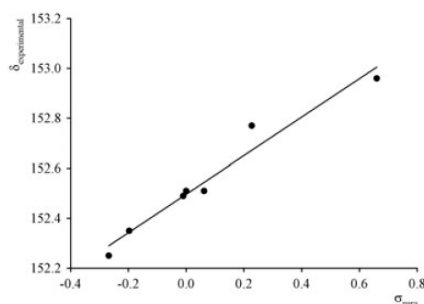
Figure 9. The correlation of carbon C-4 chemical shifts with σ_{para} Hammett constants.

that 6-azidopurine exists in solid state as a pure tetrazole form.[48] The energy calculations suggest that the azido-azomethine form **15b** is the most stable form in vacuum (Table 4). In DMSO, the energies of **15a** and **15b** are very close, and we might speculate that if the solvent was treated explicitly, the tetrazole form **15a** would be more stabilized. The importance of solvation by polar solvents may be estimated from a huge difference between calculated dipole moments of the tetrazole and azido-azomethine forms (11.45 Debye for **15a** and 6.26 Debye for **15b**). The azido-azomethine form **15c** has the highest energy in both vacuum and PCM calculations. From the correlations of calculated shieldings with experimental chemical shifts, it is clear that the tetrazole form **15a** is the only species (or highly predominant) in the DMSO solution (e.g. Fig. 4, where the forms **15b** and **15c** are very far from the linear correlation for carbon C-2).

For the series of *para*-substituted phenyl derivatives **17**–**24**, we observed a linear correlation of the purine carbon C-4 chemical shi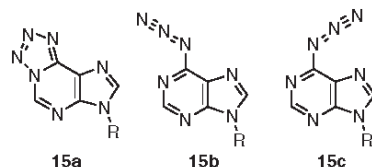fts on σ_{para} Hammett constants[49] (Fig. 9). This good correlation is quite surprising, given the very small range of the experimental shifts. However, for other carbon and nitrogen atoms, the correlation of chemical shifts with Hammett constants was poorer (data not shown).

Conclusions

We measured the ^{1}H, ^{13}C and ^{15}N chemical shifts for a series of 24 purine derivatives bearing a norbornane substituent in position 9 and various substituents in position 6. The experimental data were complemented with DFT calculations on smaller systems, where the bicycloheptane substituent was replaced by

a methyl group. The correlation of calculated shieldings and experimental chemical shifts made it possible to obtain information about the tautomer and conformational equilibria of the studied compounds in DMSO solution.

References

[1] H. Rosemeyer. *Chem. Biodivers.* **2004**, *1*, 361–401.
[2] M. Legraverend, D. S. Grierson. *Bioorg. Med. Chem.* **2006**, *14*, 3987–4006.
[3] M. T. Crimmins. *Tetrahedron* **1998**, *54*, 9229–9272.
[4] L. Agrofoglio, E. Suhas, A. Farese, R. Condom, S. R. Challand, R. A. Earl, R. Guedj. *Tetrahedron* **1994**, *50*, 10611–10670.
[5] A. D. Borthwick, K. Biggadike. *Tetrahedron* **1992**, *48*, 571–623.
[6] S. W. Schneller. *Curr. Top. Med. Chem.* **2002**, *2*, 1087–1092.
[7] C. Simons, Q. P. Wu, T. T. Htar. *Curr. Top. Med. Chem.* **2005**, *5*, 1191–1203.
[8] L. A. Agrofoglio. *Curr. Org. Chem.* **2006**, *10*, 333–362.
[9] V. E. Marquez, M. A. Siddiqui, A. Ezzitouni, P. Russ, J. Y. Wang, R. W. Wagner, M. D. Matteucci. *J. Med. Chem.* **1996**, *39*, 3739–3747.
[10] V. E. Marquez, S. H. Hughes, S. Sei, R. Agbaria. *Antiviral Res.* **2006**, *71*, 268–275.
[11] M. Šála, A. M. De Palma, H. Hřebabecký, R. Nencka, M. Dračínský, P. Leyssen, J. Neyts, A. Holý. *Bioorg. Med. Chem.* **2010**, *18*, 4374–4384.
[12] M. Šála, A. M. De Palma, H. Hřebabecký, M. Dejmek, M. Dračínský, P. Leyssen, J. Neyts, H. Mertlíková-Kaiserová, R. Nencka. *Bioorg. Med. Chem. Lett.* **2011**, *21*, 4271–4275.
[13] S. Standara, K. Maliňáková, R. Marek, J. Marek, M. Hocek, J. Vaara, M. Straka. *Phys. Chem. Chem. Phys.* **2010**, *12*, 5126–5139.
[14] R. Marek, J. Brus, J. Tousek, L. Kovacs, D. Hockova. *Magn. Res. Chem.* **2002**, *40*, 353–360.
[15] O. Tsikouris, T. Bartl, J. Tousek, N. Lougiakis, T. Tite, P. Marakos, N. Pouli, E. Mikros, R. Marek. *Magn. Reson. Chem.* **2008**, *46*, 643–649.
[16] M. T. Chenon, R. J. Pugmire, D. M. Grant, R. P. Panzica, L. B. Townsend. *J. Am. Chem. Soc.* **1975**, *97*, 4627–4636.
[17] J. Kongsted, K. Aidas, K. V. Mikkelsen. *Phys. Chem. Chem. Phys.* **2010**, *12*, 761–768.
[18] N. C. Gonnella, H. Nakanishi, J. B. Holtwick, D. S. Horowitz, K. Kanamori, N. J. Leonard, J. D. Roberts. *J. Am. Chem. Soc.* **1983**, *105*, 2050–2055.
[19] T. Bartl, Z. Zacharová, P. Sečkářová, E. Kolehmainen, R. Marek. *Eur. J. Org. Chem.* **2009**, 1377–1383.
[20] M. Dračínský, P. Jansa, J. Chocholoušová, J. Vacek, S. Kovačková, A. Holý. *Eur. J. Org. Chem.* **2010**, 777–785.
[21] M. Dračínský, P. Jansa, K. Ahonen, M. Buděšínský. *Eur. J. Org. Chem.* **2011**, 1544–1551.
[22] R. Marek, V. Sklenář. *Annu. Rep. NMR Spectrosc.* **2004**, *54*, 201–242.
[23] I. Alkorta, J. Elguero, G. S. Denisov. *Magn. Reson. Chem.* **2008**, *46*, 599–624.
[24] W. Willker, D. Leibfritz, R. Kerssebaum, W. Bermel. *Magn. Reson. Chem.* **1993**, *31*, 287–292.
[25] A. Bax, M. F. Summers. *J. Am. Chem. Soc.* **1986**, *108*, 2093–2094.
[26] M. J. Frisch, G. W. Trucks, H. B. Schlegel, G. E. Scuseria, M. A. Robb, J. R. Cheeseman, G. Scalmani, V. Barone, B. Mennucci, G. A. Petersson, H. Nakatsuji, X. Caricato, X. Li, H. P. Hratchian, A. F. Izmaylov, J. Bloino, G. Zheng, J. L. Sonnenberg, M. Hada, M. Ehara, K. Toyota, R. Fukuda, J. Hasegawa, M. Ishida, T. Nakajima, Y. Honda, O. Kitao, H. Nakai, T. Vreven, J. J. A. Montgomery, J. E. Peralta, F. Ogliaro, M. Bearpark, J. J. Heyd, E. Brothers, K. N. Kudin, V. N. Staroverov, R. Kobayashi, J. Normand, K. Raghavachari, A. Rendell, J. C. Burant, S. S. Iyengar, J. Tomasi, M. Cossi, N. Rega, J. M. Millam, M. Klene, J. E. Knox, J. B. Cross, V. Bakken, C. Adamo, J. Jaramillo, R. Gomperts, R. E. Stratmann, O. Yazyev, A. J. Austin, R. Cammi, C. Pomelli, J. W. Ochterski, R. L. Martin, K. Morokuma, V. G. Zakrzewski, G. A. Voth, P. Salvador, J. J. Dannenberg, S. Dapprich, A. D. Daniels, O. Farkas, J. B. Foresman, J. V. Ortiz, J. Cioslowski, D. J. Fox, *Gaussian 09, Revision A.02*, Gaussian, Inc., Wallingford CT, **2009**.

185

[27] A. D. Becke. *J. Chem. Phys.* **1993**, *98*, 5648–5652.

[28] C. T. Lee, W. T. Yang, R. G. Parr. *Phys. Rev. B* **1988**, *37*, 785–789.

[29] V. Barone, M. Cossi. *J. Phys. Chem. A* **1998**, *102*, 1995–2001.

[30] M. Cossi, N. Rega, G. Scalmani, V. Barone. *J. Comput. Chem.* **2003**, *24*, 669–681.

[31] M. Dračínský, P. Bouř. *J. Chem. Theory Comput.* **2010**, *6*, 288–299.

[32] M. Dračínský, J. Kaminský, P. Bouř. *J. Phys. Chem. B* **2009**, *113*, 14698–14707.

[33] M. Dračínský, J. Kaminský, P. Bouř. *J. Chem. Phys.* **2009**, *130*, 094106.

[34] M. T. Chenon, R. J. Pugmire, D. M. Grant, R. P. Panzica, L. B. Townsend. *J. Am. Chem. Soc.* **1975**, *97*, 4636–4642.

[35] A. Laxer, D. T. Major, H. E. Gottlieb, B. Fischer. *J. Org. Chem.* **2001**, *66*, 5463–5481.

[36] C. F. Guerra, F. M. Bickelhaupt, S. Saha, F. Wang. *J. Phys. Chem. A* **2006**, *110*, 4012–4020.

[37] R. Ramaekers, G. Maes, L. Adamowicz, A. Dkhissi. *J. Mol. Struct.* **2001**, *560*, 205–221.

[38] G. G. Sheina, S. G. Stepanian, E. D. Radchenko, Y. P. Blagoi. *J. Mol. Struct.* **1987**, *158*, 275–292.

[39] L. Pazderski, I. Lakomska, A. Wojtczak, E. Szlyk, J. Sitkowski, L. Kozerski, B. Kamienski, W. Kozminski, J. Tousek, R. Marek. *J. Mol. Struct.* **2006**, *785*, 205–215.

[40] J. W. Engels, K. Worner, T. Strube. *Helv. Chim. Acta* **1999**, *82*, 2094–2104.

[41] K. Yamanari, M. Kida, M. Yamamoto, T. Fujihara, A. Fuyuhiro, S. Kaizaki. *J. Chem. Soc. Dalton Trans.* **1996**, *25*, 305–309.

[42] K. Quiggle, M. L. Wejrowski, S. Chladek. *Biochemistry* **1978**, *17*, 94–101.

[43] C. Temple, M. C. Thorpe, W. C. Coburn, J. A. Montgomery. *J. Org. Chem.* **1966**, *31*, 935–938.

[44] A. Masternak, B. Skalski, J. Milecki. *J. Label. Compd. Radiopharm.* **2007**, *50*, 43–46.

[45] C. Temple, C. L. Kussner, J. Montgome. *J. Org. Chem.* **1966**, *31*, 2210–2215.

[46] T. Lioux, G. Gosselin, C. Mathe. *Eur. J. Org. Chem.* **2003**, 3997–4002.

[47] J. D. Sutherland, J. N. Whitfield. *Tetrahedron* **1997**, *53*, 11595–11626.

[48] J. P. Glusker, D. v. d. Helm, W. E. Love, J. A. Minkin, A. L. Patterson. *Acta Cryst. B* **1968**, *B 24*, 359–366.

[49] D. H. McDaniel, H. C. Brown. *J. Org. Chem.* **1958**, *23*, 420–427.

V.

A Switchable Intramolecular Hydrogen Bond in Polysubstituted 5-Nitrosopyrimidines

Eliška Procházková, Lucie Čechová, Zlatko Janeba,* and Martin Dračínský*

Institute of Organic Chemistry and Biochemistry, Academy of Sciences of the Czech Republic, Flemingovo nam. 2, 166 10 Prague, Czech Republic

S Supporting Information

ABSTRACT: The formation of strong intramolecular hydrogen bonds was observed in a series of 2-amino-5-nitrosopyrimidines with alkylamino and arylamino substituents at positions 4 and 6. Mixtures of two rotamers differing in the orientation of the nitroso group were observed in the NMR spectra of the compounds where two distinct intramolecular hydrogen bonds could be formed. The ratio of the two rotamers depends strongly on the character of the substituents at positions 4 and 6 and can be finely tuned over a broad range of conformation ratios. The experimental results were supported by DFT calculations, which also made it possible to explain the apparent contradiction in the experimental dependence of the rotamer ratio on the Hammett constants for the arylamino substituents. The UV/vis spectra of the compounds also significantly depend on the nature of the substituents; however, the orientation of the nitroso group does not have any influence on the position of the absorption bands in the spectra.
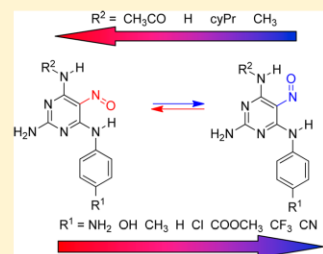
■ INTRODUCTION

The formation of intramolecular hydrogen bonds has a very pronounced effect on molecular structure and properties. For example, molecules mask their polarity from the environment, become more lipophilic, and might thus display a higher membrane permeability.[1] High stability of intramolecular hydrogen bonds has often been observed when a six-membered ring is formed and when the linker atoms are sp^2-hybridized (amides, heteroaromatic rings), leading to planar, conjugated systems. The high stability of these intramolecular hydrogen bonds has been termed resonance-assisted hydrogen bonding (RAHB) and can be rationalized by enhanced π-delocalization.[2] RAHB has recently been reviewed.[3−5] The high propensity to form resonance-assisted hydrogen bonds has been used in the design of new kinase inhibitors.[6] On the basis of the known bicyclic kinase inhibitor scaffold, pyrimidin-4-ylureas were suggested as bioisosteres. Molecules containing this substructure indeed turned out to be inhibitors of multiple kinases, and the binding mode was confirmed by a cocrystal structure. The literature contains a number of further examples where six-membered hydrogen-bonded pseudorings effectively mimic aromatic rings.[7−11] Nevertheless, the concept of RAHB was later criticized. It was found in a series of enols of β-diketones and β-enaminones that the RAHB effect is not the primary reason behind the strength of their intramolecular hydrogen bonds, which is simply a consequence of the structure of the σ-skeleton of the system that keeps the hydrogen-bond donor and acceptor coplanar and closer to each other.[12]

Conjugated nitrosoamines belong to the same family as the enols of β-diketones and other conjugated systems with intramolecular hydrogen bonds. Therefore, the formation of strong intramolecular hydrogen bonds may be expected, and indeed, these hydrogen bonds were found in the solid-state structures of 3-amino-2-nitrosocyclohex-2-en-1-one,[13] 5-amino-4-nitrosopyrazole,[14] and 6-amino-5-nitrosopyrimidines.[15−18]

Nitrosopyrimidine derivatives are not naturally occurring, but their interesting biological properties have been described. The cytostatic activity of 5-nitrosopyrimidines is well-known,[19,20] just like their antifungal effects.[21] They are also useful as direct precursors for the synthesis of biologically relevant heterocyclic systems, such as heteroatomic diazoles[22] and pteridines.[23,24] 5-Nitrosopyrimidines have also been shown to be able to form complexes with a variety of metal ions both in solution and in the solid state.[25−28]

In this work, a series of 32 2-amino-5-nitrosopyrimidine derivatives with a *para*-substituted phenylamino substituent at position 6 and an unsubstituted or substituted amino group (cycloalkylamino, alkylamino, acetylamino) at position 4 were prepared. A new microwave-assisted methodology for the synthesis of the derivatives has been developed. The prepared 5-nitrosopyrimidines have two competing NH groups that can form an intramolecular hydrogen bond with the nitroso group (Figure 1). The ratio of the two rotamers was determined by NMR spectroscopy, and the results were supported by DFT calculations. The effect of the substituent in the *para* position of the phenylamino group on the electronic structure was also observed by UV/vis spectroscopy.

Rotamer A   Rotamer B

R¹ = H, CH₃, OH, NH₂, CN, Cl, COOCH₃, CF₃
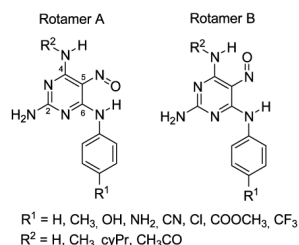R² = H, CH₃, cyPr, CH₃CO

Figure 1. The two possible geometries of the nitroso group at position 5 of the studied compounds. Rotamer A (left) has the C6—C5—N—O torsion angle close to 0°, whereas rotamer B (right) has the C6—C5—N—O torsion angle close to 180°.

■ RESULTS AND DISCUSSION

Synthesis. A series of polysubstituted 5-nitrosopyrimidines were synthesized starting from 2-amino-4,6-dimethoxy-5-nitrosopyrimidine (**1**).[29] In the first step, compound **1** was treated with a variety of *para*-substituted anilines **2a–h** in dimethylformamide (DMF) to give the intermediates **3a–h** (Scheme 1). It is known that aminolysis of the 4- and 6-methoxy groups on the pyrimidine ring takes place because of their activation by the electron-withdrawing nitroso group at position 5.[30] Depending on the nature of the R¹ substituent in anilines **2a–h**, the aromatic nucleophilic substitution can be performed either under conventional heating or, more conveniently, in a closed vessel under microwave irradiation, especially in the case of less reactive anilines (e.g., **2a** and **2b**).

Subsequently, the remaining methoxy group of intermediates **3a–h** was replaced by a reaction with selected amines, namely, methylamine, cyclopropylamine, and ammonia (Scheme 1). Again, differences in the reactivity of various amines were observed, as reactions of compounds **3a–h** with methylamine in EtOH/DMF to obtain the products **4a–h** took place at room temperature while the analogous reactions with cyclo-

propylamine in DMF (to give **5a–h**) and aqueous ammonia (to give **6a–h**) required conventional heating to reach full conversion (Scheme 1). The reactivity of acetamide with the methoxy group of pyrimidines **3a–h** in the aromatic nucleophilic reaction is too low, and no desired product **7** was observed even under microwave irradiation at temperatures up to 180 °C, whereas at higher temperatures, decomposition of DMF (used as a solvent) and the subsequent formation of 4-(*N,N*-dimethylamino)pyrimidines were observed (UPLC-MS).[31] An alternative approach to *N*-acetyl derivatives **7a–f** involved treating compounds **6a–f** with acetic anhydride at 80 °C (Scheme 1).[32] Unfortunately, the treatment of **6g** and **6h** with acetic anhydride at 80 °C did not lead to the formation of the desired products **7g** and **7h**, respectively, as there seemed to be preferential acetylation of the *p*-hydroxy and *p*-amino groups on the aryl ring at position 6. For the subsequent NMR studies, the 4-(dimethylamino)phenylamino derivatives **6i** and **7i** were prepared instead, using the reaction of compound **1** with *N,N*-dimethyl-*p*-phenylenediamine (to give **3i**) followed by ammonolysis of **3i** (to give **6i**) and finally by acetylation of **6i** (to give **7i**).

In several cases, the formation of two distinct rotamers in the final products **4–7** was observed as two spots using TLC or as cleft signals in the UPLC-MS spectra.

The reactivities of the *para*-substituted anilines **2a–h** in aromatic nucleophilic substitution can be evaluated/measured in two different ways: (a) by comparing the Hammett constants and (b) by comparing their basicities using pK_b values. To compare their genuine reactivities, the anilines **2a–h** were reacted with 2-amino-4,6-dimethoxy-5-nitrosopyrimidine (**1**) in DMF under integrated conditions (160 °C, MW-assisted heating, monitoring by UPLC-MS); the data are summarized in Table 1. According to our expectations, we observed that the reaction time steadily increased in the order $NH_2 < OH < CH_3 < H < Cl < COOCH_3 \approx CF_3 \approx CN$.

NMR Spectroscopy. In compounds **3a–h**, the nitroso oxygen atom and the NH hydrogen atom from the aniline residue form an intramolecular hydrogen bond, whose presence

Scheme 1. Synthesis of Polysubstituted Pyrimidines[a]

a R¹=CN
b R¹=CF₃
c R¹=COOCH₃
d R¹=Cl
e R¹=H
f R¹=CH₃
g R¹=OH
h R¹=NH₂
i R¹=N(CH₃)₂
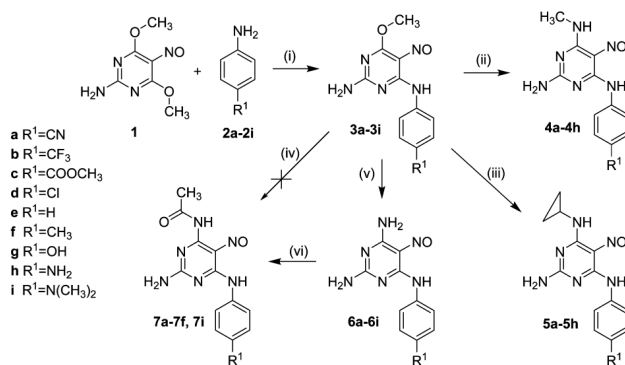
[a]Conditions: (i) DMF, MW or conventional heating; (ii) 33% CH₃NH₂ in EtOH, DMF, rt; (iii) cyclopropylamine, DMF, conventional heating (70–90 °C); (iv) acetamide, DMF, MW-assisted heating (100–180 °C); (v) ammonia, conventional heating (50 °C); (vi) acetic anhydride, conventional heating (80 °C).

Table 1. Comparison of the Reactivities and Properties of the Anilines 2a–h Depending on the Nature of the *para* Substituent R¹

compound	R¹	Hammett constant[33]	aniline pK_b[34]	reaction time (min)
2a	CN	0.70	1.74[35]	240
2b	CF₃	0.53	2.57	220
2c	COOCH₃	0.44	2.30	260
2d	Cl	0.24	3.81	80
2e	H	0	4.58	20
2f	CH₃	−0.14	5.07	25
2g	OH	−0.38	5.50	9
2h	NH₂	−0.57	6.08	3

was clearly confirmed by NMR spectroscopy. The signal of the NH hydrogen was found in the low-field region (13.5–13.7 ppm), which is a typical value for hydrogen atoms involved in strong hydrogen bonds. The signal of the NH hydrogen in similar compounds without the 5-nitroso group was found at 8–10 ppm.[36] Furthermore, we observed four-bond correlations between the NH hydrogen and carbon atom C2 in the HMBC spectra. Four-bond correlations are usually observed when the atoms in the coupling path are in a W-like arrangement (see Figure 2). The presence of the NH–C2 cross-peak and the absence of the NH–C4 cross-peak provide clear evidence of the arylamino residue conformation with the NH hydrogen heading toward the nitroso group. Similarly, the W-like arrangement can be found between the hydrogen atoms in the 2-amino group and carbon atoms C4 or C6. The two NH₂ hydrogens are not equivalent because of a slow rotation around the C2–NH₂ bond, and the two four-bond correlations are observable in the HMBC spectra (Figure 2).

Interestingly, the 6-NH hydrogen chemical shifts have an unexpected dependence on the substituent at the *para* position of the attached phenyl group. An electron-withdrawing substituent at the *para* position of an aniline derivative usually increases the chemical shift of the amino protons because of the lower electron density in the phenyl ring and the amino group, whereas electron-donating substituents have the opposite effect. For example, the NH₂ chemical shift of 4-aminobenzonitrile (2a) is 2 ppm higher than that of 1,4-diaminobenzene

(2h).[37,38] In the series of compounds 3a–i, we observed the opposite order of NH chemical shifts, as the 4-cyanophenyl derivative 3a has a lower chemical shift than the 4-aminophenyl derivative 3h by 0.2 ppm (Table 2). It should be noted,

Table 2. Experimental Chemical Shifts of the 6-NH Hydrogen in Compounds 3a–i (Measured in DMSO)

compound	R¹	δ_{NH} (ppm)
3a	CN	13.45
3b	CF₃	13.47
3c	COOCH₃	13.53
3d	Cl	13.46
3e	H	13.51
3f	CH₃	13.52
3g	OH	13.54
3h	NH₂	13.65
3i	N(CH₃)₂	13.67

however, that in 3a–i the whole molecule has a system of conjugated π electrons, and therefore, the electronic effects of the substituent at the *para* position of the aniline fragment are spread throughout the molecule. Thus, an electron-withdrawing substituent also lowers the electron density in the nitroso group, making it a poorer hydrogen-bond acceptor. Poorer hydrogen-bond acceptors may form weaker hydrogen bonds with the 6-NH group, leading to a decrease of the 6-NH chemical shift. Therefore, the effect of the *para* substituent on the 6-NH chemical shift can be divided into two contributions: (a) the influence on the NH electron density and (b) the influence on the electron density of the nitroso group. The two effects have the opposite sign and almost cancel each other out, leaving only a modest NH chemical shift dependence on the *para* substituent with the former effect (a) being slightly overridden by the latter (b).

In the case of compounds 4–7, two intramolecular hydrogen bonds are possible, differing in the orientation of the nitroso group (Figure 1). Both of them were formed in the solutions of all the compounds studied, and two sets of signals were observed in both the ¹H and ¹³C NMR spectra. The chemical shift of the hydrogen atom involved in the hydrogen bond was close to 14 ppm, whereas the chemical shift of the unbound
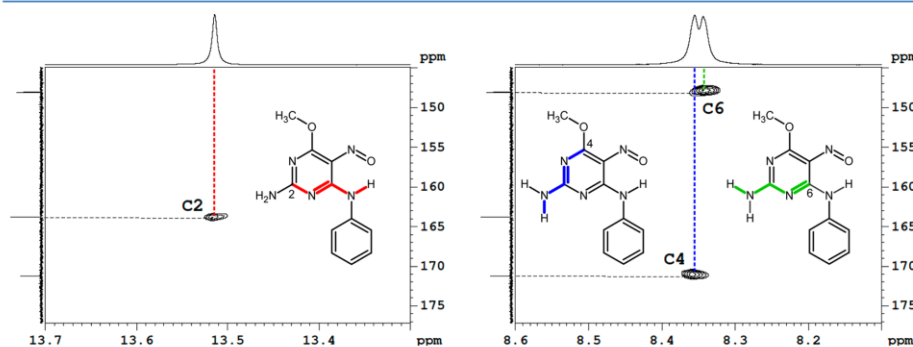
Figure 2. HMBC correlations of compound 3e with the W-like arrangement between the aniline NH hydrogens and C2 (left) and between the amino hydrogens and C4/C6 (right).

amino hydrogen was close to 10 ppm. Furthermore, the orientation of the nitroso group has a significant influence on the chemical shifts of the carbon atoms C4 and C6, as shown in Table 3. For example, in rotamer A of compound **5e**, where the

Table 3. Experimental Pyrimidine Carbon Chemical Shifts of Rotamer A of Compound 5e and the Experimental and Calculated [B3LYP/6-31+G(d,p)] Chemical-Shift Differences between the Two Rotamers

atom	$\delta_{A,exptl}$ (ppm)	$\Delta\delta_{A-B}$ (ppm)	
		exptl	calcd
C2	164.5	0.1	−0.1
C4	164.2	12.1	16.2
C5	135.9	0.0	0.2
C6	148.4	−13.1	−17.2

nitroso oxygen atom is turned to the NH group at position 6, the C6 carbon atom is more shielded (148.4 ppm) than in rotamer B (161.5 ppm). The carbon chemical-shift differences between the rotamers were also confirmed by DFT calculations (see below).

We also measured the ^{1}H NMR spectra of compound **5e** at variable temperatures up to 140 °C [Figure S1 in the Supporting Information (SI)]. The two nonequivalent signals of the protons in the 2-amino group of both rotamers merged already at 50 °C. On the other hand, the NH signals corresponding to rotamer A did not merge with the NH signals of rotamer B over the whole temperature range into one signal set, as would be expected for a system with a fast interconversion between forms A and B. The signals of both forms became only slightly broader. The low limit of the barrier for the conformational change between the two forms was estimated from the NMR line shape analysis of the NH protons to be 21 kcal/mol. It should be noted, however, that the NH proton signal broadening is caused only partly by the rotamer interconversion and that the line broadening may be a result of other exchange processes, such as exchange of the NH protons

with the traces of water present in the sample or with the 2-amino protons. The presence of these exchange processes is evidenced by a high-field shift of all of the NH proton signals (i.e., toward the water and NH$_2$ signals) at higher temperatures. Therefore, the estimated rotamer interconversion barrier is only a lower limit estimation, and the actual barrier may be significantly higher. An alternative approach for the determination of the exchange rate, and hence the barrier for the rotamer interconversion, relies on the determination of the coalescence temperature of the signals corresponding to the two rotamers. The coalescence temperature is defined as the temperature at which two separate peaks of the spectrum merge into one. At this temperature, an approximate equation for the exchange rate may be used: $k = \pi\Delta\nu_0/\sqrt{2}$, where $\Delta\nu_0$ is the separation of the signals (in Hz) in the slow-exchange limit. This approach could be applied only for the *meta*- and *para*-hydrogen signals of the phenyl ring because the other signals did not merge in the whole temperature range. The *meta*-hydrogens were separated by 11.2 Hz at room temperature and merged at 120 °C, whereas the *para*-hydrogens were separated by 20.0 Hz and merged at 140 °C. The free energies of activation were calculated to be 20.7 and 21.4 kcal/mol at 120 and 140 °C, respectively. It should be noted, however, that this approach also leads only to an estimation of the reaction barrier because the splitting of the signals caused by *J* coupling made the exact coalescence temperature difficult to determine.

The ratio of the two conformers depends significantly on the substituents at positions 4 and 6 of the pyrimidine ring. The observed molar ratios of the two conformers are summarized in Table 4, and a graphical representation is shown in Figure S2 in the SI. For example, for compounds **4a–h** with the methylamino group at position 4, the percentage of rotamer A ranged from 32 to 70% depending on the *para* substituent of the phenylamino group at position 6, and the percentages correlated well with the Hammett coefficients (Figure 3). Electron-withdrawing substituents decrease the concentration of the form A, whereas electron-donating substituents have the opposite effect. The ratios of the two conformers in the

Table 4. Observed Percentages of Rotamer A in the DMSO Solutions of Compounds 4–7 and the Calculated Data [B3LYP/6-31+G(d,p), vacuum]

| compound	R^2	R^1	ΔG_{exptl} (kcal/mol)	% A exptl	% A calcd	compound	R^2	R^1	ΔG_{exptl} (kcal/mol)	% A exptl	% A calcd
4a	CH$_3$	CN	−0.45	32	42	6a	H	CN	−0.12	45	61
4b	CH$_3$	CF$_3$	−0.32	37	37	6b	H	CF$_3$	0.00	50	54
4c	CH$_3$	COOCH$_3$	−0.22	41	40	6c	H	COOCH$_3$	0.14	56	61
4d	CH$_3$	Cl	−0.14	44	46	6d	H	Cl	0.22	59	66
4e	CH$_3$	H	0.07	53	43	6e	H	H	0.39	66	64
4f	CH$_3$	CH$_3$	0.14	56	42	6f	H	CH$_3$	0.50	70	64
4g	CH$_3$	OH	0.27	61	49	6g	H	OH	0.68	76	70
4h	CH$_3$	NH$_2$	0.50	70	57	6h	H	NH$_2$	0.82	80	76
						6i	H	N(CH$_3$)$_2$	0.79	79	77
5a	cyPr	CN	−0.42	33	39	7a	COCH$_3$	CN	0.17	57	79
5b	cyPr	CF$_3$	−0.32	37	37	7b	COCH$_3$	CF$_3$	0.27	61	69
5c	cyPr	COOCH$_3$	−0.22	41	36	7c	COCH$_3$	COOCH$_3$	0.34	64	79
5d	cyPr	Cl	−0.17	43	44	7d	COCH$_3$	Cl	0.39	66	82
5e	cyPr	H	0.00	50	37	7e	COCH$_3$	H	0.62	74	82
5f	cyPr	CH$_3$	0.14	56	41	7f	COCH$_3$	CH$_3$	0.72	77	79
5g	cyPr	OH	0.27	61	46	7g	COCH$_3$	OH	n.a.	n.a.	84
5h	cyPr	NH$_2$	0.47	69	52	7h	COCH$_3$	NH$_2$	n.a.	n.a.	88
						7i	COCH$_3$	N(CH$_3$)$_2$	0.98	84	88
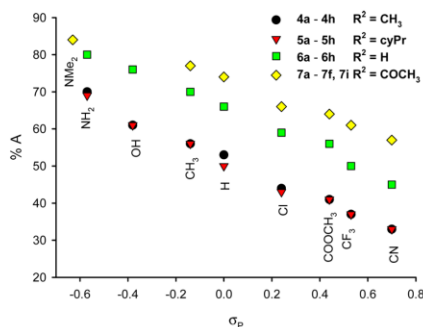
Figure 3. Dependence of the observed rotamer ratio of compounds **4**−**7** on the Hammett constant σ_p for the substituent at the *para* position of the phenylamino group (R[1]).

compounds **5a**−**5h** with the cyclopropylamino group in the position 4 were almost identical to those found for the compounds **4a**−**4h**. In the 4-amino derivatives **6a**−**6h**, the A form was consistently slightly more preferred, namely by 10−15%, when compared with **4a**−**4h**, and the acetamino group in the compounds **7** promoted the formation of the conformer A by further 5−12%.

Calculations. We optimized the geometries of both rotamers of compounds **4**−**7** and determined the free energy differences and the rotamer ratios in equilibrium. The calculated rotamer ratios agree reasonably well with the experimental ones (Table 4), with the highest error being 16%. Part of the error may be ascribed to the neglect of solvation in the calculations. We also performed the geometry optimization of compounds **5e** and **5g** using a polarizable continuum solvent model, but it did not improve the calculated rotamer ratios. The specific solvation of the polar pyrimidines is probably important in the DMSO solutions. Unfortunately, these specific interactions cannot be modeled well with the implicit solvation model.[39]

Electron-donating substituents in the *para* position of the phenyl ring (R[1] in Figure 1) increase the concentration of form A, whereas electron-withdrawing substituents do the opposite. This behavior might seem surprising at first sight, as electron-donating groups increase the electron density in the aniline residue including the NH nitrogen, making the NH group less acidic and a poorer hydrogen-bond donor. The expected substituent effect was found previously for hydrogen-bonded

complexes of substituted phenols with a water molecule, where the strength of the XPhOH⋯OH$_2$ complexes increased for electron-withdrawing substituents X[40] (i.e., the hydrogen-bond stability increased in the reverse order than in our compounds). In our case, however, as already discussed, the whole molecules contain systems of conjugated π-electrons, enabling the transfer of the electronic substituent effects throughout the molecule. Therefore, electron-donating substituents increase the electron density also at the nitroso oxygen atom, making it a better hydrogen-bond acceptor, as can be seen from the plots of electrostatic potentials in Figure 4 and also by comparing the calculated Mulliken charges of the oxygen atom ($-0.02e$ difference between R[1] = NH$_2$ and R[1] = CN). The influence of the substituents on the rotamer ratio can be then explained as follows: electron-donating groups increase the electron density in both the phenyl and the pyrimidine parts of the molecule. The electrostatic potential at the aniline NH hydrogen is affected by substituent R[1] to a lower extent than that at the amino hydrogen at position 4; the corresponding differences in the Mulliken atomic charges when going from R[1] = NH$_2$ to R[1] = CN are $-0.001e$ and $-0.015e$ for the aniline and amino NH hydrogens, respectively. Electron-donating substituents thus make the 4-amino hydrogen a poorer hydrogen-bond donor, which results in the higher stability of form A.

The strength of the hydrogen bonds could be also estimated from their calculated lengths. However, in our conjugated pyrimidine derivatives, where the substituents change the properties of both the hydrogen-bond donor and acceptor, no significant changes in the bond lengths were observed. The calculated hydrogen-bond lengths are listed in the SI.

We also looked for a transition-state structure for the rotamer interconversion. The first-order saddle-point structure on the reaction coordinate for compound **5e** was localized by using the QST3 method,[41,42] and the free energy barriers to transition were calculated in vacuo and with a polarizable continuum model of solvation. The transition state is visualized in Figure 5. The free energy barrier heights calculated in vacuum (27.8 kcal/mol) and in DMSO (30.0 kcal/mol) were slightly higher than the rough estimates from the NMR experiments.

UV/Vis Spectroscopy. The UV/vis spectra of the nitrosopyrimidines in DMSO solution exhibit one weak electronic transition in the visible region (430−600 nm) and two strong transitions in the UV region (260−350 nm), which could be assigned on the basis of time-dependent density functional theory (TD-DFT) calculations (see below). The color of the solutions (green or yellow-red) arises from the weak n → π^* electronic transitions, and the UV bands are caused by $\pi \rightarrow \pi^*$
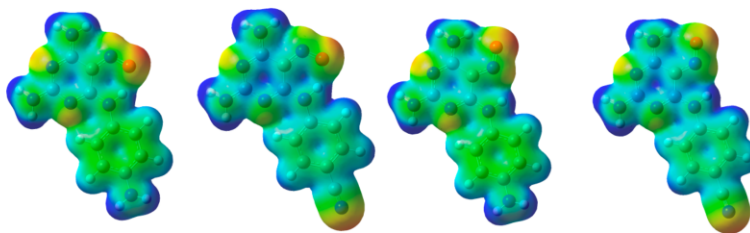

Figure 4. Electrostatic potential plots for the two rotamers of compounds **6a** and **6h**.

Figure 5. Transition state of compound **5e** found by QST3 calculations.

transitions. The maximum-intensity wavelengths for compounds **3a**–**i** are summarized in Table 5. The position of the

Table 5. Experimental and Calculated UV/Vis Absorption Maxima for Compounds 3a–i

compound	R^i	λ_{max1}^{expt} (nm)	λ_{max2}^{expt} (nm)	λ_{max1}^{expt} (nm)	λ_{max1}^{calcd} (nm)
3a	CN	$-^a$	342	596	619
3b	CF$_3$	$-^a$	342	602	615
3c	COOCH$_3$	276	342	600	617
3d	Cl	264	338	596	609
3e	H	260	338	594	608
3f	CH$_3$	260	338	592	606
3g	OH	260	336	582	602
3h	NH$_2$	274	336	436	598
3i	N(CH$_3$)$_2$	$-^a$	336	442	597

^{a}The absorption maximum overlapped with other maxima.

maximum in the visible region (λ_{max1}) depends significantly on the *para* substituent, with a bathochromic shift for electron-withdrawing substituents and a hypsochromic shift for electron-donating substituents. The absorption bands for the amino derivative **3h** and the dimethylamino derivative **3i** are significantly broader and shifted to lower wavelengths than the bands for the other compounds in the series (see the SI). The position of the first UV maximum (λ_{max2} in Table 5) is almost independent of the nature of the substituent, whereas the position of the second UV maximum (λ_{max3}) slightly varies in the series. However, no clear Hammett-like correlation of λ_{max3} was observed. We also measured the electronic spectra of compound **3e** in a series of solvents and observed a significant solvatochromic effect, with λ_{max1} found at 608, 594, 552, and 540 nm in acetone, DMSO, ethanol, and methanol, respectively. The solutions of compound **3e** had different colors in these solvents (see Figure S4 in the SI for a photo of the solutions).

The UV/vis absorption maxima of derivatives **4**–**7** are shifted by an almost constant shift with respect to the
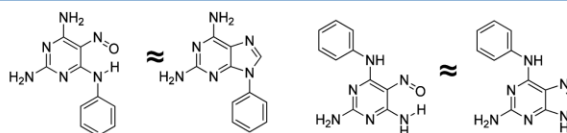
corresponding methoxy derivatives **3** (see the SI), indicating that the orientation of the nitroso group does not affect the electronic spectrum.

The TD-DFT calculations predicted the positions of the absorption maxima well (see Table 5 and the SI), making it possible to explain the observed experimental spectra. We calculated the five lowest-energy electronic transitions for compounds **3a**–**i**. Typically, one transition in the visible range with a very low oscillator strength (corresponding to a weak intensity of the peak in the experimental spectrum) and two transitions with high oscillator strengths in the UV region were found among the calculated transitions. Additional weak transitions were found in the UV region of some derivatives; however, these bands are probably overlapped by the intense bands in the experimental spectra. In the calculated transitions for the amino derivative **3h**, one of the $\pi \to \pi^*$ transitions is close to the n $\to \pi^*$ transition, which could explain the unusually broad experimental signal in the visible range. Furthermore, the lowest-energy transitions in the visible range for compounds **3a**–**g** correspond to excitation from the HOMO to the LUMO, whereas for the amino derivative **3h**, the lowest-energy transition corresponds to excitation from the HOMO−1 orbital.

■ CONCLUSIONS

We prepared a series of polysubstituted 5-nitrosopyrimidine derivatives capable of forming strong intramolecular hydrogen bonds. Mixtures of two forms with distinct hydrogen-bond patterns were found in the solutions of compounds with two hydrogen-bond donors neighboring the nitroso group. The ratio of the two forms was significantly substituent-dependent, and the concentrations of the two forms can be found in a broad range. Furthermore, the rotamer ratio can be predicted well by DFT calculations. It has been speculated previously that 5-nitrosopyrimidines might mimic purine derivatives.[43] Our switchable 5-nitrosopyrimidines might thus mimic two different purine derivatives depending on the orientation of the nitroso group. For example, form A of compound **6e** (Figure 6) resembles 2-amino-9-phenyladenine, which can act as a phosphatidylinositol-kinase inhibitor,[44] whereas form B of the same compound resembles 2-amino-6-phenylaminopurine, which can act as a cytokinin-receptor activator.[45] Theoretically, one compound may hence target two different metabolic pathways. Studies of the biological properties of the polysubstituted 5-nitrosopyrimidines are in progress.

■ EXPERIMENTAL SECTION

Instrumentation and Calculations. The NMR spectra were measured at room temperature on a spectrometer operating at 499.9 MHz for ^{1}H and at 125.7 MHz for ^{13}C in DMSO-d_6 (2 mg of the compound dissolved in 0.6 mL of the solvent). A combination of 1D and 2D experiments (COSY, HSQC, HMBC) was used for the

Figure 6. The two forms of 5-nitrosopyrimidine **6e** as purine mimics.

assignment of all of the ^{1}H and ^{13}C resonances. The general numbering scheme for the assignment of the NMR signals of the polysubstituted pyrimidines is shown in Figure 7. The rotamer
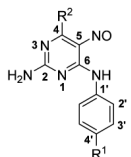

Figure 7. General numbering scheme for the assignment of the NMR signals of the polysubstituted pyrimidines.

mixtures of compounds **4–7** were allowed to equilibrate for 24 h prior to the NMR measurements, and we checked that the equilibrium composition did not change over 4 weeks. High-resolution electrospray mass spectrometry (HRMS) was performed using an Orbitrap spectrometer.

All of the structures were optimized at the DFT level of theory using the B3LYP functional[46,47] and a standard 6-31+G(d,p) basis set. The NMR parameters were calculated using the GIAO method. The calculations were done for the molecules in vacuum, but for comparison we also optimized the geometries of compounds **5e** and **5g** in DMSO using the PCM method.[30,31] The Gaussian 09 program package was used throughout this study.[48] The QST3 optimization method[41,42] was applied in the search for the transition state of the rotamer interconversion of compound **5e** in vacuum, that is, the structures of the reactants and products and an estimate of the transition state were used. Once the transition state had been optimized in vacuum, a single-point energy and frequency calculation was performed with the PCM method of solvation. The vibrational frequencies and free energies were calculated for all of the optimized structures, and the character of each stationary point (a minimum or a first-order saddle point) was thus confirmed. The electronic spectra were calculated using the TD-DFT method[49] with the PCM method of DMSO solvation.

All of the microwave-assisted reactions were carried out in a CEM Discover (Explorer) microwave apparatus with a 24-position system for 10 mL vessels sealed with a Teflon septum. It was operated at a frequency of 2.45 GHz with continuous irradiation power from 0 to 300 W. The solutions were steadily stirred during the reaction. The temperature was measured with an IR sensor on the outer surface of the process vessel. The vials were cooled to ambient temperature with a gas jet cooling system. The pressure was measured with an inboard CEM Explorer pressure control system (0–21 bar).

Preparation of 5-Nitrosopyrimidines. *General Procedure A: Synthesis of 2-Amino-6-arylamino-4-methoxy-5-nitrosopyrimidines* ***3a–i.*** A mixture of compound **1** and 1.1 equiv of the corresponding *para*-substituted aniline (**2a–i**) in DMF (3 mL per 1 mmol of **1**) was stirred and heated under conventional heating (conv.) or microwave-assisted (MW) heating until full conversion (as judged by TLC). The reaction mixture was evaporated in vacuum, and the product was isolated by silica gel column chromatography (5–8% MeOH in CHCl$_3$). In the case of compounds **3a** and **3f**, the solid residues after solvent evaporation were dissolved in acetone and methanol, respectively, and the products were filtered off, washed, and dried. Compounds **3a–c** and **3f** were crystallized.

4-[(2-Amino-4-methoxy-5-nitrosopyrimidin-6-yl)amino]-benzonitrile (3a). Treatment of **1** (600 mg, 3.3 mmol) and 4-aminobenzonitrile (**2a**) (429 mg, 3.6 mmol) by general procedure A (MW, 170 °C, 2 h) gave **3a** (267 mg, 30%) as green crystals (from methanol/acetone, 1:1) with mp = 245 °C. ^{1}H NMR (DMSO-d_6): δ 13.45 (1H, s, 6-NH), 8.57 and 8.53 (2H, bs, 2-NH$_2$), 8.06 (2H, m, H2'), 7.79 (2H, m, H3'), 4.10 (3H, s, O−CH$_3$). ^{13}C NMR (DMSO-d_6): δ 171.2 (C4), 163.7 (C2), 147.5 (C6), 142.1 (C1'), 138.4 (C5), 133.2 (C3'), 123.2 (C2'), 119.0 (CN), 106.6 (C4'). UV/vis (DMSO):

λ_{max} = 342, 596 nm. ESI MS *m/z*: 293.2 [M + Na]$^+$, 271.2 [M + H]$^+$. HRMS (ESI) *m/z*: calcd for C$_{12}$H$_{11}$N$_6$O$_2$ [M + H]$^+$ 271.0938, found 271.0938.

4-Methoxy-5-nitroso-N^6-[4-(trifluoromethyl)phenyl]pyrimidine-2,6-diamine (3b). Treatment of **1** (600 mg, 3.3 mmol) and 4-(trifluoromethyl)aniline (**2b**) (585 mg, 3.6 mmol) by general procedure A (MW, 170 °C, 2 h) gave **3b** (310 mg, 30%) as green crystals (from methanol) with mp = 217−219 °C. ^{1}H NMR (DMSO-d_6): δ 13.47 (1H, s, 6-NH), 8.48 (2H, bs, 2-NH$_2$), 8.05 (2H, m, H2'), 7.69 (2H, m, H3'), 4.11 (3H, s, O−CH$_3$). ^{13}C NMR (DMSO-d_6): δ 171.3 (C4), 163.8 (C2), 147.8 (C6), 141.3 (C1', $J_{C1'-F}$ = 1.1 Hz), 138.5 (C5), 126.0 (C3', $J_{C3'-F}$ = 3.8 Hz), 124.8 (C4', $J_{C4'-F}$ = 32.0 Hz), 124.4 (CF$_3$, J_{C-F} = 271.8 Hz), 123.4 (C2'), 54.7 (O−CH$_3$). UV/vis (DMSO): λ_{max} = 342, 602 nm. ESI MS *m/z*: 336.0 [M + Na]$^+$, 314.0 [M + H]$^+$. HRMS (ESI) *m/z*: calcd for C$_{12}$H$_{11}$F$_3$N$_5$O$_2$ [M + H]$^+$ 314.0859, found 314.0859.

Methyl 4-[(2-Amino-4-methoxy-5-nitrosopyrimidin-6-yl)amino]-benzoate (3c). Treatment of **1** (600 mg, 3.3 mmol) and methyl 4-aminobenzoate (**2c**) (549 mg, 3.6 mmol) by general procedure A (MW, 170 °C, 1 h) gave **3c** (630 mg, 63%) as red crystals with mp = 230 °C (decomp.). ^{1}H NMR (DMSO-d_6): δ 13.53 (1H, s, 6-NH), 8.50 (2H, bs, 2-NH$_2$), 8.00 (2H, m, H2'), 7.92 (2H, m, H3'), 4.11 (3H, s, O−CH$_3$), 3.84 (3H, s, COOCH$_3$). ^{13}C NMR (DMSO-d_6): δ 171.2 (C4), 165.8 (C4'−CO), 163.8 (C2), 147.6 (C6), 142.1 (C1'), 138.5 (C5), 130.2 (C3'), 125.4 (C4'), 122.6 (C2'), 54.7 (O−CH$_3$), 52.2 (COOCH$_3$). UV/vis (DMSO): λ_{max} = 276, 342, 600 nm. ESI MS *m/z*: 326.1 [M + Na]$^+$, 304.1 [M + H]$^+$. HRMS (ESI) *m/z*: calcd for C$_{13}$H$_{14}$N$_5$O$_4$ [M + H]$^+$ 304.1040, found 304.1039.

N^6-(4-Chlorophenyl)-4-methoxy-5-nitrosopyrimidine-2,6-diamine (3d). Treatment of **1** (400 mg, 2.2 mmol) and 4-chloroaniline (**2d**) (309 mg, 2.4 mmol) by general procedure A (MW, 160 °C, 1 h) gave **3d** (474 mg, 77%) as a green solid with mp = 219 °C. ^{1}H NMR (DMSO-d_6): δ 13.46 (1H, s, 6-NH), 8.40 (2H, bs, 2-NH$_2$), 7.85 (2H, m, H2'), 7.40 (2H, m, H3'), 4.09 (3H, s, O−CH$_3$). ^{13}C NMR (DMSO-d_6): δ 171.2 (C4), 163.7 (C2), 147.9 (C6), 138.4 (C5), 136.4 (C1'), 128.9 (C3'), 128.9 (C4'), 124.8 (C2'), 54.7 (O−CH$_3$). UV/vis (DMSO): λ_{max} = 264, 338, 596 nm. ESI MS *m/z*: 302.0 [M + Na]$^+$, 280.0 [M + H]$^+$. HRMS (ESI) *m/z*: calcd for C$_{11}$H$_{10}$ClN$_5$O$_2$Na [M + Na]$^+$ 302.0410, found 302.0414.

4-Methoxy-5-nitroso-N^6-phenylpyrimidine-2,6-diamine (3e). Treatment of **1** (900 mg, 4.9 mmol) and aniline (**2e**) (502 mg, 2.0 mmol) by general procedure A (MW, 160 °C, 20 min) gave **3e** (1.01 g, 84%) as a red solid with mp = 204−210 °C. ^{1}H NMR (DMSO-d_6): δ 13.51 (1H, s, 6-NH), 8.36 (1H, s, 2-NH^B), 8.34 (1H, s, 2-NH^A), 7.80 (2H, m, H2'), 7.37 (2H, m, H3'), 7.17 (1H, m, H4'), 4.09 (3H, s, O−CH$_3$). ^{13}C NMR (DMSO-d_6): δ 171.2 (C4), 163.8 (C2), 148.0 (C6), 138.4 (C5), 137.3 (C1'), 129.1 (C3'), 125.1 (C4'), 123.1 (C2'), 54.6 (O−CH$_3$). UV/vis (DMSO): λ_{max} = 260, 338, 594 nm. ESI MS *m/z*: 268.0 [M + Na]$^+$, 246.0 [M + H]$^+$. HRMS (ESI) *m/z*: calcd for C$_{11}$H$_{12}$N$_5$O$_2$ [M + H]$^+$ 246.0985, found 246.0985.

4-Methoxy-5-nitroso-N^6-(p-tolyl)pyrimidine-2,6-diamine (3f). Treatment of **1** (900 mg, 4.9 mmol) and *p*-toluidine (**2f**) (577 mg, 5.4 mmol) by general procedure A (MW, 160 °C, 20 min) gave **3f** (939 mg, 74%) as red crystals (from methanol) with mp = 210 °C. ^{1}H NMR (DMSO-d_6): δ 13.52 (1H, s, 6-NH), 8.32 (1H, bs, 2-NH^B), 8.31 (1H, bs, 2-NH^A), 7.68 (2H, m, H2'), 7.17 (2H, m, H3'), 4.08 (3H, s, O−CH$_3$), 2.29 (3H, s, CH$_3$). ^{13}C NMR (DMSO- d_6): δ 171.2 (C4), 163.7 (C2), 148.0 (C6), 138.3 (C5), 134.7 (C1'), 134.4 (C4'), 129.5 (C3'), 123.1 (C2'), 54.6 (O−CH$_3$), 20.7 (CH$_3$). UV/vis (DMSO): λ_{max} = 260, 338, 592 nm. ESI MS *m/z*: 282.1 [M + Na]$^+$, 260.1 [M + H]$^+$. HRMS (ESI) *m/z*: calcd for C$_{12}$H$_{14}$N$_5$O$_2$ [M + H]$^+$ 260.1142, found 260.1141.

4-[(2-Amino-4-methoxy-5-nitrosopyrimidin-6-yl)amino]phenol (3g). Treatment of **1** (200 mg, 1.1 mmol) and 4-aminophenol (**2g**) (132 mg, 1.2 mmol) by general procedure A (conv., 70 °C, 6 h) gave **3g** (163 mg, 56%) as an orange solid with mp = 230 °C (decomp.). ^{1}H NMR (DMSO-d_6): δ 13.54 (1H, s, 6-NH), 9.49 (1H, s, 4'-OH), 8.21 (2H, bs, 2-NH$_2$), 7.58 (2H, m, H2'), 6.75 (2H, m, H3'), 4.07 (3H, s, O−CH$_3$). ^{13}C NMR (DMSO-d_6): δ 171.1 (C4), 163.7 (C2), 155.0 (C4'), 147.9 (C6), 138.2 (C5), 128.5 (C1'), 124.7 (C2'), 115.6 (C3'),

54.5 (O−CH₃). UV/vis (DMSO): λ_{max} = 260, 336, 582 nm. ESI MS m/z: 284.1 [M + Na]⁺, 262.1 [M + H]⁺. HRMS (ESI) m/z: calcd for C₁₁H₁₁N₅O₃Na [M + Na]⁺ 284.0754, found 284.0754.

N⁶-(4-Aminophenyl)-4-methoxy-5-nitrosopyrimidine-2,6-diamine (3h). Treatment of **1** (1.00 g, 5.4 mmol) and benzene-1,4-diamine (**2h**) (643 mg, 5.9 mmol) by general procedure A (conv., 90 °C, 24 h) gave **3h** (1.23 g, 88%) as a red solid with mp = 220 °C (decomp.). ¹H NMR (DMSO-d_6): δ 13.65 (1H, s, 6-NH), 8.14 (2H, bs, 2-NH₂), 7.45 (2H, m, H2′), 6.56 (2H, m, H3′), 5.16 (2H, s, 4′-NH₂), 4.06 (3H, s, O−CH₃). ¹³C NMR (DMSO-d_6): δ 171.0 (C4), 163.5 (C2), 147.7 (C6), 146.7 (C4′), 138.1 (C5), 125.6 (C1′), 124.3 (C2′), 114.0 (C3′), 54.5 (O−CH₃). UV/vis (DMSO): λ_{max} = 274, 336, 436 nm. ESI MS m/z: 283.1 [M + Na]⁺, 261.1 [M + H]⁺. HRMS (ESI) m/z: calcd for C₁₁H₁₂N₆O₂Na [M + Na]⁺ 283.0913, found 283.0914.

N⁶-(4-(Dimethylamino)phenyl)-4-methoxy-5-nitrosopyrimidine-2,6-diamine (3i). Treatment of **1** (1.00 g, 5.4 mmol) and *N,N*-dimethyl-*p*-phenylenediamine (**2i**) (809 mg, 5.9 mmol) by general procedure A (conv., 80 °C, 5 h) gave **3i** (1.11 g, 71%) as a black solid with mp = 220 °C. ¹H NMR (DMSO-d_6): δ 13.67 (1H, s, 6-NH), 8.18 (2H, bs, 2-NH₂), 7.60 (2H, m, H2′), 6.70 (2H, m, H3′), 4.07 (3H, s, O−CH₃), 2.89 (6H, s, N(CH₃)₂). ¹³C NMR (DMSO-d_6): δ 171.1 (C4), 163.6 (C2), 148.2 (C4′), 147.8 (C6), 138.2 (C5), 126.1 (C1′), 124.2 (C2′), 112.5 (C3′), 54.5 (O−CH₃), 40.3 (N(CH₃)₂). UV/vis (DMSO): λ_{max} = 336, 442 nm. ESI MS m/z: 311.0 [M + Na]⁺, 289.0 [M + H]⁺. HRMS (ESI) m/z: calcd for C₁₃H₁₇N₆O₂ [M + H]⁺ 289.1407, found 289.1407.

General Procedure B: Synthesis of N⁴,N⁶-Disubstituted 5-Nitrosopyrimidine-2,4,6-triamines 4−6. The corresponding amine (1.1 equiv) or an excess of aq. ammonia was added dropwise to the mixture of the corresponding compound **3a−i** (1.0 equiv) in DMF (20 mL per 1 mmol of **3**), and the reaction mixture was stirred at room temperature (rt) or under conventional heating (conv.) for 3−24 h. The solvents were evaporated, and the corresponding product **4a−h**, **5a−h**, or **6a−i** was obtained by silica gel column chromatography (3−20% MeOH in CHCl₃).

4-[(2-Amino-4-(methylamino)-5-nitrosopyrimidin-6-yl)amino]-benzonitrile (4a). Treatment of **3a** (100 mg, 0.37 mmol) with methylamine (33% ethanolic solution, 17 μL) in DMF by general procedure B (rt, 4 h) gave **4a** (40 mg, 40%) as a red solid with mp = 300 °C. ¹H NMR (DMSO-d_6): Rotamer A: δ 14.15 (1H, s, 6-NH), 9.02 (1H, q, $J_{NH−CH_3}$ = 4.8 Hz, 4-NH), 8.08 (2H, m, H2′), 7.98 (2H, bs, 2-NH₂), 7.77 (2H, m, H3′), 2.96 (3H, d, $J_{CH_3−NH}$ = 4.8 Hz, N−CH₃). Rotamer B: δ 11.34 (1H, q, $J_{NH−CH_3}$ = 5.0 Hz, 4-NH), 10.64 (1H, s, 6-NH), 8.31 (2H, m, H2′), 7.95 (1H, bs, 2-NHᴮ), 7.89 (1H, bs, 2-NHᴬ), 7.76 (2H, m, H3′), 2.89 (3H, d, $J_{CH_3−NH}$ = 5.0 Hz, NH−CH₃). ¹³C NMR (DMSO-d_6): Rotamer A: δ 164.3 (C2), 163.2 (C4), 148.3 (C6), 142.7 (C1′), 136.0 (C5), 133.2 (C3′), 122.7 (C2′), 119.1 (CN), 106.0 (C4′), 27.6 (NH−CH₃). Rotamer B: δ 163.8 (C2), 161.9 (C6), 151.0 (C4), 143.6 (C1′), 136.5 (C5), 132.8 (C3′), 121.8 (C2′), 119.4 (CN), 104.8 (C4′) 26.2 (NH−CH₃). UV/vis (DMSO): λ_{max} = 574 nm. ESI MS m/z: 270.2 [M + H]⁺. HRMS (ESI) m/z: calcd for C₁₂H₁₂N₇O [M + H]⁺ 270.1097, found 270.1098.

N⁴-Methyl-5-nitroso-N⁶-[4-(trifluoromethyl)phenyl]pyrimidine-2,4,6-triamine (4b). Treatment of **3b** (100 mg, 0.32 mmol) with methylamine (33% ethanolic solution, 15 μL) in DMF by general procedure B (rt, 16 h) gave **4b** (90 mg, 90%) as an orange solid with mp = 220 °C. ¹H NMR (DMSO-d_6): δ 14.16 (1H, s, 6-NH, A), 11.39 (1H, q, $J_{NH−CH_3}$ = 5.0 Hz, 4-NH, B), 10.62 (1H, s, 6-NH, B), 9.02 (1H, q, $J_{NH−CH_3}$ = 4.9 Hz, 4-NH, A), 8.26 (2H, m, H2′, B), 8.07 (2H, m, H2′, A), 7.96 and 7.94 (2H, bs, 2-NH₂, A), 7.84 (2H, bs, 2-NH₂, B), 7.64−7.68 (4H, m, H3′, A and B), 2.97 (3H, d, $J_{CH_3−NH}$ = 4.9 Hz, CH₃, A), 2.90 (3H, d, $J_{CH_3−NH}$ = 5.0 Hz, CH₃, B). ¹³C NMR (DMSO-d_6): Rotamer A: δ 164.4 (C2), 163.2 (C4), 148.4 (C6), 141.9 (C1′, $J_{C1'−F}$ = 1.3 Hz), 136.0 (C5), 126.0 (C3′, $J_{C3'−F}$ = 3.8 Hz), 124.4 (CF₃, $J_{C−F}$ = 271.5 Hz), 124.2 (C4′, $J_{C4'−F}$ = 32.4 Hz), 122.8 (C2′), 27.6 (NH−CH₃). Rotamer B: δ 164.0 (C2), 162.0 (C6), 151.2 (C4), 142.9 (C1′, $J_{C1'−F}$ = 1.2 Hz), 136.5 (C5), 125.6 (C3′, $J_{C3'−F}$ = 3.8 Hz), 124.6 (CF₃, $J_{C−F}$ = 271.5 Hz), 123.3 (C4′, $J_{C4'−F}$ = 32.8 Hz), 122.2 (C2′) 26.2

(NH−CH₃). UV/vis (DMSO): λ_{max} = 570 nm. ESI MS m/z: 335.1 [M + Na]⁺, 313.1 [M + H]⁺. HRMS (ESI) m/z: calcd for C₁₂H₁₃F₃N₆O [M + H]⁺ 313.1019, found 313.1018.

Methyl 4-[(2-Amino-4-(methylamino)-5-nitrosopyrimidin-6-yl)-amino]benzoate (4c). Treatment of **3c** (121 mg, 0.40 mmol) with methylamine (33% ethanolic solution, 18 μL) in DMF by general procedure B (rt, 24 h) gave **4c** (77 mg, 64%) as a pink solid with mp = 223−228 °C. ¹H NMR (DMSO-d_6): Rotamer A: δ 14.19 (1H, s, 6-NH), 9.00 (1H, q, $J_{NH−CH_3}$ = 4.8 Hz, 4-NH), 8.01 (2H, m, H2′), 7.95 and 7.94 (2H, bs, 2-NH₂), 7.91 (2H, m, H3′), 3.84 (3H, s, O−CH₃), 2.97 (3H, d, $J_{CH_3−NH}$ = 4.8 Hz, N−CH₃). Rotamer B: δ 11.38 (1H, q, $J_{NH−CH_3}$ = 5.0 Hz, 4-NH), 10.56 (1H, s, 6-NH), 8.22 (2H, m, 2′-H), 7.90 (2H, m, 3′-H), 7.85 (2H, bs, 2-NH₂), 3.84 (3H, s, O−CH₃), 2.90 (3H, d, $J_{CH_3−NH}$ = 5.0 Hz, N−CH₃). ¹³C NMR (DMSO-d_6): Rotamer A: δ 165.9 (C4′−CO), 164.4 (C2), 163.2 (C4), 148.2 (C6), 142.8 (C1′), 136.0 (C5), 129.8 (C3′), 124.9 (C4′), 122.1 (C2′), 52.2 (O−CH₃), 27.6 (N−CH₃). Rotamer B: δ 166.1 (C4′−CO), 164.0 (C2), 161.8 (C6), 151.1 (C4), 143.7 (C1′), 136.5 (C5), 129.8 (C3′), 123.9 (C4′), 121.4 (C2′), 52.1 (O−CH₃), 26.2 (N−CH₃). UV/vis (DMSO): λ_{max} = 570 nm. ESI MS m/z: 325.2 [M + Na]⁺, 303.2 [M + H]⁺. HRMS (ESI) m/z: calcd for C₁₃H₁₅N₆O₃ [M + H]⁺ 303.1200, found 303.1199.

N⁶-(4-Chlorophenyl)-N⁴-methyl-5-nitrosopyrimidine-2,4,6-triamine (4d). Treatment of **3d** (100 mg, 0.36 mmol) with methylamine (33% ethanolic solution, 16 μL) in DMF by general procedure B (rt, 6 h) gave **4d** (78 mg, 78%) as a pink solid with mp = 261 °C. ¹H NMR (DMSO-d_6): Rotamer A: δ 14.13 (1H, s, 6-NH), 8.95 (1H, q, $J_{NH−CH_3}$ = 4.9 Hz, 4-NH), 7.88 (2H, m, H2′), 7.85 (2H, bs, 2-NH₂), 7.38 (2H, m, H3′), 2.96 (3H, d, $J_{CH_3−NH}$ = 4.9 Hz, N−CH₃). Rotamer B: δ 11.44 (1H, q, $J_{NH−CH_3}$ = 5.0 Hz, 4-NH), 10.42 (1H, s, 6-NH), 8.05 (2H, m, H2′), 7.75 (2H, bs, 2-NH₂), 7.36 (2H, m, H3′), 2.89 (3H, d, $J_{CH_3−NH}$ = 5.0 Hz, N−CH₃). ¹³C NMR (DMSO-d_6): Rotamer A: δ 164.4 (C2), 163.2 (C4), 148.4 (C6), 137.0 (C1′), 135.9 (C5), 128.9 (C3′), 128.3 (C4′), 124.2 (C2′), 27.6 (N−CH₃). Rotamer B: δ 164.1 (C2), 161.6 (C6), 151.6 (C4), 138.1 (C1′), 136.3 (C5), 128.3 (C3′), 127.3 (C4′), 123.9 (C2′), 26.2 (N−CH₃). UV/vis (DMSO): λ_{max} = 564 nm. ESI MS m/z: 301.1 [M + Na]⁺, 279.1 [M + H]⁺. HRMS (ESI) m/z: calcd for C₁₁H₁₂ClN₆O [M + H]⁺ 279.0755, found 279.0758.

N⁴-Methyl-5-nitroso-N⁶-phenylpyrimidine-2,4,6-triamine (4e). Treatment of **3e** (100 mg, 0.41 mmol) with methylamine (33% ethanolic solution, 19 μL) in DMF by general procedure B (rt, 8 h) gave **4e** (65 mg, 65%) as a red solid with mp = 260 °C. ¹H NMR (DMSO-d_6): Rotamer A: δ 14.12 (1H, s, 6-NH), 8.94 (1H, q, $J_{NH−CH_3}$ = 4.9 Hz, 4-NH), 7.84 (2H, m, H2′), 7.81 (2H, bs, 2-NH₂), 7.35 (2H, m, H3′), 7.13 (1H, m, H4′), 2.96 (3H, d, $J_{CH_3−NH}$ = 4.9 Hz, N−CH₃). Rotamer B: δ 11.48 (1H, q, $J_{NH−CH_3}$ = 5.0 Hz, 4-NH), 10.28 (1H, s, 6-NH), 7.98 (2H, m, H2′), 7.72 (2H, bs, 2-NH₂), 7.33 (2H, m, H3′), 7.09 (1H, m, H4′), 2.89 (3H, d, $J_{CH_3−NH}$ = 5.0 Hz, N−CH₃). ¹³C NMR (DMSO-d_6): Rotamer A: δ 164.5 (C2), 163.3 (C4), 148.5 (C6), 138.0 (C1′), 136.0 (C5), 129.1 (C3′), 124.5 (C4′), 122.7 (C2′), 27.6 (N−CH₃). Rotamer B: δ 164.2 (C2), 161.6 (C6), 151.3 (C4), 138.1 (C1′), 136.3 (C5), 128.6 (C3′), 123.6 (C4′), 122.3 (C2′), 26.1 (N−CH₃). UV/vis (DMSO): λ_{max} = 564 nm. ESI MS m/z: 267.1 [M + Na]⁺, 245.1 [M + H]⁺. HRMS (ESI) m/z: calcd for C₁₁H₁₃N₆O [M + H]⁺ 245.1145, found 245.1144.

N⁴-Methyl-5-nitroso-N⁶-(p-tolyl)pyrimidine-2,4,6-triamine (4f). Treatment of **3f** (100 mg, 0.39 mmol) with methylamine (33% ethanolic solution, 18 μL) in DMF by general procedure B (rt, 3 h) gave **4f** (68 mg, 68%) as a red solid with mp = 240 °C. ¹H NMR (DMSO-d_6): Rotamer A: δ 14.12 (1H, s, 6-NH), 8.91 (1H, q, $J_{NH−CH_3}$ = 4.9 Hz, 4-NH), 7.77 (2H, bs, 2-NH₂), 7.71 (2H, m, H2′), 7.15 (2H, m, H3′), 2.95 (3H, d, $J_{CH_3−NH}$ = 4.9 Hz, N−CH₃), 2.28 (3H, s, 4′-CH₃). Rotamer B: δ 11.50 (1H, q, $J_{NH−CH_3}$ = 5.0 Hz, 4-NH), 10.21 (1H, s, 6-NH), 7.83 (2H, m, H2′), 7.67 (2H, bs, 2-NH₂), 7.13 (2H, m, H3′), 2.89 (3H, d, $J_{CH_3−NH}$ = 5.0 Hz, N−CH₃), 2.28 (3H, s, 4′-CH₃).

^{13}C NMR (DMSO-d_6): Rotamer A: δ 164.5 (C2), 163.3 (C4), 148.4 (C6), 136.2 (C5), 135.4 (C1'), 133.8 (C4'), 129.5 (C3'), 122.6 (C2'), 27.5 (N–CH$_3$), 20.7 (4'-CH$_3$). Rotamer B: δ 164.3 (C2), 161.4 (C6), 151.4 (C4), 136.5 (C5), 135.9 (C1'), 132.7 (C4'), 129.0 (C3'), 122.4 (C2'), 26.1 (N–CH$_3$), 20.6 (4'-CH$_3$). UV/vis (DMSO): λ_{max} = 562 nm. ESI MS m/z: 281.1 [M + Na]$^+$, 259.2 [M + H]$^+$. HRMS (ESI) m/z: calcd for C$_{12}$H$_{15}$N$_6$O [M + H]$^+$ 259.1301, found 259.1302.

4-[(2-Amino-4-(methylamino)-5-nitrosopyrimidin-6-yl)amino]-phenol (4g). Treatment of **3g** (118 mg, 0.45 mmol) with methylamine (33% ethanolic solution 20 μL) in DMF by general procedure B (rt, 24 h) gave **4g** (71 mg, 59%) as a red solid with mp = 273 °C (decomp.). ^{1}H NMR (DMSO-d_6): Rotamer A: δ 14.12 (1H, s, 6-NH), 9.43 (1H, s, 4'-OH), 8.84 (1H, q, $J_{NH–CH_3}$ = 4.9 Hz, 4-NH), 7.66 (2H, m, 2-NH$_2$), 7.62 (2H, m, H2'), 6.74 (2H, m, H3'), 2.94 (3H, d, $J_{CH_3–NH}$ = 4.9 Hz, N–CH$_3$). Rotamer B: δ 11.54 (1H, q, $J_{NH–CH_3}$ = 5.0 Hz, 4-NH), 10.09 (1H, s, 6-NH), 9.27 (1H, s, 4'-OH), 7.68 (2H, m, H2'), 7.57 (2H, m, 2-NH$_2$), 6.72 (2H, m, H3'), 2.88 (3H, d, $J_{CH_3–NH}$ = 5.0 Hz, N–CH$_3$). ^{13}C NMR (DMSO-d_6): Rotamer A: δ 164.5 (C2), 163.3 (C4), 154.6 (C4'), 148.2 (C6), 135.8 (C5), 129.2 (C1'), 124.2 (C2'), 115.5 (C3'), 27.5 (N–CH$_3$). Rotamer B: δ 164.4 (C2), 161.2 (C6), 154.0 (C4'), 151.5 (C4), 136.2 (C5), 130.5 (C1'), 124.3 (C2'), 115.0 (C3'), 26.1 (N–CH$_3$). UV/vis (DMSO): λ_{max} = 546 nm. ESI MS m/z: 283.1 [M + Na]$^+$, 261.1 [M + H]$^+$. HRMS (ESI) m/z: calcd for C$_{11}$H$_{13}$N$_6$O$_2$ [M + H]$^+$ 261.1094, found 261.1094.

N^6-(4-Aminophenyl)-N^4-methyl-5-nitrosopyrimidine-2,4,6-triamine (4h). Treatment of **3h** (100 mg, 0.38 mmol) with methylamine (33% ethanolic solution, 17 μL) in DMF by general procedure B (rt, 12 h) gave **4h** (74 mg, 75%) as a red solid with mp = 239 °C. ^{1}H NMR (DMSO-d_6): δ 14.18 (1H, s, 6-NH, A), 11.57 (1H, q, $J_{CH_3–NH}$ = 5.0 Hz, 4-NH, B), 9.94 (1H, s, 6-NH, B), 8.79 (1H, q, $J_{CH_3–NH}$ = 4.9 Hz, 4-NH, A), 7.59 and 7.58 (2H, 2-NH$_2$, A), 7.49–7.52 (4H, m, 2-NH$_2$, H2', B), 7.48 (2H, m, H2', A), 6.55 (2H, m, H3', A), 6.54 (2H, m, H3', B), 5.10 (2H, bs, 4'-NH$_2$, A), 4.95 (2H, bs, 4'-NH$_2$, B), 2.94 (3H, d, $J_{CH_3–NH}$ = 4.9 Hz, N–CH$_3$, A), 2.88 (3H, d, $J_{CH_3–NH}$ = 5.0 Hz, N–CH$_3$, B). ^{13}C NMR (DMSO-d_6): Rotamer A: δ 164.4 (C2), 163.3 (C4), 147.9 (C6), 146.2 (C4'), 135.7 (C5), 126.4 (C1'), 123.9 (C2'), 114.1 (C3'), 27.5 (N–CH$_3$). Rotamer B: δ 164.4 (C2), 160.9 (C6), 151.6 (C4), 145.6 (C4'), 136.1 (C5), 127.8 (C1'), 124.2 (C2'), 113.7 (C3'), 26.0 (N–CH$_3$). UV/vis (DMSO): λ_{max} = 482 nm. ESI MS m/z: 282.1 [M + Na]$^+$, 260.1 [M + H]$^+$. HRMS (ESI) m/z: calcd for C$_{11}$H$_{14}$N$_7$ONa [M + Na]$^+$ 282.1073, found 282.1074.

4-[(2-Amino-4-(cyclopropylamino)-5-nitrosopyrimidin-6-yl)-amino]benzonitrile (5a). Treatment of **3a** (120 mg, 0.44 mmol) with cyclopropylamine (28 mg, 0.48 mmol) in DMF by general procedure B (conv., 80 °C, 5 h) gave **5a** (62 mg, 48%) as a violet solid with mp = 267 °C. ^{1}H NMR (DMSO-d_6): δ 14.13 (1H, s, 6-NH, A), 11.62 (1H, s, $J_{NH–CH}$ = 5.6 Hz, 4-NH, B), 10.66 (1H, s, 6-NH, B), 8.97 (1H, d, $J_{NH–CH}$ = 5.4 Hz, 4-NH, A), 8.31 (2H, m, H2', B), 8.08 (2H, m, H2', A), 7.99–8.07 (4H, m, 2-NH$_2$, A and B), 7.75–7.79 (4H, m, H3', A and B), 3.20 (1H, m, CH$_{cypr}$, A), 3.09 (1H, m, CH$_{cypr}$, B), 0.79–0.83 (4H, m, CH$_2^A{}_{cypr}$, A and B), 0.72 (2H, m, CH$_2^B{}_{cypr}$, A), 0.66 (2H, m, CH$_2^B{}_{cypr}$, B). ^{13}C NMR (DMSO-d_6): Rotamer A: δ 164.2 (C4), 164.1 (C2), 148.1 (C6), 142.7 (C1'), 135.9 (C5), 133.2 (C3'), 122.8 (C2'), 119.1 (CN), 106.0 (C4'), 24.4 (CH$_{cypr}$), 6.1 (CH$_{2cypr}$). Rotamer B: δ 163.9 (C2), 161.8 (C6), 151.8 (C4), 143.5 (C1'), 136.0 (C5), 132.8 (C3'), 121.9 (C2'), 119.4 (CN), 104.9 (C4'), 22.8 (CH$_{cypr}$), 7.0 (CH$_{2cypr}$). UV/vis (DMSO): λ_{max} = 570 nm. ESI MS m/z: 296.3 [M + H]$^+$. HRMS (ESI) m/z: calcd for C$_{14}$H$_{14}$N$_7$O [M + H]$^+$ 296.1254, found 296.1254.

N^4-Cyclopropyl-5-nitroso-N^6-[4-(trifluoromethyl)phenyl]-pyrimidine-2,4,6-triamine (5b). Treatment of **3b** (100 mg, 0.32 mmol) with cyclopropylamine (20 mg, 0.35 mmol) in DMF by general procedure B (conv., 80 °C, 12 h) gave **5b** (45 mg, 42%) as a violet solid with mp = 228–230 °C. ^{1}H NMR (DMSO-d_6): δ 14.13 (1H, s, 6-NH, A), 11.16 (1H, d, $J_{NH–CH}$ = 5.7 Hz, 4-NH, B), 10.63 (1H, s, 6-NH, B), 8.95 (1H, d, $J_{NH–CH}$ = 5.4 Hz, 4-NH, A), 8.26 (2H, m, H2', B), 8.08 (2H, m, H2', A), 7.91–8.01 (4H, m, 2-NH$_2$, A and B), 7.64–7.68 (4H, m, H3', A and B), 3.20 (1H, m, CH$_{cypr}$,

CH$_{cypr}$, B), 0.79–0.83 (4H, m, CH$_2^A{}_{cypr}$, A and B), 0.73 (2H, m, CH$_2^B{}_{cypr}$, A), 0.65 (2H, m, CH$_2^B{}_{cypr}$, B). ^{13}C NMR (DMSO-d_6): Rotamer A: δ 164.4 (C4), 164.1 (C2), 148.3 (C6), 141.9 (C1', $J_{C1'–F}$ = 1.3 Hz), 135.9 (C5), 129.0 (C3', $J_{C3'–F}$ = 3.9 Hz), 124.4 (CF$_3$, $J_{C–F}$ = 270.9 Hz), 124.3 (C4', $J_{C4'–F}$ = 32.1 Hz), 122.8 (C2'), 24.4 (CH$_{cypr}$), 6.1 (CH$_{2cypr}$). Rotamer B: δ 164.1 (C2), 161.8 (C6), 151.9 (C4), 142.8 (C1', $J_{C1'–F}$ = 1.3 Hz), 136.0 (C5), 125.6 (C3', $J_{C3'–F}$ = 3.8 Hz), 124.6 (CF$_3$, $J_{C–F}$ = 271.3 Hz), 123.4 (C4', $J_{C4'–F}$ = 31.8 Hz), 122.3 (C2'), 22.8 (CH$_{cypr}$), 7.0 (CH$_{2cypr}$). UV/vis (DMSO): λ_{max} = 568 nm. ESI MS m/z: 361.1 [M + Na]$^+$, 339.1 [M + H]$^+$. HRMS (ESI) m/z: calcd for C$_{14}$H$_{14}$F$_3$N$_6$O [M + H]$^+$ 339.1175, found 339.1175.

Methyl 4-[(2-Amino-4-(cyclopropylamino)-5-nitrosopyrimidin-6-yl)amino]benzoate (5c). Treatment of **3c** (100 mg, 0.33 mmol) with cyclopropylamine (21 mg, 0.36 mmol) in DMF (10 mL) by general procedure B (conv., 70 °C, 12 h) gave **5c** (92 mg, 85%) as a red solid with mp = 211 °C. ^{1}H NMR (DMSO-d_6): δ 14.16 (1H, s, 6-NH, A), 11.66 (1H, d, $J_{NH–CH}$ = 5.6 Hz, 4-NH, B), 10.59 (1H, s, 6-NH, B), 8.94 (1H, d, $J_{NH–CH}$ = 5.4 Hz, 4-NH, A), 8.22 (2H, m, H2', B), 8.02 (2H, m, H2', A), 7.98 (2H, bs, 2-NH$_2$, B), 7.94 (2H, bs, 2-NH$_2$, A), 7.91 (2H, m, H3', A), 7.90 (2H, m, H3', B), 3.84 (6H, s, COOCH$_3$, A and B), 3.20 (1H, m, CH$_{cypr}$, A), 3.10 (1H, m, CH$_{cypr}$, B), 0.79–0.83 (4H, m, CH$_2^A{}_{cypr}$, A and B), 0.73 (2H, m, CH$_2^B{}_{cypr}$, A), 0.66 (2H, m, CH$_2^B{}_{cypr}$, B). ^{13}C NMR (DMSO-d_6): Rotamer A: δ 165.9 (C4'–CO), 164.3 (C2), 164.1 (C4), 148.2 (C6), 142.8 (C1'), 135.9 (C5), 130.2 (C3'), 124.9 (C4'), 122.2 (C2'), 52.2 (COOCH$_3$), 24.4 (CH$_{cypr}$), 6.1 (CH$_{2cypr}$). Rotamer B: δ 166.1 (C4'–CO), 164.1 (C2), 161.7 (C6), 151.9 (C4), 143.6 (C1'), 136.0 (C5), 129.8 (C3'), 124.0 (C4'), 121.5 (C2'), 52.1 (COOCH$_3$), 22.8 (CH$_{cypr}$), 7.0 (CH$_{2cypr}$). UV/vis (DMSO): λ_{max} = 568 nm. ESI MS m/z: 351.1 [M + Na]$^+$, 329.1 [M + H]$^+$. HRMS (ESI) m/z: calcd for C$_{15}$H$_{16}$N$_6$O$_3$Na [M + Na]$^+$ 351.1176, found 351.1174.

N^6-(4-Chlorophenyl)-N^4-cyclopropyl-5-nitrosopyrimidine-2,4,6-triamine (5d). Treatment of **3d** (100 mg, 0.36 mmol) with cyclopropylamine (22 mg, 0.39 mmol) in DMF by general procedure B (conv., 90 °C, 5 h) gave **5d** (80 mg, 73%) as a red solid with mp = 220 °C. ^{1}H NMR (DMSO-d_6): δ 14.11 (1H, s, 6-NH, A), 11.74 (1H, d, $J_{NH–CH}$ = 5.6 Hz, 4-NH, B), 10.46 (1H, s, 6-NH, B), 8.92 (1H, d, $J_{NH–CH}$ = 5.4 Hz, 4-NH, A), 8.05 (2H, m, H2', B), 7.89 (2H, m, H2', A), 7.86 and 7.92 (4H, bs and m, 2-NH$_2$, A and B), 7.38 (2H, m, H3', A), 7.36 (2H, m, H3', B), 3.18 (1H, m, CH$_{cypr}$, A), 3.08 (1H, m, CH$_{cypr}$, B), 0.78–0.82 (4H, m, CH$_2^A{}_{cypr}$, A and B), 0.71 (2H, m, CH$_2^B{}_{cypr}$, A), 0.64 (2H, m, CH$_2^B{}_{cypr}$, B). ^{13}C NMR (DMSO-d_6): Rotamer A: δ 164.4 (C2), 164.1 (C4), 148.3 (C6), 137.0 (C1'), 135.8 (C5), 128.9 (C3'), 128.3 (C4'), 124.3 (C2'), 24.4 (CH$_{cypr}$), 6.1 (CH$_{2cypr}$). Rotamer B: δ 164.2 (C2), 161.5 (C6), 152.0 (C4), 138.1 (C1'), 135.9 (C5), 128.3 (C3'), 127.4 (C4'), 124.0 (C2'), 22.8 (CH$_{cypr}$), 7.0 (CH$_{2cypr}$). UV/vis (DMSO): λ_{max} = 564 nm. ESI MS m/z: 327.1 [M + Na]$^+$, 305.1 [M + H]$^+$. HRMS (ESI) m/z: calcd for C$_{13}$H$_{13}$ClN$_6$ONa [M + Na]$^+$ 327.0731, found 327.0730.

N^4-Cyclopropyl-5-nitroso-N^6-phenylpyrimidine-2,4,6-triamine (5e). Treatment of **3e** (100 mg, 0.41 mmol) with cyclopropylamine (26 mg, 0.45 mmol) in DMF by general procedure B (conv., 90 °C, 12 h) gave **5e** (81 mg, 74%) as a violet solid with mp = 222 °C. ^{1}H NMR (DMSO-d_6): δ 14.09 (1H, s, 6-NH, A), 11.77 (1H, d, $J_{NH–CH}$ = 5.6 Hz, 4-NH, B), 10.29 (1H, s, 6-NH, B), 8.86 (1H, d, $J_{NH–CH}$ = 5.4 Hz, 4-NH, A), 7.98 (2H, m, H2', B), 7.79–7.86 (6H, m, 2-NH$_2$, A and B; H2', A), 7.35 (2H, m, H3', A), 7.35 (2H, m, H3', B), 7.14 (1H, m, H4', A), 7.10 (1H, m, H4', B), 3.19 (1H, m, CH$_{cypr}$, A), 3.09 (1H, m, CH$_{cypr}$, B), 0.78–0.83 (4H, m, CH$_2^A{}_{cypr}$, A and B), 0.72 (2H, m, CH$_2^B{}_{cypr}$, A), 0.64 (2H, m, CH$_2^B{}_{cypr}$, B). ^{13}C NMR (DMSO-d_6): Rotamer A: δ 164.5 (C2), 164.2 (C4), 148.4 (C6), 138.0 (C1'), 135.9 (C5), 129.1 (C3'), 124.6 (C4'), 122.7 (C2'), 24.4 (CH$_{cypr}$), 6.1 (CH$_{2cypr}$). Rotamer B: δ 164.3 (C2), 161.6 (C6), 152.1 (C4), 139.0 (C1'), 135.8 (C5), 128.5 (C3'), 123.7 (C4'), 122.4 (C2'), 22.7 (CH$_{cypr}$), 7.0 (CH$_{2cypr}$). UV/vis (DMSO): λ_{max} = 562 nm. ESI MS m/z: 293.1 [M + Na]$^+$, 271.1 [M + H]$^+$. HRMS (ESI) m/z: calcd for C$_{13}$H$_{15}$N$_6$O [M + H]$^+$ 271.1301, found 271.1302.

N^4-Cyclopropyl-5-nitroso-N^6-(p-tolyl)pyrimidine-2,4,6-triamine (5f). Treatment of **3f** (100 mg, 0.39 mmol) with cyclopropylamine (25

mg, 0.43 mmol) in DMF by general procedure B (conv., 90 °C, 3 h) gave **5f** (75 mg, 68%) as a red solid with mp = 193–195 °C. ^{1}H NMR (DMSO-d_6): δ 14.08 (1H, s, 6-NH, A), 11.72 (1H, d, J_{NH-CH} = 5.5 Hz, 4-NH, B), 10.21 (1H, s, 6-NH, B), 8.81 (1H, d, J_{NH-CH} = 5.3 Hz, 4-NH, A), 7.82 (2H, m, H2′, B), 7.76–7.80 (4H, m, 2-NH$_2$, A and B), 7.71 (2H, m, H2′, A), 7.15 (2H, m, H3′, A), 7.13 (2H, m, H3′, B), 3.18 (1H, m, CH$_{cypr}$, A), 3.08 (1H, m, CH$_{cypr}$, B), 2.28 (6H, s, 4′-CH$_3$, A and B), 0.77–0.82 (4H, m, CH$_2^A{}_{cypr}$, A and B), 0.71 (2H, m, CH$_2^B{}_{cypr}$, A), 0.63 (2H, m, CH$_2^B{}_{cypr}$, B). ^{13}C NMR (DMSO-d_6): Rotamer A: δ 164.5 (C2), 164.1 (C4), 148.3 (C6), 135.8 (C5), 135.3 (C1′), 133.8 (C4′), 129.5 (C3′), 122.6 (C2′), 24.4 (CH$_{cypr}$), 20.7 (C4′–CH$_3$), 6.1 (CH$_{2cypr}$). Rotamer B: δ 164.3 (C2), 161.3 (C6), 152.1 (C4), 136.4 (C1′), 135.8 (C5), 132.8 (C4′), 129.0 (C3′), 122.5 (C2′), 22.7 (CH$_{cypr}$), 20.7 (C4′–CH$_3$), 7.0 (CH$_{2cypr}$). UV/vis (DMSO): λ_{max} = 562 nm. ESI MS m/z: 307.2 [M + Na]$^+$, 285.2 [M + H]$^+$. HRMS (ESI) m/z: calcd for C$_{14}$H$_{17}$N$_6$O [M + H]$^+$ 285.1458, found 285.1458.

4-[(2-Amino-4-(cyclopropylamino)-5-nitrosopyrimidin-6-yl)-amino]phenol (5g). Treatment of **3g** (147 mg, 0.56 mmol) with cyclopropylamine (35 mg, 0.62 mmol) in DMF by general procedure B (conv., 80 °C, 8 h) gave **5g** (92 mg, 58%) as an orange solid with mp = 274–279 °C. ^{1}H NMR (DMSO-d_6): δ 14.09 (1H, s, 6-NH, A), 11.58 (1H, d, J_{NH-CH} = 5.7 Hz, 4-NH, B), 11.15 (1H, s, 6-NH, B), 9.44 (1H, s, 4′-OH, A), 9.28 (1H, s, 4′-OH, B), 8.77 (1H, d, J_{NH-CH} = 5.4 Hz, 4-NH, A), 7.61–7.73 (8H, m, 2-NH$_2$, A and B; H2′, A and B), 6.74 (2H, m, H3′, A), 6.72 (2H, m, H3′, B), 3.17 (1H, m, CH$_{cypr}$, A), 3.07 (1H, m, CH$_{cypr}$, B), 0.76–0.82 (4H, m, CH$_2^A{}_{cypr}$, A and B), 0.71 (2H, m, CH$_2^B{}_{cypr}$, A), 0.63 (2H, m, CH$_2^B{}_{cypr}$, B). ^{13}C NMR (DMSO-d_6): Rotamer A: δ 164.5 (C2), 164.1 (C4), 154.6 (C4′), 148.2 (C6), 135.7 (C5), 129.2 (C1′), 124.2 (C2′), 115.5 (C3′), 24.4 (CH$_{cypr}$), 6.1 (CH$_{2cypr}$). Rotamer B: δ 164.4 (C2), 161.0 (C6), 154.1 (C4′), 152.2 (C4), 135.7 (C5), 130.4 (C1′), 124.4 (C2′), 115.0 (C3′), 22.7 (CH$_{cypr}$), 7.0 (CH$_{2cypr}$). UV/vis (DMSO): λ_{max} = 550 nm. ESI MS m/z: 309.1 [M + Na]$^+$, 287.1 [M + H]$^+$. HRMS (ESI) m/z: calcd for C$_{13}$H$_{15}$N$_6$O$_2$ [M + H]$^+$ 287.1251, found 287.1251.

N^6-(4-Aminophenyl)-N^4-cyclopropyl-5-nitrosopyrimidine-2,4,6-triamine (5h). Treatment of **3h** (100 mg, 0.38 mmol) with cyclopropylamine (24 mg, 0.42 mmol) in DMF by general procedure B (conv., 90 °C, 24 h) gave **5h** (99 mg, 92%) as a red solid with mp = 236–237 °C. ^{1}H NMR (DMSO-d_6): δ 14.15 (1H, s, 6-NH, A), 11.89 (1H, d, J_{NH-CH} = 5.7 Hz, 4-NH, B), 9.96 (1H, s, 6-NH, B), 8.70 (1H, d, J_{NH-CH} = 5.4 Hz, 4-NH, A), 7.57–7.64 (4H, m, 2-NH$_2$, A and B), 7.50 (2H, m, H2′, B), 7.48 (2H, m, H2′, A), 6.55 (2H, m, H3′, A), 6.53 (2H, m, H3′, B), 5.11 (2H, bs, 4′-NH$_2$, A), 4.96 (2H, bs, 4′-NH$_2$, B), 3.16 (1H, m, CH$_{cypr}$, A), 3.07 (1H, m, CH$_{cypr}$, B), 0.75–0.81 (4H, m, CH$_2^A{}_{cypr}$, A and B), 0.70 (2H, m, CH$_2^B{}_{cypr}$, A), 0.62 (2H, m, CH$_2^B{}_{cypr}$, B). ^{13}C NMR (DMSO-d_6): Rotamer A: δ 164.4 (C2), 164.1 (C4), 147.8 (C6), 146.2 (C4′), 135.7 (C5), 126.3 (C1′), 123.9 (C2′), 114.1 (C3′), 24.3 (CH$_{cypr}$). Rotamer B: δ 164.5 (C2), 160.7 (C6), 152.3 (C4), 145.6 (C4′), 135.7 (C5), 127.7 (C1′), 124.3 (C2′), 113.7 (C3′), 22.6 (CH$_{cypr}$), 7.0 (CH$_{2cypr}$). UV/vis (DMSO): λ_{max} = 516 nm. ESI MS m/z: 308.1 [M + Na]$^+$, 286.1 [M + H]$^+$. HRMS (ESI) m/z: calcd for C$_{13}$H$_{16}$N$_7$O [M + H]$^+$ 286.1410, found 286.1410.

4-[(2,4-Diamino-5-nitrosopyrimidin-6-yl)amino]benzonitrile (6a). Treatment of **3a** (100 mg, 0.37 mmol) with ammonia (25% aqueous solution, 20 mL) by general procedure B (conv., 50 °C, 4 h) gave **6a** (42 mg, 45%) as an orange solid with mp > 300 °C. ^{1}H NMR (DMSO-d_6): δ 13.92 (1H, s, 6-NH, A), 10.68 (1H, s, 6-NH, B), 10.28 (1H, d, J_{GEM} = 4.6 Hz, 4-NH^A, B), 8.49 (1H, bs, 4-NH^A, A), 8.32 (2H, m, H2′, B), 8.07–8.10 (3H, m, H2′, A; 4-NH^B, B), 7.91 (1H, bs, 2-NH^A, A), 7.84 (1H, bs, 2-NH^A, B), 7.75–7.80 (5H, m, H3′, A; H3′, B; 2-NH^B, A), 7.72 (1H, bs, 4-NH^B, A), 7.69 (1H, bs, 2-NH^B, B). ^{13}C NMR (DMSO-d_6): Rotamer A: δ 165.9 (C4), 164.6 (C2), 148.1 (C6), 142.7 (C1′), 136.2 (C5), 133.2 (C3′), 122.7 (C2′), 119.1 (CN), 105.9 (C4′). Rotamer B: δ 164.1 (C2), 162.0 (C6), 150.9 (C4), 143.6 (C1′), 137.4 (C5), 132.8 (C3′), 121.8 (C2′), 119.4 (CN), 104.8 (C4′). UV/vis (DMSO): λ_{max} = 350, 578 nm. ESI MS m/z: 278.1 [M + Na]$^+$, 256.1 [M + H]$^+$. HRMS (ESI) m/z: calcd for C$_{11}$H$_{10}$N$_7$O [M + H]$^+$ 256.0941, found 256.0941.

5-Nitroso-N^6-[4-(trifluoromethyl)phenyl]pyrimidine-2,4,6-tria-mine (6b). Treatment of **3b** (100 mg, 0.32 mmol) with ammonia (25% aqueous solution, 20 mL) by general procedure B (conv., 50 °C, 5 h) gave **6b** (34 mg, 36%) as a red solid with mp = 253–255 °C. ^{1}H NMR (DMSO-d_6): δ 13.92 (1H, s, 6-NH, A), 10.65 (1H, s, 6-NH, B), 10.32 (1H, d, J_{GEM} = 4.7 Hz, 4-NH^A, B), 8.48 (1H, bs, 4-NH^A, A), 8.26 (2H, m, H2′, B), 8.06–8.09 (3H, m, H2′, A; 4-NH^B, B), 7.84 (1H, bs, 2-NH^A, A), 7.76 (1H, bs, 2-NH^B, A), 7.74 (1H, bs, 2-NH^A, B), 7.72 (1H, bs, 4-NH^B, A), 7.64–7.68 (5H, m, H3′, A; H3′, B; 2-NH^B, B). ^{13}C NMR (DMSO-d_6): Rotamer A: δ 166.0 (C4), 164.7 (C2), 148.3 (C6), 141.4 (C1′, $J_{C1′-F}$ = 1.3 Hz), 136.3 (C5), 126.0 (C3′, $J_{C3′-F}$ = 3.9 Hz), 124.5 (CF$_3$, J_{C-F} = 3270.8 Hz), 124.2 (C4′, $J_{C4′-F}$ = 32.0 Hz), 122.8 (C2′). Rotamer B: δ 164.3 (C2), 162.1 (C6), 151.0 (C4), 142.9 (C1′, $J_{C1′-F}$ = 1.3 Hz), 137.4 (C5), 125.6 (C3′, $J_{C3′-F}$ = 3.9 Hz), 124.6 (CF$_3$, J_{C-F} = 271.7 Hz), 123.3 (C4′, $J_{C4′-F}$ = 32.1 Hz), 122.2 (C2′). UV/vis (DMSO): λ_{max} = 346, 576 nm. ESI MS m/z: 321.1 [M + Na]$^+$, 299.1 [M + H]$^+$. HRMS (ESI) m/z: calcd for C$_{11}$H$_{10}$F$_3$N$_6$O [M + H]$^+$ 299.0862, found 299.0863.

Methyl 4-[(2,4-Diamino-5-nitrosopyrimidin-6-yl)amino]benzoate (6c). Treatment of **3c** (100 mg, 0.32 mmol) with ammonia (25% aqueous solution, 20 mL) by general procedure B (conv., 50 °C, 20 h) gave **6c** (46 mg, 50%) as a pink solid with mp = 295–299 °C. ^{1}H NMR (DMSO-d_6): Rotamer A: δ 13.95 (1H, s, 6-NH), 8.47 (1H, bs, 4-NH^A), 8.02 (2H, m, H2′), 7.91 (2H, m, H3′), 7.85 (1H, bs, 2-NH^A), 7.75–7.77 (1H, m, 2-NH^B), 7.71 (1H, bs, 4-NH^B), 3.84 (3H, s, COOCH$_3$). Rotamer B: δ 10.60 (1H, s, 6-NH), 10.31 (1H, d, J_{GEM} = 4.7 Hz, 4-NH^A), 8.23 (2H, m, H2′), 8.07 (1H, d, J_{GEM} = 4.7 Hz, 4-NH^B), 7.90 (2H, m, H3′), 7.75–7.77 (1H, m, 2-NH^A), 7.67 (1H, m, 2-NH^B), 3.84 (COOCH$_3$). ^{13}C NMR (DMSO-d_6): Rotamer A: δ 166.0 (C4), 165.9 (C4′–CO), 164.7 (C2), 148.1 (C6), 142.8 (C1′), 136.2 (C5), 130.2 (C3′), 124.8 (C4′), 122.1 (C2′), 52.2 (COOCH$_3$). Rotamer B: δ 166.1 (C4′–CO), 164.2 (C2), 162.0 (C6), 150.9 (C4), 143.8 (C1′), 137.4 (C5), 129.8 (C3′), 123.8 (C4′), 121.4 (C2′), 52.1 (COOCH$_3$). UV/vis (DMSO): λ_{max} = 348, 576 nm. ESI MS m/z: 311.2 [M + Na]$^+$, 289.2 [M + H]$^+$. HRMS (ESI) m/z: calcd for C$_{12}$H$_{12}$N$_6$O$_3$Na [M + Na]$^+$ 311.0863, found 311.0863.

N^6-(4-Chlorophenyl)-5-nitrosopyrimidine-2,4,6-triamine (6d). Treatment of **3d** (100 mg, 0.36 mmol) with ammonia (25% aqueous solution, 20 mL) by general procedure B (conv., 50 °C, 3 h) gave **6d** (55 mg, 58%) as an orange solid with mp = 274–277 °C. ^{1}H NMR (DMSO-d_6): Rotamer A: δ 13.88 (1H, s, 6-NH), 8.41 (1H, bs, 4-NH^A), 7.88 (2H, m, H2′), 7.76 (1H, m, 2-NH^A), 7.65–7.68 (2H, m, 2-NH^B and 4-NH^B), 7.38 (2H, m, H3′). Rotamer B: δ 10.45 (1H, s, 6-NH), 10.45 (1H, d, J_{GEM} = 4.8 Hz, 4-NH^A), 8.05 (2H, m, H2′), 8.02 (1H, d, J_{GEM} = 4.8 Hz, 4-NH^B), 7.65–7.68 (1H, m, 2-NH^A), 7.58 (1H, bs, 2-NH^B), 7.36 (2H, m, H3′). ^{13}C NMR (DMSO-d_6): Rotamer A: δ 165.9 (C4), 164.7 (C2), 148.3 (C6), 137.0 (C1′), 136.2 (C5), 128.8 (C3′), 128.2 (C4′), 124.2 (C2′). Rotamer B: δ 164.3 (C2), 161.8 (C6), 151.0 (C4), 138.2 (C1′), 137.3 (C5), 128.3 (C3′), 127.2 (C4′), 123.9 (C2′). UV/vis (DMSO): λ_{max} = 340, 564 nm. ESI MS m/z: 287.1 [M + Na]$^+$, 265.1 [M + H]$^+$. HRMS (ESI) m/z: calcd for C$_{10}$H$_{10}$ClN$_6$O [M + H]$^+$ 265.0599, found 265.0599.

5-Nitroso-N^6-phenylpyrimidine-2,4,6-triamine (6e). Treatment of **3e** (100 mg, 0.38 mmol) with ammonia (25% aqueous solution, 20 mL) by general procedure B (conv., 50 °C, 3 h) gave **6e** (63 mg, 72%) as a pink solid with mp = 266 °C. ^{1}H NMR (DMSO-d_6): Rotamer A: δ 13.88 (1H, s, 6-NH), 8.38 (1H, s, 4-NH^A), 7.83 (2H, m, H2′), 7.71 (1H, m, 2-NH^A), 7.61–7.63 (2H, m, 2-NH^B and 4-NH^B), 7.35 (2H, m, H3′), 7,13 (1H, m, H4′). Rotamer B: δ 10.40 (1H, d, J_{GEM} = 4.7 Hz, 4-NH^A), 10.30 (1H, s, 6-NH), 7.97–8.00 (3H, m, H2′ and 4-NH^B), 7.61–7.63 (1H, m, 2-NH^A), 7.53 (1H, bs, 2-NH^B), 7.33 (2H, m, H3′), 7.09 (1H, m, H4′). ^{13}C NMR (DMSO-d_6): Rotamer A: δ 166.0 (C4), 164.8 (C2), 148.4 (C6), 138.6 (C1′), 136.2 (C5), 129.0 (C3′), 124.5 (C4′), 122.7 (C2′). Rotamer B: δ 164.5 (C2), 161.7 (C6), 151.1 (C4), 139.1 (C1′), 137.2 (C5), 128.5 (C3′), 123.6 (C4′), 122.4 (C2′). UV/vis (DMSO): λ_{max} = 342, 568 nm. ESI MS m/z: 253.1 [M + Na]$^+$, 231.1 [M + H]$^+$. HRMS (ESI) m/z: calcd for C$_{10}$H$_{10}$N$_6$ONa [M + Na]$^+$ 253.0808, found 253.0808.

5-Nitroso-N^6-(p-tolyl)pyrimidine-2,4,6-triamine (6f). Treatment of **3f** (100 mg, 0.39 mmol) with ammonia (25% aqueous solution, 20

mL) by general procedure B (conv., 50 °C, 14 h) gave **6f** (66 mg, 70%) as an orange solid with mp = 250−251 °C. ^{1}H NMR (DMSO-d_6): Rotamer A: δ 13.88 (1H, s, 6-NH), 8.35 (1H, bs, 4-NH^A), 7.71 (2H, m, H2′), 7.67 (1H, m, 2-NH^A), 7.56−7.60 (2H, m, 2-NH^B and 4-NH^B), 7.15 (2H, m, H3′), 2.28 (3H, s, CH$_3$). Rotamer B: δ 10.41 (1H, d, J_{GEM} = 5.0 Hz, 4-NH^A), 10.23 (1H, s, 6-NH), 7.96 (1H, d, J_{GEM} = 5.0 Hz, 4-NH^B), 7.83 (2H, m, H2′), 7.56−7.60 (1H, m, 2-NH^A), 7.49 (1H, bs, 2-NH^B), 7.13 (2H, m, 3′-H), 2.29 (3H, s, CH$_3$). ^{13}C NMR (DMSO-d_6): Rotamer A: δ 166.0 (C4), 164.8 (C2), 148.3 (C6), 136.2 (C5), 135.3 (C1′), 133.7 (C4′), 129.5 (C3′), 122.6 (C2′), 20.6 (CH$_3$). Rotamer B: δ 164.5 (C2), 161.6 (C6), 151.1 (C4), 137.2 (C5), 136.5 (C1′), 132.7 (C4′), 128.9 (C3′), 122.5 (C2′), 20.6 (CH$_3$). UV/vis (DMSO): λ_{max} = 340, 564 nm. ESI MS m/z: 267.2 [M + Na]$^+$, 245.2 [M + H]$^+$. HRMS (ESI) m/z: calcd for C$_{11}$H$_{13}$N$_6$O [M + H]$^+$ 245.1145, found 245.1145.

4-[(2,4-Diamino-5-nitrosopyrimidin-6-yl)amino]phenol (6g). Treatment of **3g** (100 mg, 0.38 mmol) with ammonia (25% aqueous solution, 20 mL) by general procedure B (conv., 50 °C, 14 h) gave **6g** (48 mg, 51%) as an orange solid with mp = 288 °C (decomp.). ^{1}H NMR (DMSO-d_6): Rotamer A: δ 13.88 (1H, s, 6-NH), 8.28 (1H, bs, 4-NH^A), 7.60 (2H, m, H2′), 7.56 (1H, bs, 2-NH^A), 7.52 (1H, bs, 4-NH^B), 7.46−7.49 (1H, m, 2-NH^B), 6.73 (2H, m, H3′). Rotamer B: δ 10.44 (1H, d, J_{GEM} = 3.4 Hz, 4-NH^A), 10.11 (1H, s, 6-NH), 7.90 (1H, d, J_{GEM} = 3.4 Hz, 4-NH^B), 7.67 (2H, m, H2′), 7.46−7.49 (1H, m, 2-NH^A), 7.40 (1H, bs, 2-NH^B), 6.72 (2H, m, H3′). ^{13}C NMR (DMSO-d_6): Rotamer A: δ 165.9 (C4), 164.90 (C2), 154.9 (C4′), 148.1 (C6), 136.1 (C5), 129.0 (C1′), 124.2 (C2′), 115.6 (C3′). Rotamer B: δ 164.6 (C2), 161.4 (C6), 154.1 (C4′), 151.2 (C4), 137.1 (C5), 130.4 (C1′), 124.4 (C2′), 115.0 (C3′). UV/vis (DMSO): λ_{max} = 334, 550−560 nm. ESI MS m/z: 269.1 [M + Na]$^+$, 247.7 [M + H]$^+$. HRMS (ESI) m/z: calcd for C$_{10}$H$_{10}$N$_6$O$_2$Na [M + Na]$^+$ 269.0757, found 269.0757.

N^6-(4-Aminophenyl)-5-nitrosopyrimidine-2,4,6-triamine (6h). Treatment of **3h** (100 mg, 0.38 mmol) with ammonia (25% aqueous solution, 20 mL) by general procedure B (conv., 50 °C, 28 h) gave **6h** (71 mg, 77%) as a red solid with mp = 268−270 °C. ^{1}H NMR (DMSO-d_6): δ 13.94 (1H, s, 6-NH, A), 10.47 (1H, d, J_{GEM} = 5.1 Hz, 4-NH^A, B), 9.97 (1H, s, 6-NH, B), 8.23 (1H, bs, 4-NH^A, A), 7.88 (1H, d, J_{GEM} = 5.1 Hz, 4-NH^B, B), 7.49−7.51 (4H, m, H2′, B; 4-NH^B and 2-NH^A, A), 7.47 (2H, m, H2′), 7.41−7.43 (2H, m, 2-NH^A B; 2-NH^B, A), 7.35 (1H, m, 2-NH^B, B), 6.55 (2H, m, H3′, A), 6.54 (2H, m, H3′, B), 4.97−5.14 (4H, m, 4′-NH$_2$, A; 4′-NH$_2$, B). ^{13}C NMR (DMSO-d_6): Rotamer A: δ 165.9 (C4), 164.8 (C2), 147.9 (C6), 146.2 (C4′), 136.0 (C5), 126.3 (C1′), 123.9 (C2′), 114.1 (C3′). Rotamer B: δ 164.6 (C2), 161.1 (C6), 151.3 (C4), 145.5 (C4′), 137.1 (C5), 127.1 (C1′), 124.3 (C2′), 113.7 (C3′). UV/vis (DMSO): λ_{max} = 330, 422 nm. ESI MS m/z: 268.2 [M + Na]$^+$, 246.2 [M + H]$^+$. HRMS (ESI) m/z: calcd for C$_{10}$H$_{12}$N$_7$O [M + H]$^+$ 246.1097, found 246.1097.

N^6-(4-(Dimethylamino)phenyl)-5-nitrosopyrimidine-2,4,6-triamine (6i). Treatment of **3i** (200 mg, 0.69 mmol) with ammonia (25% aqueous solution, 30 mL) by general procedure B (conv., 60 °C, 5 h) gave **6i** (160 mg, 77%) as a black solid with mp = 251−254 °C. ^{1}H NMR (DMSO-d_6): δ 13.97 (1H, s, 6-NH, A), 10.46 (1H, d, J_{GEM} = 5.2 Hz, 4-NH^A, B), 10.10 (1H, s, 6-NH, B), 8.26 (1H, bs, 4-NH^A, A), 7.88 (1H, d, J_{GEM} = 5.2 Hz, 4-NH^B, B), 7.69 (2H, m, H2′, B), 7.63 (2H, m, H2′, A), 7.52 (1H, bs, 2-NH^A, A), 7.51 (1H, bs, 4-NH^B, A), 7.45 (2H, m, 2-NH^B, A; 2-NH^A, B), 7.38 (1H, bs, 2-NH^B, B), 6.68−6.71 (4H, m, H3′, A and B), 2.89 (6H, s, N(CH$_3$)$_2$, A), 2.88 (6H, s, N(CH$_3$)$_2$, B). ^{13}C NMR (DMSO-d_6): Rotamer A: δ 165.9 (C4), 164.8 (C2), 148.0 (C4′), 147.9 (C6), 136.1 (C5), 126.9 (C1′), 123.8 (C2′), 112.6 (C3′), 40.4 (N(CH$_3$)$_2$). Rotamer B: δ 164.6 (C2), 161.2 (C6), 151.3 (C4), 147.5 (C4′), 137.2 (C5), 128.6 (C1′), 124.1 (C2′), 112.5 (C3′), 40.6 (N(CH$_3$)$_2$). UV/vis (DMSO): λ_{max} = 278, 330, 428 nm. ESI MS m/z: 296.1 [M + Na]$^+$, 274.1 [M + H]$^+$. HRMS (ESI) m/z: calcd for C$_{12}$H$_{16}$N$_7$O [M + H]$^+$ 274.1410, found 274.1411.

General Procedure C: Synthesis of Acetamides 7a−f and 7i. A mixture of 5-nitrosopyrimidine **6a−f** or **6i** in acetic anhydride (10 mL per 1 mmol of **6**) was stirred at 80 °C (conv.). After completion (TLC), the reaction mixture was evaporated to dryness (in vacuum),

and the final product **7a−f** or **7i** was obtained by silica gel column chromatography (5% or 10% MeOH in CHCl$_3$) as a solid.

N-[2-amino-6-[(4-cyanophenyl)amino]-5-nitrosopyrimidin-4-yl]-acetamide (7a). Treatment of **6a** (100 mg, 0.39 mmol) by general procedure C (30 min) gave **7a** (20 mg, 17%) as a green solid with mp = 224 °C. ^{1}H NMR (DMSO-d_6): δ 13.25 (1H, s, 6-NH, A), 12.61 (1H, s, 4-NH, B), 10.96 (1H, s, 6-NH, B), 10.59 (1H, s, 4-NH, A), 8.52−8.62 (4H, m, 2-NH$_2$, A and B), 8.27 (2H, m, H2′, B), 8.09 (2H, m, H2′, A), 7.80−7.83 (4H, m, H3′, A and B), 2.49 (3H, s, CH$_3$CO, B), 2.45 (3H, s, CH$_3$CO, A). ^{13}C NMR (DMSO-d_6): Rotamer A: δ 169.6 (CO), 163.9 (C2), 162.3 (C4), 147.3 (C6), 141.9 (C1′), 136.5 (C5), 133.3 (C2), 123.2 (C2′), 119.0 (CN), 106.76 (C4′), 26.0 (CH$_3$). Rotamer B: δ 172.7 (CO), 163.8 (C2), 162.2 (C6), 145.2 (C4), 143.1 (C1′), 136.5 (C5), 132.9 (C3′), 122.6 (C2′), 119.33 (CN), 105.7 (C4′), 27.6 (CH$_3$). UV/vis (DMSO): λ_{max} = 600 nm. ESI MS m/z: 320.1 [M + Na]$^+$, 298.1 [M + H]$^+$. HRMS (ESI) m/z: calcd for C$_{13}$H$_{11}$N$_7$O$_2$Na [M + Na]$^+$ 320.0866, found 320.0863.

N-[2-Amino-5-nitroso-6-[(4-(trifluoromethyl)phenyl)amino]-pyrimidin-4-yl]acetamide (7b). Treatment of **6b** (200 mg, 0.67 mmol) by general procedure C (10 min) gave **7b** (116 mg, 51%) as a green solid, which was crystallized (from acetone) to afford green crystals with mp = 240−243 °C. ^{1}H NMR (DMSO-d_6): δ 13.25 (1H, s, 6-NH, A), 12.65 (1H, s, 4-NH, B), 10.94 (1H, bs, 6-NH, B), 10.57 (1H, bs, 4-NH, A), 8.44−8.55 (4H, m, 2-NH$_2$, A and B), 8.20 (2H, m, H2′, B), 8.06 (2H, m, H2′, A), 7.68−7.71 (4H, m, H3′, A and B), 2.50 (3H, s, CH$_3$CO, B), 2.46 (3H, s, CH$_3$CO, A). ^{13}C NMR (DMSO-d_6): Rotamer A: δ 169.7 (CO), 163.9 (C2), 162.3 (C4), 147.5 (C6), 141.1 (C1′), 136.5 (C5), 124.9 (C4′, $J_{C4′−F}$ = 32.2 Hz), 124.4 (CF$_3$, $J_{C−F}$ = 271.5 Hz), 126.1 (C3′, $J_{C3′−F}$ = 3.8 Hz), 123.4 (C2′), 26.0 (CH$_3$). Rotamer B: δ 172.8 (CO), 163.9 (C2), 162.3 (C6), 145.3 (C4), 142.3 (C1′), 136.5 (C5), 125.7 (C4′, $J_{C4′−F}$ = 3.8 Hz), 124.5 (CF$_3$, $J_{C−F}$ = 271.8 Hz), 124.1 (C3′, $J_{C3′−F}$ = 33.0 Hz), 123.1 (C2′), 27.6 (CH$_3$). UV/vis (DMSO): λ_{max} = 598 nm. ESI MS m/z: 363.0 [M + Na]$^+$, 341.0 [M + H]$^+$. HRMS (ESI) m/z: calcd for C$_{13}$H$_{12}$F$_3$N$_6$O$_2$ [M + H]$^+$ 341.0968, found 341.0968.

Methyl 4-[(4-Acetamido-2-amino-5-nitrosopyrimidin-6-yl)-amino]benzoate (7c). Treatment of **6c** (100 mg, 0.35 mmol) by general procedure C (15 min) gave **7c** (40 mg, 35%) as a green solid with mp = 247−248 °C. ^{1}H NMR (DMSO-d_6): δ 13.32 (1H, s, 6-NH, A), 12.65 (1H, s, 4-NH, B), 10.90 (1H, s, 6-NH, B), 10.57 (1H, s, 4-NH, A), 8.47−8.57 (4H, m, 2-NH$_2$, A and B), 8.18 (2H, m, H2′, B), 8.02 (2H, m, H2′, A), 7.92−7.95 (4H, m, H3′, A and B), 3.84−3.85 (COOCH$_3$, m, 6H, A and B), 2.50 (3H, s, CH$_3$CO, B), 2.45 (3H, s, CH$_3$CO, A). ^{13}C NMR (DMSO-d_6): Rotamer A: δ 169.6 (CO), 165.88 (**C**OOCH$_3$), 163.9 (C2), 162.3 (C4), 147.3 (C6), 141.9 (C1′), 136.5 (C5), 130.2 (C3′), 125.5 (C4′), 122.7 (C2′), 52.3 (COO**C**H$_3$), 26.0 (CH$_3$). Rotamer B: δ 172.8 (CO), 166.0 (**C**OOCH$_3$), 163.9 (C2), 162.1 (C6), 145.3 (C4), 143.1 (C1′), 136.5 (C5), 129.8 (C3′), 124.7 (C4′), 122.2 (C2′), 52.2 (COO**C**H$_3$), 27.6 (CH$_3$). UV/vis (DMSO): λ_{max} = 596 nm. ESI MS m/z: 353.1 [M + Na]$^+$, 331.1 [M + H]$^+$. HRMS (ESI) m/z: calcd for C$_{14}$H$_{14}$N$_6$O$_4$Na [M + Na]$^+$ 353.0968, found 353.0968.

N-[2-Amino-6-[(4-chlorophenyl)amino]-5-nitrosopyrimidin-4-yl]-acetamide (7d). Treatment of **6d** (300 mg, 1.13 mmol) by general procedure C (30 min) gave **7d** (135 mg, 39%) as a green solid, which was crystallized (from methanol) to afford green crystals with mp = 230 °C. ^{1}H NMR (DMSO-d_6): Rotamer A: δ 13.23 (1H, s, 6-NH), 10.51 (1H, s, 4-NH), 8.44 (2H, bs, 2-NH$_2$), 7.86 (2H, m, H2′), 7.41 (2H, m, H3′), 2.45 (3H, s, CH$_3$). Rotamer B: δ 12.72 (1H, s, 4-NH), 10.76 (1H, s, 6-NH), 8.39 and 8.38 (2H, bs, 2-NH$_2$), 7.98 (2H, m, H2′), 7.40 (2H, m, H3′), 2.49 (3H, s, CH$_3$). ^{13}C NMR (DMSO-d_6): Rotamer A: δ 169.7 (CO), 163.9 (C2), 162.2 (C4), 147.5 (C6), 136.4 (C5), 136.2 (C4′), 129.1 (C1′), 128.9 (C3′), 124.8 (C2′), 26.0 (CH$_3$). Rotamer B: δ 172.8 (CO), 164.0 (C2), 161.9 (C6), 145.3 (C4), 137.5 (C1′), 136.4 (C5), 128.4 (C3′), 128.2 (C4′), 124.8 (C2′), 27.6 (CH$_3$). UV/vis (DMSO): λ_{max} = 592 nm. ESI MS m/z: 329.0 [M + Na]$^+$, 307.0 [M + H]$^+$. HRMS (ESI) m/z: calcd for C$_{12}$H$_{11}$ClN$_6$O$_2$Na [M + Na]$^+$ 329.0524, found 329.0523.

N-[2-Amino-5-nitroso-6-(phenylamino)pyrimidin-4-yl]acetamide (7e). Treatment of **6e** (189 mg, 0.82 mmol) by general procedure C

(30 min) gave **7e** (62 mg, 28%) as a green solid with mp = 229–231 °C. ^{1}H NMR (DMSO-d_6): Rotamer A: δ 13.28 (1H, s, 6-NH), 10.48 (1H, s, 4-NH), 8.40 (2H, bs, 2-NH$_2$), 7.82 (2H, m, H2′), 7.38 (2H, m, H3′), 7.18 (1H, m, H4′), 2.46 (3H, s, CH$_3$). Rotamer B: δ 12.76 (1H, s, 4-NH), 10.64 (1H, s, 6-NH), 8.35 and 8.32 (2H, bs, 2-NH$_2$), 7.92 (2H, m, H2′), 7.37 (2H, m, H3′), 7.15 (1H, m, H4′), 2.50 (3H, s, CH$_3$). ^{13}C NMR (DMSO-d_6): Rotamer A: δ 169.7 (CO), 163.9 (C2), 162.1 (C4), 147.6 (C6), 137.1 (C1′), 136.4 (C5), 129.1 (C3′), 125.2 (C4′), 123.1 (C2′), 26.0 (CH$_3$). Rotamer B: δ 172.9 (CO), 164.0 (C2), 161.9 (C6), 145.4 (C4), 138.4 (C1′), 136.5 (C5), 128.6 (C3′), 124.4 (C4′), 123.3 (C2′), 27.6 (CH$_3$). UV/vis (DMSO): λ_{max} = 590 nm. ESI MS m/z: 295.2 [M + Na]$^+$, 273.2 [M + H]$^+$. HRMS (ESI) m/z: calcd for C$_{12}$H$_{12}$N$_6$O$_2$Na [M + Na]$^+$ 295.0913, found 295.0914.

N-[2-Amino-5-nitroso-6-(p-tolylamino)pyrimidin-4-yl]acetamide (**7f**). Treatment of **6f** (184 mg, 0.77 mmol) by general procedure C (60 min) gave **7f** (94 mg, 43%) as a green solid with mp = 238 °C. ^{1}H NMR (DMSO-d_6): Rotamer A: δ 13.29 (1H, s, 6-NH), 10.46 (1H, s, 4-NH), 8.36 (2H, bs, 2-NH$_2$), 7.69 (2H, m, H2′), 7.18 (2H, m, H3′), 2.46 (3H, s, CO–CH$_3$), 2.29 (3H, s, 4′-CH$_3$). Rotamer B: δ 12.79 (1H, s, 4-NH), 10.58 (1H, s, 6-NH), 8.30 and 8.28 (2H, bs, 2-NH$_2$), 7.77 (2H, m, H2′), 7.16 (2H, m, H3′), 2.49 (3H, s, CO–CH$_3$), 2.30 (3H, s, 4′-CH$_3$). ^{13}C NMR (DMSO-d_6): Rotamer A: δ 169.7 (CO), 163.9 (C2), 162.1 (C4), 147.5 (C6), 136.3 (C5), 134.5 and 129.6 (C1′ and C4′), 129.6 (C3′), 123.1 (C2′), 26.0 (CO–CH$_3$), 20.74 (4′-CH$_3$). Rotamer B: δ 172.9 (CO), 164.1 (C2), 161.7 (C6), 145.4 (C4), 136.3 (C5), 135.9 (C1′), 133.6 (C4′), 129.0 (C3′), 123.4 (C2′), 27.6 (CO–CH$_3$), 20.7 (4′-CH$_3$). UV/vis (DMSO): λ_{max} = 586 nm. ESI MS m/z: 309.2 [M + Na]$^+$, 287.2 [M + H]$^+$. HRMS (ESI) m/z: calcd for C$_{13}$H$_{14}$N$_6$O$_2$Na [M + Na]$^+$ 309.1070, found 309.1069.

N-(2-Amino-6-(4-(dimethylamino)phenylamino)-5-nitrosopyrimidin-4-yl)acetamide (**7i**). Treatment of **6i** (100 mg, 0.37 mmol) by general procedure C (rt, 20 min) gave **7i** (56 mg, 48%) as a black solid with mp = 220–222 °C. ^{1}H NMR (DMSO-d_6): δ 13.44 (1H, s, 6-NH, A), 12.89 (1H, s, 4-NH, B), 10.48 (1H, s, 6-NH, B), 10.40 (1H, s, 4-NH, A), 8.25 and 8.24 (2H, bs, 2-NH$_2$, A), 8.18 and 8.17 (2H, bs, 2-NH$_2$, B), 7.62–7.65 (4H, m, H2′, A and B), 6.69–6.73 (4H, m, H3′, A and B), 2.90 (6H, s, N(CH$_3$)$_2$, A), 2.89 (6H, s, N(CH$_3$)$_2$, B), 2.49 (3H, s, CO–CH$_3$, B), 2.46 (3H, s, CO–CH$_3$, A). ^{13}C NMR (DMSO-d_6): Rotamer A: δ 169.7 (CO), 163.8 (C2), 161.9 (C4), 148.2 (C4′), 147.1 (C6), 136.1 (C5), 125.8 (C1′), 124.2 (C2′), 112.55 (C3′), 40.3 (N(CH$_3$)$_2$), 26.0 (CO–CH$_3$). Rotamer B: δ 172.9 (CO), 164.0 (C2), 161.2 (C6), 148.0 (C4′), 145.5 (C4), 136.2 (C5), 127.7 (C1′), 124.8 (C2′), 112.3 (C3′), 40.5 (N(CH$_3$)$_2$), 27.6 (CO–CH$_3$). UV/vis (DMSO): λ_{max} = 458 nm. ESI MS m/z: 338.1 [M + Na]$^+$, 316.1 [M + H]$^+$. HRMS (ESI) m/z: calcd for C$_{14}$H$_{18}$N$_7$O$_2$ [M + H]$^+$ 316.1516, found 316.1516.

■ ASSOCIATED CONTENT

Ⓢ Supporting Information

Temperature dependence of the ^{1}H NMR spectra of compound **5e**; ^{1}H and ^{13}C NMR, HRMS, and UV–vis spectra of the new compounds; and computational details. This material is available free of charge via the Internet at http://pubs.acs.org.

■ AUTHOR INFORMATION

Corresponding Authors

*E-mail: janeba@uochb.cas.cz.
*E-mail: dracinsky@uochb.cas.cz.

Notes

The authors declare no competing financial interest.

■ ACKNOWLEDGMENTS

■ REFERENCES

(1) Kuhn, B.; Mohr, P.; Stahl, M. *J. Med. Chem.* **2010**, *53*, 2601–2611.

(2) Gilli, G.; Bellucci, F.; Ferretti, V.; Bertolasi, V. *J. Am. Chem. Soc.* **1989**, *111*, 1023–1028.

(3) Bolvig, S.; Hansen, P. E. *Curr. Org. Chem.* **2000**, *4*, 19–54.

(4) Sobczyk, L.; Grabowski, S. J.; Krygowski, T. M. *Chem. Rev.* **2005**, *105*, 3513–3560.

(5) Lyssenko, K. A.; Antipin, M. V. *Russ. Chem. Bull.* **2006**, *55*, 1–15.

(6) Furet, P.; Caravatti, G.; Guagnano, V.; Lang, M.; Meyer, T.; Schoepfer, J. *Bioorg. Med. Chem. Lett.* **2008**, *18*, 897–900.

(7) Hodge, C. N.; Pierce, J. *Bioorg. Med. Chem. Lett.* **1993**, *3*, 1605–1608.

(8) Furet, P.; Bold, G.; Hofmann, F.; Manley, P.; Meyer, T.; Altmann, K. H. *Bioorg. Med. Chem. Lett.* **2003**, *13*, 2967–2971.

(9) Menear, K. A.; Adcock, C.; Alonso, F. C.; Blackburn, K.; Copsey, L.; Drzewiecki, J.; Fundo, A.; Le Gall, A.; Gomez, S.; Javaid, H.; Lence, C. F.; Martin, N. M. B.; Mydlowski, C.; Smith, G. C. M. *Bioorg. Med. Chem. Lett.* **2008**, *18*, 3942–3945.

(10) Lord, A. M.; Mahon, M. F.; Lloyd, M. D.; Threadgill, M. D. *J. Med. Chem.* **2009**, *52*, 868–877.

(11) Osmialowski, B.; Kolehmainen, E.; Kowalska, M. *J. Org. Chem.* **2012**, *77*, 1653–1662.

(12) Sanz, P.; Mo, O.; Yanez, M.; Elguero, J. *J. Phys. Chem. A* **2007**, *111*, 3585–3591.

(13) Gilli, P.; Bertolasi, V.; Ferretti, V.; Gilli, G. *J. Am. Chem. Soc.* **2000**, *122*, 10405–10417.

(14) Holschbach, M. H.; Sanz, D.; Claramunt, R. M.; Infantes, L.; Motherwell, S.; Raithby, P. R.; Jimeno, M. L.; Herrero, D.; Alkorta, I.; Jagerovic, N.; Elguero, J. *J. Org. Chem.* **2003**, *68*, 8831–8837.

(15) Marchal, A.; Nogueras, M.; Sanchez, A.; Low, J. N.; Naesens, L.; De Clercq, E.; Melguizo, M. *Eur. J. Org. Chem.* **2010**, 3823–3830.

(16) Urbelis, G.; Susvilo, I.; Tumkevicius, S. *J. Mol. Model.* **2007**, *13*, 219–224.

(17) Susvilo, I.; Brukstus, A.; Tumkevicius, S. *Tetrahedron Lett.* **2005**, *46*, 1841–1844.

(18) Melguizo, M.; Quesada, A.; Low, J. N.; Glidewell, C. *Acta Crystallogr., Sect. B* **2003**, *59*, 263–276.

(19) O'Brien, D. E.; Baiocchi, F.; Robins, R. K.; Cheng, C. C. *J. Med. Chem.* **1963**, *6*, 467–471.

(20) Arris, C. E.; Boyle, F. T.; Calvert, A. H.; Curtin, N. J.; Endicott, J. A.; Garman, E. F.; Gibson, A. E.; Golding, B. T.; Grant, S.; Griffin, R. J.; Jewsbury, P.; Johnson, L. N.; Lawrie, A. M.; Newell, D. R.; Noble, M. E. M.; Sausville, E. A.; Schultz, R.; Yu, W. *J. Med. Chem.* **2000**, *43*, 2797–2804.

(21) Olivella, M.; Marchal, A.; Nogueras, M.; Sanchez, A.; Melguizo, M.; Raimondi, M.; Zacchino, S.; Giannini, F.; Cobo, J.; Enriz, R. D. *Bioorg. Med. Chem.* **2012**, *20*, 6109–6122.

(22) Yavolovskii, A. A.; Kishichenko, V. D.; Oliinichenko, O. A.; Ivanov, E. I. *Russ. J. Gen. Chem.* **2005**, *75*, 457–460.

(23) Zhang, F. L.; Schweizer, W. B.; Xu, M.; Vasella, A. *Helv. Chim. Acta* **2007**, *90*, 521–534.

(24) Weinstock, J.; Dunoff, R. Y.; Sutton, B.; Trost, B.; Kirkpatrick, J.; Farina, F.; Straub, A. S. *J. Med. Chem.* **1968**, *11*, 549–556.

(25) Lopez-Garzon, R.; Arranz-Mascaros, P.; Godino-Salido, M. L.; Gutierrez-Valero, M. D.; Cuesta, R.; Moreno, J. M. *Inorg. Chim. Acta* **2003**, *355*, 41–48.

(26) Lopez-Garzon, R.; Arranz-Mascaros, P.; Godino-Salido, M. L.; Gutierrez-Valero, M. D.; Perez-Cadenas, A.; Cobo-Domingo, J.; Moreno, J. M. *Inorg. Chim. Acta* **2000**, *308*, 59–64.

(27) Colacio, E.; Lopez-Magana, C.; McKee, V.; Romerosa, A. *J. Chem. Soc., Dalton Trans.* **1999**, 2923–2926.

(28) Colacio, E.; Dominguezvera, J. M.; Escuer, A.; Kivekäs, R.; Romerosa, A. *Inorg. Chem.* **1994**, *33*, 3914–3924.

(29) Marchal, A.; Melguizo, M.; Nogueras, M.; Sanchez, A.; Low, J. N. *Synlett* **2002**, 255–258.

(30) Melguizo, A.; Marchal, A.; Nogueras, M.; Sanchez, A.; Low, J. N. *J. Heterocycl. Chem.* **2002**, *39*, 97−103.

(31) Čechová, L.; Jansa, P.; Šála, M.; Dračínský, M.; Holý, A.; Janeba, Z. *Tetrahedron* **2011**, *67*, 866−871.

(32) Mesguiche, V.; Parsons, R. J.; Arris, C. E.; Bentley, J.; Boyle, F. T.; Curtin, N. J.; Davies, T. G.; Endicott, J. A.; Gibson, A. E.; Golding, B. T.; Griffin, R. J.; Jewsbury, P.; Johnson, L. N.; Newell, D. R.; Noble, M. E. M.; Wang, L. Z.; Hardcastle, I. R. *Bioorg. Med. Chem. Lett.* **2003**, *13*, 217−222.

(33) Smith, M. B.; March, J. *March's Advanced Organic Chemistry: Reactions, Mechanisms, and Structure*, 5th ed.; Wiley: New York, 2001.

(34) Brown, H. C. *Determination of Organic Structures by Physical Methods*; Academic Press: New York, 1955.

(35) Fickling, M. M.; Fischer, A.; Mann, B. R.; Packer, J.; Vaughan, J. *J. Am. Chem. Soc.* **1959**, *81*, 4226−4230.

(36) Britsun, V. N.; Borisevich, A. N.; Lozinskii, M. O. *Russ. J. Org. Chem.* **2007**, *43*, 907−910.

(37) Cantillo, D.; Baghbanzadeh, M.; Kappe, C. O. *Angew. Chem., Int. Ed.* **2012**, *51*, 10190−10193.

(38) Zhang, D. Y.; Sun, H. F.; Zhang, L.; Zhou, Y.; Li, C. P.; Jiang, H. L.; Chen, K. X.; Liu, H. *Chem. Commun.* **2012**, *48*, 2909−2911.

(39) Dračínský, M.; Bouř, P. *J. Chem. Theory Comput.* **2010**, *6*, 288−299.

(40) Jorgensen, W. L.; Jensen, K. P.; Alexandrova, A. N. *J. Chem. Theory Comput.* **2007**, *3*, 1987−1992.

(41) Peng, C.; Schlegel, H. B. *Isr. J. Chem.* **1994**, *33*, 449−454.

(42) Peng, C.; Ayala, P. Y.; Schlegel, H. B.; Frisch, M. J. *J. Comput. Chem.* **1996**, *17*, 49−56.

(43) Quesada, A.; Marchal, A.; Melguizo, M.; Nogueras, M.; Sanchez, A.; Low, J. N.; Cannon, D.; Farrell, D. M. M.; Glidewell, C. *Acta Crystallogr., Sect. B* **2002**, *58*, 300−315.

(44) Young, R. C.; Jones, M.; Milliner, K. J.; Rana, K. K.; Ward, J. G. *J. Med. Chem.* **1990**, *33*, 2073−2080.

(45) Spichal, L.; Gemrotova, M.; Zatloukal, M.; Frebortova, J.; Galuszka, P.; Werner, T.; Schmulling, T.; Dolezal, K.; Strnad, M. Substituted 6-Anilinopurine Derivatives as Inhibitors of Cytokinin Oxidase/Dehydrogenase and Preparations Containing These Derivatives. U.S. Patent 20100190806 A1, 2010.

(46) Becke, A. D. *J. Chem. Phys.* **1993**, *98*, 5648−5652.

(47) Lee, C. T.; Yang, W. T.; Parr, R. G. *Phys. Rev. B* **1988**, *37*, 785−789.

(48) Frisch, M. J.; Trucks, G. W.; Schlegel, H. B.; Scuseria, G. E.; Robb, M. A.; Cheeseman, J. R.; Scalmani, G.; Barone, V.; Mennucci, B.; Petersson, G. A.; Nakatsuji, H.; Caricato, X.; Li, X.; Hratchian, H. P.; Izmaylov, A. F.; Bloino, J.; Zheng, G.; Sonnenberg, J. L.; Hada, M.; Ehara, M.; Toyota, K.; Fukuda, R.; Hasegawa, J.; Ishida, M.; Nakajima, T.; Honda, Y.; Kitao, O.; Nakai, H.; Vreven, T.; Montgomery, J. A., Jr.; Peralta, J. E.; Ogliaro, F.; Bearpark, M.; Heyd, J. J.; Brothers, E.; Kudin, K. N.; Staroverov, V. N.; Kobayashi, R.; Normand, J.; Raghavachari, K.; Rendell, A.; Burant, J. C.; Iyengar, S. S.; Tomasi, J.; Cossi, M.; Rega, N.; Millam, J. M.; Klene, M.; Knox, J. E.; Cross, J. B.; Bakken, V.; Adamo, C.; Jaramillo, J.; Gomperts, R.; Stratmann, R. E.; Yazyev, O.; Austin, A. J.; Cammi, R.; Pomelli, C.; Ochterski, J. W.; Martin, R. L.; Morokuma, K.; Zakrzewski, V. G.; Voth, G. A.; Salvador, P.; Dannenberg, J. J.; Dapprich, S.; Daniels, A. D.; Farkas, Ö.; Foresman, J. B.; Ortiz, J. V.; Cioslowski, J.; Fox, D. J. *Gaussian 09*, revision A.02; Gaussian, Inc.: Wallingford, CT, 2009.

(49) Bauernschmitt, R.; Ahlrichs, R. *Chem. Phys. Lett.* **1996**, *256*, 454−464.

VI.

ChemComm

COMMUNICATION

Separation of planar rotamers through intramolecular hydrogen bonding in polysubstituted 5-nitrosopyrimidines†‡

L. Čechová,§[ab] E. Procházková,§[ac] I. Císařová,[c] M. Dračínský*[a] and Z. Janeba*[a]

While purifying new polysubstituted 5-nitrosopyrimidines, the unique separation of pairs of rotamers as chemical species, stabilized by a single intramolecular hydrogen bond and differing only in nitroso group orientation, was achieved. This interesting stereochemical phenomenon is compared to the well-known atropisomerism.

The ability to form strong hydrogen bonds is one of the most important properties of biologically active compounds. Intermolecular hydrogen bonding is crucial for encoding genetic information (Watson–Crick base pairs); intramolecular hydrogen bonding is pivotal to the formation of biologically relevant three-dimensional structures of macromolecules, such as nucleic acids and proteins. Nevertheless, the ability to form intramolecular hydrogen bonds (IMHBs) also has a great impact on the molecular structure and physico-chemical properties of small organic molecules, making the closed form (with an IMHB) more lipophilic and the open form more water-soluble.[1] Furthermore, the cyclic system formed due to the presence of an IMHB can mimic the structural motifs of other biologically relevant molecules. Thus, replacing the real ring with a "pseudo" ring in drug-like molecules has become an important medicinal chemistry strategy in the search for new lead compounds.[1,2]

The high stability of IMHBs has often been observed in planar systems where a six-membered ring is formed and the linker

atoms are sp²-hybridized (as in amides, enols of β-diketones and β-enaminones, heteroaromatic rings, *etc.*).[1] Some researchers suggest that the stability of such systems is due to stabilization by a resonance-assisted hydrogen bond (RAHB).[3] Others believe that RAHB is not the primary reason behind the strength of the IMHBs in a series of enols of β-diketones and β-enaminones, but rather that the molecular structure (σ-skeleton) keeps the hydrogen donor and hydrogen acceptor coplanar and, therefore, closer to each other.[4]

An effect of the internal hydrogen bond on the conformational isomerism of 2-amino-2-methylpropanol was theoretically studied by Andrade *et al.*[5] Recently, conformers of C-nitroso derivatives of indolizines and azaindolizines with restricted rotation about the C–NO bond were studied by the Katritzky group using solution NMR methods.[6] Conjugated nitrosamines can evidently form planar systems with enhanced π-delocalization and, thus, belong to a class of compounds able to form strong IMHBs.[7] During recent studies of 5-nitrosopyrimidines bearing distinct amino substituents in the C4 and C6 positions, two possible rotamers, stabilized by strong IMHBs, were identified as two sets of signals in ¹H NMR spectra.[8] In our previous paper,[8d] the ratio of the two rotamers was found to be significantly substituent-dependent with a broad range of conformation ratios. NMR spectroscopy showed that the interconversion barriers of these rotamers were as high (>20 kcal mol⁻¹) as those reported for atropisomers,[9] which are conformational isomers isolable through sterically hindered rotation. The high interconversion barriers of these rotamers led us to wonder: could the use of low temperatures with appropriately substituted amino groups in positions C4 and/or C6 potentially lead to the separation of a pair of IMHB-stabilized rotamers? As non-covalent interactions (*e.g.* hydrogen bonds) are considerably less stable compared to covalent bonds, it has been suggested by Szumna[10] that separation of isomers based on a single hydrogen bond is not possible, unless additional auxiliaries are introduced. Indeed, the isolation of such isomers has so far been successful either in relatively complex molecules with an ability to form cooperative robust systems of many hydrogen bonds,[11] or in the case of relatively stable formamide rotamers.[12]

[a] Institute of Organic Chemistry and Biochemistry, Academy of Sciences of the Czech Republic, v.v.i., Flemingovo nám. 2, CZ-166 10 Prague 6, Czech Republic.
E-mail: janeba@uochb.cas.cz, dracinsky@uochb.cas.cz
[b] Department of Chemistry of Natural Compounds, Institute of Chemical Technology Prague, Technická 5, CZ-166 28 Prague 6, Czech Republic
[c] Faculty of Science, Charles University in Prague, Hlavova 2030, CZ-128 40 Prague 2, Czech Republic
† This paper is dedicated to the memory of Professor Alan R. Katritzky, who died on February 10, 2014.
‡ Electronic supplementary information (ESI) available: Supplementary figures and Table, X-ray diffraction data, kinetics, DFT calculations, synthesis and characterization of the prepared compounds. CCDC 1001296 and 1001297. For ESI and crystallographic data in CIF or other electronic format see DOI: 10.1039/c4cc06978a
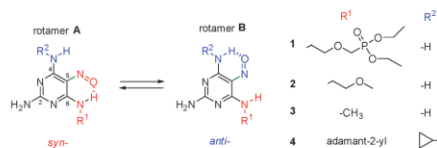§ L.C. and E.P. contributed equally to this work.

Fig. 1   Two possible geometries of the nitroso group in position C5 for compounds **1–4**. Rotamer **A** has a torsion angle C6–C5–N–O close to 0°; rotamer **B** has a torsion angle C6–C5–N–O close to 180°.

Fig. 2   General characteristics of atropisomerism and the herein reported stereochemical phenomenon. A ≠ B and A′ ≠ B′, A/A′ has priority over B/B′.

Although spatial separation using an electric field has recently been developed to enable the study of small molecule conformers,[13] the isolation and full characterization of small molecule rotamers of aromatic compounds as separate chemical species stabilized by a single resonance-assisted IMHB has not yet been reported.

In this paper, we present unique examples of the separation and full characterization of such planar rotamers isolable through a single intramolecular hydrogen bond.

Our previously described methodology[8d] (see ESI‡) was used to prepare a new set of polysubstituted 5-nitrosopyrimidines bearing two different hydrogen-bond donors in positions C4 and C6 of the pyrimidine moiety. While purifying compounds **1–4** (Fig. 1), two products were observed as partially separated UPLC peaks and as well-separated spots on thin layer chromatography (TLC) plates. These products were isolated by routine silica gel chromatography and, to our surprise, found to have identical mass and subsequently identified as **A** and **B** rotamer pairs (Fig. 1), differing only in their 5-nitroso group orientation. The purification of compounds **1** and **2** led to the isolation of pure rotamers **1A/1B** and **2A/2B**. In the case of compounds **3** and **4**, it was only possible to isolate **3A** and **4A** as pure isomers; **3B** and **4B** were always, to some extent, contaminated by **3A** and **4A**, respectively.

We were quite astonished by the fact that we were able to separate rotamers **A** and **B** (Fig. 1) at room temperature and characterize them using just standard spectroscopic methods. Initially, we considered this phenomenon to be a special case of atropisomerism because atropisomers are, by definition,[9] stereoisomers with restricted rotation around a single bond where the rotational barrier is high enough to permit isolation of the isomeric species. However, we quickly realized that there were significant differences between typical atropisomers and our rotamers, the most obvious being their mode of stabilization. Steric hindrance stabilizes atropisomers, but our planar rotamers were stabilized by intramolecular hydrogen bonding (Fig. 2).

Having made this distinction, we explored further similarities and differences between atropisomers and our planar rotamers. We found that there are two necessary preconditions for both the phenomena. The first precondition is a rotationally stable axis, which, in our case, lies along the C5–NO bond. Analogous to the axis of the most common class of atropisomers represented by biaryl compounds (the sp²–sp² family),[9] the herein reported rotamers are characterized by a rotationally stable bond between sp² carbon (C5) and sp² nitrogen (nitroso group) atoms. The second precondition involves the presence of different substituents on
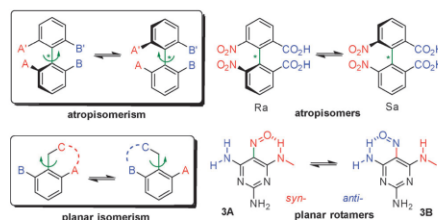
both sides of the axis; in our case, there are differently substituted amino groups in the C4 and C6 positions, and an oxygen and free electron pair on the nitrosyl nitrogen. However, unlike atropisomers,[9] which contain an element of chirality (usually through the axis), our planar rotamers (shortly planamers), precisely because they are planar, lack any element of chirality.

The solid-state ¹³C cross polarization-magic angle spinning (CP-MAS) NMR spectra of rotamers **1A** and **1B** obtained after gentle evaporation of the solvents from the chromatographic fractions are depicted in Fig. 3 and Fig. S1 (ESI‡). According to these spectra, both rotamers were pure; the amount of the second one in the pair was lower than the solid-state NMR detection limit (*ca.* 5%). The ¹³C NMR signals of rotamer **1A** are sharp, indicating long-range order in the solid, while the spectrum of rotamer **1B** exhibits the features typical of amorphous structures; namely, broad signals with multiple overlapped resonances. Interestingly, the solid-state ¹³C NMR spectra show that while the crystalline rotamer **1A** was perfectly stable at room temperature, the solid amorphous rotamer **1B** slowly re-crystallized, over a period of months, into the crystalline rotamer **1A** (Fig. 3 and Fig. S1 in ESI‡).

The solid-state IR spectra of rotamers **1A** and **1B** were acquired on samples dispersed in KBr pellets. Similar to the NMR spectra, there were significant differences between the rotamers. For example, a difference of up to 40 cm⁻¹ was observed between their antisymmetric N–H vibrations. Furthermore, as with the NMR spectra, the signals of the amorphous isomer **1B** were slightly
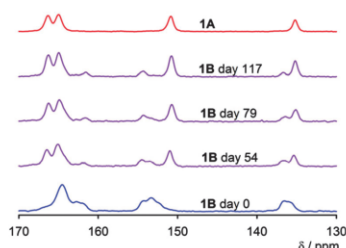

Fig. 3   The aromatic region of ¹³C CP-MAS solid-state NMR spectra of planar rotamers **1A** and **1B**. Solid amorphous **1B** slowly transforms into solid crystalline **1A**. The full spectrum is available in Fig. S1 in ESI.‡
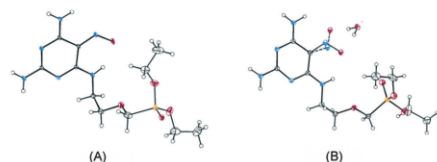
Fig. 4 X-ray crystallographic analysis of pure rotamer **1A** (A) and of the monohydrate of compound **1** (B). Carbon is shown in grey, nitrogen in blue, oxygen in red and phosphorus in yellow. The less occupied position of the nitroso group of rotamer **1B** is drawn with dashed lines (B). The displacement ellipsoids are drawn at a 30% probability level. The disordered atoms of the phosphonate moiety and solvating water molecule are omitted for clarity.

Fig. 5 Interconversion of rotamers **1A** and **1B**. Interconversion was monitored by ^{1}H NMR spectroscopy in a DMSO-d_6 solution. $R^1 = CH_2-CH_2-O-CH_2-P(O)(OEt)_2$.

broader than those of the crystalline isomer **1A**, with no visible contamination by each other (Fig. S2 in ESI‡).

After the re-crystallization of compound **1** (a mixture of **1A** and **1B**) from dry acetone, a monocrystal suitable for X-ray diffraction (XRD) was obtained (Fig. 4A). XRD confirmed that the orientation of the nitroso group corresponded to that of pure rotamer **1A**. The solid-state ^{13}C NMR spectrum of this recrystallized material was identical to the spectrum of **1A** obtained by column chromatography. However, following re-crystallization from an acetone–water mixture, a monohydrate of compound **1** was obtained. In this monohydrate (Fig. 4B), both rotamers were present, **1A** being predominant (*ca.* 80%). Clearly, in a solid state, the conformational stability of a rotamer depends on the polymorphic/crystalline form of the parent compound. In this way, our planamers meet Oki's criterion for atropisomers:[14] physically separable species at a given temperature, having a half-life (τ) of at least 1000 s ($\sim$16.7 min), which is the time considered to be the minimum lifetime for a molecule to be isolable.

Immediately after dissolution of the separated rotamers **A** or **B** in DMSO-d_6 or CD$_3$OD, their ^{1}H and ^{13}C NMR spectra contained one major set of signals together with the low intensity signals of its corresponding second rotamer, **B** or **A**, respectively. Gradually, the **A/B** signal ratio changed until, after several hours, equilibrium was reached. The kinetics of these transformations were determined by solution-state ^{1}H NMR spectroscopy (Fig. 5 and Fig. S3 in ESI‡). The NH hydrogen signals of the two rotamers were usually well separated and, thus, their integration enabled the mixture composition to be determined at various times after dissolution. Table S1 (see ESI‡) summarizes the rate constants (calculated according to the procedure in ESI‡) and the concentrations of rotamers **1A–4A** in equilibrium in various solvents. It is evident that the rotamer equilibrium ratio was not only strongly substituent dependent, but also solvent dependent.

The signals of the NH hydrogens involved in the hydrogen bond were shifted downfield (10–13 ppm) with respect to the signals of the free NH hydrogens (7–9 ppm). The position and orientation of the hydrogen-bond donor atom was confirmed both by the splitting of the signal, which resulted from indirect spin–spin interactions with neighbouring hydrogen atoms, and by the two- and three-bond correlations observed in the HMBC spectra. We also observed four-bond correlations between the
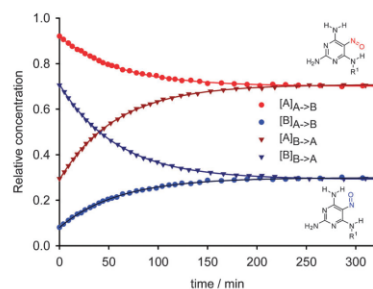
NH hydrogen atoms and the pyrimidine carbon atoms. These correlations were observed when the atoms involved were arranged in the form of a W-like coupling path (Fig. S4 in ESI‡). Furthermore, the orientation of the nitroso group had a significant influence on the chemical shifts of C4 and C6: by *ca.* 12 ppm, the C6 carbon was more shielded in rotamer **A** and the C4 carbon more shielded in rotamer **B**.

Fig. 6 shows the progress of the isotope exchange of hydrogen C6–NH for compound **1** in a DMSO-d_6–CD$_3$OD mixture. As can be seen from the rates of the hydrogen-to-deuterium exchange reaction, the formation of intramolecular hydrogen bonds reduced the accessibility of the solvent to the hydrogen bond donors. In rotamer **1A**, where C6–NH is involved in the hydrogen bond, the exchange reaction was much slower than in rotamer **1B**. As is normal for free amino groups, the hydrogen atoms of the amino group in position C2 were completely replaced by deuterium before the first spectrum could be acquired. Interestingly, both amino hydrogens in position C4 in isomer **1B** were also fully replaced before the first data acquisition. We assume that this was caused by the fast isotope exchange of the unbound amino hydrogen followed by fast rotation around the C4–NH$_2$
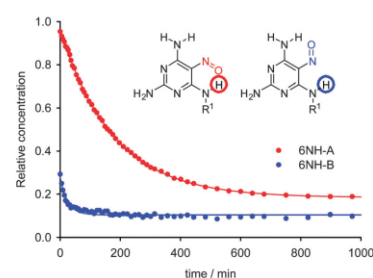

Fig. 6 The progress of the H−D exchange of hydrogen atoms of the amino group in position C6 in the equilibrium mixture of rotamers **1A** and **1B** in a DMSO-d_6–CD$_3$OD mixture (9 : 1).

bond. This hypothesis is supported by the density functional theory (DFT) calculations for the C4–NH$_2$ rotation barrier, which was found to be 5.6 kcal mol^{-1} lower than the rotation of the nitroso group around the C5–NO bond (see ESI‡).

In summary, we succeeded in preparation of planar rotamers which, like atropisomers, are characterized by a high interconversion barrier that enables their separation by column chromatography at room temperature. Herein, we have isolated and fully characterized planar rotamers structurally derived from polysubstituted 5-nitrosopyrimidines. Unlike atropisomers, whose separation is achieved through steric hindrance (and display chirality), the isolation of our planar rotamers is achieved through intramolecular hydrogen bonding (and are achiral). To make a distinction from relatively common atropisomerism, we suggest a term 'planamerism' and define 'planamers' as small aromatic molecule rotamers with a planar conjugated moiety that are isolable as chemical species. It is possible that the reported stereochemical phenomenon has a role to play in disciplines involving weak and reversible non-covalent interactions, such as supramolecular assemblies, host molecules, or in the development of novel drug-like molecules. Therefore, to more clearly understand the scale and scope of this phenomenon, we are currently synthesizing other substituted (hetero)aromatic derivatives likely to be capable of forming strong intramolecular hydrogen bonds and, consequently, separable rotamers.

Notes and references

1 B. Kuhn, P. Mohr and M. Stahl, *J. Med. Chem.*, 2010, **53**, 2601.
2 (a) C. N. Hodge and J. Pierce, *Bioorg. Med. Chem. Lett.*, 1993, **3**, 1605; (b) P. Furet, G. Bold, F. Hofmann, P. Manley, T. Meyer and K.-H. Altmann, *Bioorg. Med. Chem. Lett.*, 2003, **13**, 2967; (c) P. Furet, G. Caravatti, V. Guagnano, M. Lang, T. Meyer and J. Schoepfer, *Bioorg. Med. Chem. Lett.*, 2008, **18**, 897; (d) K. A. Menear, C. Adcock, F. C. Alonso, K. Blackburn, L. Copsey, J. Drzewiecki, A. Fundo, A. Le Gall, S. Gomez, H. Javaid, C. F. Lence, N. M. B. Martin, C. Mydlowski and G. C. M. Smith, *Bioorg. Med. Chem. Lett.*, 2008, **18**, 3942; (e) A.-M. Lord, M. F. Mahon, M. D. Lloyd and M. D. Threadgill, *J. Med. Chem.*, 2009, **52**, 868.
3 (a) G. Gilli, F. Bellucci, V. Ferretti and V. Bertolasi, *J. Am. Chem. Soc.*, 1989, **111**, 1023; (b) S. Bolvig and P. E. Hansen, *Curr. Org. Chem.*, 2000, **4**, 19; (c) L. Sobczyk, S. J. Grabowski and T. M. Krygowski, *Chem. Rev.*, 2005, **105**, 3513; (d) K. A. Lyssenko and M. Y. Antipin, *Russ. Chem. Bull.*, 2006, **55**, 1.
4 P. Sanz, O. Mó, M. Yáñez and J. Elguero, *J. Phys. Chem. A*, 2007, **111**, 3585.
5 L. A. F. Andrade, J. M. Silla and M. P. Freitas, *J. Mol. Struct.*, 2014, **1072**, 203.
6 I. Ghiviriga, B. E.-D. M. El-Gendy, H. Martinez, D. Fedoseyenko, E. P. Metais, A. Fadli and A. R. Katritzky, *Org. Biomol. Chem.*, 2010, **8**, 3518.
7 P. Gilli, V. Bertolasi, V. Ferretti and G. Gilli, *J. Am. Chem. Soc.*, 2000, **122**, 10405.
8 (a) I. Susvilo, A. Brukstus and S. Tumkevicius, *Tetrahedron Lett.*, 2005, **46**, 1841; (b) G. Urbelis, I. Susvilo and S. Tumkevicius, *J. Mol. Model.*, 2007, **13**, 219; (c) A. Marchal, M. Nogueras, A. Sánchez, J. N. Low, L. Naesens, E. De Clercq and M. Melguizo, *Eur. J. Org. Chem.*, 2010, 3823; (d) E. Procházková, L. Čechová, Z. Janeba and M. Dračínský, *J. Org. Chem.*, 2013, **78**, 10121.
9 (a) E. L. Eliel and S. H. Wilen, *Stereochemistry of Organic Compounds*, John Wiley & Sons, Inc., New York, 1994; (b) I. Alkorta, J. Elguero, C. Roussel, N. Vanthuyne and P. Piras, *Adv. Heterocycl. Chem.*, 2012, **105**, 1.
10 A. Szumna, *Chem. Soc. Rev.*, 2010, **39**, 4274.
11 K. Mishiro, T. Furuta, T. Sasamori, K. Hayashi, N. Tokitoh, S. Futaki and T. Kawabata, *J. Am. Chem. Soc.*, 2013, **135**, 13644.
12 M. Geffe, L. Andernach, O. Trapp and T. Opatz, *Beilstein J. Org. Chem.*, 2014, **10**, 701.
13 (a) F. Filsinger, J. Küpper, G. Meijer, J. L. Hansen, J. Maurer, J. H. Nielsen, L. Holmegaard and H. Stapelfeldt, *Angew. Chem., Int. Ed.*, 2009, **48**, 6900; (b) T. S. Zwier, *Nat. Chem.*, 2009, **1**, 687.
14 K. Oki, Recent Advances in Atropisomerism, *Topics in Stereochemistry*, Wiley Interscience, New York, 1983, vol. 14, pp. 1–76.

VII.

Dračínský, M. – **Procházková, E.** – Kessler, J. – Šebestík, J. – Matějka, J. – Bouř, P.:

Resolution of organic polymorphic crystals by Raman spectroscopy.

J. Phys. Chem. B. **2013**; 117, 7297–7307.

Resolution of Organic Polymorphic Crystals by Raman Spectroscopy

Martin Dračínský,[†,‡] Eliška Procházková,[†] Jiří Kessler,[†] Jaroslav Šebestík,[†] Pavel Matějka,[§] and Petr Bouř*[†]

[†]Institute of Organic Chemistry and Biochemistry, Academy of Sciences, Flemingovo nám. 2, 166 10 Prague, Czech Republic
[‡]Department of Chemistry, Durham University, South Road, Durham DH1 3LE, United Kingdom
[§]Department of Physical Chemistry, Institute of Chemical Technology, Technická 5, 166 28 Prague, Czech Republic

S *Supporting Information*

ABSTRACT: Depending on crystallization conditions, many organic compounds can form crystals of different structure. Their proper characterization is important, for example, in the pharmaceutical industry. While the X-ray diffractometry established as a standard method, alternative techniques are desirable for broader application flexibility and economic reasons. In the present study, Raman spectroscopy combined with the density functional calculations is suggested as a complementary method to the X-ray and other higher resolution techniques. The potential to discriminate structural differences in polymorphic crystalline forms is documented on three model compounds of industrial importance. Methacrylamide, piracetam, and 2-thiobarbituric acid were crystallized under various conditions, and their Raman spectra were recorded using 532 and 1064 nm laser excitations. X-ray diffractometry and nuclear magnetic resonance spectroscopy were used as complementary techniques to verify sample composition and structure. To interpret the observed differences in Raman frequencies and intensities, three computational strategies were explored based on single molecule, a cluster model, and a plane-wave periodic boundary conditions calculation. The single-molecule modeling was found inadequate, whereas the plane-wave approach provides the most realistic spectra. For all compounds, the differences in the Raman spectra of polymorphic forms could be unambiguously assigned to the simulations. The modeling revealed that the spectral differences were caused by the molecular structure itself as well as by crystal packing. The relative importance of these factors significantly varied across the investigated samples. Owing to its simplicity, Raman spectroscopy appears to be a promising technique capable of reliable discriminating between organic crystal polymorphic states.
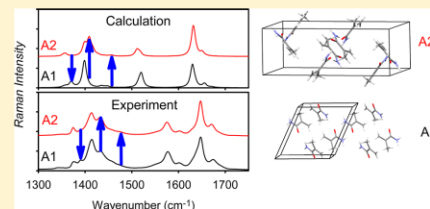
■ INTRODUCTION

Many elements, ionic compounds, or molecules can form crystals of more than one structure. This behavior, polymorphism, is also encountered in single-component organic crystals.[1] Individual crystal forms can then exhibit different physical or even chemical properties.[2] The identification of polymorphic forms is therefore of crucial importance, for example, in the pharmaceutical industry. Various pharmaceutical processes yield different polymorphs, hydrates, and solvates of drugs.[3−5] In particular, the crystalline state of a given compound influences its bioavailability, or just the production cost, as it may be easier to make drugs from one polymorph than from another. Drug regulatory authorities such as FDA in USA demand information about polymorphism before granting licenses for product distribution. Even patents have been made on the basis of the discovery of new polymorphs.[6−8]

Apart from polymorphs that have the same molecular composition, organic substances can form various solvates or hydrates, which is sometimes referred to as pseudopolymorphism.[9] Inclusion of more than one molecule in the asymmetric part of the unit cell ($Z' > 1$) represents yet another interesting crystal variation.[10,11] Complementary to the standard diffraction methods, the ^{13}C cross-polarization (CP) magic-angle spinning (MAS) NMR is also an efficient way of determining Z' by means of comparing the number of observed resonances with the number of nonequivalent carbon atoms present in the molecule.[5,12] Polymorphic crystals were also successfully studied by neutron diffraction.[13]

In the present study, we explore the potential of Raman spectroscopy to reliably distinguish three model polymorphic crystals. The low-resolution spectroscopic methods are often more practical than the X-ray diffraction or NMR, e.g., samples are easier to prepare and/or a smaller amount is required, and the spectra can be collected faster. Raman scattering is very sensitive to fine structural details in crystals and is thus increasingly used in analytical chemistry.[14−19] It measures the relative intensity of scattered light as dependent on its shift from the laser excitation frequency, usually caused by

vibrational motions in molecules. In terms of sample preparation, the Raman technique resembles X-ray powder diffraction, where polycrystalline samples are used as well.

Lately, the vibrational Raman spectroscopy in the solid state has been boosted by the possibility to reliably simulate spectra of infinite periodic systems by accurate quantum-chemical methods. In particular, the plane-wave density functional theory (DFT) methodology is convenient as it allows for the crystalline translational symmetry.[20] However, we are not aware of any systematic accuracy test with respect to the discrimination of the polymorphic crystal vibrational spectra. Especially for organic molecules bound by weak crystal forces, high-precision computations are required to detect the finer crystal structure differences.

To assess the potential for structural studies for the Raman experiment combined with the computations, we chose methacrylamide (A), piracetam (B), and 2-thiobarbituric acid (C) as model molecules representing typical organic systems forming polymorphic crystals (Figure 1). The differences
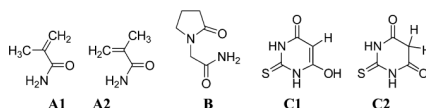
Figure 1. Methacrylamide (**A1** and **A2**, *s-cis* and *s-trans* conformers), piracetam (**B**), and 2-thiobarbituric acid (**C1** and **C2**, enol and keto forms) as model molecules examined in the present study.

between their polymorphs range from a subtle change in the crystal packing (piracetam) over conformational (methacrylamide) and tautomeric (2-thiobarbituric acid) variations. Within DFT, we model Raman spectra of isolated molecules as well as take into account the crystal environment of model systems. A cluster crystal model and a periodic-boundary condition plane-wave computation are employed.

The industrially important compound methacrylamide is, for example, a key intermediate in the acetonecyanohydrin process employed in manufacturing methyl methacrylate.[3] Of the two known polymorphs, the monoclinic form I (denoted here as **A1**) contains only the *s-cis* molecules, whereas the ortho-rhombic form II (**A2**) is exclusively formed by the *s-trans* conformer.[3]

Similarly, piracetam (2-oxo-pyrrolidineacetamide) is a nootropic agent, currently marketed by UCB Pharma as Nootropil. It is used to treat the age-related mental decline and similar disorders of the nervous system. Five polymorphs have been identified and their structures determined.[21] Among them, stable forms II (**B1**, triclinic, of *P*-1 symmetry) and III (**B2**, monoclinic, *P21/n*) can be prepared by recrystallization from various solvents under ambient conditions. For example, propan-2-ol and methanol provide forms II and III, respectively. Crystal structures of both forms have also been reported.[22,23] Unlike in **A**, however, molecular conformations **B1** and **B2** are almost identical. Two approximately planar parts, the pyrrolidine ring and the acetamide group (Figure 1), are almost perpendicular. The crystals are formed from dimers linked by two N–H···O hydrogen bonds. The crystal packing of the two forms looks quite similar if projected on the *ac* or *bc* crystallographic planes and differs most if observed along the *c*-axis (projection to *ab* plane).

Above 400 K both forms transform into form I (triclinic, *P*-1),[21,24] which at ambient temperature can be converted to phase II. High-pressure recrystallization of aqueous and methanolic solutions of piracetam resulted in the formation of yet another high-pressure polymorph IV, structurally characterized by single-crystal X-ray diffractometry.[21] A compression of form II by 0.45–0.70 GPa causes a reversible single-crystal to single-crystal transition to the last form V.[21]

As for 2-thiobarbituric acid, a substance valued since long time for its pharmacological properties,[25] six polymorphs have been isolated and characterized.[26,27] We have chosen forms II (**C1**) and III (**C2**) that can be prepared by recrystallization from absolute ethanol and dry acetonitrile, respectively. In **C1**, the molecules are present in the enol form, whereas only the keto isomer is present in **C2**. The other 2-thiobarbituric polymorphs and a hydrate also contain these two isomers; details can be found elsewhere.[26]
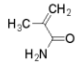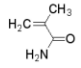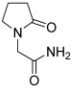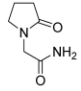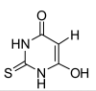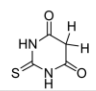
■ METHODS

Crystal Preparation, X-ray, and NMR Characterization.
Methacrylamide, piracetam, and 2-thiobarbituric acid were obtained from Sigma-Aldrich, and samples of different polymorphs were prepared as described in the literature listed above. Briefly, crystals of **A1** were obtained by recrystallization from a hot chloroform solution, and **A2** was prepared by slow cooling of warm water solution of methacrylamide. **B1** and **B2** were obtained by recrystallization of piracetam from propan-2-ol and methanol solutions, respectively. Polymorphs **C1** and **C2** were obtained by recrystallization of 2-thiobarbituric acid from dry ethanol and dry acetonitrile, respectively. Sample **C2** contained traces of **C1** (~5%), and its contribution was subtracted from each resultant Raman spectrum of **C2**. Solid-state NMR spectra were recorded with Bruker Avance II 500 spectrometer operating at 499.8 MHz in the ^{1}H and at 125.7 MHz in the ^{13}C experiments, using rotors 3.2 mm in diameter. The chemical shifts were referenced to crystalline α-glycine as a secondary reference (δ_{st} = 176 ppm for carbonyl group carbon). The ramped amplitude shape pulse was used during the cross-polarization. The contact time in the basic ^{13}C experiments was 2 ms, the relaxation delay 4 s, and the spinning rate 12 kHz. The identity of the methacrylamide sample was also verified by X-ray measurement on KappaCCD four-circle diffractometer with a CCD area detector and Mo Kα radiation. The structures were solved by direct methods[28] and refined by full-matrix least-squares based on F2[29] with absorption neglected.

Raman Experiments.
Solid-state Raman spectra within the 100–2000 cm^{-1} range were collected with BioTools ChiralRA-MAN-2X instrument based on a design of Hug[30] (532 nm excitation wavelength, 32–128 scans, 1.03 s illumination time, laser power at sample 50–300 mW) and processed using in-house software.[31] Calibration was carried out with a neon lamp and verified with crystalline α-glycine. First, one polymorph was recorded and then the second one; this was repeated three times. As another control, the mixture of both polymorphic materials was measured and compared with individual polymorphs. Polycrystalline samples were measured in fused silica sample cell.

Alternatively, a near-infrared (NIR) Fourier spectrometer Equinox 55/S fitted with a Raman module FRA 106/S (Bruker, Germany) was employed to collect spectra excited by a Nd:YAG laser (1064 nm excitation, 1024 or 2048 scans, 2 cm^{-1} resolution, at least four spectra were averaged per sample).

Table 1. Overview of Studied Compounds and Their Crystal Structure

	Compound	Form **1**	Crystal[a] $a\,b\,c$ (Å) $\alpha\,\beta\,\gamma$ (deg.)	Form **2**	Crystal[a] $a\,b\,c$ (Å) $\alpha\,\beta\,\gamma$ (deg.)
A	methacrylamide Ref. [3]		WANSAG02 9.365 6.086 9.743 90.00 115.30 90.00		WANSAG01 5.934 10.242 16.436 90.00 90.00 90.00
B	Piracetam Ref. [22]		BISMEV 6.403 6.618 8.556 79.85 102.39 91.09		BISMEV01 6.525 6.440 16.463 90.00 92.19 90.00
C	2-thiobarbituric acid Ref. [26]		PABNAJ 9.874 8.776 7.066 90.00 109.30 90.00		THBARB01 9.523 7.703 8.002 90.00 105.68 90.00

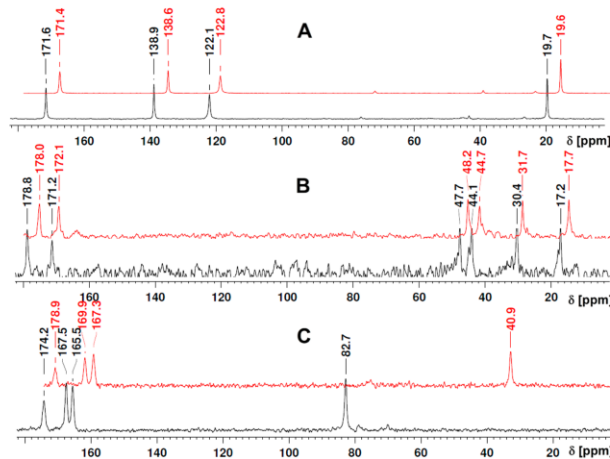[a]Cambridge Structural Database ID and unit cell parameters.

Figure 2. ^{13}C solid-state NMR spectra of polymorphic crystals. From top to bottom: **A1** vs **A2**, **B1** vs **B2**, and **C1** vs **C2**. For clarity, the forms **A1**, **B1**, and **C1** are plotted in red and offset by ~4 ppm; in **A**, the three low-intensity signals in the 20−80 ppm region correspond to spinning side bands of the sp[2] carbon atoms.

Powdered sulfur was used as a reference sample to check the wavenumber scale. A ChiralRAMAN-2X spectrometer provided a stronger signal, whereas the NIR-excited measurement reduced the fluorescence and provided a wider range of frequencies (−300 to 4500 cm^{-1}). The NIR Raman spectra are shown by default.

Raman and NMR Spectra Calculations. The atomic coordinates of the polymorphs of methacrylamide, piracetam, and 2-thiobarbituric acid were derived from the Cambridge Crystallographic Database[32] (see Table 1 for the reference codes). The shielding values of the infinite crystals, harmonic force fields, and Raman intensities were calculated by using the CASTEP program.[33] The calculations were based on X-ray structures with positions of all atoms optimized by energy

minimization; the experimental lattice parameters were kept fixed. The generalized gradient approximation (GGA) functional of Perdew, Burke, and Ernzerhof (PBE)[34] and norm-conserving pseudopotentials were employed. Harmonic force field and Raman intensities within the periodic boundary conditions[35] were calculated at the same level as for the optimization. To verify reliability of the results, two combinations of the plane-wave cutoff energy and Monkhorst−Pack[36] grid spacing were applied (600 eV and 0.08 Å^{-1} and 900 eV and 0.05 Å^{-1}; the latter setup providing better results on average is presented by default). With the optimized geometries, NMR shielding was calculated using the gauge-including projector-augmented wave approach (GIPAW)[37] and the "on the fly" pseudopotentials at 550 eV cutoff.[38]
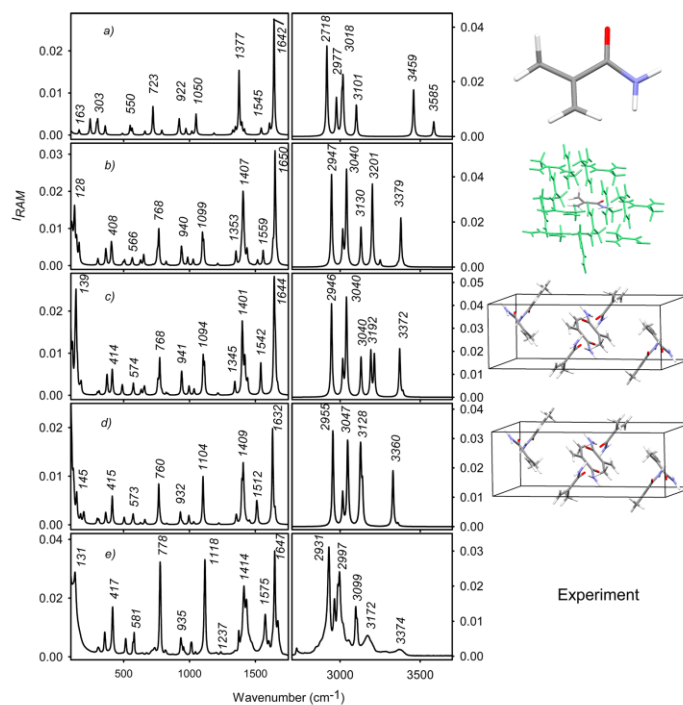
Figure 3. Raman spectra of methacrylamide, **A2**, computed for (a) single molecule and (b) a cluster. The (0,0,0) mode signals of the periodic elementary cell are in the (c) and (d) panels, while (e) is the experimental spectrum. Spectra a–c were obtained at the B3PW91/6-311++G**/6-31G/CPCM level and x-scaled by a factor of 0.96; (d) was obtained by the plane-wave simulation with the PBE functional.

As an alternative to the CASTEP "plane-wave" (PW) approach described above, we computed the Raman spectra with a cluster model and Gaussian atomic orbitals. First, the crystal cell obtained for each simulated system from the database was propagated to a "3 × 3 × 3" packing geometry, replicating elementary cell directions. Then clusters of a molecule chosen in the center and neighboring molecules closer than 4 Å were created with our own software. Finally, the geometries of the clusters were optimized in normal mode vibrational coordinates[39,40] with ω_{max}[41] of 300 cm^{-1}. Note that such constrained optimization leaves the crystal geometry virtually unchanged, whereas the vibrational coordinates relevant to Raman spectrum (frequencies typically greater than ω_{max}) can be relaxed.

The force field and polarizability derivatives of the clusters were then calculated by the Gaussian[42] program and transferred[43,44] back to the crystal cell. The BPW91[45] functional with the 6-31G and 6-31G** basis sets and the B3PW91[46,47] functional with the 6-311++G** and 6-31G basis sets for the central and neighboring molecules, respectively, were used. The reduction of the basis set was necessary to obtain results in a reasonable computational time. Supposedly, however, the effect

of this approximation on the precision is limited as the diagonal force constants most important for the vibrational frequencies[48] were obtained from the central molecule with the larger basis set. The results were quite similar given the differences between the polymorphic forms; only the B3PW91/6-311++G**/6-31G calculations are shown, with the surrounding crystal environment simulated by placing the clusters in the CPCM model solvent[49] with relative electric permittivity $\varepsilon_r = 78$. We used the water permittivity as reported earlier[50] to approximately mimic the dielectric properties of polar organic crystals. While the CPCM correction provided slightly better results than vacuum computations, we verified that the simulated spectra were fairly independent of the variation of ε_r.

From the plane wave model and cluster force fields, zero (0, 0, 0) crystal phonon mode vibrational frequencies were calculated. Involvement of phonon modes with nonzero wave vectors had a negligible effect on the simulated intensities. Theoretical spectra were simulated with the Lorentzian bands, and the full width at half-maximum (Δ) was set 10 cm^{-1}, while applying the Boltzmann temperature correction. The spectrum at frequency ω was obtained from the computed backscattering Raman intensities (I_{180}) of each mode i with the harmonic
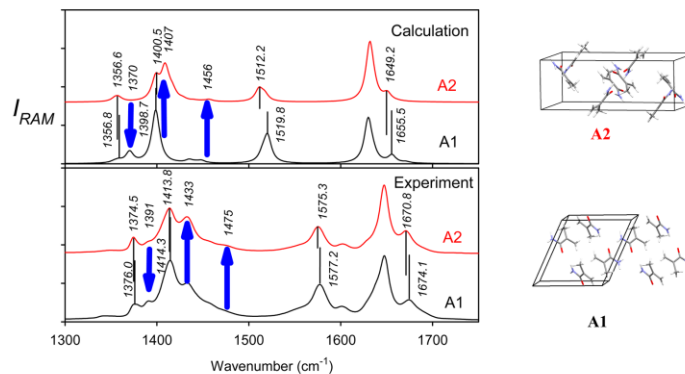
Figure 4. Calculated (top, plane wave) and experimental (bottom, NIR) Raman spectra of the two methacrylamide crystal forms, within 1300−1750 cm^{-1}. Main intensity changes are indicated by the blue arrows; selected peak maxima are indicated.

vibrational frequency ω_i as $S(\omega) = \omega_i^{-1}\{1 - \exp[-\omega_i/(kT)]\}^{-1}\{4[(\omega - \omega_i)/\Delta]^2 + 1\}^{-1}I_{180}$, where k is the Boltzmann constant and T is the temperature.

■ RESULTS

NMR Analysis. The NMR results were not the focus of the present study, as the detection of polymorphic forms by this technique has been previously described for a number of compounds.[5,26,51] In Figure 2, ^{13}C solid-state NMR spectra of polymorphic forms of methacrylamide (**A1**, **A2**), piracetam (**B1**, **B2**), and 2-thiobarbituric acid (**C1**, **C2**) are plotted. It can be clearly seen that the crystal packing induces specific shielding; i.e., the samples used in the Raman measurement correspond to the required forms.

Curiously, only nonpure preparations of methacrylamide batches, i.e., those also containing one or the other form, have been described so far.[3] As it is apparent from the NMR spectra (Figure 2), we did obtain pure forms of this compound. However, when sample **A2** (prepared from water solution) was not completely dried before the CP-MAS experiment, it slowly transformed to **A1**. The process could be monitored in a series of successive CP-MAS spectra, in which the **A2** signals were decreasing while the **A1** ones were increasing. The **A2** to **A1** transformation may have been facilitated by the combined effect of residual solvent and higher pressure in the MAS rotor spinning at 12 kHz because it was not observed when the sample was dry or wet and stored without spinning.

The calculations reproduce the experimental differences in chemical shifts of the polymorphic forms quite well. Except for one atom, all predicted signs agree with the experiment, with a small average error of 1.5 ppm (δ, see Table S1). These results are in accord with our earlier study, where the solid state NMR spectroscopy was found to be very suitable for identification of the polymorphic forms and the crystal packing.[51] The crystal packing is reflected in the chemical shift in two ways; it directly affects the electronic shielding by neighboring molecules and the geometry or conformational changes due to the packing itself.[52,53] Either of these contributions can be estimated by the comparison shifts calculated for an isolated molecule (while employing either X-ray data or optimized geometry; see second

and third column in Table S1). However, as expected, the full periodic boundary computation (fourth column in Table S1) is needed to reach the best agreement with the experiment.

Theoretical Models Adopted for Raman Spectra. To understand the Raman spectral pattern, we adopted various models for its simulation. This is exemplified by the spectra of the **A2** form plotted in Figure 3. The single-molecule computation performed at the B3PW91/6-31++G**/CPCM level (panel a in Figure 3) is compared to the spectrum of the cluster (b). In addition, the elementary cell signal was obtained from (b) by the CCT transfer[44] (c) and as the plane-wave PBE result (d). The experiment is plotted in panel e. The B3PW91 frequencies were scaled by a factor of 0.96 for an easier comparison.

The effect of the packing interactions is clearly manifested in spectra shown in Figure 3. The isolated molecule (a) provides the basic spectral pattern; however, it deviates in some features from the experiment (e). For example, there is no signal (except for the weak band of methyl rotation at 163 cm^{-1}) at the lowest wavenumbers, unlike in the experiment with a strong peak at 131 cm^{-1}; the experimental band at 1575 cm^{-1} does not have a clear counterpart in the simulation, and the simulated bands at 3459 and 3585 cm^{-1} (in- and out-of-phase NH stretching, respectively) are too high.

The cluster model (b) provides a more realistic spectrum. In particular, the lowest wavenumber (∼100−600 cm^{-1}) signal rises and is better structured than on (a), which reflects the crystal packing forces. These modes are to a large extent composed of delocalized translations/rotations of various molecular parts. Also, the NH out-of-phase stretching frequency dramatically falls to 3379 cm^{-1}, and the in-phase mode (3201 cm^{-1} in (b)) is even below the CH$_2$ group stretching. This corresponds to the uneven length of the NH···O hydrogen bonds in the crystal, 2.029 and 2.093 Å,[3] contributing to the splitting of the NH stretching modes. It is also interesting to note that the PCM approximation of the bulk crystal adopted for the single-molecule spectrum a does not adequately represent the NH stretching frequency affected by the hydrogen bonding. Such inability of the polarizable continuum solvent models to fully describe the directional and

partially covalent hydrogen bonds has been well documented elsewhere.[54−60]

Finally, spectra c and d obtained from the periodic elementary cell and the (0, 0, 0) phonon mode are the most realistic ones. The cluster-based model (c) provides a more realistic hydrogen-stretching pattern, in particular the 3192 cm^{-1} signal observable at 3172 cm^{-1}, and intensities above 1200 and below 200 cm^{-1}. On the other hand, some features, mostly within 200−1200 cm^{-1}, are better reproduced by the plane-wave calculation (d).

A visualization of the normal mode displacement reveals an interesting shift of the amide I (C=O stretching) mode, in the single-molecule (a) hidden at the signal around 1642 cm^{-1}. This vibration heavily mixes with the in-phase NH bending and shifts downward in the crystal, to 1542 cm^{-1} for the cluster model c, experimentally at 1575 cm^{-1}. Note that the plane-wave approach can take into account the longer-scale electron conjugation and periodicity of the crystal structure, whereas the cluster model comprises interactions of the neighboring molecules only. On the other hand, the cluster approach enables one to use a more advanced functional (B3PW91, containing the Hartree−Fock exchange) and the more economical Gaussian basis set.

A1 and A2 Polymorphs. The differences between the individual polymorph spectra of methacrylamide (**A1** vs **A2**, calculation vs experiment) are documented in Figure 4 showing the 1300−1750 cm^{-1} interval where the most significant spectral changes occurred. As it can be seen, individual polymorphs of this molecule differ in minor shape changes of the Raman bands.

The relative intensity and frequency changes between individual peaks in **A1** and **A2** spectra can easily be inspected visually (Figure 4). Experimentally, for example, the intensity at 1374.5 cm^{-1} of **A2** partially moves to 1391 cm^{-1} for **A1**. Corresponding calculated peaks at 1356.6 and 1370 cm^{-1} reveal that this is caused by changes in mode coupling, rather than by shifts of the vibrational frequencies themselves. In particular, the CH_3 umbrella CH bending vibrations (experimentally $\sim$1376 cm^{-1}) couple differently with the other modes (NH_2, CH_2 bending, C−C stretching), providing thus the intensity boost at 1370 cm^{-1} in **A1**.

Similarly, another strong signal for **A2**, experimentally at 1433 cm^{-1}, calculated at 1407 cm^{-1}, originates in CH scissoring modes coupled with other CH bending and C−C stretching. A minor band of **A2** at 1475 cm^{-1} is caused primarily by CH_3 scissoring vibrations. The calculated band at 1512.2 cm^{-1} in **A2** shifts to 1519.8 cm^{-1} in **A1**, as in experiment, although the observed change is smaller and the absolute frequency higher, at $\sim$1576 cm^{-1}. Because this frequency is underestimated in the cluster model as well (e.g., at 1542 cm^{-1}, spectrum c, Figure 3), the lack of anharmonic corrections in the model is the most likely scenario. Presently, we are not aware of any other method providing reliable anharmonic corrections for systems of this size.

It is important to understand that the main differences in the polymorphic spectra have in this case their origin in the crystal packing. The cis and trans conformations of individual methacrylamide molecules provide different spectra (cf. Figure S1) but do not explain the crystal features (Figure 3) or the polymorphic differences (Figure 4). Interestingly, the **A1** and **A2** crystal Raman spectra (see Figure S2 for a comparison in the entire range of frequencies) resemble more each other than those of the isolated cis and trans conformers (Figure S1). In

other words, crystal packing appears to smear the differences in the spectra of individual isomers.

Polymorphs B1 and B2. Piracetam behaves somewhat differently than methacrylamide. The **B1** and **B2** polymorphic forms are composed of very similar rotamers. The conformation in which the amide group is approximately perpendicular to the nearly planar five-membered ring is also conserved. The differences in the Raman spectra primarily arise from the different crystal packing, with the P-1 symmetry in **B1** and $P21/n$ in **B2**. Even then, the packing is quite similar,[22] with a piracetam dimer being the basic unit held together by a dispersion attraction of the five-membered rings, and by hydrogen bonds between the NH_2 and exocyclic carbonyl groups. In **B1**, the dimer hydrogen bonds are slightly shorter (1.953 Å), and the ring is slightly more puckered than in **B2** (cf. the $N-C_O-C-C$ angle of 7°, Figure 5).
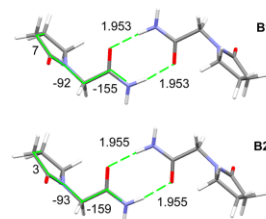

Figure 5. Piracetam dimer structure in two polymorphic crystal forms (distances in Å, torsional angles in deg).

The great degree of similarity between **B1** and **B2** causes only minor changes in the Raman spectra. The small effect of the packing on the spectra in an organic crystal is in agreement e.g. with a recent study[61] about vibronic effects and solid state circular dichroism. However, as it can be seen in Figure 6 where the experiment from the 1064 nm excitation is compared to the plane-wave calculation, the differences exhibited as fine frequency and intensity changes occur within the entire range of frequencies and are reasonably matched by the computation.
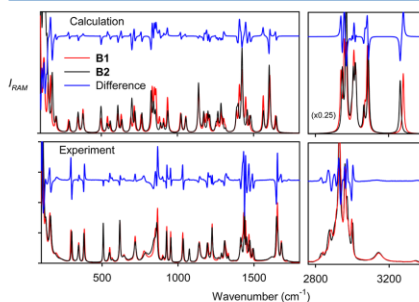

Figure 6. Calculated (top) and experimental (bottom) Raman spectra of the piracetam polymorphs **B1** and **B2**. The intensity scale is arbitrary, but consistent in calculation and experiment; the intensities in the upper right panel are scaled down by a factor of 0.25.

The experimental spectrum obtained with the 532 nm laser is quite similar, and its comparison with a computed spectrum is shown in Figure S3. The correspondence between the simulation and the experiment is less clear in the hydrogen stretching region (2800–3400 cm^{-1}, Figure 6), most likely due to anharmonic forces[62] that are difficult to include in the computation.[63] However, the theory provides correct signs of the intensity shifts of most bends including the most important intensity features of the difference spectrum plotted in Figure 6 in blue.

Alternatively, one can inspect the frequency change of individual vibrational bands for the two polymorphic forms. This analysis is more laborious than visual comparison of intensities as the corresponding peaks need to be identified. Nevertheless, as shown in Figure 7 where 10 vibrational bands
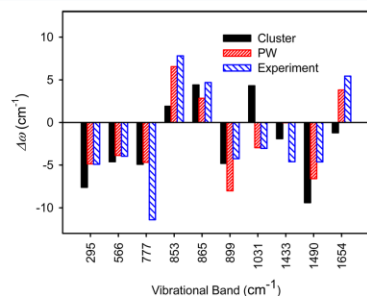

Figure 7. Ten largest frequency differences in the Raman bands between piracetam polymorphs, $\Delta\omega = \omega(\mathbf{B1}) - \omega(\mathbf{B2})$, calculated by the cluster and plane-wave method, and measured experimentally.

with the largest changes were selected, the frequency changes can also be quite reliably reproduced by the calculations. The plane-wave method appears to be more reliable than the cluster model; the latter one even yielded a frequency difference for the 1031 cm^{-1} Raman band with a wrong sign. Overall, however, the main trends are reproduced well. The large differences between the computation and experimental changes for 777 and 1433 cm^{-1} bands are at least partially explicable by an interference of close vibrations, indistinguishable at the currently available experimental resolution. On average, the changes computed by the PW method match the experiment with an error of only about 2 cm^{-1} and correlation coefficient of 0.739; the cluster results are noticeably worse (Figure S4).

The higher frequency (>2000 cm^{-1}) modes were not included in the statistics as they are difficult to assign and prone to anharmonic perturbations.[62,64] Quite often, modes involving large hydrogen atom movements provide the largest frequency differences. These include the backbone torsion and CH$_2$ group rotation (experimentally at 295 cm^{-1}), NH$_2$ bending (853 cm^{-1}), torsion (865 cm^{-1}), or CH$_2$ scissor modes (1433 and 1490 cm^{-1}). The modes involving the amide oxygen (out-of-plane deviation at 566 cm^{-1} and C=O stretching at 1606 cm^{-1}) also provide large frequency differences of about 5 cm^{-1} (Figure 7).

On piracetam, we can also demonstrate the effect of the energy cutoff and grid size on the computed Raman spectra (Figure S5). Both computational setups provided a reasonable

spectral shape, and for some bands the cruder model (500 eV, 0.08 Å) gave a better agreement with the experiment than the finer one (900 eV, 0.05 Å). However, the finer setup clearly performed overall better in terms of frequencies and relative peak intensities. The differences between the two polymorphic forms were significantly overestimated by the cruder model. Higher computational precision is thus required to capture the tiny differences in Raman spectra, as caused by crystal packing.

2-Thiobarbituric Acid Polymorphs C1 and C2. This compound exhibits yet another behavior than the previous two systems, with the greatest differences among the Raman spectra of its polymorphs. The simulated (plane-wave) and NIR Raman experimental spectra are plotted in Figure 8. In the hydrogen stretching region (~2800–3300 cm^{-1}), for example, the **C1** form has only one distinct peak in the experimental spectrum (3104 cm^{-1}), whereas **C2** has three. This observation corresponds to the more extensive hydrogen bond network only compatible with the enol form **C1** (cf. Table 1).[26] Computation yields more peaks in this region, but we can suppose that the NH stretching signals (3110, 3126, and 3222 cm^{-1} in Figure 8) are manifested as a broad background only in the experiment, due to the strong anharmonic effects and polarity of the hydrogen bond, similarly as for the OH stretching.

The plane-wave computation provided an unreasonable value of the OH stretching frequency (~2000 cm^{-1}, not shown), most probably due to the inaccuracy of the PBE functional unable to describe the very short hydrogen bond and a rather long OH bond observed in the crystal. The =O···H and O–H distances were determined as 1.44 and 1.097 Å, respectively.[26] Indeed, the OH vibration can be better reproduced with the cluster model where the B3PW91 functional can be used and where the signal at 2000 cm^{-1} disappears. However, this does not improve the overall agreement with the experiment (cluster computation, Figure S6). As expected, the single-molecule spectra, also plotted in Figure S6, are not realistic either. Most probably, the weak experimental signals of the OH and NH stretching bands are caused by anharmonic interactions and consequent inhomogeneous band broadening; the experimental band at 3104 cm^{-1} can then be assigned to C–H stretching.

In the experimental Raman spectrum of **C2**, three strong bands appear in the high-frequency region (Figure 8). The peaks at 2874 and 2979 cm^{-1} are reproduced by the calculation (2886 and 3036 cm^{-1}) as C–H stretching bands. Interestingly, the rather unusual low frequency of the experimental 2874 cm^{-1} band seems to be caused by a weak hydrogen bond involving an aliphatic hydrogen and keto group oxygen. The third experimental band at the highest frequency (3097 cm^{-1}) is reproduced as a split 3108/3131 cm^{-1} signal, which unmasks yet another loophole in the theory regarding the polar hydrogen bonding.

The spectra of the **C1** and **C2** forms are even more complex in the lower-frequency region (<1800 cm^{-1}, Figure 8), and the theory can faithfully reproduce only some experimental features. It should be also noted that the experimental spectrum **C1** may contain incompletely subtracted contributions from **C2**. However, by a careful comparison, a reliable assignment of most peaks is possible. Only the **C2** form provides the C=O stretching ("amide I") peak at 1717 cm^{-1} in the experiment, reproduced at 1657 cm^{-1} by the model. In **C1**, this mode is mixed with C=C stretching, providing only a weak signal as reproduced by the calculation. The amide II mode (largely N–C stretching) shifts from the experimental 1553 cm^{-1} peak in
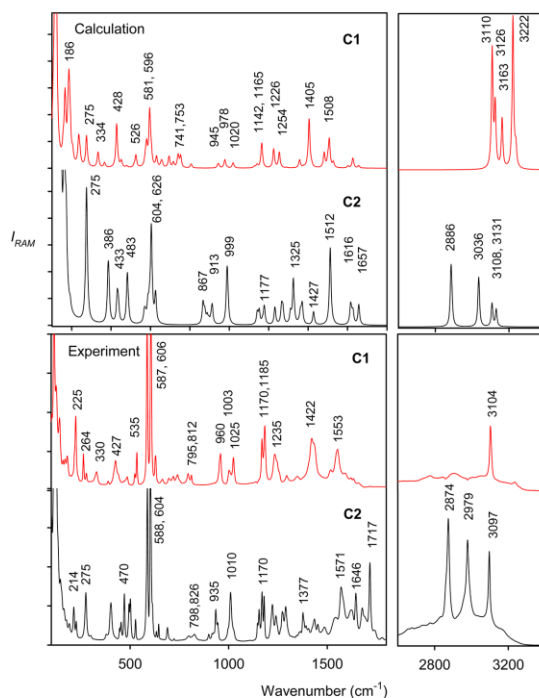
Figure 8. 2-Thiobarbituric acid: calculated (plane-wave) and NIR experimental Raman spectra of the two polymorphic forms **C1** and **C2**.

C1 to 1571 cm^{-1} in **C2**, similarly as in theory (1508 → 1512 cm^{-1}). A ring deformation in **C1** gives a strong signal both in the theoretical (1405 cm^{-1}) and observed (1422 cm^{-1}) spectrum, similarly as for the CH$_2$ scissoring mode in **C2** (exptl 1377 cm^{-1}, calcd 1325 cm^{-1}). The experimental C=S stretching band moves down from 1025 cm^{-1} (**C1**) to 1010 cm^{-1} (**C2**), as does the theoretical one (1020 → 999 cm^{-1}). A visual inspection of the normal modes reveals that C=S stretching is also mixed with C=N stretching, contributing to the signal around 1170 cm^{-1}.

A rather specific signal, clearly stronger in the **C2** form, is due to out-of-plane motions, such as NH bending; it is experimentally observed at 798–935 cm^{-1} and calculated at 867–913 cm^{-1}. The strongest experimental intensities, detected at 587–606 cm^{-1}, are underestimated by the computation. They originate in the out-of-plane C=O, C=S, and C–H group motions, which are notoriously difficult to describe within the harmonic approximation.[57,65] Finally, the lowest-wavenumber region is also rich in information, involving, for example, the 526/535 (calcd/exptl) cm^{-1} or the 428/427 cm^{-1} ring deformation band characteristic for **C1** and a very stable C=S bending frequency (experimentally at 264/275 cm^{-1} for **C1/C2**).

Although the polymorphic differences can be reliably reproduced by our models, an accuracy improvement is certainly still needed. It as very likely that the accuracy of the GGA force field and Raman intensities obtained within the PW computations represent the limiting factor; the cluster approach is more flexible in the basis set and functional choice but limited in the physical model. The absolute Raman intensities in particular are extremely sensitive to the basis set variations.[66] For the **C1/C2** polymorphic forms, a correction for anharmonic forces can potentially improve the hydrogen-stretching region (2800–3200 cm^{-1}). However, this is currently impossible for a system of this size. Additionally, larger deviations between the simulations and the experiment are also encountered in the lower-frequency region. Although this region is presumably well described at the harmonic level, frequency shifts of several cm^{-1} caused by anharmonic forces cannot be excluded. Future improvements of the method are thus dependent on the efficiency of implementing more precise electronic and vibrational quantum chemical methods.

Other structural information might also be hidden in the lattice modes, not analyzed in the present study. Our spectrometers do not enable measurement below ∼100 cm^{-1}. These vibrations are difficult to analyze because of the large background signal and a limited precision of calculated force

fields. Another important practical issue in the Raman spectra interpretation is the use of coordinates determined by X-ray diffraction. If one wants to replace X-ray spectroscopy, a pure a priory generation could be considered in the future for the initial coordinates as well. Currently, we propose the Raman technique as a convenient complementary way of examining the polymorphic forms in analytical practice.

CONCLUSIONS

We succeeded in preparing model polymorphic crystal forms of three model compounds including those of practical importance and characterized them by NMR and Raman spectroscopy. Pure polymorphs of methacrylamide were prepared, which has not been reported so far.

The NMR data confirmed sample purity and good performance of the technique in polymorphic discrimination. Raman spectroscopy proved to be an equally viable technique, as the spectra of different polymorphs exhibited distinct features that could be reliably reproduced by the density functional computations. Compared to green (532 nm) laser, excitation by a near-infrared one was somewhat more suitable as it suppressed sample fluorescence. The spectral shapes were similar in both experiments.

In spite of minor inconsistencies, the plane-wave approach, inherently comprising the crystal symmetry and periodicity, made it possible to reliably simulate spectral frequencies and intensities. Occasionally, the cluster-based computations were more advantageous as they could be combined with more theoretical approaches, in particular with different functionals. The studied examples represent a wide array of interpolymorphic differences manifested in the Raman spectra, from an almost pure crystal packing influence (piracetam) to profound changes in molecular structures (methacrylamide, 2-thiobarbituric acid). The computational models could successfully handle all cases, and we aim to further improve them so that even more complex systems can be reliably examined in the future. In any case, we demonstrated that Raman spectroscopy combined with computational modeling can significantly enhance the structural analysis of organic compounds' polymorphic forms.

ASSOCIATED CONTENT

ⓈSupporting Information

Calculated and experimental chemical shifts, additional computational and experimental details. This material is available free of charge via the Internet at http://pubs.acs.org.

AUTHOR INFORMATION

Corresponding Author

*E-mail: bour@uochb.cas.cz (P.B.).

Notes

The authors declare no competing financial interest.

ACKNOWLEDGMENTS

REFERENCES

(1) Bernstein, E. R. Polymorphism - a Perspective. *Cryst. Growth Des.* **2011**, *11*, 632−650.

(2) Grant, D. J. W. Theory and Origin of Polymorphsm. In *Polymorphysm in Pharmaceutical Solids*; Brittain, H. G., Ed.; Marcel Dekker, Inc.: New York, 1999.

(3) Guo, C. Y.; Hickey, M. B.; Guggenheim, E. R.; Enkelmann, V.; Foxman, B. M. Conformational Polymorphism of Methacrylamide. *Chem. Commun.* **2005**, *17*, 2220−2222.

(4) Anderson, K. M.; Steed, J. W. Comment on "On the Presence of Multiple Molecules in the Crystal Asymmetric Unit (Z′ > 1)" by Gautam R. Desiraju. *CrystEngComm* **2007**, *9*, 328−330.

(5) Harris, R. K. NMR Studies of Organic Polymorphs & Solvates. *Analyst* **2006**, *131*, 351−373.

(6) Saurabh, G.; Kaushal, C. Pharmaceutical Solid Polymorphism in Abbreviated New Drug Application (ANDA) - a Regulatory Perspective. *J. Chem. Pharm. Res.* **2011**, *3*, 6−17.

(7) Datta, S.; Grant, D. J. W. Crystal Structures of Drugs: Advances in Determination, Prediction and Engineering. *Nat. Rev. Drug Discovery* **2004**, *3*, 42−57.

(8) Wu, V.; Rades, T.; Saville, D. J. Stability of Polymorphic Forms of Ranitidine Hydrochloride. *Pharmazie* **2000**, *55*, 508−512.

(9) Seddon, K. R. Perspective - Pseudopolymorph: A Polemic. *Cryst. Growth Des.* **2004**, *4*, 1087−1087.

(10) Anderson, K. M.; Probert, M. R.; Whiteley, C. N.; Rowland, A. M.; Goeta, A. E.; Steed, J. W. Designing Co-Crystals of Pharmaceutically Relevant Compounds That Crystallize with Z′ > 1. *Cryst. Growth Des.* **2009**, *9*, 1082−1087.

(11) Rummel, R. J. *Applied Factor Analysis*; Northwestern University Press: Evanston, 1970.

(12) Aliev, A. E.; Mann, S. E.; Rahman, A. S.; McMillan, P. F.; Cora, F.; Iuga, D.; Hughes, C. E.; Harris, K. D. M. High-Resolution Solid-State 2H NMR Spectroscopy of Polymorphs of Glycine. *J. Phys. Chem. A* **2011**, *115*, 12201−12211.

(13) Langan, P.; Mason, S. A.; Myles, D.; Schoenborn, B. P. Structural Characterization of Crystals of Alpha-Glycine during Anomalous Electrical Behaviour. *Acta Crystallogr., Sect. B* **2002**, *58*, 728−733.

(14) Pagliai, M.; Miranda, M. M.; Cardini, G.; Schettino, V. Raman and Infrared Spectra of Minerals from Ab Initio Molecular Dynamics Simulations: The Spodumene Crystal. *J. Mol. Struct.* **2011**, *993*, 151−154.

(15) Dračínský, M.; Benda, L.; Bouř, P. Comparison of Fused Silica, Crystal Quartz, and Water Raman Spectra. *Chem. Phys. Lett.* **2011**, *512*, 54−59.

(16) McGrane, S. D.; Barber, J.; Quenneville, J. Anharmonic Vibrational Properties of Explosives from Temperature-Dependent Raman. *J. Phys. Chem. A* **2005**, *109*, 9919−9927.

(17) Schweitzer-Stenner, R.; Sieler, G.; Mirkin, N. G.; Krimm, S. Intermolecular Coupling in Liquid and Crystalline States of Trans-N-Methylacetamide Investigated by Polarized Raman and FT-IR Spectroscopies. *J. Phys. Chem. A* **1998**, *102*, 118−127.

(18) Kim, I.; Krimm, S. Raman Longitudinal Acoustic Mode Studies of Poly(Ethylene Oxide) and Alpha, Omega-Methoxylated Poly-(Ethylene Oxide) Fractions during Isothermal Crystallization from the Melt. *J. Polym. Sci., Part B: Polym. Phys.* **1997**, *35*, 1117−1126.

(19) Othman, S.; Richaud, P.; Vermeglio, A.; Desbois, A. Evidence for a Proximal Histidine Interaction in the Structure of Cytochromes C′ in Solution - a Resonance Raman Study. *Biochemistry* **1996**, *35*, 9224−9234.

(20) Frenkel, D.; Smit, B. *Understanding Molecular Simulation*, 2nd ed.; Academic: London, 2002.

(21) Fabbiani, F. P. A.; Allan, D. R.; David, W. I. F.; Davidson, A. J.; Lennie, A. R.; Parsons, S.; Pulham, C. R.; Warren, J. E. High-Pressure Studies of Pharmaceuticals: An Exploration of the Behavior of Piracetam. *Cryst. Growth Des.* **2007**, *7*, 1115−1124.

(22) Admiraal, G.; Eikelenboom, J. C.; Vos, A. Structures of the Triclinic and Monoclinic Modifications of (2-Oxo-1-Pyrrolidinyl)-Acetamide. *Acta Crystallogr., Sect. B* **1982**, *38*, 2600−2605.

(23) Bandoli, G.; Clemente, D. A.; Grassi, A.; Pappalardo, G. C. Molecular Determinants for Drug-Receptor Interactions. 1. Solid-State Structure and Conformation of the Novel Nootropic Agent 2-Pyrrolidone-N-Acetamide - X-Ray and Theoretical SCF-MO Studies. *Mol. Pharmacol.* **1981**, *20*, 558−564.

(24) Louër, D.; Louër, M.; Dzyabchenko, V. A.; Agafonov, V.; Céolin, R. Structure of a Metastable Phase of Piracetam from X-Ray-Powder Diffraction Using Atom-Atom Potential Method. *Acta Crystallogr., Sect. B* **1995**, *51*, 182−187.

(25) Bondock, S.; Tarhoni, A. E.; Fadda, A. A. *Phosphorus, Sulfur Silicon Relat. Elem.* **2007**, *182*, 1915−1936.

(26) Chierotti, M. R.; Ferrero, L.; Garino, N.; Gobetto, R.; Pellegrino, L.; Braga, D.; Grepioni, F.; Maini, L. The Richest Collection of Tautomeric Polymorphs: The Case of 2-Thiobarbituric Acid. *Chem.—Eur. J.* **2010**, *16*, 4347−4358.

(27) Calas, M. R.; Martinez, J. Determination de la Structure Cristalline de l'Acide Thiobarbiturique. *C. R. Acad. Sci., Ser. C* **1967**, *265*, 631−631.

(28) Altomare, A.; Cascarano, G.; Giacovazzo, C.; Guagliardi, A.; Burla, M. C.; Polidori, G.; Camalli, M. SIR92 - a Program for Automatic Solution of Crystal Structures by Direct Methods. *J. Appl. Crystallogr.* **1994**, *27*, 435.

(29) Sheldrick, G. M. A Short History of SHELX. *Acta Crystallogr., Sect. A* **2007**, *64*, 112−122.

(30) Hug, W.; Hangartner, G. A Novel High-Throughput Raman Spectrometer for Polarization Difference Measurements. *J. Raman Spectrosc.* **1999**, *30*, 841−852.

(31) Šebestík, J.; Bouř, P. Raman Optical Activity of Methyloxirane Gas and Liquid. *J. Phys. Chem. Lett.* **2011**, *2*, 498−502.

(32) Allen, F. H. The Cambridge Structural Database: A Quarter of a Million Crystal Structures and Rising. *Acta Crystallogr., Sect. B* **2002**, *58*, 380−388.

(33) Clark, S. J.; Segall, M. D.; Pickard, C. J.; Hasnip, P. J.; Probert, M. J.; Refson, K.; Payne, M. C. First Principles Methods Using CASTEP. *Z. Kristallogr.* **2005**, *220*, 567−570.

(34) Perdew, J. P.; Burke, K.; Ernzerhof, M. Generalized Gradient Approximation Made Simple. *Phys. Rev. Lett.* **1996**, *77*, 3865−3868.

(35) Refson, K.; Tulip, P. R.; Clark, S. J. Variational Density-Functional Perturbation Theory for Dielectrics and Lattice Dynamics. *Phys. Rev. B* **2006**, *73*, 155114.

(36) Monkhorst, H. J.; Pack, J. D. Special Points for Brillouin-Zone Integrations. *Phys. Rev. B* **1976**, *13*, 5188−5192.

(37) Pickard, C. J.; Mauri, F. All-Electron Magnetic Response with Pseudopotentials: NMR Chemical Shifts. *Phys. Rev. B* **2001**, *6324*, 245101.

(38) Yates, J. R.; Pickard, C. J.; Mauri, F. Calculation of NMR Chemical Shifts for Extended Systems Using Ultrasoft Pseudopotentials. *Phys. Rev. B* **2007**, *76*, 024401.

(39) Bouř, P.; Keiderling, T. A. Partial Optimization of Molecular Geometry in Normal Coordinates and Use as a Tool for Simulation of Vibrational Spectra. *J. Chem. Phys.* **2002**, *117*, 4126−4132.

(40) Bouř, P. Convergence Properties of the Normal Mode Optimization and Its Combination with Molecular Geometry Constraints. *Collect. Czech. Chem. Commun.* **2005**, *70*, 1315−1340.

(41) Hudecová, J.; Hopmann, K. H.; Bouř, P. Correction of Vibrational Broadening in Molecular Dynamics Clusters with the Normal Mode Optimization Method. *J. Phys. Chem. B* **2012**, *116*, 336−342.

(42) Frisch, M. J.; Trucks, G. W.; Schlegel, H. B.; Scuseria, G. E.; Robb, M. A.; Cheeseman, J. R.; Scalmani, G.; Barone, V.; Mennucci, B.; Petersson, G. A.; et al. *Gaussian 09, Revision B01*; Gaussian, Inc.: Wallingford, CT, 2009.

(43) Bouř, P.; Sopková, J.; Bednárová, L.; Maloň, P.; Keiderling, T. A. Transfer of Molecular Property Tensors in Cartesian Coordinates: A New Algorithm for Simulation of Vibrational Spectra. *J. Comput. Chem.* **1997**, *18*, 646−659.

(44) Yamamoto, S.; Li, X.; Ruud, K.; Bouř, P. Transferability of Various Molecular Property Tensors in Vibrational Spectroscopy. *J. Chem. Theory Comput.* **2012**, *8*, 977−985.

(45) Becke, A. Density-Functional Exchange-Energy Approximation with Correct Asymptotic Behavior. *Phys. Rev. A* **1988**, *38*, 3098−3100.

(46) Perdew, J. P.; Burke, K.; Wang, Y. Generalized Gradient Approximation for the Exchange-Correlation Hole of a Many-Electron System. *Phys. Rev. B* **1996**, *54*, 16533−16539.

(47) Becke, A. D. Density-Functional Thermochemistry. III. The Role of Exact Exchange. *J. Chem. Phys.* **1993**, *98*, 5648−5652.

(48) Bouř, P.; Andrushchenko, V.; Kabeláč, M.; Maharaj, V.; Wieser, H. Simulations of Structure and Vibrational Spectra of Deoxyoctanucleotides. *J. Phys. Chem. B* **2005**, *109*, 20579−20578.

(49) Klamt, A. COSMO and COSMO-RS. In *The Encyclopedia of Computational Chemistry*; Schleyer, P. R., Allinger, N. L., Clark, T., Gasteiger, J., Kollman, P. A., Schaefer III, H. F., Schreiner, P. R., Eds.; John Wiley & Sons: Chichester, 1998; Vol. *1*, pp 604−615.

(50) Kapitán, J.; Baumruk, V.; Kopecký, V., Jr.; Pohl, R.; Bouř, P. Proline Zwitterion Dynamics in Solution, Glass and Crystalline State. *J. Am. Chem. Soc.* **2006**, *128*, 13451−13462.

(51) Dračínský, M.; Buděšínský, M.; Warzajtis, B.; Rychlewska, U. Solution and Solid-State Effects on NMR Chemical Shifts in Sesquiterpene Lactones: NMR, X-Ray, and Theoretical Methods. *J. Phys. Chem. A* **2012**, *116*, 680−688.

(52) Dračínský, M.; Bouř, P. Computational Analysis of Solvent Effects in NMR Spectroscopy. *J. Chem. Theory Comput.* **2010**, *6*, 288−299.

(53) Uldry, A. C.; Griffin, J. M.; Yates, J. R.; Perez-Torralba, M.; Maria, M. D. S.; Webber, A. L.; Beaumont, M. L. L.; Samoson, A.; Claramunt, R. M.; Pickard, C. J.; Brown, S. P. Quantifying Weak Hydrogen Bonding in Uracil and 4-Cyano-4'-Ethynylbiphenyl: A Combined Computational and Experimental Investigation of NMR Chemical Shifts in the Solid State. *J. Am. Chem. Soc.* **2008**, *130*, 945−954.

(54) Ganim, Z.; Chung, H. S.; Smith, A. W.; Deflores, L. P.; Jones, K. C.; Tokmakoff, A.; Amide, I. Two-Dimensional Infrared Spectroscopy of Proteins. *Acc. Chem. Res.* **2008**, *41*, 432−441.

(55) Lee, K. K.; Hahn, S.; Oh, K. I.; Choi, J. S.; Joo, C.; Lee, H.; Han, H.; Cho, M. Structure of N-Acetylproline Amide in Liquid Water: Experimentally Measured and Numerically Simulated Infrared and Vibrational Circular Dichroism Spectra. *J. Phys. Chem. B* **2006**, *110*, 18834−18843.

(56) Choi, J. H.; Kim, J. S.; Cho, M.; Amide, I. Vibrational Circular Dichroism of Polypeptides: Generalized Fragmentation Approximation Method. *J. Chem. Phys.* **2005**, *122*, 174903.

(57) Andrushchenko, V.; Matějka, P.; Anderson, D. T.; Kaminský, J.; Horníček, J.; Paulson, L. O.; Bouř, P. Solvent Dependence of the N-Methylacetamide Structure and Force Field. *J. Phys. Chem. A* **2009**, *113*, 9727−9736.

(58) Bouř, P.; Michalík, D.; Kapitán, J. Empirical Solvent Correction for Multiple Amide Group Vibrational Modes. *J. Chem. Phys.* **2005**, *122*, 144501.

(59) Bouř, P. On the Influence of the Water Electrostatic Field on the Amide Group Vibrational Frequencies. *J. Chem. Phys.* **2004**, *121*, 7545−7548.

(60) Bouř, P.; Keiderling, T. A. Empirical Modeling of the Peptide Amide I Band IR Intensity in Water Solution. *J. Chem. Phys.* **2003**, *119*, 11253−11262.

(61) Pescitelli, G.; Padula, D.; Santoro, F. Intermolecular Exciton Coupling and Vibronic Effects in Solid-State Circular Dichroism: A Case Study. *Phys. Chem. Chem. Phys.* **2013**, *15*, 795−802.

(62) Daněček, P.; Bouř, P. Comparison of the Numerical Stability of Methods for Anharmonic Calculations of Vibrational Molecular Energies. *J. Comput. Chem.* **2007**, *28*, 1617−1624.

(63) Dračínský, M.; Bouř, P. Vibrational Averaging of the Chemical Shift in Crystalline α-Glycine. *J. Comput. Chem.* **2012**, *33*, 1080−1089.

(64) Temelso, B.; Shields, G. C. The Role of Anharmonicity in Hydrogen-Bonded Systems: The Case of Water Clusters. *J. Chem. Theory Comput.* **2011**, *7*, 2804−2817.

(65) Kapitán, J.; Hecht, L.; Bouř, P. Raman Spectral Evidence of Methyl Rotation in Liquid Toluene. *Phys. Chem. Chem. Phys.* **2008**, *10*, 1003−1008.

7306

dx.doi.org/10.1021/jp404382f | *J. Phys. Chem. B* 2013, 117, 7297−7307

(66) Zuber, G.; Hug, W. Rarefied Basis Sets for the Calculation of Optical Tensors. 1. The Importance of Gradients on Hydrogen Atoms for the Raman Scattering Tensor. *J. Phys. Chem. A* **2004**, *108*, 2108–2118.

7307

dx.doi.org/10.1021/jp404382f | *J. Phys. Chem. B* 2013, 117, 7297–7307

VIII.

Procházková, E. – Jansa, P. – Březinová, A. – Čechová, L. - Mertlíková-Kaiserová, H. – Holý, A. – Dračínský, M.:

Compound instability in dimethyl sulphoxide, case studies with 5-aminopyrimidines and the implications for compound storage and screening.

Contents lists available at SciVerse ScienceDirect

Bioorganic & Medicinal Chemistry Letters

Compound instability in dimethyl sulphoxide, case studies with 5-aminopyrimidines and the implications for compound storage and screening

Eliška Procházková, Petr Jansa, Anna Březinová, Lucie Čechová, Helena Mertlíková-Kaiserová, Antonín Holý, Martin Dračínský *

Institute of Organic Chemistry and Biochemistry, Academy of Sciences of the Czech Republic, Flemingovo nam. 2, 166 10 Prague, Czech Republic

ABSTRACT

The oxidation reactions of 5-aminopyrimidine derivatives in dimethyl sulphoxide (DMSO) were studied. The DMSO solutions of the studied compounds became deeply coloured within a few hours or days. The oxidation products can undergo further condensation reactions with the starting pyrimidines to yield bipyrimidines and/or pyrimidopteridines. The reaction mechanism of the oxidation-condensation reaction was also supported by reactions of the 5-aminopyrimidines with alloxan (2,4,5,6-tetraoxopyrimidine). DMSO is often used as the solvent in in vitro tests of biological activities, but it is also an oxidising agent and may react with solute molecules and significantly affect the quality of the generated biochemical data.

© 2012 Elsevier Ltd. All rights reserved.

Substituted pyrimidines play a key role in many biochemical processes; for instance, they form the basic building blocks of nucleic acids and are found in high-energy molecules with higher specificity than adenosine-5'-triphospate (ATP). Cytosine-5'-triphosphate (CTP) works as a coenzyme in glycerophospholipid synthesis or in glycosylation reactions of proteins.[1] Synthetically prepared aminopyrimidine derivatives display a wide range of biological activities such as antibacterial,[2] antitumor[3] and antiviral.[4,5] Therefore, the substituted aminopyrimidine structural motif can be found in diverse clinically approved drugs. Interestingly, a substituted aminopyrimidine moiety was also suggested to account for the antioxidant activity of folic acid, and this was hypothesised to play a role in the protective effects of folic acid against cardiovascular, neurological or haematological pathologies.[6]

In our previous work,[7] we studied the antioxidative activities of a series of 5-aminopyrimidines and observed that some of the compounds were unstable in DMSO solutions; within a few hours or days, the solutions coloured and the antioxidative activities decreased. The deleterious effect of DMSO on the performance of certain antioxidant assays owing to its ability to act as a hydroxyl radical scavenger has long been known.[8] However, when working with poorly soluble compounds, DMSO is sometimes impossible to avoid for in vitro screening. The feasibility of the use of DMSO

as a solvent in the evaluation of new potential antioxidants has been contradictory. Recent studies have suggested that DMSO is a tolerable vehicle in the antioxidant assays supposing that the relevant controls are provided and that the final DMSO concentration is kept below 5%.[9] However, the stability of the potential antioxidants in DMSO solutions is rarely addressed in the literature in spite of the
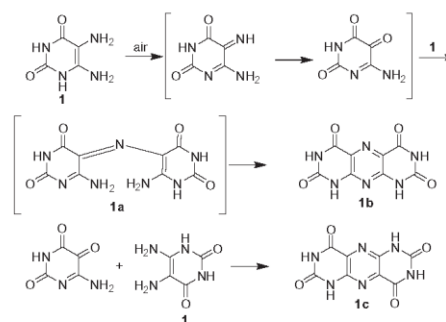
Scheme 1. The proposed reaction mechanism of the oxidative self-condensation of compound **1** in water in the presence of air.[10]

---

* Corresponding author. Tel.: +420 220 183 139; fax: +420 220 183 123.
E-mail address: dracinsky@uochb.cas.cz (M. Dračínský).

fact that DMSO is a redox-active agent theoretically capable of oxidising the tested compounds.

We hypothesise that DMSO could oxidise 5-aminopyrimidines similarly to other oxidation agents (e.g. air,[10] potassium ferricyanide[11] or mercury oxide[12]). The oxidative self-condensation of 5,6-diaminopyrimidines has been known for a long time.[10] The proposed reaction mechanism[10] is depicted in Scheme 1. The initial step of the reaction is the oxidation of the starting pyrimidine derivative (1) to the pyrimidine-quinone-imine, which may undergo hydrolysis under the reaction conditions to give quinone. Subsequent condensation of quinone-imine or the quinone with the 5-aminogroup of unchanged 1 can yield the bipyrimidine intermediate 1a, which can undergo third-ring closure by direct loss of ammonia or by preliminary hydrolysis followed by dehydration; the final product of the reaction is the pyrimidopteridine product 1b (bis-alloxazine). Alternatively, the condensation of quinone-imine or the quinone with the 6-aminogroup of unchanged 1 would lead to pyrimidopteridine 1c.[10]

The pyrimidopteridine products of the reaction are highly insoluble and deeply coloured. Several pyrimidopteridine derivatives were prepared as potential coronary vasodilators, but their pharmacological evaluation did not prove their clinical usefulness.[13] On the other hand, it is possible to use these pyrimidopteridines as electron-transfer particles, which work as low reduction potential flavin mimics.[14,15]

The aim of this work was to study the decomposition of 5-aminopyrimidines in DMSO solutions, to identify the products and to propose the reaction mechanism of the reactions.

The studied compounds were dissolved in DMSO and the solutions were stirred at room temperature. Immediately after dissolution, the solutions were colourless. Typically, deep colour changes were apparent within a few hours. The progress of the reactions was monitored by UV/VIS and NMR spectroscopy.

Compound 1 was transformed into a mixture of compounds 1b and 1c after stirring overnight in DMSO. The products are the same as in the previously described air oxidation of 1.[10]

The solution of compound 2 changed its colour to deep purple overnight. After two months, the purple colour changed to light yellow and a yellow precipitate appeared in the reaction mixture (see Fig. S2 in SI). In the UV/VIS spectra, we observed that compound 2 was first transformed into a purple intermediate product 2a (with absorption maxima at 347 and 550 nm) and within a few more days it was consequently converted into a yellow product 2b (with an absorption maximum at 397 nm), which is stable (see Fig. 1). The isosbestic point at 365 nm provides the evidence for the successive reactions taking place (2→2a→2b).

Figure 2. The time evolution of the ¹H NMR spectra of compound 2 in DMSO. The starting compound 2 (■) reacts in DMSO to generate the intermediate product 2a (●). Simultaneously, the ammonium cation occurs (○). Consequently, 2a is converted to the final product 2b (*).

The kinetics of these transformations were also monitored by ¹H NMR spectroscopy. For illustration, the time-response changes in the ¹H NMR spectra of compound 2 are displayed in Figure 2. The NMR signal of the starting compound (■; 6.35 ppm) practically disappears from the reaction mixture by day 7. The signal of the purple intermediate product 2a (●; 8.30 and 8.60 ppm) appears within only one day of incubation. On day 2, the signal of an ammonium cation is detected (○; 7.09 ppm, J = 51 Hz). In a few months, it is possible to observe the NMR signal of the final prod-
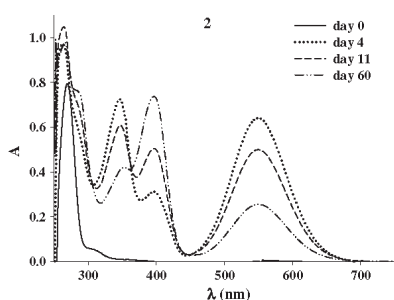

Figure 1. The changes in the absorption spectra of a 10 mM solution of compound 2 in DMSO over a period of two months at room temperature. For the UV/VIS spectra measurement, the solutions were diluted to 0.2 mM concentration.
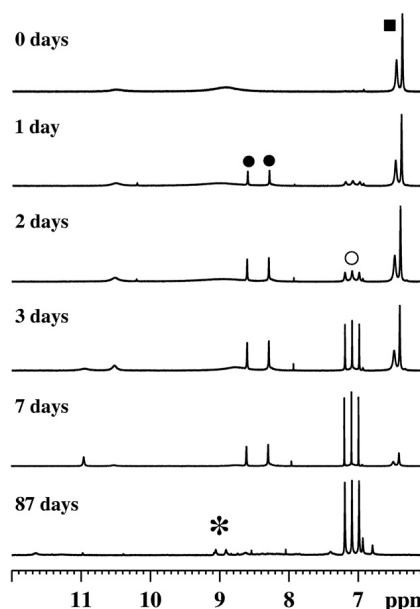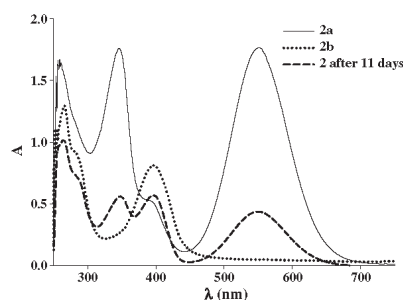

Figure 3. The absorption spectra characterising the individual products (2a, 2b) isolated from the DMSO solution of compound 2 compared to the DMSO solution of compound 2 standing at room temperature for 11 days.

uct of a successive reaction of **2a**, the yellow **2b** (*, 8.9 and 9.0 ppm). The low intensity of these signals is caused by the low solubility of **2b** in DMSO.

We isolated the two products of the reaction (**2a** and **2b**). The absorption spectra of the isolated products are shown in Figure 3. The absorption maxima of the individual products (**2a** and **2b**) are in agreement with the maxima observed in the reaction mixture after 11 days at room temperature, that is at 347 and 550 nm for **2a** and 397 nm for **2b**.

The high-resolution mass spectra (HRMS) revealed the compositions of the products **2a** and **2b** to be $C_8H_{10}N_9O_2$ and $C_8H_8N_9O$, respectively. The hydrolysis of compound **2b** with sodium nitrite and dilute hydrochloric acid yielded compound **1b** of molecular formula $C_8H_4N_6O_4$, the UV/VIS spectrum of which was identical with the previously published spectrum of bis-alloxazine.[10] The structures of compounds **2a** and **2b** together with the proposed mechanism of the oxidation reaction are depicted in Scheme 2. First, compound **2** is oxidised by DMSO to the pyrimidine-quinone-imine while an ammonium cation (which was observed in the ^{1}H NMR spectra) is released. The quinone-imine can subsequently condense with the 5-aminogroup of another molecule **2**, after which the intermediate **2a** can undergo a new ring closure to give **2b** as the final product of the reaction. In the ^{13}C NMR spectrum of compound **2a**, we observed four signals, which is in agreement with the proposed structure of **2a**, where the iminogroup of one ring can be in fast tautomer exchange equilibrium with the amino group of the second ring. Unfortunately, the very low solubility of pyrimidopteridines did not allow us to acquire the ^{13}C NMR spectrum of compound **2b**. Interestingly, we did not observe the formation of a condensation product analogical to the compound **1c**.

We performed the reaction also in dried DMSO under an inert atmosphere, and the reaction rates were unchanged. When the reaction was performed in larger quantities, the smell of dimethyl sulphide (DMS) was apparent. These observations are in agreement with the proposed mechanism. Interestingly, when the DMSO solution was alkalised with a drop of NaOH solution, we were not able to detect the purple intermediate **2a** and the reaction to **2b** was completed in 24 h. Conversely, when a drop of HCl was added to the DMSO solution, the reaction was slowed down.

The solution of tetraaminopyrimidine **3** in DMSO changed from colourless to orange overnight. The oxidation products of compound **3**, two constitutional isomers **3b** (yellow) and **3c** (red), were isolated and their absorption spectra were compared with the reaction mixture in DMSO (see Fig. S3 in SI). The molecular formula $C_8H_8N_{10}$ was determined by HRMS for both compounds **3b** and **3c**. The 'open form' similar to the intermediate **2a** was not detected in this case because the second condensation reaction is probably too fast. The reason for the different reactivity might be in different acido-basic properties of the two compounds. After hydrolysis of the amino groups of both isomers with sodium nitrite in dilute hydrochloric acid, we obtained compounds **1b** and **1c**, respectively
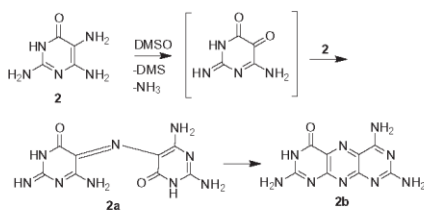
Scheme 2. The proposed mechanism of compound **2** oxidation and self-condensation.

(see Scheme 3). Compound **1c** was also prepared (for the comparison of spectral properties) by a known oxidation reaction of 5-aminouracil with potassium ferricyanide.[11]

Another studied compound was 5-aminobarbituric acid (**4**). The reaction was observed by UV/VIS spectroscopy and ^{1}H NMR spectroscopy. In the DMSO solution, the ammonium cation released (observed by ^{1}H NMR) and the 'open form' **4a** (i.e. a metalochromic indicator murexide, see Scheme 3) was detected, but no subsequent intramolecular condensation was observed. This is not surprising, because no aminogroup is present in **4a**. Product **4a** has its absorption maximum at 532 nm and by comparison with the commercially available sample of murexide, its structure was unambiguously confirmed.

The DMSO oxidation of 5,6-diamino-4-oxo-2-thiopyrimidine (**5**) was also studied. The changes in the UV/VIS spectra and the presence of ammonia cation observed in ^{1}H NMR suggest that similar oxidation and condensation reactions take place. However, a complex mixture of products appeared in the solution and the isolation of the products failed. Some unidentified subsequent reactions involving the reactive SH group (e.g. oxidation of the SH group) probably took place. The DMSO solution of 2,5-diamino-4,6-dimethoxypyrimidine (**6**) slowly changed its colour to orange. However, the only change we were able to detect in the ^{1}H NMR spectra was the hydrolysis of one of the methoxy groups (signals of methanol appeared in the spectra together with an amidic proton and one methoxy group). Apparently, the hydrolysed product may undergo further reactions (hydrolysis of the other methoxy group, oxidation and condensation), which leads to colour changes, but the subsequent reactions were so slow that the products were below the NMR detection limit even after two months. The DMSO solution of 2,5-diamino-4,6-dichloropyrimidine (**7**) slowly changed its colour to dark red, which was further converted into yellow. However, both the NMR and MS spectra revealed that a complicated mixture of products was formed. The chlorine atoms might have been hydrolysed and/or substituted, because the typical isotopic pattern of chlorinated compounds was not observed in the MS spectra.

To support further the proposed reaction mechanism and the structures of the condensation products, we performed condensation reactions of compounds **1**, **2**, **3**, **4** and **6** with alloxan (2,4,5,6-tetraoxopyrimidine). The reactions were performed in DMSO by mixing equimolar amounts of alloxan with a substituted 5-aminopyrimidine. Compound **1** gave bipyrimidine **1d**, which gave pyrimidopteridine **1b** after heating to 120 °C. Similarly, we obtained bipyrimidine **2d** and pyrimidopteridine **2e** from compound **2**. The product **2e** was hydrolysed with sodium nitrite to **1b**.

We were not able to isolate the bipyrimidine derivative from the reaction mixture of compound **3** with alloxan; the only product of the reaction was pyrimidopteridine **3e**, which was also hydrolysed with sodium nitrite to **1b**. 5-Aminobarbituric acid (**4**) gave murexide (**4a**) after reaction with alloxan, and compound **6** condensed with alloxan to a bipyrimidine derivative **6d**.

We have also studied a series of disubstituted 5-aminopyrimidines (with hydrogen atom in position 2 or 6). They were oxidised more slowly than the trisubstituted derivatives **1–6**. In the UV/VIS spectra of these compounds, we observed similar changes like for compounds **1–6**. However, we were not able to isolate the oxidation products for the majority of the disubstituted 5-aminopyrimidines in sufficient quantity for proper characterisation. The full discussion of these compounds is given in the SI.

For comparison, we dissolved 2,6-diamino-4-oxopyrimidine (i.e. compound **2** without the 5-aminogroup) in DMSO and we did not observe any changes in the UV/VIS or NMR spectra. Obviously, the 5-aminogroup is crucial for the oxidation reaction. Neither did we observe any reaction of this compound with alloxan.

All of the reactions were monitored by UV/VIS spectroscopy; the spectra are shown in the SI. The isolated products were charac-
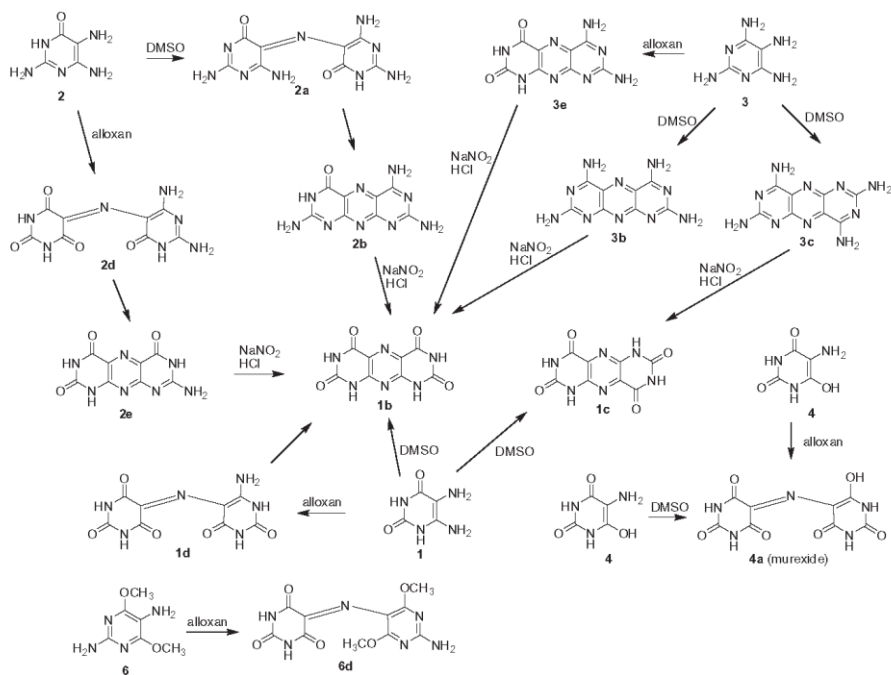
Scheme 3. The observed oxidation-condensation reactions of 5-aminopyrimidines in DMSO.

terised by UV/VIS spectra and high-resolution mass spectra. The UV/VIS spectra are shown in the SI; the absorption maxima are summarised in Table 1. The wavelength of the absorption maxima is dependent on the number of oxo- and amino-substituents, for example in the series of compounds **1b**, **2e**, **3e**, **2b** and **3b** the number of aminogroups goes from zero to four and the absorption maximum goes from 360 to 424 nm.

Unfortunately, the pyrimidopteridine products of the reactions are very poorly soluble and we were not able to acquire ^{13}C NMR spectra for the majority of them. In the ^{1}H NMR spectra, the signals of the exchangeable protons (NH and OH) were very broad, probably because of fast tautomer interconversions. The positions of the

proton signals were also very dependent on the conditions of the measurement; minor changes of temperature or pH probably cause shifts in the tautomer equilibria. In some cases, we did not obtain identical ^{1}H NMR spectra for the same products obtained from two different reactions. Therefore, we do not believe that the ^{1}H NMR spectra are particularly useful for the characterisation of this type of compound.

The DMSO solutions of the substituted 5-aminopyrimidines exhibited signs of instability during storage (colour changes). The antioxidative activity of the coloured samples was clearly lower than that of the freshly prepared solutions.[7] In this study, we have shown that 5-aminopyrimidines can undergo oxidation and subsequent condensation reactions in DMSO. Bipyrimidines and pyrimidopteridines are formed during the reactions. Importantly, the rate of the decomposition of 5-aminopyrimidines in DMSO appears to correlate with their antioxidative activity.[7] The trisubstituted 5-aminopyrimidines (**1–3** and **5**) were found to be more active in the antioxidant assays and were also faster transformed to their oxidation products in DMSO. On the other hand, the antioxidative activities of the disubstituted 5-aminopyrimidines were much lower or not detected at all and they were also more stable in DMSO. We observed that the more electron-donor substituents are attached to the pyrimidine skeleton, the faster the DMSO oxidation of 5-aminopyrimidines is.

Here, we would like to point out that the antioxidative activities of various antioxidants (reducing agents) can be negatively affected by reaction with DMSO (an oxidising agent). We can speculate that some very strong antioxidants will turn totally inactive

after their dissolution in DMSO. This fact may also complicate a direct comparison of the antioxidant activity data on certain groups of compounds between different laboratories. Furthermore, many other biochemical assays have colourimetric end points and highly coloured impurities (such as those observed in this study) may affect the results significantly. Therefore, the storage of tested compounds in DMSO solutions should be avoided and freshly prepared solutions are desirable for biochemical screening.

Acknowledgment

Supplementary data

Supplementary data associated with this article can be found, in the online version, at http://dx.doi.org/10.1016/j.bmcl.2012.08.065.

References and notes

1. Eggens, I.; Eriksson, L. C.; Chojnacki, T.; Dallner, G. *Cancer Res.* **1984**, *44*, 799.
2. Hawser, S.; Lociuro, S.; Islam, K. *Biochem. Pharmacol.* **2006**, *71*, 941.
3. Lee, J.; Kim, K. H.; Jeong, S. *Bioorg. Med. Chem. Lett.* **2011**, *21*, 4203.
4. Gadhachanda, V. R.; Wu, B. G.; Wang, Z. W.; Kuhen, K. L.; Caldwell, J.; Zondler, H.; Walter, H.; Havenhand, M.; He, Y. *Bioorg. Med. Chem. Lett.* **2007**, *17*, 260.
5. Hockova, D.; Holy, A.; Masojidkova, M.; Andrei, G.; Snoeck, R.; De Clercq, E.; Balzarini, J. *J. Med. Chem.* **2003**, *46*, 5064.
6. Rezk, B. M.; Haenen, G. R.; van der Vijgh, W. J.; Bast, A. *FEBS Lett.* **2003**, *555*, 601.
7. Procházková, E.; Jansa, P.; Dračínský, M.; Holý, A.; Mertlíková-Kaiserová, H. *Free Radical Res.* **2012**, *46*, 61.
8. Halliwell, B.; Gutteridge, J. M. C.; Aruoma, O. I. *Anal. Biochem.* **1987**, *165*, 215.
9. Sanmartin-Suarez, C.; Soto-Otero, R.; Sanchez-Sellero, I.; Mendez-Alvarez, E. *J. Pharmacol. Toxicol. Methods* **2011**, *63*, 209.
10. Taylor, E. C.; Loux, H. M.; Falco, E. A.; Hitchings, G. H. *J. Am. Chem. Soc.* **1955**, *77*, 2243.
11. Baudisch, O.; Davidson, D. *J. Biol. Chem.* **1927**, *71*, 497.
12. Hartman, W. W.; Simppabd, O. E. *Org. Synth.* **1932**, *12*, 84.
13. Kaminsky, D.; Lutz, W. B.; Lazarus, S. *J. Med. Chem.* **1966**, *9*, 610.
14. Skibo, E. B.; Bruice, T. C. *J. Am. Chem. Soc.* **1986**, *108*, 1650.
15. Skibo, E. B.; Bruice, T. C. *J. Am. Chem. Soc.* **1983**, *105*, 3304.